CLARKSON UNIVERSITY

Equation-Oriented Modeling of Dividing Wall Columns

A Dissertation

by

Jingsong Zhou

Department of Chemical and Biomolecular Engineering

Submitted in partial fulfillment of the requirements

for the degree of

Doctor of Philosophy
(Chemical Engineering)

April 2019

Accepted by the Graduate School

_____, _____
Date, Dean of the Graduate School

The undersigned have examined the thesis entitled “Equation-Oriented Modeling of Dividing Wall Columns” presented by Jingsong Zhou, a candidate for the degree of Doctor of Philosophy in Chemical and Biomolecular Engineering, and hereby certify that it is worthy of acceptance.

Date	Prof. Ross Taylor (Advisor)
	Prof. Ruth Baltus
	Prof. Yuncheng Du
	Prof. Marcias Martinez
	Prof. Richard McCluskey

Abstract

Dividing wall columns (DWCs) have been widely studied over the last decade, mainly because of their potentials in energy and capital savings. It is often stated that no commercial simulation software package offers DWC as a standard module; hence engineers employ multi-column models for simulations of such columns. In such simulations, a DWC is divided into different independent segments, with each segment modeled using a conventional column model. However, this sequential solving approach is sometimes challenging when the column system is complicated. A parallel column model is proposed in this research that is equation-based in nature. That means all of the equations that describe the column system are solved at the same time. The proposed model is shown capable of modeling DWCs of arbitrary configurations. Extensive DWC simulations are used to test the model, and it is concluded that the equation-based PCM exhibits better numerical performance, compared to sequential-modular multi-column models.

The parallel column model is validated using the pilot DWC data from University of Texas at Austin; good agreement is observed between model predictions and experimental data. The CAPE-OPEN is a standard allowing interoperability between different simulation software. The parallel column model is a CAPE-OPEN compliant and can be used in any CAPE-OPEN compliant process flowsheet simulation package as a standard DWC module. Examples of flowsheet intensification using the parallel column model in a CAPE-OPEN flowsheet simulation package are demonstrated.

Acknowledgements

I would like to express my sincere gratitude to my academic advisor, Professor Ross Taylor, for your continuous support of my Ph.D. study and research. Having worked with you for more than five years at Clarkson University, you are so much more than an advisor to me. I admire the ingenuity and insights you have to various problems, and your enthusiasm to scientific challenges; I also appreciate your integrity. Your kind advice on my research and career are something priceless that I will always bear in mind in my future life.

I would also like to offer many thanks to Dr. Hendrik A. Kooijman, who has provided me with considerable support of my research. I have gained much valuable industrial knowledge from you during our cooperation, and I am deeply grateful for your kindness and patience. An unforgettable memory is sitting with you at the cafeteria close to the train station in Florence after the Distillation and Absorption 2018 conference, you gave me some insightful opinions and encouragement in finding a job.

My sincere thanks also goes to the other members of my thesis committee: Professor Ruth Baltus, Professor Yuncheng Du, Professor Marcias Martinez, and Professor Richard McCluskey, for your brilliant comments, suggestions, and challenging questions, which helped me to broaden my research perspectives.

A special thanks to the late Professor Marco A. Satyro, who was a Professor at Clarkson University from 2015 to 2016. I appreciate the guidance and instruction he offered me in thermodynamics. I love his passion for science, and his patience as a teacher: he was always willing to answer questions from students no matter how busy he was.

Last but not the least, I would like to express my appreciation to my parents, friends, and anyone who supported me. Without you, this thesis would not be possible.

Table of Contents

Abstract i

Acknowledgements ii

List of Tables vii

List of Figures x

List of Variables xiv

CHAPTER 1 Introduction and Literature Review 1

1.1 Introduction to Dividing Wall Column 1

1.2 Thermodynamic Analysis 4

1.3 Simulation and Design 6

1.3.1 Approximate Design Methods 6

1.3.2 Rigorous Simulation Strategies 7

1.3.3 Rate-Based (or Non-equilibrium) DWC Model 10

1.4 Heat Transfer across the Dividing Wall 10

1.5 Pressure Balancing and Vapor Split 12

1.6 Experimental Work on DWC 14

1.7 Summary and Outline of this Thesis 15

Reference 17

CHAPTER 2 Equilibrium Stage Parallel Column Model 22

2.1 Model Description 24

2.1.1 Numbering Stages 24

2.1.2 A Parallel Column Model 28

2.1.3 Heat Transfer across Dividing Wall(s) 32

2.1.4 Summary of Specification 36

2.1.5 Method of Solution 37
2.2 Model Verification 39
2.2.1 Aromatics Complex Separation 39
2.2.2 Satellite Column Simulation 45
2.3 Other Applications 52
2.3.1 Heat Transfer across Dividing Wall 53
2.3.2 Column with Multiple Condensers 57
2.3.3 Additional Case Studies 60
2.4 Performance Summary 60
2.5 Usage in a Commercial Simulation Program 62
2.6 Remarks 63
Software Used in This Work 65
Reference 65
CHAPTER 3 Rate-Based Parallel Column Model 68
3.1 Model Description 68
3.2 Method of Solution 75
3.3 Aromatics Processing Case Study 78
3.3.1 Simulation Description 79
3.3.2 Simulation Results 81
3.4 Remarks 84
Reference 85
CHAPTER 4 Model Validation with Pilot Data 87
4.1 Validation with the Pilot Data from University of Texas at Austin 87
4.1.1 Simulation with the Equilibrium-Stage PCM 88

4.1.2 Simulation with the Rate-Based PCM 96
4.1.3 Simulation Results 97
4.2 Validation with the Mutalib Pilot Data 100
4.3 Remarks 102
Reference 102
CHAPTER 5 Multiple Steady-State Solutions in a Dividing Wall Column Simulation 104
5.1 Introduction 104
5.2 Case Study 105
5.3 Discussion 111
5.4 Conclusion 112
Reference 112
CHAPTER 6 Process Plant Intensification with DWCs 114
6.1 LPG Recovery Plant 114
6.1.1 Process Description 115
6.1.2 Simulation of the LPG Recovery 118
6.1.3 Summary 124
6.2 Shell Higher Olefin Process (SHOP) 125
6.2.1 Oligomerization Reaction 127
6.2.2 Process Simulation 129
6.2.3 Simulations at Different Growth Factors 151
6.2.4 Remarks 155
Reference 157
CHAPTER 7 Conclusions and Future Work 159
7.1 Conclusions 159

7.2 Future Work 161

Appendix A: Counting Stages – Additional Discussion 163

Appendix B: PCM Initialization..... 167

Appendix C: Additional Case Studies and Supplementary Material to Chapter 2..... 172

Appendix D: Simulation Results of Cases from Roach (2017) 199

List of Tables

Table 2.1 Stage-connection information for a simple DWC. 28

Table 2.2 Summary of simulation parameters and specified variables for a DWC simulation. 37

Table 2.3 Summary of simulation parameters for aromatics column 41

Table 2.4 Pressure specifications of the four-column model. 41

Table 2.5 Comparisons of product purities with the ChemCAD results from Dejanović (2017). 45

Table 2.6 Summary of the satellite column specifications. 48

Table 2.7 Interaction parameters of NRTL model from UniSim® Design. 48

Table 2.8 Comparison of the product compositions. 50

Table 2.9 Simulation specifications of the pentane/hexane/heptane case from Benyounes et al. (2015) 54

Table 2.10 Binary interaction parameters of PR model from UniSim® Design. 54

Table 2.11 Comparisons of product purities with and without considering heat transfer (HT) effects. 56

Table 2.12 Product purities in the EDWC predicted from the PCM. 59

Table 2.13 PCM performance for DWC simulations. 61

Table 3.1 Basic dimensions and estimated pressure drop in each packed bed section. . 82

Table 3.2 Selected product mole fractions as a function of stage height. 83

Table 4.1 Summary of pilot tests in the thesis of Roach (2017). 89

Table 4.2 Specifications for the selected DWC simulations (from Roach, 2017). 91

Table 4.3 Parameters used in Kooijman et al. (2002) pressure drop model for Sulzer M500Y packing. 96

Table 4.4 Specifications for selected dividing wall column simulations 99

Table 4.5 Comparison of the simulated purity and those provided in the paper of Mutalib et al. (1998). 102

Table 5.1 Specifications for dividing wall column simulation 106

Table 5.2 Summary of multiple steady state solutions 107

Table 6.1 Natural gas feed (from Mostafa et al. 2019). 116

Table 6.2 Streams sent to the LPG recovery section (from Mostafa et al. 2019). 117

Table 6.3 Product purities from the conventional column sequence simulation. 120

Table 6.4 Product purities from the DWC simulation. 123

Table 6.5 Comparison of the reboiler duty between direct sequence and DWC column. 123

Table 6.6 Ethylene oligomerization product compositions at different K-factors. 129

Table 6.7 Simulation results for the oligomerization reactor inlet and outlet streams. 131

Table 6.8 Inlet and outlet stream information of column DC2=. 133

Table 6.9 Summary of the product streams simulated with the conventional method. 135

Table 6.10 Summary of column specifications and some simulation results. 136

Table 6.11 Comparison between the conventional and the "3-3-2" configurations. 144

Table 6.12 Summary of the product streams simulated with the configuration "3-3-2". 144

Table 6.13 Comparison between the conventional and the "3-2-3" configurations. 147

Table 6.14 Summary of streams information in the configuration “3-2-3”. 147

Table 6.15 Comparison between the conventional and the "3-4" configurations..... 150

Table 6.16 Summary of the product stream information in the configuration "3-4". ... 150

Table 6.17 Comparison between the conventional and the "3-3-2" configurations for separations at K-factor equals 0.60. 153

Table 6.18 Comparison between the conventional and the "3-3-2" configurations for separations at K-factor equals 0.65. 154

Table 6.19 Comparison between the conventional and the "3-3-2" configurations for separations at K-factor equals 0.70. 155

List of Figures

Figure 1.1 Diagram of a simple DWC 2

Figure 1.2 Conventional column sequences for ternary system separation 3

Figure 1.3 (a) Pre-fractionator arrangement, (b) Petlyuk arrangement, and (c) DWC 3

Figure 1.4 More operable Petlyuk arrangement 8

Figure 1.5 Four-column DWC model 9

Figure 1.6 Pumparound DWC model 9

Figure 2.1 Diagram of the DWC with one wall and four sections 25

Figure 2.2 Diagram of sections in a DWC and the corresponding equilibrium stage model 29

Figure 2.3 Schematic diagram of a DWC example 31

Figure 2.4 Schematic diagram of a DWC intersection 34

Figure 2.5 Schematic diagram of cases with (a) equal and (b) unequal number of stages on two sides of the wall 35

Figure 2.6 Results of (a) flowrate and (b) temperature profiles from the PCM, with an HETP value of 0.4 m from Dejanović et al. (2011). 44

Figure 2.7 Liquid composition profiles for five components from the PCM simulation of the aromatic column. 44

Figure 2.8 Diagrams of (a) the satellite column system, and (b) the equivalent DWC structure. 46

Figure 2.9 Flowsheet of seven-column model in UniSim® Design. 49

Figure 2.10 Results of (a) vapor flowrate and (b) liquid flowrate profiles from the PCM, assuming equal HETP. 51

Figure 2.11 Temperature profiles of satellite column system predicted from the PCM, assuming equal HETP. 51

Figure 2.12 Liquid composition profiles predicted with the PCM, assuming equal HETP. 52

Figure 2.13 Comparison of temperature profiles with and without heat transfer, assuming equal HETP. 56

Figure 2.14 Liquid composition profiles assuming equal HETP (a) with no heat transfer effects, and (b) with heat transfer effects. 57

Figure 2.15 Flowsheet of the EDWC simulation with three-column model and the PCM (right). 58

Figure 2.16 Temperature profiles of the EDWC predicted from the PCM. 60

Figure 2.17 A flowsheet for the work-up section of an alpha-olefins plant created with COFE containing DWCs modeled using the PCM in which a direct separation sequence of 5 columns has been replaced by two DWCs. 63

Figure 3.1: Schematic diagram of sections in dividing wall column and corresponding stage model. 69

Figure 3.2 Stage alignment at the foot of a dividing wall. 74

Figure 3.3 Diagram of the DWC with packed beds (left); model setup in the PCM (right). 79

Figure 3.4 Temperature profiles of the aromatic DWC predicted from the rate-based PCM.. 83

Figure 4.1 (left) Schematic diagram of the DWC with four packed beds (numbers indicate stages in model); (right) Initial liquid split at the top and vapor split at the bottom of the wall (specified by Roach, 2017). 90

Figure 4.2 Temperature profiles of case A10ii (data from Roach, 2017). 92

Figure 4.3 Temperature profiles of case H1 (data from Roach, 2017). 93

Figure 4.4 Predicted temperature profiles in case H12 using equilibrium-stage PCM with (a) no heat transfer, and (b) U_{atm} = 85.4 W/m^{2}K, U_{wall} = 850 W/m^{2}K. Data from Roach (2017). 94

Figure 4.5 Parity plot of temperatures for all case studies in Roach (2017), predicted with the equilibrium-stage PCM. 95

Figure 4.6 Temperature profiles in the DWC of two different systems described in Table 4.4. Data from Roach (2017). 98

Figure 4.7 Predicted temperature profiles in hydrocarbon case H12 with (a) no heat transfer, and (b) U_{atm} = 85.4 W/m^{2}K, U_{wall} = 1238 W/m^{2}K. Data from Roach (2017). 98

Figure 4.8 Parity plots of temperatures in dividing wall sections for all case studies in Roach (2017). 100

Figure 4.9 Schematic diagram of the pilot DWC in the work of Mutalib et al. (1998) (numbers indicate stages in the PCM). 101

Figure 5.1 (a) Diagram of the packed DWC; (b) Diagram of the DWC with numbers indicating stages in model 106

Figure 5.2 Temperature profiles of three steady-state solutions 107

Figure 5.3 Flowrate and liquid phase mole fraction profiles for three steady-state solutions for the dividing wall column in Table 6.1 108

Figure 5.4 Product purity as a function of side product mass flowrates: (a) top product purity, and (b) middle product purity vs. side product mass flowrate. Points represent the solution in Figure 6.2 and 6.3 109

Figure 5.5 Multiple steady-state solutions obtained when varying side product and bottom product flowrates simultaneously: (a) Purity of main compound in the distillate (left), and (b) mole fraction of main product in the sidedraw..... 110

Figure 6.1 NGL recovery process simulated in COCO. 117

Figure 6.2 LPG recovery flowsheet of the conventional method simulated in COCO.... 119

Figure 6.3 DWC model for LPG recovery column (numbers represent stages in the PCM). 121

Figure 6.4 LPG recovery flowsheet of the DWC method simulated in COCO. 122

Figure 6.5 Temperature profiles of the DWC. 122

Figure 6.6 The entire flowsheet of the DWC method setup in COCO. 124

Figure 6.7 Schulz-Flory type distribution (plotted at K = 0.65). 128

Figure 6.8 Simulation of the oligomerization reaction system in COCO. 130

Figure 6.9 Flowsheet of α-olefin product separation using conventional direct sequence of columns..... 134

Figure 6.10 Reflux ratio as a function of vapor and liquid split ratios (point indicates the found minimum reflux ratio) 139

Figure 6.11 DWC configuration separating $C_{6=}$ and $C_{8=}$. 139

Figure 6.12 Two solutions of the temperature profiles of the DWC simulation. 140

Figure 6.13 Two solutions of the flowrate profiles of the DWC simulation. 141

Figure 6.14 Flowsheet of the “3-3-2” configuration. 143

Figure 6.15 Flowsheet of the "3-2-3" configuration. 145

Figure 6.16 Flowsheet of the "3-4" configuration. 148

Figure 6.17 Diagram of the DWC2 in the "3-4" configuration (numbers indicate stage numbers in the PCM). 149

Figure 6.18 New flowsheet of the "3-3-2" configuration. 152

List of Variables

A	heat transfer area, m^2
B	pressure balance equation, Pa
c	number of components
C	proportional constants
E	energy balance equation, W
F	molar flowrate of the feed, kmol/s
G	interlinked molar flows, kmol/s
h	height in Eq. (3.11)
H	enthalpy, J/kmol K
H	height of the dividing wall, m
H	hydraulic equation, Pa
J	Jacobian matrix
K	equilibrium ratio
L	molar flowrate of the liquid phase, kmol/s
M	material balance equation, kmol/s
N	number of stages
$\mathcal{N}$	mass transfer rate, kmol/s
Q	heat removal, W
Q	interface equilibrium equation
r	radius of the column intersection, m
R	mass transfer rate equation, kmol/s
s	number of stages in the column
S	summation equation
S	side stream molar flowrate, kmol/s
T	temperature, K
U	overall heat transfer coefficient, W/m^2K
V	molar flowrate of the vapor phase, kmol/s
w	number of dividing walls
W	width of the dividing wall, m
x	mole fraction in liquid phase
y	mole fraction in vapor phase
z	mole fraction of the feed

Greek letters

α	liquid split ratio
β	vapor split ratio
δ	ratio of the flows between two stages
$\mathcal{E}$	energy transfer rate, W
ϑ	angle in Figure 2.4

ρ	density, kg/m^3
τ	sum of temperature differences in Eq. (B.8)

Subscripts

DW	dividing wall
f	referring to feed
i	referring to components
j	referring to stage number
k	referring to dividing wall
L (or left)	left hand side
m	referring to stage number
r	referring to right hand side in Eq. (2.9)
R (or right)	right hand side
t	referring to total mixture

Superscripts

dynamic	referring to dynamic part of pressure drop
F	feed
I	phase interface
L, V	liquid and vapor phases
k	iteration index
P	phase
static	referring to static part of pressure drop
S	column shell
W	dividing wall

Publications that resulted from this work:

- Zhou, J., Kooijman, H. A., Taylor, R., 2018. A rate-based equation-oriented parallel column model: application to dividing wall columns. *Chemical Engineering Transactions*, ***69***, 247-252
  DOI: 10.3303/CET1869042

- Zhou, J., Kooijman, H. A., Taylor, R., 2018. Multiple steady-state solutions in a dividing wall column simulation. *Chemical Engineering Transactions*, **69**, 355-360
  DOI: 10.3303/CET1869060

- Zhou, J., Kooijman, H.A., Taylor, R., 2019. Parallel column model for dividing wall column simulations. *Computers and Chemical Engineering*, **125**, 114-133
  DOI: 10.1016/j.compchemeng.2019.02.008

- Zhou, J., Kooijman, H.A., Taylor, R., 2019. A rate-based equation-oriented parallel column model: application to dividing wall columns. *Chemical Engineering Research and Design*, **146**, 48-59
  DOI: doi.org/10.1016/j.cherd.2019.03.034

Presentations that resulted from this work (* presenter if not J. Zhou):

- Process Optimization using CAPE-OPEN Tools
  R. Taylor*, H.A. Kooijman, J. Zhou
  CAPE-OPEN 2017 Annual Meeting, Sunbury, UK, October 12-13, 2017

- An Equation-Based Parallel Column Model
  J. Zhou, H.A. Kooijman, R. Taylor
  AIChE 2017 Fall Meeting, Minneapolis, MN, USA, October 29 – November 3, 2017

- Rate-Based Equation-Oriented Parallel Column Model: Application to Dividing Wall Columns
  J. Zhou, H.A. Kooijman, R. Taylor
  AIChE 2018 Spring Meeting, Orlando, FL, USA, April 22-26, 2018

- A Rate-Based Equation-Oriented Parallel Column Model: Application to Dividing Wall Columns
  J. Zhou, H.A. Kooijman, R. Taylor
  Distillation and Absorption 2018, Florence, Italy, Sep 16-19, 2018

- A Rate-Based Equation-Oriented Parallel Column Model: Application to Dividing Wall Columns
  J. Zhou, H.A. Kooijman*, R. Taylor
  CAPE-OPEN 2018 Annual Meeting, Ludwigshafen, Germany, Oct 9-10, 2018

- Design Packed Columns to Handle Maldistribution
  H.A. Kooijman, J. Zhou, R. Taylor*
  AIChE 2019 Spring Meeting, New Orleans, LA, March 31 – April 4, 2019

CHAPTER 1 Introduction and Literature Review

1.1 Introduction to Dividing Wall Column

Distillation is widely known as one of the most commonly used processes in the chemical industries. However, this process is capital and energy intensive; “distillation operations in the chemicals and petroleum refining industries alone account for almost 53% of the total separation energy used” (Oak Ridge National Laboratory, 2005). Dividing wall columns (DWCs) are attracting considerable attention in the scientific and patent literature (see Tian et al., 2018) because of their potential for saving capital and energy costs. It is claimed that DWCs may be able to save up to 30% of the energy when compared to conventional column sequences (Becker et al., 2001; Fidkowski and Królikowski, 1987; Triantafyllou and Smith, 1992). In addition, a DWC is installed in a single column shell, thereby (usually) saving a significant percentage of the capital cost (Schultz et al., 2002).

The concept of a dividing wall column (DWC) was originally proposed by Richard Wright in 1949 (Wright, 1949), in which he claimed that a vertical partition at about the middle section of the column can effectively prevent the side stream product from being contaminated by the lighter and heavier components, and three relatively pure products may be obtained from a single column. A diagram of a simple DWC is shown in Figure 1.1, which resembles a side-stream column except that it has a partition in the middle. Unlike a side-stream column, where the purity of middle product is limited, a DWC has superior separation abilities, due primarily to the fact that the vertical partition effectively prevents lateral mixing in the column.

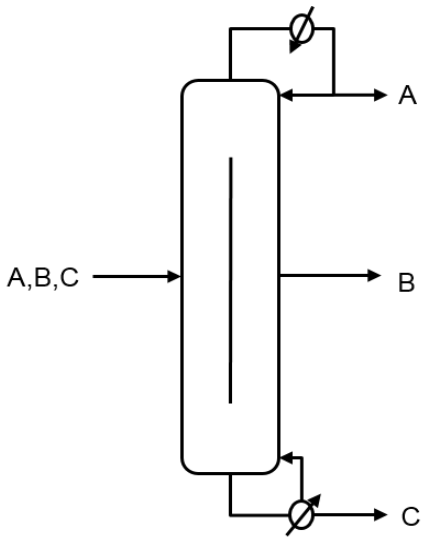

Figure 1.1 Diagram of a simple DWC

Figure 1.2a and b shows the direct and indirect column sequence for ternary separations. Another possible sequence, also known as the sloppy sequence, is shown in Figure 1.2c. Note that, in the sloppy sequence, the bottom flow from the second column and the top flow from the third column are both product B, these two columns can be combined as one single column with a side product (Figure 1.3a). Further modifications can be made by replacing the condenser and reboiler on the first column with vapor and liquid material flows (Figure 1.3b); this is known as the fully thermally coupled (FC) configuration or Petlyuk arrangement (Petlyuk et al., 1965).

The pre-fractionator in the Petlyuk arrangement can be integrated into the main-fractionator, where the two columns share the same column shell (Figure 1.3c). The fact that a DWC incorporates two columns into one shell underlies the ability of a DWC to obtain a side stream product with high purity. For the same ternary mixture separation, the conventional direct (or indirect) sequence needs two column shells, two condensers, and two reboilers; while a DWC needs one shell, one condenser, and one reboiler. Therefore, for the same task, a DWC can achieve significant capital savings, and, obviously, needs a smaller footprint.

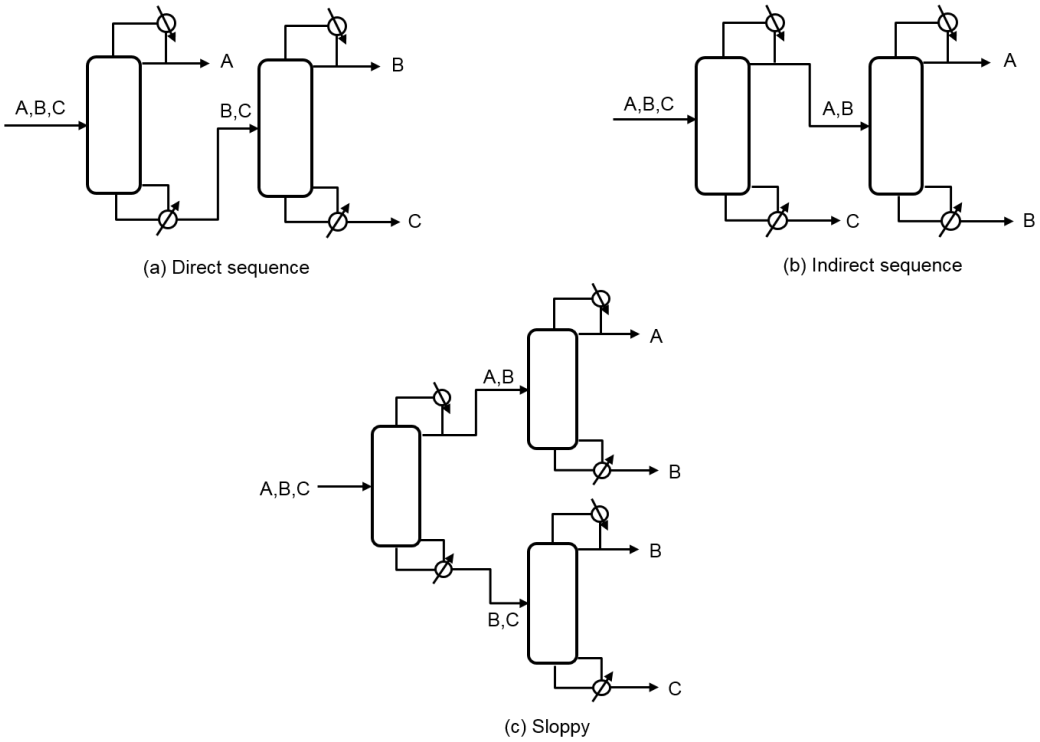

Figure 1.2 Conventional column sequences for ternary system separation

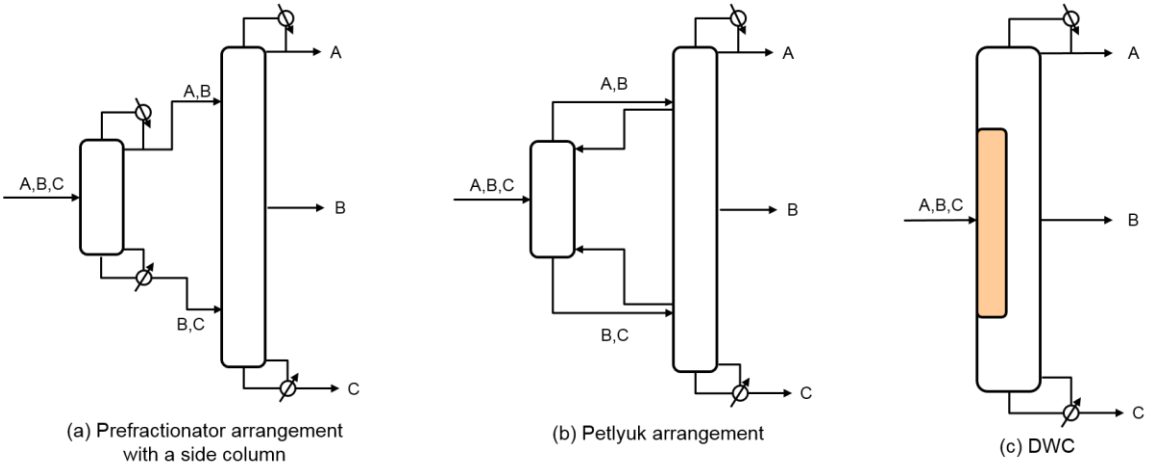

Figure 1.3 (a) Pre-fractionator arrangement, (b) Petlyuk arrangement, and (c) DWC

From the perspective of thermodynamics, the Petlyuk arrangement and a simple DWC are equivalent structures, assuming heat transfer across the dividing wall is zero (Schultz et al., 2002). The conventional direct or indirect sequences are considered thermodynamically inefficient, due primarily to the existence of remixing of the internal

streams (Smith, 2005). In the first column of the direct sequence, the concentration of B reaches a peak value on a tray near the bottom; as the heaviest component C is predominant at the bottom, the concentration of B then starts to decrease on stages ever closer to the bottom of the column. The decrease in the concentration is the main source of inefficiency, which should be avoided in the operation. A similar explanation applies to the indirect sequence. In contrast, the Petlyuk arrangement avoids this remixing problem by conducting a non-sharp separation in the pre-fractionator. In addition, the entropy of mixing between the feed composition and the composition at the feed stage can be effectively reduced in the pre-fractionator (Smith, 2005). Therefore, by avoiding these thermodynamic inefficiencies, DWCs can save up to 30% of energy cost compared to conventional direct and indirect sequences. Additional commentary on the thermodynamic analysis of DWCs will be discussed in the following section.

1.2 Thermodynamic Analysis

Since the Petlyuk column and DWC configurations are thermodynamically equivalent as long as the wall is adiabatic, anything we conclude about the Petlyuk column should also be applicable to the equivalent DWC configuration. Many studies have been conducted on the thermodynamic aspects of the Petlyuk configuration (Fidkowski and Krolikowski, 1986; Agrawal and Fidkowski, 1998a; Halvorsen and Skogestad, 2001; Hernández et al., 2006; Hernandez-Gaona et al., 2005; Rev et al., 2001; Stichlmair and Stemmer, 1989). Fidkowski and Królikowski (1986) compared the minimized energy requirements for an assumed ideal ternary mixture separation using four different configurations (Petlyuk column, direct sequence, indirect sequence, and separation complex), and found that the Petlyuk column requires the least energy of the four configurations. Later on, they compared the Petlyuk column with other three thermally coupled configurations (inner column, side-rectifier, and side-stripper) for the separation of a near-ideal ternary mixture (Fidkowski and Królikowski, 1987), the Petlyuk column again needs the minimum

energy requirement. In their work, they used the sum of vapor flow rates from all reboilers to approximate energy requirements.

Although the Petlyuk column has been said to have the ability to save, on average, 30% of the energy compared to conventional direct and indirect sequences (Triantafyllou and Smith, 1992), that does not mean the Petlyuk column is perfect. Agrawal and Fidkowski (1998) were the first to analyze the thermodynamic efficiency of different configurations. They studied five different configurations for ideal ternary mixture separation of mixtures with different feed compositions and different relative volatilities. They found that, based on the combination of feed compositions and relative volatilities, the Petlyuk column usually is not the most thermodynamically efficient configuration, while the side-rectifier and side-stripper configurations show higher thermodynamic efficiency more often than does the Petlyuk configuration.

Halvorsen and Skogestad (2001) evaluated the minimum entropy production (second law) of the reversible and irreversible (adiabatic) Petlyuk column, and they concluded that even if the reversible arrangement is optimal with respect to entropy production (second law), the adiabatic Petlyuk column has the lowest energy consumption (first law). Hernandez-Gaona et al. (2005) studied several different column sequences for ternary and quaternary separations, and they applied exergy analysis in evaluating the efficiencies for each configuration.

In summary, from the perspective of the first law, the Petlyuk column requires less energy than conventional configurations for the same task; however, in terms of the second law, the Petlyuk column has a lower thermodynamic efficiency for most cases, resulting in large temperature ranges.

1.3 Simulation and Design

1.3.1 Approximate Design Methods

Although DWCs possess significant capital and energy savings, they are not constructed as frequently as conventional distillation columns. This is mainly because the simulation and control of DWCs remains somewhat immature (Kaibel, 2014). Unlike conventional distillation columns, DWCs have more degrees of freedom in design and simulation studies. Considerable research work has been conducted towards developing short-cut methods for DWC design, because a good short-cut method can, most likely, guarantee a fast convergence of a rigorous simulation of DWC.

Fidkowski and Krolikowski (1986) optimized a model that can quickly calculate the minimum energy requirement for the Petlyuk column. Later, they applied this approach to other thermally coupled systems, including side-rectifiers and side-strippers (Fidkowski and Królikowski, 1987). However, Dünnebier and Pantelides (1999) questioned the appropriateness and accuracy of the model.

Triantafyllou and Smith (1992) presented a short-cut design method for the Petlyuk arrangement based on Fenske-Underwood-Gilliland model (FUG), which is a combination of models widely used for making preliminary designs and optimizations of simple distillation columns. They optimized the three-column model by minimizing the reboiler duty (energy requirement) and the number of stages (capital cost) at the same time. Vapor and liquid flows in the main column were considered not independent of the vapor and liquid flows fed to the pre-fractionator.

Amminudin et al. (2001) pointed out some drawbacks in Triantafyllou and Smith's work. They thought the Gilliland correlations can cause significant errors if used to compute number of stages for the Petlyuk arrangement; the Kirkbride equation can also cause errors when rigorous simulation is conducted. Based on the equilibrium stage

composition concept, they proposed a semi-rigorous model that can provide an initial design close to the rigorous simulation results.

Sotudeh and Hashemi Shahraki (2007) believed that the Fenske equation is inappropriate for the estimation of the minimum number of stages in a DWC. This is because the composition of the vapor stream going to the main column and the composition of the liquid stream going back from the main column are not equal, while the equality of these compositions is the prerequisite of using the Fenske equation. Therefore, their short-cut model is based on the Underwood equations.

Apart from the above-mentioned methods, that are mainly based on all, or a portion of, the Fenske-Underwood-Gilliland-Kirkbride model combination, other short-cut methods are based on entirely different techniques. These include the “moving triangle” technique (Holland et al., 2004), and genetic algorithms (Gómez-Castro et al., 2008; Vazquez–Castillo et al., 2009; Gutiérrez-Antonio and Briones-Ramírez, 2009).

1.3.2 Rigorous Simulation Strategies

Unlike conventional distillation columns, DWCs have more degrees of freedom for design and simulation. Furthermore, there is no standard DWC module in commercial software packages, such as ASPEN PLUS™, ChemCAD or Aspen HYSYS®, that can be used directly for design and simulation, and one has to arrange the conventional columns in sequences to simulate DWCs (Kaibel, 2014; Dejanović et al., 2010; Becker et al., 2001; Kiss, 2013). There are several strategies of simulating a simple DWC using commercial simulation packages, each with pros and cons discussed in what follows.

The first approach is the two-column model, where the DWC is modeled as the Petlyuk arrangement. However, the original Petlyuk arrangement (Figure 1.3b) has a potential issue in that the pressure at the top of the pre-fractionator should be greater than the pressure of the point of connection in the main-fractionator, while the pressure at the

bottom of pre-fractionator should be less than the pressure at the point of connection in the main-fractionator. This is a significant restriction on the pressure and on the pressure drop for the two columns. Agrawal and Fidkowski (1998b) discussed some more operable arrangements, e.g. Figure 1.4, in this arrangement, the pressure of the second column can be slightly higher than that of the first column. Simulation of this arrangement makes use of two distillation columns, so conventional sequential modular simulators can solve these systems iteratively. However, these simulations may exhibit poor convergence because of the strong interaction between the units. In large columns containing complex mixtures, the computational costs can become excessive (Becker et al., 2001).

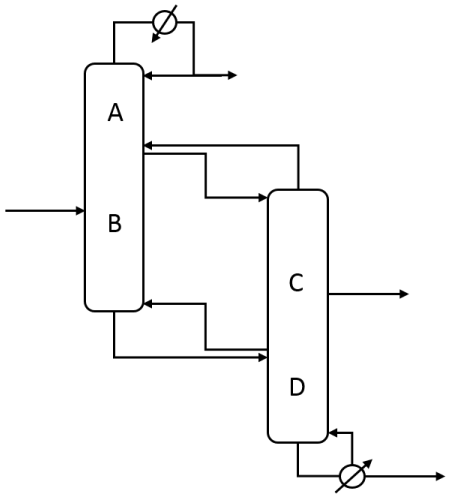

Figure 1.4 More operable Petlyuk arrangement

The second approach is to split a conventional DWC into four individual column sections with two columns in the middle section representing the pre-fractionator and side product section connected in parallel (Figure 1.5) (see, e.g. Górak and Olujic, 2014). This four-column model is considered to be the best suitable structure for the study of dynamic simulations and process control. However, this four-column model requires four initial guesses for four interconnecting streams, thus exhibiting the same convergence weakness as the two-column model above.

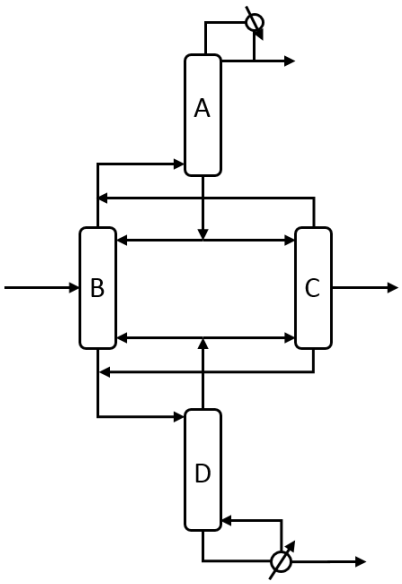

Figure 1.5 Four-column DWC model

Another commonly used method is the pumparound model shown in Figure 1.6. It uses pumparounds and vapor bypasses to simulate a DWC in a single conventional distillation unit. However, at the point between section B and section C, there is no vapor or liquid flow. This can make the model difficult to converge, or even diverge (Becker et al., 2001).

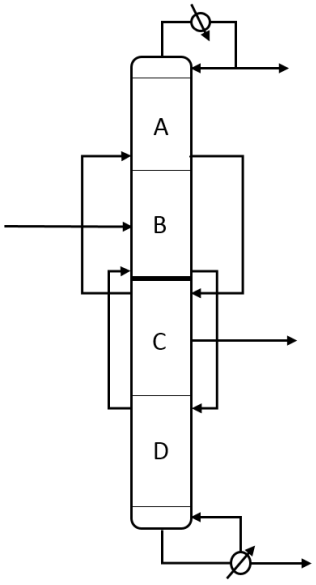

Figure 1.6 Pumparound DWC model

The last approach that is mentioned in the literature is an equation-based model, or, equivalently, equation-oriented model. By using this type of approach, the entire

flowsheet is solved simultaneously using, for example, Newton's method. This approach is considered to offer significant advantages over sequential modular approaches, as it converges more easily and quickly (Becker et al., 2001). However, there is no paper that reports on this approach in detail.

1.3.3 Rate-Based (or Non-equilibrium) DWC Model

As mentioned above, no commercial flowsheet simulation package has yet offered a DWC as a standard module; as a result, nearly all simulations of DWCs – and there are many – employ interlinked multi-column equilibrium stage models in a sequential-modular process simulator. Notable exceptions are the work of Mueller and Kenig (2007), who used a rate-based model to describe reactive distillation in dividing wall columns, and of the Fieg group (Hiller et al., 2010; Egger et al., 2018) , who described a nonequilibrium stage model for dividing wall columns. Also noteworthy (and unusual) about their work is that they used Aspen Custom Modeler (ACM), a commercial tool that employs equation-based solution techniques. This is in complete contrast to all other models in the published literature on dividing wall columns (at least those that have been described in sufficient detail). (Although models developed in ACM uses equation-based solution techniques, they cannot be generally used to model DWCs with arbitrary configuration without recreating the model if the DWC configuration changes.)

1.4 Heat Transfer across the Dividing Wall

Few studies have considered heat transfer across the dividing wall when modeling DWCs. The main reason is that there is no easy way to include wall heat transfer in the model. Some researchers (see, e.g. Mueller and Kenig, 2007; Hiller et al., 2010; Niggemann et al., 2010, 2011; Niggemann and Fieg, 2012; Egger et al., 2018) applied ACM to simulate DWCs with wall heat transfer accounted for in a relatively simple way.

The first work on heat transfer across the dividing wall was by Lestak et al. (1994), where a steady-state simulation was established in Aspen with heat exchangers positioned employed between stages on both sides of the wall. They simulated several cases, and found that, in each case, the reboiler duty would increase as the wall heat transfer coefficient increases. They claimed that heat transfer is beneficial in some regions of the wall (it can help to reduce the energy consumption), while detrimental in others; insulation should be installed in regions that have detrimental effects.

Suphanit et al. (2007) analyzed heat transfer effects by using the column grand composite curve (CGCC), together with exergy analysis. They determined the "beneficial" region of the wall in a DWC in terms of reduced exergy losses.

Ehlers et al. (2015) confirmed the conclusion from Lestak et al. (1994) that heat transfer across the dividing wall can either increase or decrease the minimum energy demand of a DWC. They also found that the heat transferred across the dividing wall would never change the minimum energy demand by more than the amount of heat being transferred.

Mueller and Kenig (2007) proposed a rate-based model for modeling either reactive or nonreactive DWCs. They considered wall heat transfer by assuming the wall is covered by one phase only. They used the pilot DWC results from Mutalib et al. (1998) to validate their nonreactive model, and analyzed the wall heat transfer effects by assuming a constant overall heat transfer coefficient, 600 W/m^2K. They concluded, based on the limited experimental results, that the changes in the product streams are marginal; further work requires the report of pilot composition profiles inside the column.

The Fieg group used their pilot DWC data to validate their DWC models, both equilibrium and nonequilibrium (Hiller et al., 2010; Niggemann et al., 2010, 2011; Niggemann and Fieg, 2012). The models consider wall heat transfer and pressure drop on both sides of the wall. In the nonequilibrium model, heat transfer is assumed to occur between liquid phases only, but the determination of the overall heat transfer coefficient should take into account multiphase heat transfer (Hiller et al., 2010). They calculated the overall heat

transfer coefficient to be 700 W/m^{2}K. The authors concluded that, for lab-scale columns, heat transfer across the dividing wall can have a significant impact on hydraulics and vapor load. Further research is needed to investigate the wall heat transfer effects in large scale DWCs.

Roach (2017) emphasized that different column internals (trays or packing) would result in different wall wettability, which is an important factor that can affect wall heat transfer. The design model proposed by Roach took into account both heat transfer across the dividing wall and heat loss to the atmosphere through a software HEEDS, which can be linked with Microsoft Excel and Aspen Plus to modify the desired variables in the Aspen input file. The simulation results were compared with extensive experimental pilot temperature data from the pilot DWC built in University of Texas at Austin.

1.5 Pressure Balancing and Vapor Split

Mutalib and Smith (1998) conducted a degrees of freedom analysis for a simple DWC, and concluded that, compared to a side draw column, a DWC has two additional degrees of freedom, namely the vapor and liquid splits. Many studies have shown the significant impact that vapor and liquid splits have on a DWC performance (see, e.g., Steacy, 2003; Dwivedi et al., 2012a; Xia et al., 2013; Kang et al., 2017). The consensus view is that the liquid split above the dividing wall can be manipulated easily and precisely by an external device (Asprion and Kaibel, 2010); however, disagreement exists on whether vapor split can be manipulated as easily as the liquid split, or even if it can be controlled at all.

Dwivedi et al. (2012) used two vapor split valves on their lab scale DWC to experimentally show that vapor split can be used as a degree of freedom during practical operations. Ge et al. (2016) proposed a vapor splitter device and conducted experimental studies; they claimed that the device can adjust the vapor split regardless of operating conditions. Similarly, research conducted by Kang et al. (2017) proposed an active vapor distributor (AVD) that can be applied to controlling the vapor split during DWC operation; they

presented their laboratory results on the AVD to show its capability. Such work on inventing a device for controlling the vapor split is only limited to the lab scale, no large scale device for industrial use has been reported yet.

On the other hand, many other researchers consider the vapor split to be a self-adjusting parameter, which is determined by balancing the pressure drops on both sides of the dividing wall (see the review papers of Kaibel, 2014; Dejanović et al., 2010; Kiss, 2013). Since the pressure drop in sections alongside the dividing wall is a complicated function of column internals, liquid load, wall positioning (cross sectional area), and so on, it then becomes possible to indirectly control the vapor split by tuning these variables. One example is the work of Mutalib and Smith (1998), who found that varying the liquid split would affect the vapor split considerably in the high liquid and vapor loading region. Dejanović et al. (2011) demonstrated the use of the free area of liquid collectors to fine-tune the pressure drop on both sides of the wall, and hence to obtain the desired vapor split. The work of Niggemann et al. (2010) shows that, for lab-scale columns, heat transfer across the dividing wall can have significant impacts on the column hydrodynamics, and thus on the vapor split. A nonequlibrium stage model proposed by Hiller et al. (2010) is able to self-adjust the vapor split according to the pressure drops on both sides of the wall; they proved that the vapor split ratio is not necessarily equal to the cross sectional area ratio.

Pressure drop correlations used in DWCs are similar to those in conventional columns. Barroso-Muñoz et al. (2010) conducted an experimental study of pressure drop in a DWC, and found that the predictions from the model of Stichlmair et al. (1989) were in good agreement with the experimental data. Rix and Olujić (2008) derived a pressure drop model for liquid collectors and distributors, and validated it with experimental data. They found, from a vacuum column example, that the pressure drop of internals (liquid collectors and distributors) took up nearly 12% of the total pressure drop, and therefore, should not be ignored in simulations.

1.6 Experimental Work on DWC

A few studies have published pilot plant data of DWC operations (both steady state and dynamic). Comprehensive reviews on the experimental work of DWCs can be found in the doctoral dissertations of Nguyen (2015) and Roach (2017).

The first experimental study in a DWC was reported by Mutalib and Smith (1998) and Mutalib et al. (1998) for separating methanol, isopropanol, and 1-butanol. The pilot DWC has a diameter of 0.305 m (about 12 inches) and an overall height of 10.97 m (about 36 feet), with Gempak 4A structured packing installed as internals. The dividing wall is positioned off-center to the pre-fractionator side, with a cross sectional area ratio of 1/1.29.

The Skogestad group studied a pilot Kaibel column built at the Norwegian University of Science and Technology (NTNU) in Trondheim (see Dwivedi et al., 2012a; b). The pilot column has no actual wall, but two parallel tubes acting as the feed and side sections of a DWC. The internal diameter of all sections is 50 mm, and glass Raschig rings are used as column internals. In this pilot plant, the vapor split ratio can be adjusted through a valve; heat transfer is not considered since the column does not have a real dividing wall.

The Fieg group reported the separation of n-hexanol, n-octanol, and n-decanol in a pilot plant at Hamburg University of Technology, Germany, in which all three products achieved high purity (>99wt%) (Niggemann et al., 2010). This pilot DWC has an inner diameter of 68 mm, with a centered welded dividing wall. The four column sections are filled with Montz B1-500 structured packing, with each section having a height of 980 mm packed bed. They used the HETP value provided by the manufacturer. The pilot data obtained from their pilot plant are used to validate the non-equilibrium stage model they proposed for DWC simulations (Hiller et al., 2010).

Nguyen and coworkers (Nguyen, 2015; Nguyen et al., 2016) studied a pilot Petlyuk column for both non-reactive and reactive systems; the pilot column was set up in their laboratory

(Toulouse, France) in 2013. The pilot plant has a total height of 5.53 m (about 18 feet), and a diameter of 80 mm in the non-wall region, and 50 mm in the wall region. The pilot plant resembles the one built at the NTNU, where the feed and side sections are two separated shells; Sulzer DX structured packing is used as column internals. They measured the HETP experimentally, which was 0.115 m (the HETP provided by Sulzer is 0.07 m). Heat transfer is not considered in their work, due to the structure of the pilot plant.

A more recent doctoral thesis of Roach (2017) reported a comprehensive experimental study of the pilot DWC built at the University of Texas, Austin (UT Austin). Roach and coworkers studied the separation of two systems, alcohol system and hydrocarbon system, at different pressures, with extensive pilot data published. The pilot column is filled with Sulzer Mellapak 500Y structured packing, and has an internal diameter of 6.63 inches. The pilot data are used for the validation of the DWC model proposed by Roach, in which heat transfer across the dividing wall and heat loss to the surroundings are both included.

1.7 Summary and Outline of this Thesis

Dividing wall columns have been studied extensively in recent years; a large number of papers were published covering various aspects of DWCs. Several comprehensive review papers or book chapters are mentioned in this chapter (e.g. Dejanović et al., 2010; Asprion and Kaibel, 2010; Kiss, 2013; Kaibel, 2014).

The main focus of this dissertation is on the simulation and modeling of DWCs; accordingly, the present situation of that can be summarized as follows:

- Most simulations of DWCs are done using multi-column models in commercial flowsheet simulation software
- Commercial software still do not contain DWC as a standard module

- Studies on rate-based (or nonequilibrium stage) modeling of DWCs are few in number and have so far been limited to simple DWCs with one wall
- Heat transfer across the dividing wall is usually ignored in the simulations, partly because there is no easy way to model it
- Different opinions exist on whether vapor split can be manipulated
- It is not easy to model a self-regulating vapor split ratio

This dissertation is composed of eight chapters and four appendices. This chapter has served to provide background and to give a summary of the latest research on DWCs, especially on the important aspects of simulation and design; both the equilibrium-stage model and rate-based (also termed as nonequlibrium) model for DWCs in the open literature were reviewed.

It has long been recognized that a simultaneous equation-based model is probably the smart tool to use for modeling of DWC. Many investigators cite a paper by Becker et al. (2001) who make such a recommendation, but they provide no evidence at all of having done so. Nor do any of the many other writers that cite Becker's work. To that end, we propose in Chapter 2 an equilibrium-stage parallel column model (PCM) that is equation-based in nature. One of the goals of this dissertation is to provide definitive evidence that a simultaneous column model can converge quickly and easily, even in cases where the multi-column models fail. The model is then verified by comparing the simulation results with those obtained from other flowsheet simulation packages using sequential modular multi-column models.

Prior work on rate-based (or nonequilibrium-stage) models for DWC is limited to three papers by Mueller and Kenig (2007), Mueller et al. (2007), and Hiller et al. (2010). Noteworthy (and unusual) about their work is that they used Aspen Custom Modeler, a commercial tool that employs equation-based solution techniques. However, Aspen Custom Modeler does not qualify as a standard DWC module, as it cannot be used to model DWCs if the configuration changes. Therefore, in Chapter 3, we describe a rate-

based PCM that can be used to model DWCs of arbitrary configuration (this includes columns with multiple walls, and multiple condensers/reboilers).

Chapter 4 serves to validate the models put forth in the previous two chapters against the pilot DWC data from University of Texas at Austin.

Chapter 5 presents multiple steady-state solutions in one DWC simulation using the equilibrium-stage PCM proposed in Chapter 2.

Chapter 7 demonstrates the use of the proposed PCM for flowsheet intensification in a flowsheet simulation package via the CAPE-OPEN mechanism.

Chapter 8 concludes this thesis and puts forth some interesting perspectives on future work concerning Dividing Wall Columns.

Reference

Agrawal, R., and Fidkowski, Z.T., 1998a. Are thermally coupled distillation columns always thermodynamically more efficient for ternary distillations? *Industrial & engineering chemistry research*, 37(8), pp.3444–3454.

Agrawal, R., and Fidkowski, Z.T., 1998b. More operable arrangements of fully thermally coupled distillation columns. *AIChE Journal*, 44(11), pp.2565–2568.

Amminudin, K.A., Smith, R., Thong, D.Y.-C., and Towler, G.P., 2001. Design and optimization of fully thermally coupled distillation columns: part 1: preliminary design and optimization methodology. *Chemical Engineering Research and Design*, 79(7), pp.701–715.

Asprion, N., and Kaibel, G., 2010. Dividing wall columns: fundamentals and recent advances. *Chemical Engineering and Processing: Process Intensification*, 49(2), pp.139–146.

Barroso-Muñoz, F.O., et al., 2010. Experimental study on pressure drops in a dividing wall distillation column. *Chemical Engineering and Processing: Process Intensification*, 49(2), pp.177–182.

Becker, H., Godorr, S., Kreis, H., and Vaughan, J., 2001. Partitioned distillation columns -- why, when & how. *Chemical Engineering*, 108(1), Jan., p.68.

Dejanović, I., Matijašević, L., Jansen, H., and Olujić, Ž., 2011. Designing a packed dividing wall column for an aromatics processing plant. *Industrial & Engineering Chemistry Research*, 50(9), pp.5680–5692.

Dejanović, I., Matijašević, L., and Olujić, Ž., 2010. Dividing wall column—a breakthrough towards sustainable distilling. *Chemical Engineering and Processing: Process Intensification*, 49(6), pp.559–580.

Dünnebier, G., and Pantelides, C.C., 1999. Optimal design of thermally coupled distillation columns. *Industrial & Engineering Chemistry Research*, 38(1), pp.162–176.

Dwivedi, D., et al., 2012a. Active vapor split control for dividing-wall columns. *Industrial & Engineering Chemistry Research*, 51(46), pp.15176–15183.

Dwivedi, D., et al., 2012b. Experimental verification on active vapor split control for dividing-wall columns. *Industrial & Engineering Chemistry Research*.

Egger, T., Hiller, C., and Fieg, G., 2018. Experimental studies of a Petlyuk column and validation of a non-equilibrium stage model. *Chemical Engineering & Technology*, 41(4), pp.827–835.

Ehlers, C., Schröder, M., and Fieg, G., 2015. Influence of heat transfer across the wall of dividing wall columns on energy demand. *AIChE Journal*, 61(5), pp.1648–1662.

Fidkowski, Z., and Krolikowski, L., 1986. Thermally coupled system of distillation columns: optimization procedure. *AIChE Journal*, 32(4), pp.537–546.

Fidkowski, Z., and Królikowski, L., 1987. Minimum energy requirements of thermally coupled distillation systems. *AIChE Journal*, 33(4), pp.643–653.

Gómez-Castro, F.I., et al., 2008. Dividing wall distillation columns: optimization and control properties. *Chemical Engineering & Technology*, 31(9), pp.1246–1260.

Górak, A., and Olujic, Z., 2014. *Distillation: equipment and processes*. Academic Press.

Gutiérrez-Antonio, C., and Briones-Ramírez, A., 2009. Pareto front of ideal Petlyuk sequences using a multiobjective genetic algorithm with constraints. *Computers & Chemical Engineering*, 33(2), pp.454–464.

Halvorsen, I.J., and Skogestad, S., 2001. Integrated column designs for minimum energy and entropy requirements in multicomponent distillation. In: *AIChE Annual Meeting, Nevada*.

Hernández, S., Segovia-Hernández, J.G., and Rico-Ramírez, V., 2006. Thermodynamically equivalent distillation schemes to the Petlyuk column for ternary mixtures. *Energy*, 31(12), pp.2176–2183.

Hernandez-Gaona, C.G., et al., 2005. Second law analysis of conventional and nonconventional distillation sequences. *Chemical and biochemical engineering quarterly*, 19(3), pp.235–241.

Hiller, C., Buck, C., Ehlers, C., and Fieg, G., 2010. Nonequilibrium stage modelling of dividing wall columns and experimental validation. *Heat and Mass Transfer*, 46(10), pp.1209–1220.

Holland, S.T., et al., 2004. Novel separation system design using “moving triangles”. *Computers & Chemical Engineering*, 29(1), pp.181–189.

Huaqiang, G., Xiangwu, C., Nan, C., and Wenyi, C., 2016. Experimental study on vapor splitter in packed divided wall column. *Journal of Chemical Technology & Biotechnology*, 91(2), pp.449–455.

Kaibel, B., 2014. Dividing-wall columns. In: *Distillation: Equipment and Processes*. Academic Press, pp.183–199.

Kang, K.J., Harvianto, G.R., and Lee, M., 2017. Hydraulic driven active vapor distributor for enhancing operability of a dividing wall column. *Industrial & Engineering Chemistry Research*, 56(22), pp.6493–6498.

Kiss, A.A., 2013. Dividing-wall column. In: *Advanced distillation technologies: design, control and applications*. John Wiley & Sons, pp.67–110.

Lestak, F., Smith, R., and Dhole, V.R., 1994. Heat transfer across the wall of dividing wall columns. *Chemical engineering research & design*, 72(5), pp.639–644.

Mueller, I., and Kenig, E.Y., 2007. Reactive distillation in a dividing wall column: rate-based modeling and simulation. *Industrial & Engineering Chemistry Research*, 46(11), pp.3709–3719.

Mueller, I., Pech, C., Bhatia, D., and Kenig, E.Y., 2007. Rate-based analysis of reactive distillation sequences with different degrees of integration. *Chemical Engineering Science*, 62(24), pp.7327–7335.

Mutalib, M.I.A., and Smith, R., 1998. Operation and control of dividing wall distillation columns: part 1: degrees of freedom and dynamic simulation. *Chemical Engineering Research and Design*, 76(3), pp.308–318.

Mutalib, M.I.A., Zeglam, A.O., and Smith, R., 1998. Operation and control of dividing wall distillation columns: part 2: simulation and pilot plant studies using temperature control. *Chemical Engineering Research and Design*, 76(3), pp.319–334.

Nguyen, T.D., 2015. *Conceptual design, simulation and experimental validation of divided wall column: application for non-reactive and reactive mixture*.

Nguyen, T.D., Rouzineau, D., Meyer, M., and Meyer, X., 2016. Design and simulation of divided wall column: experimental validation and sensitivity analysis. *Chemical Engineering and Processing: Process Intensification*, 104, pp.94–111.

Niggemann, G., and Fieg, G., 2012. Validation of dividing-wall columns based on experimental data and dynamic simulations: pilot-plant and production-scale columns. *Industrial & Engineering Chemistry Research*, 51(2), pp.931–943.

Niggemann, G., Hiller, C., and Fieg, G., 2010. Experimental and theoretical studies of a dividing-wall column used for the recovery of high-purity products. *Industrial & Engineering Chemistry Research*, 49(14), pp.6566–6577.

Niggemann, G., Hiller, C., and Fieg, G., 2011. Modeling and in-depth analysis of the start-up of dividing-wall columns. *Chemical Engineering Science*, 66(21), pp.5268–5283.

Oak Ridge National Laboratory 2005. *Materials for separation technologies: energy and emission reduction opportunities*.

Petlyuk, F.B., Platonov, V.M., and Slavinskii, D.M., 1965. Thermodynamically optimal method for separating multicomponent mixtures. *Int. Chem. Eng.*, 5(3), pp.555–561.

Rev, E., et al., 2001. Energy savings of integrated and coupled distillation systems. *Computers & Chemical Engineering*, 25(1), pp.119–140.

Rix, A., and Olujic, Z., 2008. Pressure drop of internals for packed columns. *Chemical Engineering and Processing: Process Intensification*, 47(9), pp.1520–1529.

Roach, B.J., 2017. *A design model for dividing wall distillation columns*.

Schultz, M.A., et al., 2002. Reduce costs with dividing-wall columns. *Chemical engineering progress*, 98(5), pp.64–71.

Smith, R., 2005. *Chemical process: design and integration*. John Wiley & Sons.

Sotudeh, N., and Hashemi Shahraki, B., 2007. A Method for the design of divided wall columns. *Chemical Engineering & Technology*, 30(9), pp.1284–1291.

Steacy, P.C., 2003. *Dividing wall fractionation column control system and apparatus*. US6558515B1.

Stichlmair, J., Bravo, J.L., and Fair, J.R., 1989. General model for prediction of pressure drop and capacity of countercurrent gas/liquid packed columns. *Gas Separation & Purification*, 3(1), pp.19–28.

Stichlmair, J., and Stemmer, A., 1989. Reduction of energy requirements in distillation. *Chemical engineering & technology*, 12(1), pp.163–169.

Suphanit, B., Bischert, A., and Narataruksa, P., 2007. Exergy loss analysis of heat transfer across the wall of the dividing-wall distillation column. *Energy*, 32(11), pp.2121–2134.

Tian, Y., Demirel, S.E., Hasan, M.M.F., and Pistikopoulos, E.N., 2018. An overview of process systems engineering approaches for process intensification: State of the art. *Chemical Engineering and Processing - Process Intensification*, 133, pp.160–210.

Triantafyllou, C., and Smith, R., 1992. The design and optimisation of fully thermally coupled distillation columns : process design. *Chemical engineering research & design*, 70(A2), pp.118–132.

Vazquez–Castillo, J.A., et al., 2009. Design and optimization, using genetic algorithms, of intensified distillation systems for a class of quaternary mixtures. *Computers & Chemical Engineering*, 33(11), pp.1841–1850.

Wright, R.O., 1949. *Fractionation apparatus*. US2471134A.

Xia, M., et al., 2013. Temperature control for extractive dividing-wall column with an adjustable vapor split: methylal/methanol azeotrope separation. *Industrial & Engineering Chemistry Research*, 52(50), pp.17996–18013.

CHAPTER 2 Equilibrium Stage Parallel Column Model

The common approaches to modeling DWCs were reviewed in the previous chapter. Few of the many papers on DWC modeling discuss in any detail a methodology for simulating a DWC using a multi-column model in a commercial simulator. A significant exception is the paper of Navarro et al. (2012). They propose an approach they call acyclic simulation. Essentially, this means modeling a sequence of columns without recycles. The evidence in their paper suggests that their methodology provides extremely good initial estimates for a similar sequence that includes the recycles. It does not, however, appear that this method has (as yet) been widely adopted. The first half of a paper by Waltermann and Skiborowski (2017) provides an elegant summary of various approaches to the simulation of Dividing Wall Columns (the second half is concerned with optimization and compares two different optimization approaches).

Other authors have written in somewhat non-specific terms about their general experience modeling DWCs using a commercial simulator (see, for example, Kolbe and Wenzel, 2004; Asprion and Kaibel, 2010; Dejanović et al., 2010; Okoli and Adams, 2015; Nguyen et al., 2016). Kolbe and Wenzel (2004), for example, had this to say:

Commercial process simulators are not well suited to solving the task of designing a divided-wall column easily, because manual variation of the input is necessary using the commercially available software, which is rather complex and time-consuming.

More recently, Dejanović et al. (2010) wrote:

Carrying out DWC performance simulations requires great experience and these are more or less computationally very demanding. … well established commercial software packages still do not contain a DWC as a standard model. This however will occur sooner or later, most probably as a simultaneous, equation based model.

It has long been suggested that equation-based simulators offer some advantages over sequential modular simulators in convergence stability and speed when modeling DWCs. Many investigators cite a paper by Becker et al. (2001) who make such a recommendation, but they provide no actual evidence in support of their claim. Nor do any of the many other writers that cite Becker's paper. BASF, the company that built the first DWC has long used equation-oriented models for the simulation of such columns (Benfer, 2018); but, to the best of our knowledge, has never published any details concerning the performance of their model. An extensive literature review by Tian et al. (2018) lists a number of papers that describe equation-oriented modeling of DWCs. Although models developed in process modeling environments such as Aspen Custom Modeler or gPROMS) use equation-based solution techniques, they cannot be generally used to model DWCs with arbitrary configuration without recreating the model if the DWC configuration changes (Mueller and Kenig, 2007; Hiller et al., 2010; Idris et al., 2017).

In this chapter, a flexible equation-based equilibrium-stage parallel column model (PCM), is proposed. This model can be used as a standard unit operation module within commercial simulation packages to model DWCs with arbitrary configurations. Furthermore, this equation-based PCM facilitates the inclusion of wall heat transfer effects, with no auxiliary software required.

In the latter sections, DWCs of different configurations are first modeled with the PCM ignoring heat transfer effects. Results are compared with other simulators using multi-column models to verify the PCM. Heat transfer effects are included in a subsequent case. Finally, a simulation of a DWC with multiple condensers is considered.

2.1 Model Description

2.1.1 Numbering Stages

One of the objectives behind the development of our PCM is to be able easily to model DWCs with arbitrary configurations; thus, a minor problem is to propose a consistent method for numbering stages in DWCs. This numbering exercise is avoided completely in the creation of a multi-column DWC model in a commercial simulator, but must be addressed in the development of any independent equation-oriented model.

When modeling simple columns it is common either to number stages from top to bottom or from bottom to top; condensers and reboilers (if present) sometimes are included in the numbering schemes, other times they are omitted. From a programming perspective, however, all stages, no matter what type or position in the column require a reference label (normally a number) associated with them.

We start by defining a column section as beginning and ending at either the top or bottom of the column or at the top or bottom of a wall and confined laterally by the column outer shell and/or the dividing walls inside the column. Sections are assumed to be segmental; this is not strictly necessary, it is more of a practical matter reflecting how (most) DWCs are constructed. The distributor design could be quite complicated for a non-segmental column section.

Within each column section we number the stages consecutively, starting from the top of the section. We further assume that the column configuration is known in the sense that the number of stages in each section is known, as is the presence (or absence) of any condenser and reboiler and the relative location of the feed and side product streams. Condensers and reboilers are included with their appropriate section. Thus, the condenser in the one-wall DWC in Figure 2.1 is included in the top section, the reboiler is part of the bottom section.

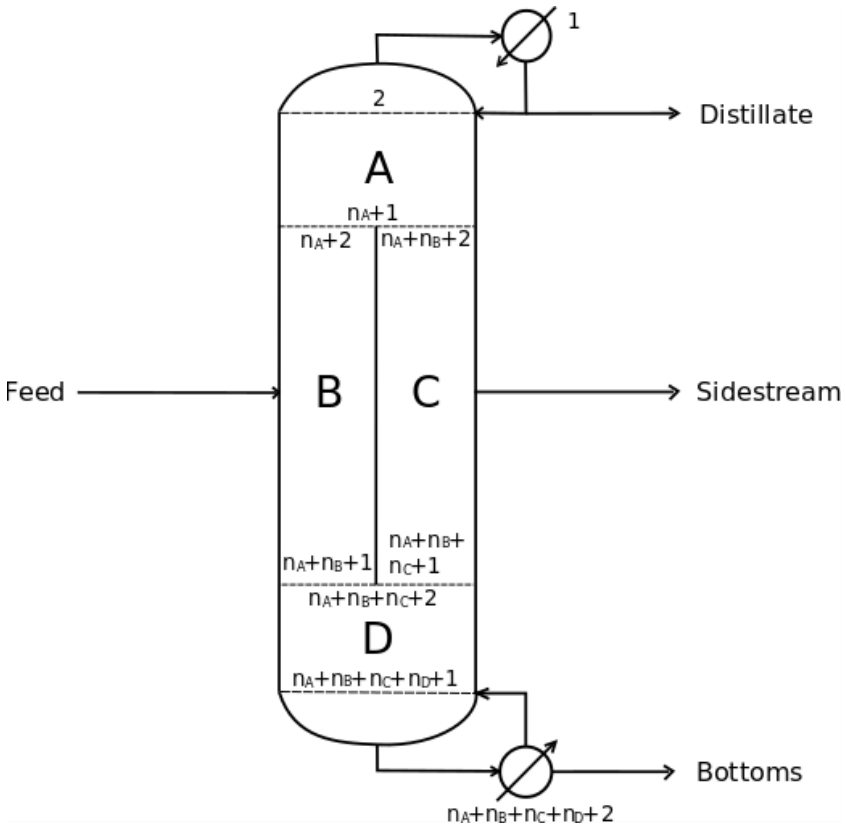

Figure 2.1 Diagram of the DWC with one wall and four sections. Roman numericals identify the section and lower case *n* is the number of stages in the section identified by the subscript.

The only question that needs to be answered before we can proceed to the numbering of all of the individual stages in the column as a whole then becomes: In what sequence should we place the various column sections?

For the one-wall, four-section column in Figure 2.1 there are 24 different ways to order the column sections. For two ten-section, three-wall columns that we will consider later (one can be found in Appendix A) there are more than three-million different ways to order the sections! Not all of these section sequences are particularly helpful when it comes to visualizing the column configuration, but there will usually be several possible section sequences that are more or less equally useful. Arguably, only 8 of the possible 24 sequences for the one-wall column are useful: ABCD, ACBD, ABDC, or ACDB; and their mirrors.

The scheme that is used in our software implementation is to number column sections following the flow of liquid down the column (i.e. starting from the top of the column). When we come to the top of a wall we arrive at what we call an "interconnection" between column sections. Each next section is assigned the next unused identity in the sequence A-Z, starting from the left hand side of the column and continuing sideways as far as necessary (usually a new wall creates just two new sections immediately below). (Note that “left” and “right” here simply refer to a graphic visualization of the column such as that in Figure 2.1. In addition, there is no need to a priori position feed streams to the left and product streams to the right. In fact, for some DWCs it will be necessary to have some feed and product streams assigned to the same “side” of the column.) When we arrive at the bottom of a wall then two (usually) sections give way to a single new section immediately below. This new section receives the next available section identity.

Section identities are assigned using these rules every time we come to the top or bottom of a wall, only stopping at the bottom of the column itself. Thus, for the simple DWC in Figure 2.1 the sequence of section numbers that results from application of these “rules” is ABCD as shown in the figure. These simple guidelines do not, however, guarantee the fewest number of non-consecutively numbered stage connecting streams (NCCs). (Liquid NCCs occur when the split leaving the bottom stage of Section S, say, goes to a stage in any section not next in the sequence A-Z, or when a vapor split leaving the top of a stage in Section S goes to any stage in a section not next in the sequence Z-A.) However, all variants of a particular DWC are formally equivalent and we have verified that our simulation code yields identical results no matter what section numbering sequence is employed.

The stages can then be numbered consecutively starting with 1 at the top of the column (usually a condenser) and then proceeding through the column, following the appropriate (alphabetical in our case) order of the sections.

(It is possible for a wall to extend all the way to the top or bottom of the shell and, as a result, for the column to be linked to multiple condensers and/or reboilers. In that situation condensers and reboilers should be associated with those column sections to which they are physically connected. An example of such a column will be considered later in this chapter.)

Further discussion of section numbering can be found in Appendix A.

2.1.1.1 Flow Splits

When the liquid reaches the top of a wall or the vapor reaches the bottom of a wall the flows are split with part going to one side of the wall or to the other side.

To specify the inter-stage flows, we introduce four parameters: phase, originating-stage, destination-stage, and the flow split ratio. The flow split ratios are defined by:

$$\alpha = \frac{Liquid\ flow\ to\ stage\ below\ left}{Liquid\ flow\ from\ stage\ above}$$

$$\beta = \frac{Vapor\ flow\ to\ stage\ above\ left}{Vapor\ flow\ from\ stage\ below}$$

With these definitions at hand, we can summarize the flow splits for the simple DWC in Figure 2.1 in Table 2.1.

It is not feasible to present generalized stage connection tables for other DWCs; there are too many potential configurations to consider.

In an equilibrium stage model it is necessary to specify the flow split ratios (or the actual flows themselves).

Table 2.1 Stage-connection information for a simple DWC.

Phase	From Stage	To Stage	Split Ratio
Liquid	$n_A + 1$	$n_A + 2$	α
		$n_A + n_B + 2$	1-α
	$n_A + n_B + 1$	$n_A + n_B + 2$	0
		$n_A + n_B + n_C + 2$	1
Vapor	$n_A + n_B + n_C + 2$	$n_A + n_B + n_C + 1$	1- β
		$n_A + n_B + 1$	β
	$n_A + n_B + 2$	$n_A + n_B + 1$	0
		$n_A + 1$	1

2.1.2 A Parallel Column Model

The parallel column model described in this chapter makes use of the equilibrium stage concept, meaning that the vapor and liquid flows leaving a stage are assumed to be in equilibrium. To assist the discussion, we show in Figure 2.2 a schematic diagram of three stages at the top of a dividing wall, with notations introduced. The vapor and liquid flowrates leaving stage *j* are denoted by V_j and L_j, respectively, and y_{ij} and x_{ij} are the mole fractions in these streams. Stream enthalpy leaving stage *j* is denoted by H_j, with the superscript indicating the stream phase. Side streams are denoted by S_j, the molar flowrate, again with superscript indicating the side stream phase. Q_j^S is the heat loss on stage *j*, with the superscript S standing for column shell. $Q_{m,j+1}^W$, represents the heat transferred across the dividing wall (if present) from stage *j+1* to stage m; this term is discussed in more detail in the next section. Interlinking flows G_{jm}^P represent the vapor and liquid traffic between stage *j* and m created by a wall that partitions the column into different segments. It is worth emphasizing that for conventional columns there are no such interlinking streams, while in divided wall columns only a few such connecting mass streams exist.

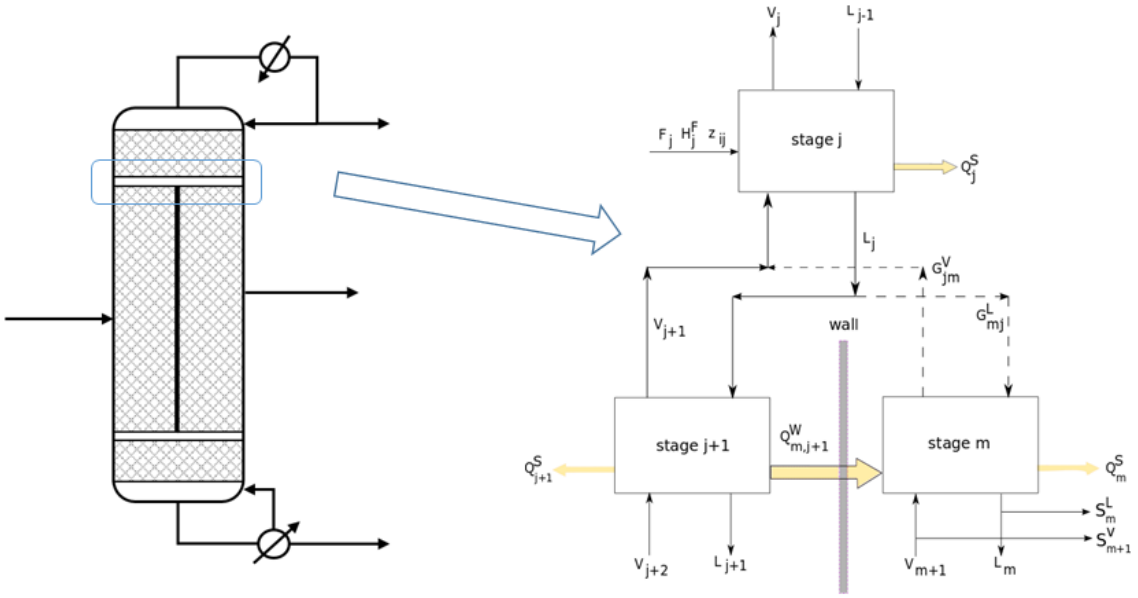

Figure 2.2 Diagram of sections in a DWC and the corresponding equilibrium stage model

A detailed description of equilibrium models for conventional distillation columns is widely available (see, e.g., Seader and Henley, 2011). In the parallel column model, we write the so-called MESH equations (MESH stands for Material balance, Equilibrium relations, composition Summation, and entHalpy balance) for stages in DWCs, with interlinked terms considered. Assume a distillation system contains *s* stages and *c* components.

1. M equations.

- Component material balance (M_c) (*c* equations for each stage)

$$M_{ij} \equiv \left(L_j + S_j^L\right)x_{ij} + \left(V_j + S_j^V\right)y_{ij} - \delta_{j,j-1}^L \cdot L_{j-1}x_{i,j-1} - \delta_{j,j+1}^V \cdot V_{j+1}y_{i,j+1} - F_j z_{ij} - \sum_{m=1}^{s}\left(G_{jm}^V y_{im} + G_{jm}^L x_{im}\right) = 0 \quad (2.1)$$

where $\delta_{j,j-1}^L$ is the ratio of the liquid flow from stage *j-1* to stage *j*, while $\delta_{j,j+1}^V$ is the ratio of the vapor flow from stage *j+1* to stage *j*. If stage *j* has no liquid connection with stage *j-1*, $\delta_{j,j-1}^L$ is set to zero, and the same applies to $\delta_{j,j+1}^V$.

- Total material balance (M_t) (one for each stage)

$$M_{tj} \equiv \left(L_j + S_j^L\right) + \left(V_j + S_j^V\right) - \delta_{j,j-1}^L \cdot L_{j-1} - \delta_{j,j+1}^V \cdot V_{j+1} - F_j - \sum_{m=1}^{s} \left(G_{jm}^V + G_{jm}^L\right) = 0 \tag{2.2}$$

2. E equations (*c* equations for each stage).

$$E_{ij} \equiv y_{ij} - K_{ij} x_{ij} = 0 \tag{2.3}$$

where K_{ij} is the K-value of component *i* on stage *j*.

3. S equations (one for each stage).

$$S_j \equiv \sum_{i=1}^{c} x_{ij} - \sum_{i=1}^{c} y_{ij} = 0 \tag{2.4}$$

4. H equations (one for each stage).

$$H_j \equiv \left(L_j + S_j^L\right)H_j^L + \left(V_j + S_j^V\right)H_j^V - \delta_{j,j-1}^L \cdot L_{j-1} H_{j-1}^L - \delta_{j,j+1}^V \cdot V_{j+1} H_{j+1}^V - F_j H_j^F - \sum_{m=1}^{s} \left(G_{jm}^V H_m^V + G_{jm}^L H_m^L\right) + Q_j^S + \sum_{m=1}^{s} Q_{mj}^W = 0 \tag{2.5}$$

An example of writing the MESH equations for a simple DWC is demonstrated below. The DWC has 30 stages in total, and the dividing wall is located in the center of the column, with 10 stages on each side of the wall. Heat transfer across the wall is ignored. A brief schematic diagram in Figure 2.3 shows stage numbers and the corresponding flow notations around the dividing wall.

In Figure 2.3, most stages only have flow connections with stages having adjacent numbers (stage *j* has connections with stage *j-1* and stage *j+1*), which is similar to the case in conventional columns. Exceptions are the stages at the top and bottom of the dividing wall. The interlinked terms, G_{jm}^P, in the MESH equations of the six stages shown in Figure 2.3 (stage 5, 6, 15, 16, 25, 26) are nonzero.

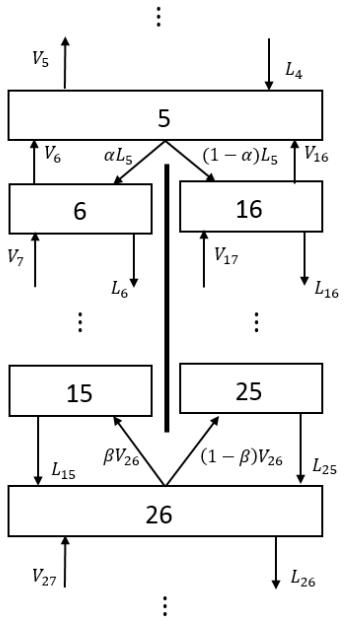

Figure 2.3 Schematic diagram of a DWC example

According to the notations introduced in Figure 2.3, the liquid flow on stage 5 splits into two streams, with a split ratio defined as α; similarly, the vapor flow on stage 26 splits with a vapor split ratio β. Note that Eqs. (2.3) and (2.4) contain no terms for adjacent stages; therefore, these two types of equations remain the same as for conventional columns. Only the material balance (M), both Eq. (2.1) and Eq. (2.2), and energy balance (H) equations, Eq. (2.5), need to be modified for stage interlinking. The M and H equations for stage 5, 6 and 16 are written as:

$$M_{t,5} \equiv L_5 + V_5 - L_4 - V_6 - V_{16} = 0$$

$$M_{i,5} \equiv L_5 x_{i,5} + V_5 y_{i,5} - L_4 x_{i,4} - V_6 y_{i,6} - V_{16} y_{i,16} = 0$$

$$H_5 \equiv L_5 H_5^L + V_5 H_5^V - L_4 H_4^L - V_6 H_6^V - V_{16} H_{16}^V = 0$$

$$M_{t,6} \equiv L_6 + V_6 - \alpha \cdot L_5 - V_7 = 0$$

$$M_{i,6} \equiv L_6 x_{i,6} + V_6 y_{i,6} - \alpha \cdot L_5 x_{i,5} - V_7 y_{i,7} = 0$$

$$H_6 \equiv L_6 H_6^L + V_6 H_6^V - \alpha \cdot L_5 H_5^L - V_7 H_7^V = 0$$

$$M_{t,16} \equiv L_{16} + V_{16} - V_{17} - (1-\alpha) \cdot L_5 = 0$$

$$M_{i,16} \equiv L_{16}x_{i,16} + V_{16}y_{i,16} - V_{17}y_{i,17} - (1-\alpha) \cdot L_5 x_{i,5} = 0$$

$$H_{16} \equiv L_{16}H_{16}^{L} + V_{16}H_{16}^{V} - V_{17}H_{17}^{V} - (1-\alpha) \cdot L_5 H_5^{L} = 0$$

Similar M and H equations are modified on stage 15, 25, and 26 to account for interlinked streams, with vapor split ratio, β, used in the equations.

2.1.3 Heat Transfer across Dividing Wall(s)

Most simulations of DWCs that have been described in the open literature neglect heat transfer across the wall. There are two main reasons for this neglect: in part it is because the inclusion of heat transfer is extremely difficult when using multi-column modular flowsheet simulations and, also, because heat transfer is not thought to be important in large DWCs (it can, however, be very important in smaller columns often used in small scale experimental work).

The first study of heat transfer effects in dividing wall was conducted by Lestak et al. (1994), using Aspen with heaters connected to each stage in the wall region. Suphanit et al. (2007) analyzed heat transfer effects by using the column grand composite curve (CGCC), together with exergy analysis. Mueller et al. (2007) and Hiller et al. (2010) used a nonequilibrium stage model to describe heat and mass transfer in DWCs. Both teams developed their models using Aspen Custom Modeler (ACM), an equation-oriented simulation environment. A recent doctoral dissertation by Roach (2017) includes a DWC model considering both heat transfer across the dividing wall, and heat loss to the atmosphere. The model simulates the heat loss and wall heat transfer through use of a software package called HEEDS, which was linked with Microsoft Excel and Aspen Plus to modify the desired variables in the Aspen input file.

The equation oriented parallel column model presented in this chapter makes it very easy to include heat transfer effects across dividing wall(s). The consideration of heat transfer effects is realized by adding a generic term, Q_{mj}^{W}, to the energy balance equations in Eq. (3.5); a positive value means that heat flows from stage *j* to stage *m*, whereas negative value indicates the opposite. Since heat transfer across dividing wall(s) occurs only in the wall region(s), all of the Q_{mj}^{W} terms for stages above and below dividing wall(s) are zero. It is important to note that the number of stages on opposite sides of a dividing wall are not necessarily equal. We will return to this point in the analysis that follows.

Heat transfer across dividing wall(s) is driven by the temperature differences on two sides of the dividing wall. For simplicity, only horizontal heat transfer is considered in our study. The amount of heat transferred from stage *j* can be expressed by

$$Q_{mj}^{W} = U_{mj} \cdot A_{mj} \cdot \Delta T_j \tag{2.6}$$

where $\Delta T_j = T_j - T_m$ is the temperature difference between the stage *j* and stage *m*; U_{mj} is the overall heat transfer coefficient from stage *j* to stage *m*; and A_{mj} is the heat transfer area from stage *j* to stage *m*.

The calculation of the heat transfer area A_{mj} requires a knowledge of the diameter of the DWC, the tray spacing (for tray columns) or HETP (for packed columns), as well as the location of the dividing wall. Since the column may not be evenly divided by a wall, the horizontal width of the wall might not equal the diameter of the column. A simple geometry is demonstrated to determine the width of the dividing wall.

Assume a DWC has vapor split ratio 70% / 30%, the dividing wall, therefore, needs to be installed off-center in order to keep the pressure drop equal on both sides of the wall (we will address pressure balancing in the subsequent chapter). Figure 2.4 shows a schematic diagram of the DWC geometry, with the straight line AB representing the width of the dividing wall. Since the vapor split ratio is 70% / 30%, the area on the left of the wall takes up approximately 70% of the total area.

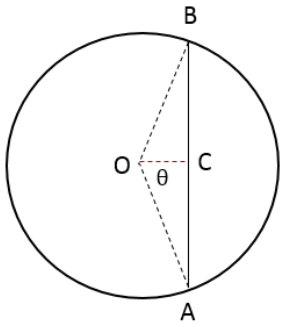

Figure 2.4 Schematic diagram of a DWC intersection

Assume the radius of the circle is *r*, the area of the right sector $\widehat{OAB}$ is calculated to be

$$A_{\widehat{OAB}} = \pi r^2 \cdot \frac{2\theta}{2\pi} \tag{2.7}$$

The area of the isosceles triangle AOB is

$$A_{AOB} = \frac{1}{2} r^2 \cdot sin\theta \tag{2.8}$$

The area on the right side of the dividing wall (A_r) can be calculated as the difference between $A_{\widehat{OAB}}$ and A_{AOB}, which takes up 30% of the whole circle, thus:

$$A_r = \pi r^2 \cdot \frac{2\theta}{2\pi} - \frac{1}{2} r^2 \cdot sin2\theta = 30\% \cdot \pi r^2 \tag{2.9}$$

θ can be solved from Eq. (2.9). Then the width of the wall, W_{DW}, is calculated from

$$W_{DW} = 2r \cdot sin\theta \tag{2.10}$$

With the width of the dividing wall known, the height of the wall for each stage-pair is needed to complete the computation of the heat transfer area. Assume the total height of the dividing wall is H_{DW}; the number of stages (or packed sections) on two sides of the dividing wall are N_L and N_R (L = left, R = right). The tray spacing (or HETP) on two sides of the wall can be determined as H_{DW}/N_L and H_{DW}/N_R, respectively.

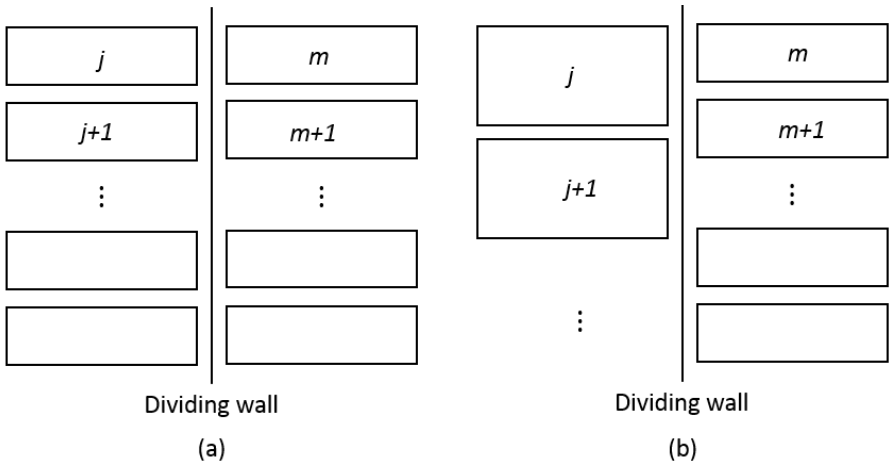

Figure 2.5 Schematic diagram of cases with (a) equal and (b) unequal number of stages on two sides of the wall

If N_L equals N_R (see Figure 2.5a), the tray spacing (or HETP) on both sides of the wall are equal. The height of the dividing wall that heat transfers from stage *j* to stage *m* can be obtained easily as H_{DW}/N_L (or H_{DW}/N_R), and thus the heat transfer area from stage *j* to stage *m* is computed in Eq. (2.11), with W_{DW} the width of the dividing wall computed before.

$$A_{mj} = W_{DW} \times \frac{H_{DW}}{N_L} \tag{2.11}$$

However, if N_L and N_R are unequal, the determination of the heat transfer area is not that straightforward. As one possible scenario shown in Figure 2.5b, stage *j* is horizontally connected both to stage m and stage m+1. The calculation of the heat transfer on stage *j* should be separated into two parts. From Figure 2.5b, the tray spacing (or HETP) on the left side of the wall is greater than the right side, which is:

$$\frac{H_{DW}}{N_L} > \frac{H_{DW}}{N_R} \tag{2.12}$$

The height on the dividing wall that heat transfers from the upper part of stage *j* to stage *m* is the tray spacing (or HETP) on the right side of the dividing wall, which is H_{DW}/N_R. Therefore, A_{mj} can be determined from Eq. (2.13) as:

$$A_{mj} = W_{DW} \times \frac{H_{DW}}{N_R} \tag{2.13}$$

The area of the lower part of stage *j* is obtained from Eq. (2.14), and this is the heat transfer area from stage *j* to stage *m+1*.

$$A_{m+1,j} = W_{DW} \times \left(\frac{H_{DW}}{N_L} - \frac{H_{DW}}{N_R}\right) \tag{2.14}$$

Note that stage *m+1* on the right side of the dividing wall has horizontal heat connections with both stage *j* and stage *j+1*. Similar calculation procedures can be conducted to determine the heat transfer area from the remainder of the stages on opposite sides of the dividing wall.

2.1.4 Summary of Specification

Table 2.2 provides a summary of specified variables and parameters.

It is worth noting that in most real DWCs it is not possible to specify the vapor flow split at the bottom of a wall. In actual operation the vapor will be distributed so as to equalize the pressure drop on both sides of the wall. It is not generally possible to calculate the pressure drop in an equilibrium stage model because there is no relationship in the model to actual equipment design. In addition, the usual way of modeling DWCs – via multi-column model in a process simulation package – makes balancing the pressure extremely difficult and is not usually done (see Dejanović et al. 2011 for an exception to our generalization). Pressure balancing can be accomplished more easily with a rate-based model, which will be discussed in the following chapter.

Table 2.2 Summary of simulation parameters and specified variables for a DWC simulation.

Specified Parameter/Variable
Configuration Parameters/Variables Number of stages (including condensers and reboilers) Number (and stage numbers) of condensers Number (and stage numbers) of reboilers Stage numbers of all feeds Stage numbers of all sidestreams Stage numbers for the top of each wall Stage numbers for the bottom of each wall
Feed Specifications Flowrate of all feeds Temperature and pressure of all feeds Composition of all feeds
Product Specifications Condenser specification (one of, e.g., reflux boilup ratio, product flow rate, mole fraction) Reboiler specification (one of, e.g., boilup ratio, product flow rate, mole fraction) Sidedraw specification(s) (one of, e.g., sidestream ratio, flow rate, mole fraction)
Other Column Specifications Pressure on all stages Heat duties for all stages except condensers and reboilers
Dividing Wall Operational Specifications Split ratio for each vapor stream at the bottom of each wall Split ratio for each liquid stream at the top of each wall Overall heat transfer coefficients for heat transfer across wall Area of each wall (or the dimensions of the column so that area can be calculated)

2.1.5 Method of Solution

The PCM equations are a combination of linear and nonlinear equations, with the nonlinearity resulting primarily from the physical properties (e.g. K-value, and enthalpy H). In this work, Newton's method is used to solve the parallel column model equations

in a manner similar to the algorithm developed by Naphtali and Sandholm (1971) and Hofeling and Seader (1978).

As discussed in the previous section, there are $(2c + 3)$ equations on each stage *j*, and the corresponding $(2c + 3)$ variables on each stage *j* are (1) vapor and liquid flowrates (V_j, L_j; 2), (2) vapor and liquid mole fractions (y_{ij}, x_{ij}; 2c), (3) stage temperature (T_j; 1). The model equations can be written in the form of Eq. (2.15).

$$\boldsymbol{F}(\boldsymbol{x}) = \mathbf{0} \tag{2.15}$$

where ***F*** is a vector containing n equations, with n the total number of equations in the column system that $n = (2c + 3) \times s$, and $\boldsymbol{x}$ is a vector of n variables:

$$\boldsymbol{x}^{\boldsymbol{T}} = \left(\boldsymbol{x}_{\mathbf{1}}^{\boldsymbol{T}}, \boldsymbol{x}_{\mathbf{2}}^{\boldsymbol{T}}, \dots, \boldsymbol{x}_{\boldsymbol{n}}^{\boldsymbol{T}}\right) \tag{2.16}$$

with $\boldsymbol{x_j}$ a vector of variables on stage *j* that:

$$\boldsymbol{x}_{\boldsymbol{j}}^{\boldsymbol{T}} = \left(V_j, y_{1,j}, y_{2,j}, \dots, y_{c,j}, T_j, x_{1,j}, x_{2,j}, \dots, x_{c,j}, L_j\right) \tag{2.17}$$

An initial guess for all variables ($\boldsymbol{x}^{(\mathbf{0})}$) are needed to initiate Newton's method, the vector of variables, $\boldsymbol{x}$, is then updated using the Eq. (2.18).

$$\boldsymbol{J}^{(\boldsymbol{k})} \cdot \left(\boldsymbol{x}^{(\boldsymbol{k}+\mathbf{1})} - \boldsymbol{x}^{(\boldsymbol{k})}\right) = -\boldsymbol{F}(\boldsymbol{x}^{(\boldsymbol{k})}) \tag{2.18}$$

where $\boldsymbol{J}^{(\boldsymbol{k})}$ is the Jacobian matrix at the kth iteration with

$$J_{ij} = \frac{\partial F_i}{\partial x_j} \tag{2.19}$$

In contrast with the equilibrium-stage model for conventional columns, the Jacobian matrix in the PCM is no longer a block-tridiagonal structure, due to the consideration of interlinked terms. The Jacobian matrix becomes a large sparse matrix with most nonzero elements located in the block-tridiagonal positions. A general Gaussian elimination method for sparse matrices can be used to solve the equations.

2.2 Model Verification

To demonstrate the correctness of the PCM discussed in Section 2.1, two DWC cases with different configurations are simulated using both the PCM and with multi-column models in other simulators. Additional cases are documented in Appendix C. All examples are taken from published papers in which the original authors used multi-column models in a commercial simulator. Heat transfer effects are neglected in this verification work, due to the fact that heat transfer was ignored in the original publications that form the basis for this phase of our work.

2.2.1 Aromatics Complex Separation

Our first example is a DWC that was investigated by Dejanović et al. (2011) to separate a 40-component platformer reactor effluent stream into three fractions, with the sidestream (often referred to as a benzene-rich cut or BRC) containing most benzene (>60 mass%). It is shown that, compared to a two-column sequence configuration, the proposed DWC configuration requires 43% less energy to get the same product specifications, and enables 51% savings in terms of total annualized cost (TAC).

2.2.1.1 Simulation Specifications

For their simulation of this column, Dejanović et al. (2011) used a four-column model in ChemCAD similar to that shown in Figure 1.5. Table 2.3 summarizes the column configuration and operating parameters of the DWC that were used in the simulations of Dejanović and coworkers (2017). The feed stream is a slightly subcooled liquid consisting of 15 components. Reflux ratio and boilup ratio are specified as mass ratios. The liquid split ratio at top of the wall is 40% / 60%, meaning that 40% of the liquid flows to the left side of the dividing wall. The vapor split is 66% / 34%.

The pressure profile in the column from Dejanović (2017) is summarized in Table 2.4, with the condenser operating at 2.7 bar, and the reboiler operating at 3.04 bar. The SRK equation of state was used as the thermodynamic model for their simulation, but no binary interaction parameters (BIPs) were given in their paper.

2.2.1.2 Simulation Setup with the PCM

The parallel column model simulates the entire DWC as a single unit operation with stage numbering as shown in Figure 2.1 with numbers of stages for each section taken from Table 2.3. In our PCM the total number of stages in the DWC model is 88 (including the condenser and reboiler), the feed stage becomes stage number 37, and the liquid side stream leaves stage 61. Other specifications for this simulation follow those in Table 2.3 and Table 2.4.

We used the Peng-Robinson (PR) equation of state thermodynamic model in our simulations with BIPs obtained from UniSim® Design, a process modeling software system from Honeywell. The BIPs for the PR EOS are provided in Appendix C.

Table 2.3 Summary of simulation parameters for aromatics column from Dejanović (2017).

Simulation Parameters	Value
Numbers of stages:	
Section A (includes condenser) (n_A+1)	27
Section B (n_B)	22
Section C (n_C)	22
Section D (included reboiler) (n_D+1)	17
Feed stage (counted in section B)	10
Side draw stage (counted in section C)	12
Feed temperature, °C	100.07
Feed pressure, bar	3.5
Feed flowrate, kg/h	31730
Top mass reflux ratio	2.74
Bottom mass boilup ratio	1.74
Side stream flowrate, kg/h	3680
Dividing wall:	
Liquid split ratio	40% / 60%
Vapor split ratio	66% / 34%

Table 2.4 Pressure specifications of the four-column model.

Top (A)		Left (B)		Right (C)		Bottom (D)	
Stages	Pres (bar)	Stages	Pres (bar)	Stages	Pres (bar)	Stages	Pres (bar)
1	2.7	1–15	3.02	1–15	3.02	1–7	3.03
2–9	3						
10–26	3.01	16–22	3.03	16–22	3.03	8–17	3.04
27	3.02						

2.2.1.3 Simulation with Multi-Column Models

The same simulation was conducted in other two software packages, COCO and UniSim® Design, using a four-column model similar to that shown in Figure 1.5. COCO is a freely

available (from www.cocosimulator.org) flowsheet simulation program that can use our model as its column simulator. This makes it an excellent vehicle for comparing the simultaneous method in our PCM to a multi-column model because the only difference then is the modular flowsheet convergence loop; the actual thermodynamics and stage model is actually using the same code minus the interconnections between non-consecutively numbered stages.

The simulations with the four-column model in two simulators use the converged results from PCM as an initial guess for the four interlinked streams. More information is available in Appendix C.

2.2.1.4 Simulation Results

For this simulation, the PCM takes only six column iterations to converge, while COCO takes more than 100 flowsheet iterations (we do not know the number of column iterations in each flowsheet iteration), even though we used the converged results from the PCM as an initial guess. The number of iterations UniSim® Design takes to converge is not known, but a randomly given initial guess would sometimes cause slow convergence, or no convergence at all.

The profiles plotted in this section and the rest of this paper for DWCs are with respect to bed elevation, provided that the HETP values are known (or in terms of "bed elevation units", if the HETP values are not known). The reason is that in DWCs there are at least one section in parallel with others, simply plotting the profiles as a function of stage number, as typically is done for conventional columns, does not adequately reflect the reality inside the column.

In Figure 2.6, the mass flowrate and temperature profiles calculated from the PCM are given, with MC denoting the main column, and PF the pre-fractionator. The results from all three simulations are in close agreement with each other. It is worth noting that COCO

and our PCM lead to identical results, but this should not be a surprise since the column model we used in COCO is the same one that underlies our PCM, but with each column section treated as an independent column.

Liquid composition profiles of five components from the PCM are shown in Figure 2.7. It can be seen that the top product is rich in isopentane and 2-methylpentane; n-hexane and benzene are the more important compounds in the middle product, and toluene represents the heavy components in the bottom. Solid lines denote the profiles in the main column, while dashed lines show the profiles in the pre-fractionator. The sidedraw position of the DWC is on a stage where the mole fraction of benzene is around its maximum.

Product purities from a ChemCAD simulation are provided by Dejanović (2017). A comparison of the purities from ChemCAD and PCM in Table 2.5 shows that they are almost the same with only slight differences. Additional results, including comparisons of the profiles, are provided in Appendix C.

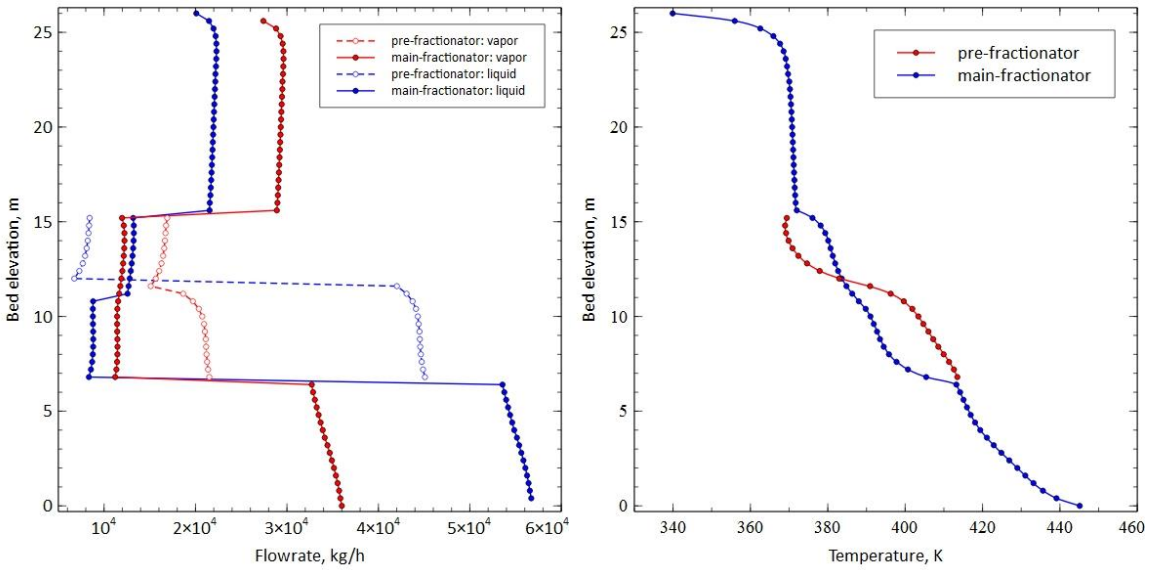

Figure 2.6 Results of (a) flowrate and (b) temperature profiles from the PCM, with an HETP value of 0.4 m from Dejanović et al. (2011).

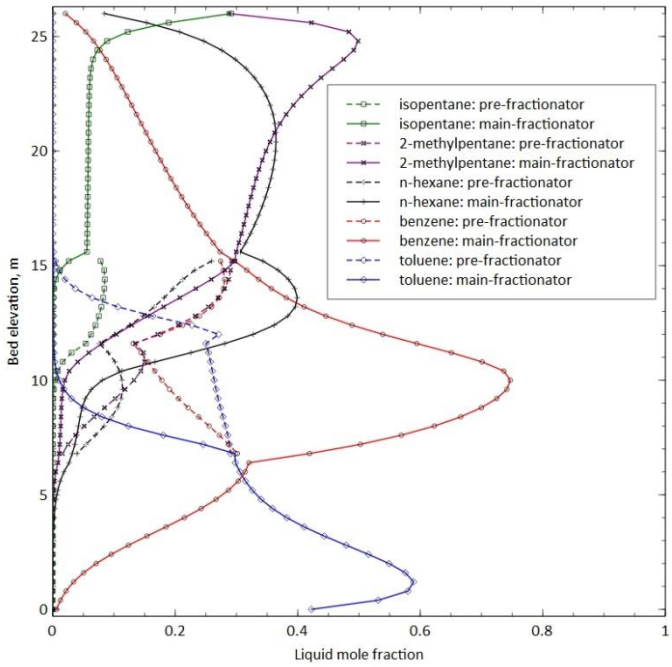

Figure 2.7 Liquid composition profiles for five components from the PCM simulation of the aromatic column.

Table 2.5 Comparisons of product purities with the ChemCAD results from Dejanović (2017).

	Feed	C5-C6 (Top)		BRC (Side)		heavies (Bottom)	
		ChemCAD	PCM	ChemCAD	PCM	ChemCAD	PCM
Total flow [t h^{-1}]	31.74	7.35	7.33	3.68	3.68	20.70	20.72
Mass fraction:							
n-Butane	0.019	0.0838	0.0840	0	0	0	0
i-Pentane	0.064	0.2764	0.2770	0	0	0	0
n-Pentane	0.045	0.1956	0.1960	0	0	0	0
2-Methylpentane	0.08	0.3329	0.3263	0.0285	0.0430	0	0
n-Hexane	0.043	0.0983	0.0955	0.1700	0.1761	0	0
Benzene	0.086	0.0130	0.0212	0.6825	0.6695	0.0050	0.0047
3-Methylhexane	0.020	0	0	0.1154	0.1077	0.0105	0.0120
Toluene	0.247	0	0	0.0036	0.0036	0.3786	0.3784
Ethylbenzene	0.035	0	0	0	0	0.0538	0.0538
p-Xylene	0.042	0	0	0	0	0.0651	0.0649
m-Xylene	0.122	0	0	0	0	0.1868	0.1867
o-Xylene	0.055	0	0	0	0	0.0841	0.0839
m-Ethyltoluene	0.047	0	0	0	0	0.0720	0.0718
1,3,5-Trimethylbenzene	0.077	0	0	0	0	0.1184	0.1182
1,4-Diethylbenzene	0.017	0	0	0	0	0.0257	0.0256

2.2.2 Satellite Column Simulation

Here we consider what is known as a satellite column system (Agrawal, 1996), by following a detailed case study provided by Tututi-Avila et al. (2017). Tututi-Avila and coworkers demonstrated a design case of using the satellite column system to separate four fractions (benzene, toluene, xylene, and heavies). Compared to the three-column direct sequence configuration, the satellite column system achieved 25% energy savings and 24% capital investment savings, resulting in about 24% reduction in the TAC.

2.2.2.1 Simulation Specifications

The satellite column system is equivalent to a three column system, with the main column located in the middle, and two additional column sections, one to each side of the main

section. Figure 2.8a shows the satellite column system, which is equivalent to a DWC structure with two parallel walls shown in Figure 2.8b.

Following Tututi-Avila et al. (2017), the system consists of a mixture of benzene, toluene, m-xylene, and 1,3,5-trimethylbenzene. A feed stream enters the system from the main column (MC), and the four products with high purities (99%) are obtained from the column system as distillate and bottom of the MC, two side products from the two side columns, SC1 and SC2.

Table 2.6 summarizes the column specifications of the satellite column system as simulated in Aspen Plus by Tututi-Avila et al. (2017). Tray pressure drop was reported to be 0.0068 atm, but, for simplicity, the column pressure in our simulation is assumed constant at 0.35 atm.

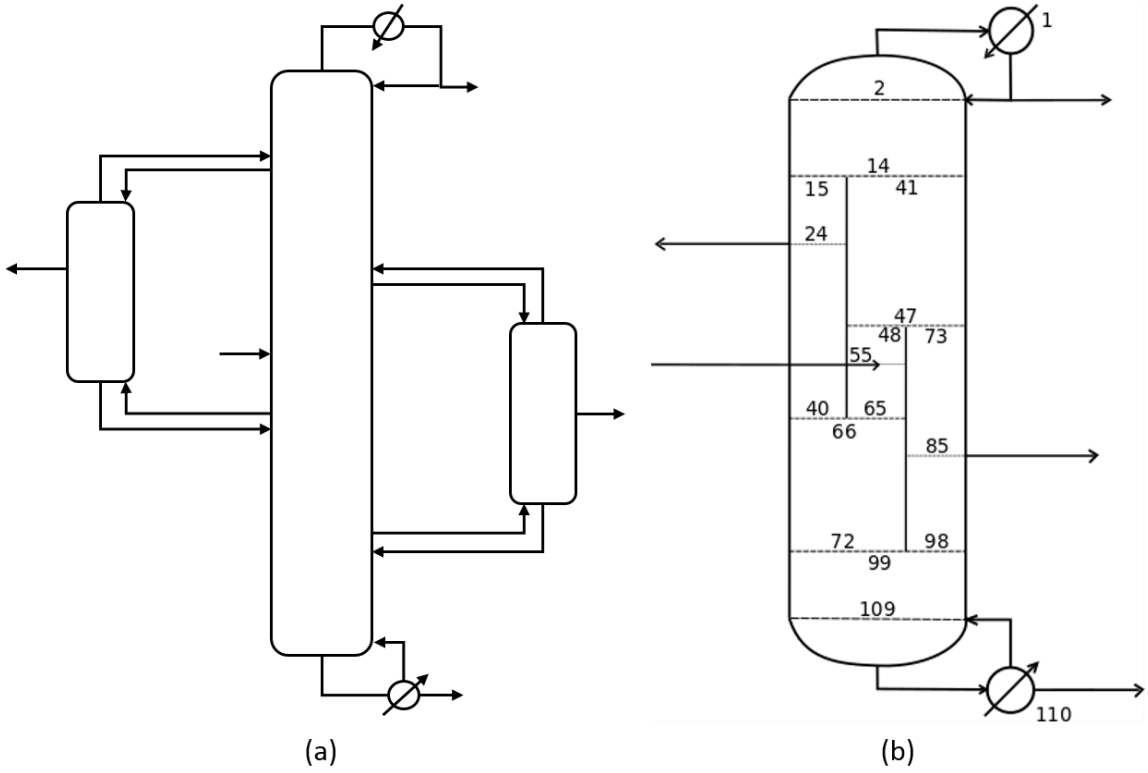

Figure 2.8 Diagrams of (a) the satellite column system, and (b) the equivalent DWC structure.

The feed stream is a saturated liquid with flowrate 114.8 kmol/h, consisting of 28.4mol% benzene, 31.7mol% toluene, 28.1mol% m-xylene, and 11.8mol% 1,3,5-trimethylbenzene. The feed pressure is not provided in the original source, so the column pressure, 0.35 atm, is used as the feed pressure. The NRTL-RK thermodynamic model was used by Tututi-Avila et al. (2017), but model parameters are not provided.

Instead of specifying product purities as was done by Tututi-Avila et al. (2017), we have specified product flowrates in our simulation. As the side stream information is not given in their work, we assume both side streams to be liquid, and the flowrates are specified as 36 kmol/h and 32 kmol/h for SC1 and SC2, respectively. The bottom product flowrate is set to 13.4 kmol/h. The same liquid and vapor split ratios from MC to SC1 and SC2, that were reported by Tututi-Avila et al. (2017) in their simulations, are used in our simulation.

2.2.2.2 Simulation Setup with PCM

In our simulation of the satellite column system with PCM the entire column is modeled as a single entity with all stages numbered sequentially in the DWC as shown in Figure 2.8b. Other specifications are as provided in the earlier section.

The NRTL model was used for liquid phase, while the vapor phase is assumed ideal in our simulation. The interaction parameters of NRTL model are taken from UniSim® Design, and given in Table 2.7. Any parameters not given in the table are set to zero.

2.2.2.3 Simulation with Multi-Column Models

The column system was also simulated with a multi-column model in both COCO and in UniSim® design. There are two possible multi-column models that one can use for this simulation: a three-column model and a seven-column model.

The three-column model uses the flowsheet shown in Figure 2.8a and is more straightforward to create. An initial guess of four interlinked streams are required to initiate the simulation. The seven-column model breaks the main columns into five connected column sections (see Figure 2.9). The convergence of the seven column model strongly depends on the initial guesses provided for the eight recycle streams. In our work, converged results from the PCM are used to provide good initial guesses for the multi-column models.

Table 2.6 Summary of the satellite column specifications.

Column	Satellite column system		
	SC1	MC	SC2
Number of Stages	26	58	26
Feed Stage(s)/Interconnection Stage	1–26	29	1–26
		14–40	
		21–47	
Side Stream Stages	10	–	13
Reflux Ratio		5.3	
Liquid Split	0.389		0.797
Vapor Split	0.375		0.407
Operating Pressure (atm)		0.35*	

* Pressure is assumed constant throughout the column system

Table 2.7 Interaction parameters of NRTL model from UniSim® Design.

Component i-j	T dependence: A+B/T				
	A-ij	A-ji	α-ij	B-ij	B-ji
Benzene – Toluene	0.000	0.000	0.303	-7.326	1.706
Benzene – m-Xylene	…	…	0.288	309.7	-228.614

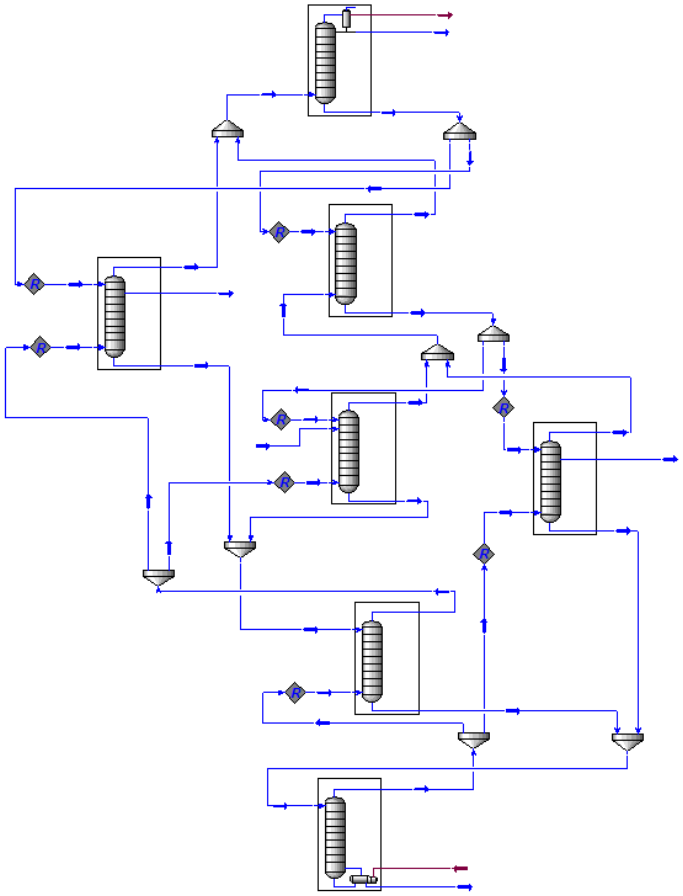

Figure 2.9 Flowsheet of seven-column model in UniSim® Design.

2.2.2.4 Simulation Results

In this simulation, the PCM takes six column iterations to converge, while COCO uses a three-column model, and takes 33 flowsheet iterations (again, the total number of column iterations required is not known). However, the seven-column model fails to converge in COCO even though the converged results from the PCM were provided as the initial guess. The seven-column model converges in UniSim® Design, but the number of iterations required is not available.

Figure 2.10 shows the vapor and liquid flowrate profiles predicted from the PCM. Figure 2.11 shows the temperature profiles of this satellite column system. Additional results are provided in Appendix C.

Simulations from COCO and UniSim® Design using multi-column models are compared with the results from the PCM, and good agreement among the three simulators can be observed. More details concerning the simulations in COCO and UniSim® Design are available in Appendix C.

Figure 2.12 shows the liquid composition profiles predicted with the PCM. Solid lines with solid symbols are the profiles of the main column, solid lines with empty symbols are the profiles of the left side column, and dash lines with empty symbols are for the right side column. From Figure 2.12 we can see that benzene accumulates at the top; 1,3,5-trimethylbenzene is the heavy key and is obtained from the bottom product of the main column. Toluene and m-xylene are found in the two side streams.

The product purities predicted from UniSim® Design and the PCM are compared in Table 2.8. The slight differences in the results between two simulators is considered acceptable.

Table 2.8 Comparison of the product compositions.

	Top product		Side stream 1	
	PCM	[a]UD	PCM	UD
Benzene	0.9754	0.9848	0.0007	0.0005
Toluene	0.0246	0.0152	0.9647	0.9703
m-Xylene	0	0	0.0346	0.0292
1,3,5-Trimethylbenzene	0	0	0	0

	Side stream 2		Bottom product	
	PCM	UD	PCM	UD
Benzene	0	0	0	0
Toluene	0.0263	0.0306	0	0
m-Xylene	0.9681	0.9671	0.0025	0.0027
1,3,5-Trimethylbenzene	0.0056	0.0023	0.9975	0.9973

[a]UD refers to UniSim® Design

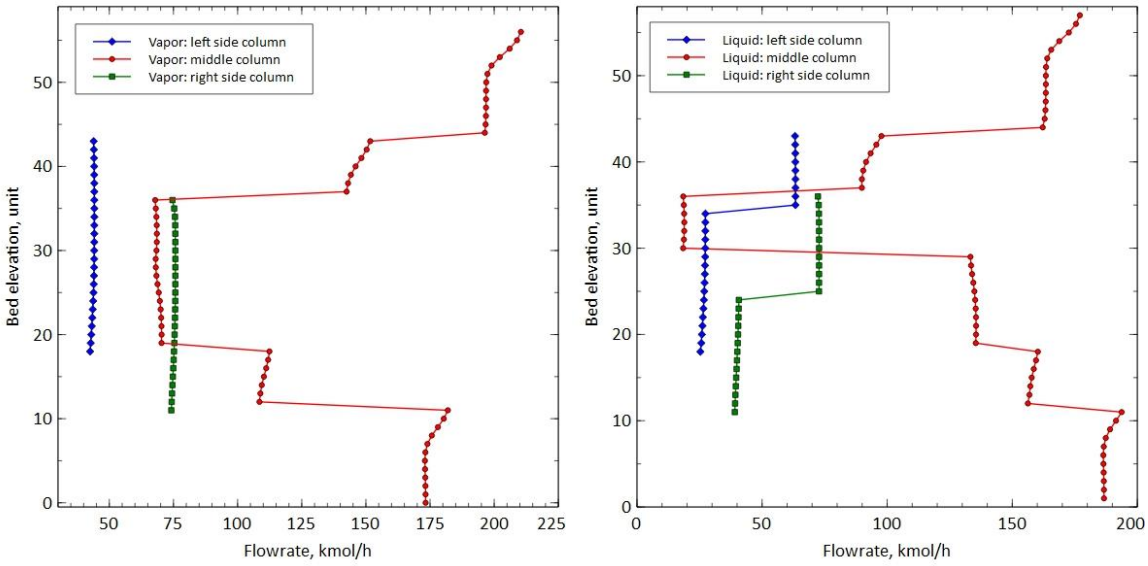

Figure 2.10 Results of (a) vapor flowrate and (b) liquid flowrate profiles from the PCM, assuming equal HETP.

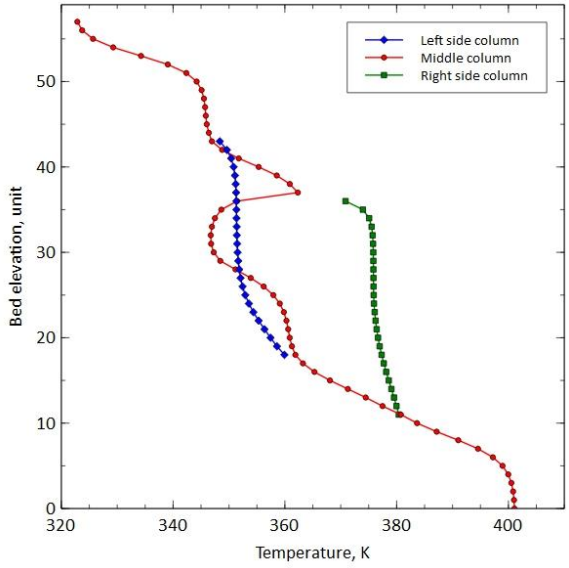

Figure 2.11 Temperature profiles of satellite column system predicted from the PCM, assuming equal HETP.

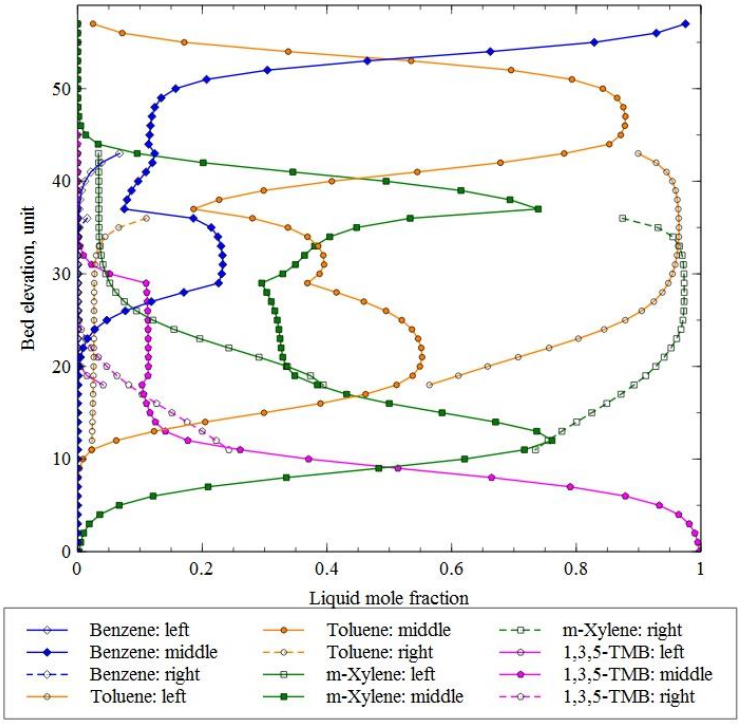

Figure 2.12 Liquid composition profiles predicted with the PCM, assuming equal HETP.

2.3 Other Applications

As demonstrated in Section 2.2, the PCM is able to model DWCs with different configurations. Note that as the number of dividing walls increases, the flowsheet created using a multi-column model become quite intricate; providing good initial guesses for the connecting streams is quite a chore.

In this section, two more case studies are shown to demonstrate the versatility of the PCM. In the first case we consider heat transfer across the dividing wall to help make the case that it is rather straightforward to include heat transfer with the PCM. The other case illustrates that the PCM is able to model DWCs with multiple condensers (and/or reboilers).

2.3.1 Heat Transfer across Dividing Wall

The case study in this section is based on one of the cases investigated by Benyounes et al. (2015). Heat transfer across the dividing wall is ignored in their simulation, but is considered in this section.

2.3.1.1 Base Case

Benyounes et al. (2015) used a two-column model (or Petlyuk column) to simulate the DWC. As reported, the pre-fractionator (PF) has 37 stages, and the main column (MC) has 50 stages. Two connecting streams are withdrawn from stage 4 and stage 42 of the MC.

A saturated liquid feed, consisting of n-pentane, n-hexane and n-heptane, enters the PF on stage 18, with flowrate and compositions given in. A liquid side product is obtained from the MC on stage 25. The column system operates at a constant pressure, 1.49 bar. Other simulation specifications from Benyounes et al. (2015) are given In Table 2.9.

Benyounes et al. (2015) used the Peng-Robinson (PR) thermodynamic model in the ProSim Plus process simulator, but the model parameters are not given. In our work, we also use the PR model with parameters from UniSim® Design as tabulated in Table 2.10.

Table 2.9 Simulation specifications of the pentane/hexane/heptane case from Benyounes et al. (2015) .

Specifications	Pentane/Hexane/Heptane
Feed:	
Compositions	0.4/0.2/0.4
Flowrate, kmol/h	45
Pressure, bar	1.49
Top:	
Reflux ratio	2.59
Sidestream:	
Flowrate, kmol/h	9
Bottom:	
Boilup ratio	3.11
Split ratio:	
Liquid	49% / 51%
Vapor	78% / 22%

Table 2.10 Binary interaction parameters of PR model from UniSim® Design.

Component	n-Pentane	n-Hexane	n-Heptane
n-Pentane	…	3.90E-04	0.00137
n-Hexane	3.90E-04	…	3.00E-04
n-Heptane	0.00137	3.00E-04	…

2.3.1.2 PCM with Heat Transfer

The DWC used in this simulation has the configuration shown in Figure 2.1 with the following numbers of stages: $n_A = 3, n_B = 37, n_C = 37, n_D = 8$ (the condenser and reboiler are not included), with the feed to stage 18 (of 37 in Section B) and the side product taken from stage 21 (of 37 in Section C). In the PCM the feed stage is number 22 and the side product drawn from stage 62.

Calculations of the heat transfer parameters follow Section 2.3. As the number of stages on both sides of the dividing wall is 37, the heat transfer area on each stage should be the same. This is computed from the product of the width of the dividing wall and the stage

height. The column diameter is 0.79 m. The wall width is determined following the procedures in Section 2.3, with vapor split ratio 78% / 22%. Accordingly, the width of the dividing wall is calculated to be 0.75 m. As there are 37 stages on each side of the dividing wall with HETP of 178 mm, the height of the wall is approximately 6.58 m. Therefore, the total area of the dividing wall can be computed to be $A_{DW} = 6.58 \times 0.75 = 4.94\ m^2$, so the heat transfer area on each stage is $0.133\ m^2$. The overall heat transfer coefficient is assumed constant for all stages alongside the dividing wall, and a reasonable value, $U = 700\ W/m^2 \cdot K$, obtained from Niggemann et al. (2010) is used in the simulation.

2.3.1.3 Simulation Results with Heat Transfer

For the abovementioned case, the PCM takes 3 iterations (about 90 ms) to converge if heat transfer is not considered; while it takes 6 iterations (about 170 ms) to converge if heat transfer is considered. Figure 2.11 shows the comparison of the temperature profiles simulated using the PCM with and without heat transfer across the dividing wall. The temperature profiles ignoring heat transfer effects are shown with dash lines, large temperature differences, up to 19K can be observed between two sides of the wall. Temperature profiles with heat transfer considered are plotted in solid lines, the temperature differences decrease as heat transfer across the dividing wall is involved. Furthermore, the heat transfer across the dividing wall can even reverse the heat transfer direction in the lower part of the dividing wall.

The significant changes in the temperature profiles lead to corresponding large changes in the composition profiles, as seen in Figure 2.14.

As shown in Table 2.11, when heat transfer is considered, the purity of n-pentane in the top product and the purity of n-hexane in the side product increase, and the purity of n-heptane in the bottom product decreases. As the overall heat transfer coefficient increases, the heat transfer resistance of the dividing wall decreases, and the

temperature differences between two sides of the wall reduces. However, heat transfer can lead to negative flowrates if the heat transfer coefficient is too large (e.g. $U > 2000\ W/m^2 \cdot K$).

Table 2.11 Comparisons of product purities with and without considering heat transfer (HT) effects.

	Top product		Side product		Bottom product	
	without HT	with HT	without HT	with HT	without HT	with HT
n-Pentane	0.9397	0.9705	0.1464	0.0776	0	0
n-Hexane	0.0603	0.0295	0.8535	0.9032	0.0136	0.0190
n-Heptane	0	0	0.0001	0.0192	0.9864	0.9810

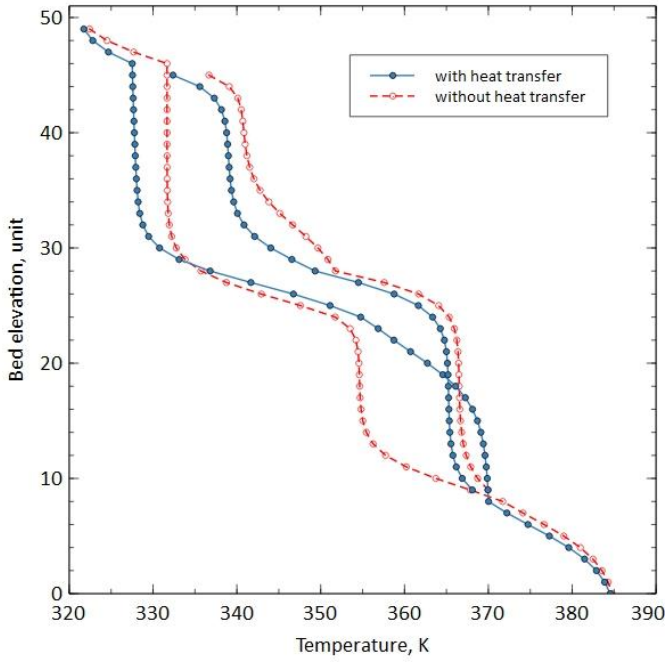

Figure 2.13 Comparison of temperature profiles with and without heat transfer, assuming equal HETP.

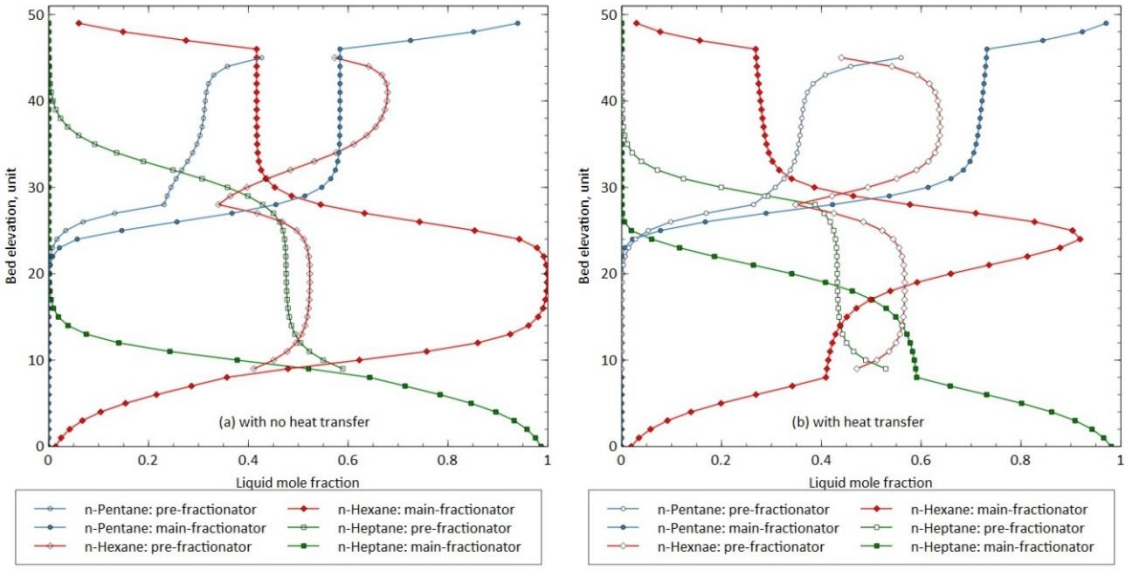

Figure 2.14 Liquid composition profiles assuming equal HETP (a) with no heat transfer effects, and (b) with heat transfer effects.

2.3.2 Column with Multiple Condensers

Dai et al. (2016) describe a process for separating the azeotropic mixture of benzene and cyclohexane (CYH) using an Extractive Dividing Wall Column (EDWC) illustrated in Figure 2.15 (left). The dividing wall in this type of column extends to the very top of the column which, therefore, divides the column top into two sections, both of which connect to a condenser.

Dai et al. (2016) used an entrainer consisting of a mixture of sulfolane and o-xylene to separate benzene and cyclohexane. The entrainer permits recovery of CYH in the overhead from the EDC-C section. Benzene is separated from the mixed entrainer in the entrainer recovery section (RC), and is recovered from the top-right section EDC-B. The entrainer mixture is obtained from Section RC and can be recycled back to Section EDC-C. A mixed entrainer was proposed in order to moderate the temperature in the entrainer recovery column; allowing water to be used for cooling thereby helping to reduce the costs of utilities. Further savings were achieved by applying the EDWC configuration. As

reported by Dai et al. (2016), an EDWC with a mixed entrainer could save 44% of energy and 36% of TAC, when compared to a conventional two-column extractive distillation arrangement with a pure component entrainer. They used a three-column model in Aspen Plus to simulate the process.

2.3.2.1 Simulation with the PCM

The EDWC was modeled using the PCM structure shown in Figure 2.15 (right). Heat transfer across the dividing wall is ignored (although the temperature difference in this column is quite substantial). Note that the second condenser is numbered as stage 37.

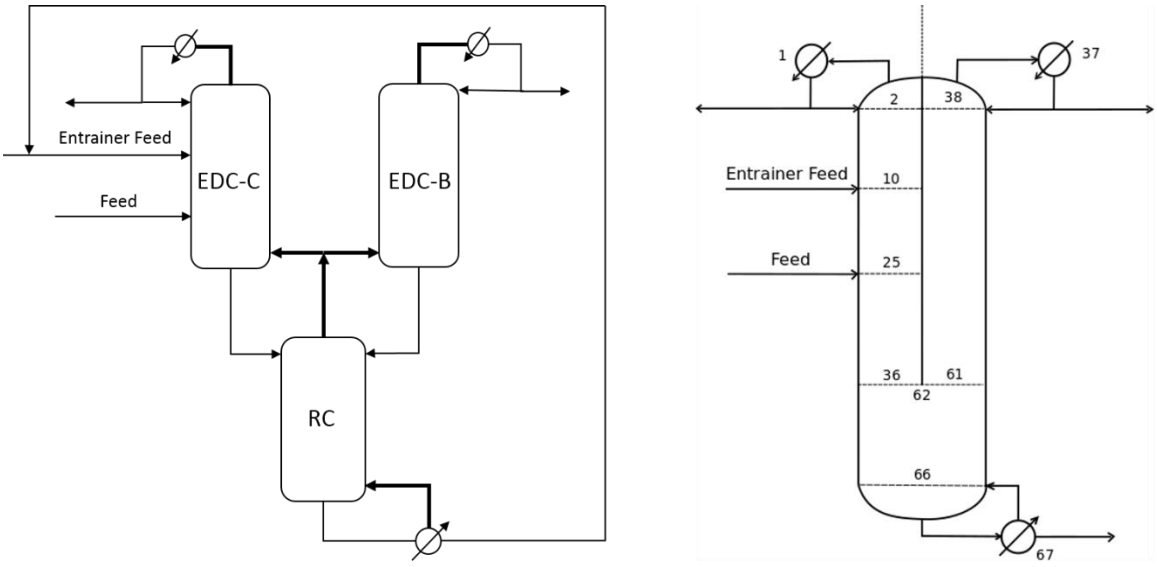

Figure 2.15 Flowsheet of the EDWC simulation with three-column model and the PCM (right).

Following Dai et al. (2016), Section EDC-C has 36 stages, Section EDC-B has 25 stages, and Section RC has 6 stages, with condensers and the reboiler counted as additional stages. The bottom product from column RC was not recycled in our simulation. The entrainer feed, consisting of 90% sulfolane and 10% o-xylene, enters Section EDC-C on stage 10,

with flowrate 110 kmol/h. An equimolar stream of benzene and cyclohexane enters Section EDC-C on stage 25, with flowrate 100 kmol/h.

The cyclohexane product purity at the top of Section EDC-C is specified as 0.998, while the reflux ratio of the condenser for Section EDC-B is set at 2.1. The bottoms flowrate of Section RC is specified as 110 kmol/h. The column pressure is assumed constant at 0.6 atm. The vapor split ratio from column RC to column EDC-C is not given by Dai et al. (2016), and is assumed to be 0.5 in our simulation. The NRTL thermodynamic model is used for this simulation.

2.3.2.2 Simulation Results

This PCM simulation required 30 iterations (about 250 ms) to converge. Figure 2.16 shows the temperature profiles of the EDWC predicted using the PCM. The temperature profiles in the top-right column and bottom column are combined. As anticipated above, the temperature differences over the wall is significant.

Calculated product purities are summarized in Table 2.12. The distillate from the top-left column contains almost pure CYH, while the distillate 2 from the top-right column is nearly pure benzene. The product from Section RC, is essentially “pure” entrainer – it contains neither of the hydrocarbons – and can be recycled back to Section EDC-C.

Table 2.12 Product purities in the EDWC predicted from the PCM.

	Distillate 1 (top-left)	Distillate 2 (top-right)	Bottom
Benzene	0.0020	0.9996	0
Cyclohexane	0.9980	0.0001	0
Sulfolane	0	0	0.9000
o-Xylene	0	0.0002	0.0999

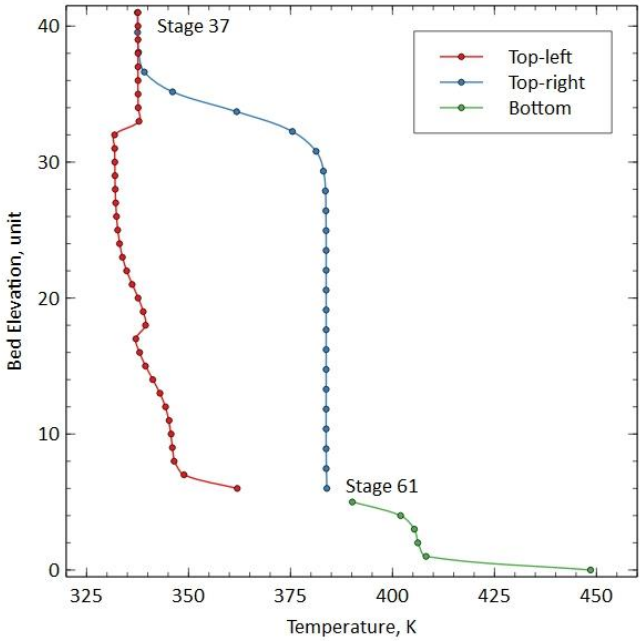

Figure 2.16 Temperature profiles of the EDWC predicted from the PCM.

2.3.3 Additional Case Studies

Two other cases are discussed in detail in Appendix C. They include a dividing wall column flowsheet for separating benzene, toluene, and o-xylene, adapted from Ling and Luyben (2009). Another case is derived from the work of Ashrafian (2014) who describes a three-wall DWC for an LNG process simulation.

2.4 Performance Summary

Table 2.13 provides a summary of the performance of our equation-oriented Parallel Column Model. For the cases described in this chapter as well as additional cases in Appendix C we report the number of iterations, the execution time, and the average rate of convergence (norm reduction). The number of iterations is that required by Newton's method and excludes the time needed for the automated initialization described in Appendix B. The average rate of convergence is found by dividing the difference between

the first and last values of the norm of the function values by the number of iterations. The execution time is reported directly by the simulation program and is an average of 10 separate runs of each case. The simulations were carried out on a Dell Precision 7710 using an Intel® Core™ i7-2760QM CPU @ 2.40 GHz processor. The operating system was Microsoft Windows 7 (64-bit version).

From Table 2.13, it can be seen that the equation-oriented PCM converges quite quickly in all of the cases we have considered here (as well as many others not discussed in this chapter).

Table 2.13 PCM performance for DWC simulations.

Cases	Number of components	Number of stages	Number of iterations	Time (seconds)	Ave. norm reduction
Aromatics Processing	15	88	6	0.71	13
Satellite Column	4	110	6	0.12	34
DWC with heat transfer	3	87	6	0.17	113
EDWC	4	67	30	0.24	2
BTX Separation	3	70	4	0.05	13
LNG Simulation	10	191	13	1.49	5

Simulation times are not provided by UniSim Design®. The number of iterations also can be difficult to ascertain and is, in any case, strongly dependent on the convergence algorithm employed at the flowsheet level and, also, on the initial guesses for the streams that connect the separate column sections. In our own verification work we made use of the converged results from our PCM in order to initialize the connecting streams in our simulations with COCO and with UniSim Design®. Our observation is that UniSIm Design® generally converged very quickly from such high quality initial estimate of stream conditions (as should only be expected, of course). It is also, however, extremely easy to provide initial estimates for the connecting stream compositions that lead to complete failure of a modular simulation. COCO does provide execution times but is using our own model for each independent column section. These factors render unfair any direct comparison of execution times for a modular simulator with our PCM. What we can say

with reasonable certainty is that the time needed to create a DWC model with our PCM is significantly less than the time needed to create a multi-column flowsheet simulation model. In addition, when provided with "reasonable" initial estimates for the connecting streams we do observe the PCM converging significantly faster than an equivalent modular simulation even though it is next to impossible to present objective data to support this observation.

Since it was beyond the scope of our work we made no attempt to investigate the use of the short cut models or the acyclic simulation technique described by Navarro et al. (2012) to initialize the modular simulation models. Such additional simulations necessarily involve a degree of effort not required by a PCM.

2.5 Usage in a Commercial Simulation Program

Many independently created software systems created for modeling chemical processes now make use of the CAPE-OPEN standards that allow software systems to work together in some defined sense. "The [CAPE-OPEN] standard defines rules and interfaces that allow CAPE (Computer-Aided Process Engineering) applications or components to interoperate" (www.colan.org). To the best of our knowledge, all major commercial flowsheeting systems are CAPE-OPEN compliant (van Baten and Pons, 2014). In practice, this means that the PCM described in this chapter, can simply be selected as the column model of choice in any CAPE-OPEN compliant flowsheeting system on any computer on which both the flowsheeting system and this model have been installed.

Figure 2.17 shows the final separation train of a process in which the last two columns are using the PCM. We used the COFE (CAPE-OPEN Flowsheeting Environment) to make this flowsheet in part because COFE is freely available, but also because COFE is the only CAPE-OPEN flowsheet simulation package with adaptable unit operation icons. In other words, a DWC column inserted into a COFE flowsheet looks like a DWC. A PCM inserted into another package (UNISIM Design for example) will be displayed using a standard icon

that that package uses for all CAPE-OPEN unit operations. The original process was the work-up section of an alpha-olefins plant separating a mixture of nineteen components using 7 columns. In the revised process shown in Figure 2.17 two DWCs replace 5 ordinary columns.

A complete description of this model being used as a column model in UNISIM Design is available in Section 5 of Appendix C. The process of using the PCM in any other commercial simulation system is very similar and the specification of the DWC itself is identical.

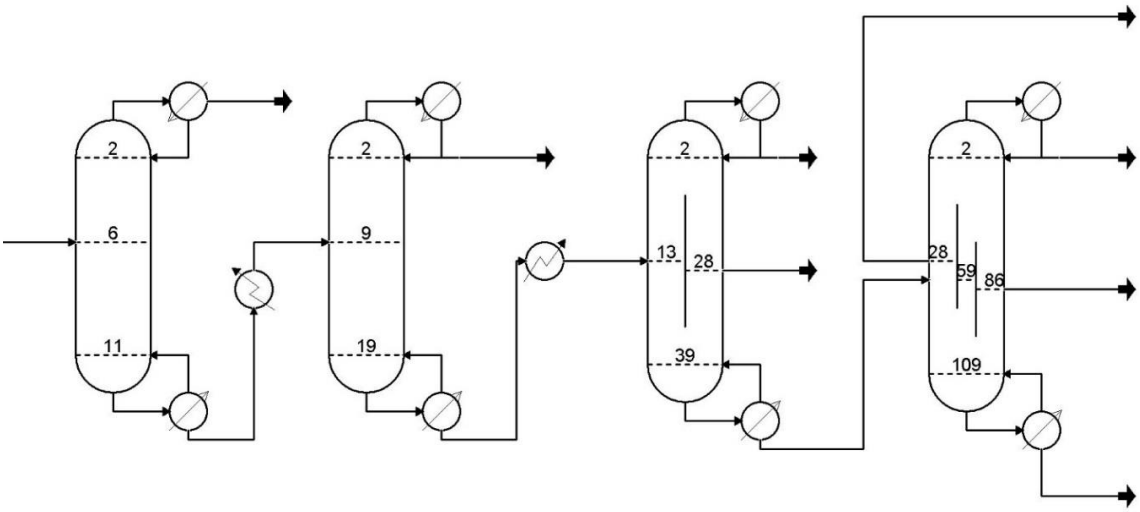

Figure 2.17 A flowsheet for the work-up section of an alpha-olefins plant created with COFE containing DWCs modeled using the PCM in which a direct separation sequence of 5 columns has been replaced by two DWCs. The top product stream from the first column is a recycle. Figure shows the actual appearance in the COFE flowsheet simulation program.

2.6 Remarks

This chapter has presented a parallel column model (PCM) and applied it to simulation of Dividing Wall Columns (DWCs). Using the PCM can effectively circumvent the tedious procedures of setting up such columns with multi-column models in a modular process

simulator. The automatic initialization option in the PCM eliminates the difficulties of providing adequate initial guesses for the connecting streams.

Two DWCs with very different structures were simulated with both the PCM and multi-column models in commercial software. The simulation results are compared with other two simulators, COCO and UniSim Design®. COCO and our PCM provide identical results as long as the specifications are the same (this is only to be expected because the COCO simulations used our own column simulator for each of the column sections in the COCO simulator). The PCM and UniSim Design® show nearly identical results, with acceptably small deviations due essentially to minor differences in the underlying physical property constants used in the thermodynamic property evaluations (critical properties, acentric factor, and ideal gas heat capacity). Additional simulations including a case with heat transfer across the walls demonstrate the greater versatility of an equation-based Parallel Column Model; an equivalent simulation using a modular process simulator is extremely difficult.

It should be possible to adapt the PCM to describe reactive distillation. Our own experience with this type of distillation process in a DWC is extremely limited. That said, we have been able to converge cases involving reaction and distillation in our equilibrium stage Parallel Column Model.

Our PCM can be used as a single unit operation model within commercial process simulation tools via the CAPE-OPEN mechanism, thereby greatly simplifying the task of building DWC models. What is more, due to its equation-based nature, the rate of convergence of the PCM can be very rapid.

Software Used in This Work

COCO (v3.3) – a modular chemical process simulator available free from www.cocosimulator.org. UniSim® Design (v6.61.0.0) – a modular process simulator available from Honeywell Inc.

Reference

Agrawal, R., 1996. Synthesis of distillation column configurations for a multicomponent separation. *Industrial & Engineering Chemistry Research*, 35(4), pp.1059–1071.

Ashrafian, R., 2014. Using dividing wall columns (DWC) in LNG production: dividing wall column, double dividing wall column, prefractionator arrangement, Petlyuk column, NGL recovery, distillation.

Asprion, N., and Kaibel, G., 2010. Dividing wall columns: fundamentals and recent advances. *Chemical Engineering and Processing: Process Intensification*, 49(2), pp.139–146.

Becker, H., Godorr, S., Kreis, H., and Vaughan, J., 2001. Partitioned distillation columns -- why, when & how. *Chemical Engineering*, 108(1), Jan., pp.68.

Benfer, R., 2018. Model meets reality: distillation simulation at BASF. Plenary lecture at Distillation and Absorption September 2018. Florence, Italy.

Benyounes, H., et al., 2015. Novel procedure for assessment of feasible design parameters of dividing-wall columns: application to non-azeotropic mixtures. *Industrial & Engineering Chemistry Research*, 54(19), pp.5307–5318.

Dai, X., et al., 2016. Energy-saving dividing-wall column design and control for benzene extraction distillation via mixed entrainer. *Chemical Engineering and Processing: Process Intensification*, 100, pp.49–64.

Dejanović, I., 2017. Private communication to R. Taylor.

Dejanović, I., Matijašević, L., Jansen, H., and Olujić, Ž., 2011. Designing a packed dividing wall column for an aromatics processing plant. *Industrial & Engineering Chemistry Research*, 50(9), pp.5680–5692.

Dejanović, I., Matijašević, L., and Olujić, Ž., 2010. Dividing wall column—a breakthrough towards sustainable distilling. *Chemical Engineering and Processing: Process Intensification*, 49(6), pp.559–580.

Hiller, C., Buck, C., Ehlers, C., and Fieg, G., 2010. Nonequilibrium stage modelling of dividing wall columns and experimental validation. *Heat and Mass Transfer*, 46(10), pp.1209–1220.

Hofeling, B.S., and Seader, J.D., 1978. A modified Naphtali-Sandholm method for general systems of interlinked, multistaged separators. *AIChE Journal*, 24(6), pp.1131–1134.

Idris, R., Hing, C.T., Harun, N., and Othman, M.R., 2017. Development of equation oriented modelling of advanced distillation process using MOSAIC: dividing wall column case study. *Australian Journal of Basic and Applied Science*, 11, pp.30-42.

Kolbe, B., and Wenzel, S., 2004. Novel distillation concepts using one-shell columns. *Chemical Engineering and Processing: Process Intensification*, 43(3), pp.339–346.

Lestak, F., Smith, R., and Dhole, V.R., 1994. Heat transfer across the wall of dividing wall columns. *Chemical Engineering Research & Design*, 72(5), pp.639–644.

Ling, H., and Luyben, W.L., 2009. New control structure for divided-wall columns. *Industrial & Engineering Chemistry Research*, 48(13), pp.6034–6049.

Mueller, I., and Kenig, E.Y., 2007. Reactive distillation in a dividing wall column: rate-based modeling and simulation. *Industrial & Engineering Chemistry Research*, 46(11), pp.3709–3719.

Naphtali, L.M., and Sandholm, D.P., 1971. Multicomponent separation calculations by linearization. *AIChE Journal*, 17(1), pp.148–153.

Navarro, M.A., Javaloyes, J., Caballero, J.A., and Grossmann, I.E., 2012. Strategies for the robust simulation of thermally coupled distillation sequences. *Computers & Chemical Engineering*, 36, pp.149–159.

Nguyen, T.D., Rouzineau, D., Meyer, M., and Meyer, X., 2016. Design and simulation of divided wall column: experimental validation and sensitivity analysis. *Chemical Engineering and Processing: Process Intensification*, 104, pp.94–111.

Niggemann, G., Hiller, C., and Fieg, G., 2010. Experimental and theoretical studies of a dividing-wall column used for the recovery of high-purity products. *Industrial & Engineering Chemistry Research*, 49(14), pp.6566–6577.

Okoli, C.O., and Adams, T.A., 2015. Design of dividing wall columns for butanol recovery in a thermochemical biomass to butanol process. *Chemical Engineering and Processing: Process Intensification*, 95, pp.302–316.

Roach, B.J., 2017. A design model for dividing wall distillation columns (Thesis).

Seader, J.D., Henley, E.J., and Roper, D.K., 2011. Separation process principles: chemical and biochemical operations. NJ John Wiley and Sons, Inc.

Suphanit, B., Bischert, A., and Narataruksa, P., 2007. Exergy loss analysis of heat transfer across the wall of the dividing-wall distillation column. *Energy*, 32(11), pp.2121–2134.

Tian, Y., Demirel, S.E., Hasan, M.M.F., and Pistikopoulos, E.N., 2018. An overview of process systems engineering approaches for process intensification: State of the art. *Chemical Engineering and Processing - Process Intensification*, 133, pp.160–210.

Tututi-Avila, S., et al., 2017. Dividing-wall columns: design and control of a Kaibel and a satellite distillation column for BTX separation. *Chemical Engineering and Processing: Process Intensification*, 114, pp.1–15.

van Baten, J., and Pons, M., 2014. CAPE-OPEN: Interoperability in industrial flowsheet simulation software. *Chemie Ingenieur Technik*, 86(7), pp.1052–1064.

Waltermann, T., and Skiborowski, M., 2017. Conceptual design of highly integrated processes – optimization of dividing wall columns. *Chemie Ingenieur Technik*, 89(5), pp.562–581.

CHAPTER 3 Rate-Based Parallel Column Model

In the last chapter, we presented an equation-based, equilibrium-stage parallel column model (PCM) and applied it to DWC simulation. This model shows great advantages over the sequential-modular multi-column models in reducing the time needed to create a DWC model while possessing excellent convergence characteristics. The equilibrium stage PCM can, via the CAPE-OPEN mechanism, be used as a standard unit operation within any CAPE-OPEN compliant commercial process simulation tool, and thereby ease the task of developing processes that include such columns.

In this chapter, the parallel column model framework is extended to use a rate-based stage model. The rate-based PCM allows for the vapor split ratios to be determined during the solution of the model equations by equalizing the pressure drop on opposite sides of the dividing wall. While it is generally recognized that pressure balancing is needed to properly determine the vapor splits, it is also not generally done in most DWC simulations that have been described in the literature. The reason for the absence of pressure balancing is that nearly all simulation studies use an equilibrium stage model that has no actual connection to real columns. The rate-based PCM also can easily incorporate heat transfer across the wall.

3.1 Model Description

Rate-based models of counter-current columns have been established now for some time. A detailed description of a rate-based model for a simple column can be found in Taylor and Krishna (1993). The building blocks of such a model are the so-called MERSHQ equations:

1. **M**aterial balances for each distinct phase
2. **E**nergy balances for each phase
3. Mass and energy transfer **R**ate equations in each phase

4. Mole fraction **S**ummation equations
5. **H**ydraulic equations to account for the pressure drop
6. Phase e**Q**uilibrium equations to model the phase interface(s)

To assist the discussion, we show, in Figure 3.1, a schematic diagram of three stages at the top of a dividing wall. Arrows represent material or energy flows, due either to physical flows from one stage to another, or to transport across the two-phase boundaries that are represented in the diagram by the wavy lines.

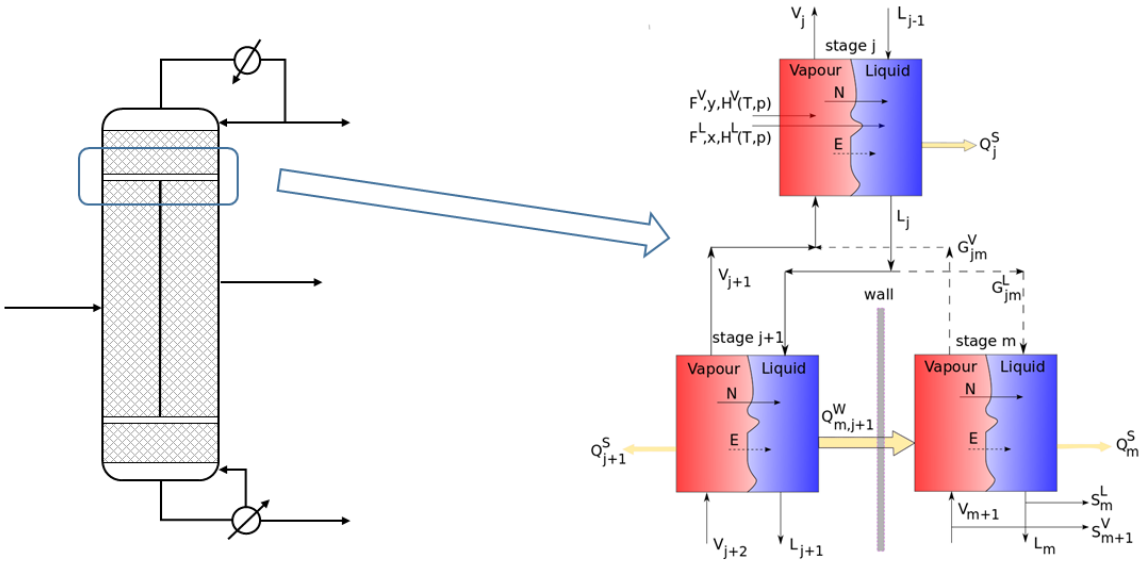

Figure 3.1: Schematic diagram of sections in dividing wall column and corresponding stage model.

It is not possible for all of the stages of a parallel column model to be numbered so that all material and energy flows are between consecutively numbered stages. Thus, the mass and energy balance equations in a PCM must account for flows between stages with any arbitrary number. It is worth noting that in a simple column there are no streams that connect non-adjacent stages and in divided wall columns there are only a few such inter-connecting streams. An extended discussion of the details of the numbering scheme is provided in Chapter 2, which includes a simple explicit example to show how the mass

balances are constructed as well as illustrations that show application of the model to DWCs with multiple walls.

The equations that need to be modified for stage-connections in DWCs are summarized below. The equations are written for an arbitrary stage *j* which could be on either side of, above or below any wall.

1. Material balances (M)

- Component Material Balances

$$M_{ij}^{V} \equiv \left(V_j + S_j^{V}\right)y_{ij} - \delta_{j,j+1}^{V} \cdot V_{j+1}y_{i,j+1} - F_j^{V}y_{ij}^{F} - \sum_{m=1}^{s} G_{jm}^{V}y_{im} + \mathcal{N}_{ij}^{V} = 0 \qquad (3.1)$$

$$M_{ij}^{L} \equiv \left(L_j + S_j^{L}\right)x_{ij} - \delta_{j,j-1}^{L} \cdot L_{j-1}x_{i,j-1} - F_j^{L}x_{ij}^{F} - \sum_{m=1}^{s} G_{jm}^{L}x_{im} - \mathcal{N}_{ij}^{L} = 0 \qquad (3.2)$$

where $\delta_{j,j+1}^{V}$ is the ratio of the vapor flow from stage *j+1* to *j*, while $\delta_{j,j-1}^{L}$ is the ratio of the liquid flow from stage *j-1* to *j*. $\delta_{j,j+1}^{V}$ and $\delta_{j,j-1}^{L}$ are in range [0,1], with zero meaning no material connection. G_{jm}^{V} and G_{jm}^{L} are the vapor and liquid flows from stage *m* to stage *j* created by a wall that partitions the column into different segments. In conventional columns, $\delta_{j,j+1}^{V}$ and $\delta_{j,j-1}^{L}$ are always one, and G_{jm}^{V} and G_{jm}^{L} are always zero. $\mathcal{N}_{ij}^{P}$ represents the mass transfer rate in phase P. The term G_{jm}^{V} contains the vapor split ratio β if *j* is the stage at the bottom of a wall (it can be the stage to either the left or the right side of the wall).

- Total Material Balances

$$M_{tj}^{V} \equiv \left(V_j + S_j^{V}\right) - \delta_{j,j+1}^{V} \cdot V_{j+1} - F_j^{V} - \sum_{m=1}^{s} G_{jm}^{V} + \mathcal{N}_{tj}^{V} = 0 \qquad (3.3)$$

$$M_{tj}^{L} \equiv \left(L_j + S_j^{L}\right) - \delta_{j,j-1}^{L} \cdot L_{j-1} - F_j^{L} - \sum_{m=1}^{s} G_{jm}^{L} - \mathcal{N}_{tj}^{L} = 0 \qquad (3.4)$$

The last term on the left-hand side of the total material balance equation, $\mathcal{N}_{tj}^{P}$, is the total mass transfer rate in phase *P*, which is the sum of all component mass transfer rates in the corresponding phase.

2. Energy Balances (E)

$$E_j^V \equiv \left(V_j + S_j^V\right)H_j^V - \delta_{j,j+1}^V \cdot V_{j+1}H_{j+1}^V - F_j^V H_j^{VF} - \sum_{m=1}^{s} G_{jm}^V H_m^V + Q_j^{S,V} + \mathcal{E}_j^V = 0 \quad (3.5)$$

$$E_j^L \equiv \left(L_j + S_j^L\right)H_j^L - \delta_{j,j-1}^L \cdot L_{j-1}H_{j-1}^L - F_j^L H_j^{LF} - \sum_{m=1}^{s} G_{jm}^L H_m^L + Q_j^{S,L} + \sum_{m=1}^{s} Q_{mj}^W - \mathcal{E}_j^L = 0 \quad (3.6)$$

where $Q_j^{S,V}$ and $Q_j^{S,L}$ are the heat losses to the surroundings from stage *j*, with *S* denoting column shell. $\mathcal{E}_j^P$ denotes the interfacial energy transfer rate in phase *P*.

Heat transfer across the dividing wall is modeled by the summation term $\sum_{m=1}^{s} Q_{mj}^W$ in Eq. (3.6), where *W* represents a dividing wall, and Q_{mj}^W is the rate of energy transfer across the wall from stage *j* to stage *m*. Heat transfer across the dividing wall in the rate-based PCM involves heat transfer between multiple phases (vapor and vapor, vapor and liquid, liquid and liquid). It can become quite complicated to consider all of the possibilities for heat transfer between phases; we therefore, assume that heat transfer occurs only between liquid phases. It is worth noting that Eq. (3.6) is valid for heat transfer across multiple walls as the summation term $\sum_{m=1}^{s} Q_{mj}^W$, covers all of the dividing walls in a column. Additional details of the heat transfer model are discussed in the equilibrium-stage PCM.

An energy balance around the phase interface gives

$$E_j^I \equiv \mathcal{E}_j^V - \mathcal{E}_j^L = 0 \quad (3.7)$$

3. Hydraulic equations (H)

The hydraulic equations in the parallel column model depend strongly on the relative positions of stages. Unlike conventional columns where stage *j* is always below stage *j-1*, in the parallel column model, the stage above stage *j* can be any arbitrary stage. To account for this, the hydraulic equations are given by

$$H_j \equiv P_j - (P_m + \Delta P_m) = 0 \quad (3.8)$$

where m is the stage located immediately above stage *j*. It must be remembered that in a PCM, the stage located above stage *j* is not necessarily numbered *j-1*. P_m is the pressure on stage *m*, and ΔP_m is the pressure drop on stage *m*. The pressure drop is of central importance in the proper modeling of DWCs; further discussion follows our introduction of a new equation, one that applies only to DWCs.

4. Pressure Balance equations (B)

   In a simple column (which, for present purposes, means one with no wall) the hydraulic equations only determine the pressure profile in the column. In a DWC, however, there exists an additional complication in that the pressure change on one side of a wall must be balanced by the pressure change on the opposite side of the wall. This pressure balance will determine how much of the vapor phase passes on each side of the wall; that is, the pressure drop determines the vapor split. We must, therefore add a pressure balance equation to the set of MERSHQ equations, but only for selected stages. (This is possible in rate-based models in which there is a direct connection with the actual equipment, but pressure balancing is not possible in an equilibrium stage simulation unless an effort is made to incorporate a pressure drop model tied to the actual equipment design. This is rarely done in practice.)

   The pressure balance equation, for dividing wall *k*, can be written as:

$$B_k \equiv \Delta P^W_{left} - \Delta P^W_{right} = 0 \qquad (3.9)$$

   There is one of these equations for each wall. The first term in Eq. (3.9), ΔP^W_{left}, represents the overall pressure drop on the left hand side of the dividing wall and is the sum of the pressure drop over all of the stages on the left side. Similarly, ΔP^W_{right} is the sum of the pressure drop over all of the stages on the right hand side of the wall. These terms are functions of the vapor flow rates (among other things) and, indirectly, of the vapor split.

The pressure drop on each stage is composed of a static part and a dynamic part;

$$\Delta P = \Delta P^{static} + \Delta P^{dynamic} \qquad (3.10)$$

with the static head given by:

$$\Delta P^{static} = \rho_v \cdot g \cdot h_{stage} \tag{3.11}$$

where ρ_v is the density of the vapor, g is the gravitational constant, and h_{stage} represents the stage height. The dynamic contribution to the pressure drop is a function of operational parameters such as vapor velocity and liquid holdup, as well as to equipment design parameters such as tray hole size, packing void fraction and so on. There are many different models for the dynamic hold up; see, for example, Lockett (1986) and Kister (1992) for useful reviews of the different approaches. We will return to this point later in the paper when we discuss how the PCM equations are solved.

The phase equilibrium equations, mole fraction summation equations and mass and energy transfer rate equations in a PCM are essentially identical to the equivalent equations in the standard rate-based model (see Taylor and Krishna, 1993). The only aspect of the rate equations that needs concern us here is to ensure that the correct column geometry be used in the calculation of the mass transfer coefficients and effective interfacial areas for those stages on either side of a dividing wall.

It should be noted out that the conventional MERSHQ equations are stage-oriented; that is, for each stage, there is one set of MERSHQ equations; however, the newly added pressure Balance equations are wall-oriented, and the number of B equations is equal to the number of walls in the columns. We add the B equations to the group of equations for the stage at the bottom left of a wall, e.g. stage L_n in Figure 3.2. (This isn't strictly necessary since we use a sparse matrix solver to solve the linearized equations that result from an application of Newton's method. The B equations can, therefore, be included anywhere in the system.)

Note that the height of the stages on opposite sides of a wall are not necessarily equal, a point emphasized by the different heights of the stages in Figure 3.2. Such differences can arise because there are different heights of packing in the two sections of the column or, rather more likely perhaps, because of different HETPs (Height Equivalent of a Theoretical

Plate) on opposite sides of the wall. The latter will clearly impact a simulation whether equilibrium stage or rate based; this is a point not previously discussed (as far as we know).

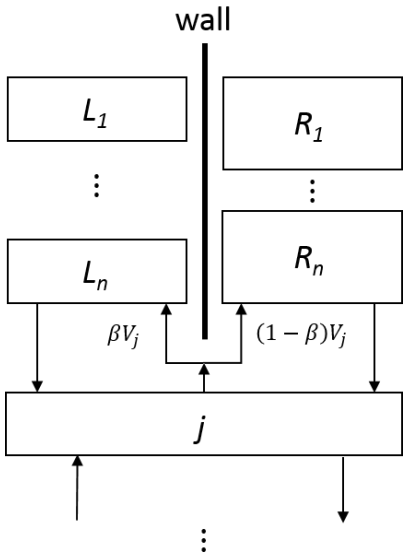

Figure 3.2 Stage alignment at the foot of a dividing wall.

To continue, we enumerate the numbers of variables and equations respectively in a DWC that has s stages (this includes all general stages, condensers and reboilers) and w dividing walls, and is separating a mixture containing c components. In what follows index i is the component index, j is used to count stages, and k identifies the wall.

There are *5c+6* variables for each non-equilibrium stage with the exception of Stage L_n:

- Vapor and liquid flow rates $(V_j, L_j;\ 2)$,
- Vapor and liquid phase compositions $(y_{ij}, x_{ij}; 2c)$,
- Vapor and liquid temperatures $(T^V, T^L; 2)$,
- Vapor and liquid interface compositions $(y_{ij}^I, x_{ij}^I; 2c)$,
- Interface temperature $(T_j^I; 1)$,
- Mass transfer rates $(\mathcal{N}_{ij}; c)$,
- Stage pressure $(P_j; 1)$.

There are 5*c*+7 variables for Stage L_n; all of the above variables plus

- The vapor split ratio $(\beta_k; 1)$.

There are 5*c*+6 equations for each non-equilibrium stage with the exception of Stage L_n:

- M: Material balance equations for vapor phase $(M_{ij}^V, M_{tj}^V; c+1)$,
- M: Material balance equations for liquid phase $\left(M_{ij}^L, M_{tj}^L; c+1\right)$,
- E: Energy balance equations $(E_j^V, E_j^L, E_j^I; 3)$,
- R: Mass transfer rate equations $(R_{ij}^V, R_{ij}^L; 2c-2)$,
- S: Summation equations $\left(S_j^{VI}, S_j^{LI}; 2\right)$,
- H: Hydraulic equations $(P_j; 1)$,
- Q: Interface equilibrium equations $(Q_{ij}^I; c)$.

There are *5c+7* equations for Stage L_n; all of the above equations plus

- B: Pressure balance equations $(B_k; 1)$, only if stage *j* is the bottom left stage of a wall.

The total number of equations and variables in a system with *C* condensers and *R* reboilers is $(s-C-R-w)\times(5c+6)+w\times(5c+7)+(C+R)\times(2c+4)$.

3.2 Method of Solution

We use Newton's method to solve the PCM equations in a manner that is largely the same as that described by Taylor et al. (1994) for a rate-based model of simple columns. An essential and critical aspect of the algorithm is the generation of initial estimates from which Newton's method will converge. Our rate-based PCM uses the initialization method developed for the equilibrium stage PCM, which is shown in Appendix B. For the simulations described in the next sections convergence was attained in most cases in around 10-12 iterations, sometimes fewer. More iterations may be needed when the wall and shell heat transfer coefficients are "large."

Newton's method requires the calculation of the partial derivatives of all of the equations with respect to all of the independent variables (see Taylor et al. (1994) for a discussion

of the calculation of the partial derivatives for a simple column). To the extent possible the necessary partial derivatives are obtained from analytical expressions. Derivatives of the mass balances and mole fraction summation equations with respect to the flow rates and mole fractions are the most straightforward. Derivatives of the mass transfer rate equations are obtained partly analytically and partly approximately as described by Taylor et al. (1994). The partial derivatives of the energy balances and the phase equilibrium equations require partial derivatives of various thermodynamic properties (vapor pressure, activity coefficients, fugacity coefficients, and enthalpy). The partial derivatives of these properties with respect to temperature, pressure and composition are the most awkward to obtain (and the ones that have the most influence on the rate of convergence). With just two exceptions (the derivatives of the excess or residual enthalpy with respect to temperature and pressure), derivatives of all thermodynamic properties are obtained analytically. Composition derivatives of activity and fugacity coefficients are with respect to the unconstrained mole fractions as described in detail (only for activity coefficients) by Taylor and Kooijman (1991).

In the rate-based PCM, because of the newly added variables, the vapor split ratios, on the bottom left stages of dividing walls, the partial derivatives of the material balance equations (these include both component and total material balance equations) and energy balance equations on such stages with respect to split ratios must be added to the Jacobian matrix. More specifically, the G_{jm}^{V} terms in Eqs. (3.1), (3.3), and (3.5) for $j = L_n$ and $j = R_n$, in Figure 3.2, should all contain the vapor split ratio β, and, hence, the derivatives of these equations with respect to β are required. Furthermore, the newly added B equations are functions of the pressure on certain stages and, indirectly, of the vapor flow rates so the partial derivatives for these terms must be included (not doing so will surely lead to failure to converge).

The precise functional form of the pressure drop equation depends on the model selected for the dynamic contribution. To a first approximation we can say that the pressure drop is approximately proportional to the square of the vapor velocity. (It may be that a given

model is exactly proportional to the square of the vapor velocity but this depends, to some extent, on the model and on the local flow regime.)

Thus, we postulate the following functional form for the pressure drop on stage l:

$$\Delta P_l^{dynamic} = C_l \cdot V_l^2 \tag{3.12}$$

where C_l is a proportionality coefficient that, in practice, is a complicated function of column internal characteristics, and physical properties. Taking the stage numbers in Figure 3.2 for example, the dynamic part of the pressure drop on the left and right side of the wall can be calculated by summing Eq. (3.12) over the stages on the corresponding side, as shown in Eqs. (3.13) and (3.14) respectively, assuming stage numbers L_1 to L_n, and stage numbers R_1 to R_n are consecutive.

$$\left(\Delta P_{left}^{w}\right)^{dynamic} \approx \sum_{l=L_1}^{L_n} C_l^L \cdot (V_l)^2 \tag{3.13}$$

$$\left(\Delta P_{right}^{w}\right)^{dynamic} \approx \sum_{l=R_1}^{R_n} C_l^R \cdot (V_l)^2 \tag{3.14}$$

$\mathrm{C_l^L}$ and $\mathrm{C_l^R}$ are the pressure drop proportionality constants for stage l on the left (L) and right (R) sides of the wall. These proportionality coefficients can be calculated quite easily following the rigorous estimation of the pressure drop for each stage and using that value in Eq. (3.12).

Substituting Eqs. (3.13) and (3.14) into Eq. (3.9) leads to the following form for the B equation:

$$B \equiv \left(\Delta P_{left}^{w}\right)^{static} - \left(\Delta P_{right}^{w}\right)^{static} + \sum_{l=L_1}^{L_n} C_l^L \cdot (V_l)^2 - \sum_{l=R_1}^{R_n} C_l^R \cdot (V_l)^2 = 0 \tag{3.15}$$

Note that Eqs. (3.12) to (3.15) are exact as long as the pressure drop proportionality equations are calculated for each stage from the pressure drop model selected for that

particular simulation. The approximation comes when we differentiate these equations for use in Newton's method.

The partial derivatives of the B equation with respect to vapor flowrates on stages alongside the dividing wall can be calculated from Eqs. (3.16) and (3.17) for the left and right side of the wall, respectively:

$$\frac{\partial B}{\partial V_l} = 2 \cdot C_l^L \cdot V_l \qquad if\ l = L_1, L_2, \dots, L_n \tag{3.16}$$

$$\frac{\partial B}{\partial V_l} = -2 \cdot C_l^R \cdot V_l \qquad if\ l = R_1, R_2, \dots, R_n \tag{3.17}$$

This formulation of the pressure balance over the wall – which, we emphasize again – is only for the purposes of approximating the partial derivatives, the balance equation itself is calculated rigorously – permits the use of any available correlation for the dynamic pressure drop; we will demonstrate this fact in a later section of this paper.

3.3 Aromatics Processing Case Study

In this section, we use the rate-based PCM to model an aromatics processing column the design of which was described in detail by Dejanović et al. (2011). The same case was simulated using the equilibrium-stage PCM in Chapter 2.

Shown to the left in Figure 3.3 is a schematic diagram of the Dejanović DWC which has seven packed beds. Montz-Pak B1-350 MN corrugated sheet metal structured packing was selected for use in their design (Dejanović et al., 2011). The shell diameter and shell height of the DWC are 1.7 m and 37.3 m, respectively. Note that the dividing wall is not flat; as shown on the left of Figure 3.3, the upper part of the wall divides the column exactly in half with equivalent diameters on two sides both 1.2 m, while the lower section of the wall is slightly offset to the right, with equivalent diameters 1.43 m and 0.92 m, respectively (Dejanović et al., 2011).

The feed stream is a slightly subcooled liquid (q = 1.064), consisting of 15 components (the feed composition is given in Table A1 in the Supplementary Material). The feed pressure is 3.5 bar, feed temperature is 100.07 ^{o}C, and feed flowrate is 31730 kg/h. According to Dejanović (2017), the reflux ratio and boilup ratio (in mass units) are 2.74 and 1.74, respectively; the liquid side draw flowrate is 3680 kg/h; the liquid split ratio above the dividing wall is 40% / 60%, while the vapor split ratio at the bottom of the wall is given as 66% / 34%. The column top pressure is 2.7 bar, and bottom pressure is 3.04 bar; pressures in between are provided by Dejanović (2017).

3.3.1 Simulation Description

The right side of Figure 3.3 shows the initial model setup for the rate-based PCM in which we follow the rules for numbering stages that were described in Chapter 2. Our base-case model of this DWC has 26 rate-based model stages (not including the condenser) in the section above the wall (this is the same as the number of equilibrium stages used in the simulations of Dejanović et al., 2011). There are 22 stages on each side of the wall, and 17 stages (including the reboiler) below the wall. The feed and side draw stages are the same as in the model of Dejanović et al. (2011) in their equilibrium-stage simulations.

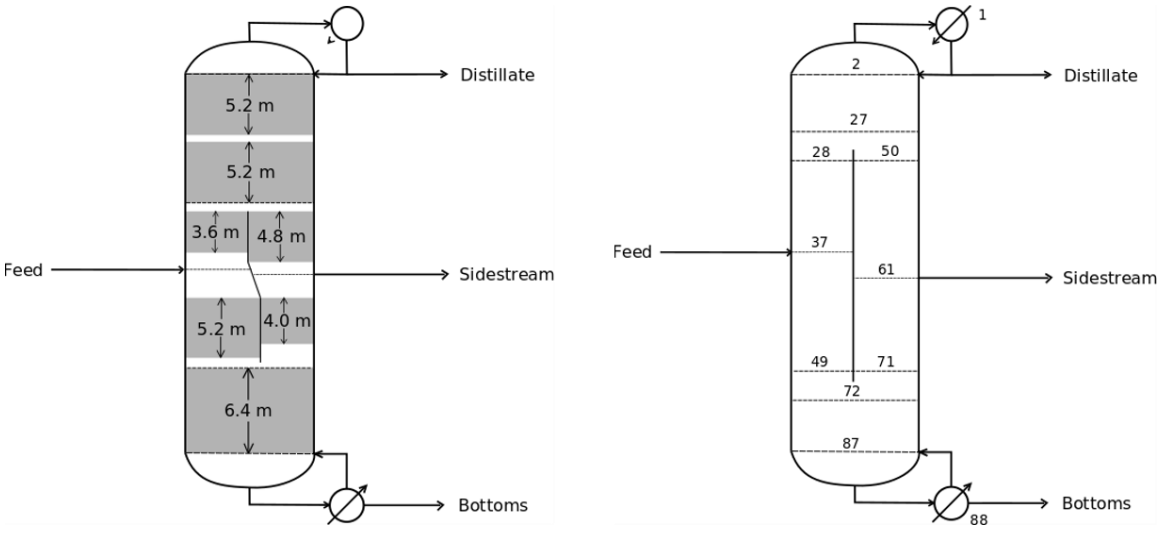

Figure 3.3 Diagram of the DWC with packed beds (left); model setup in the PCM (right).

In our rate-based PCM simulation, the vapor split ratio is predicted by equalizing the pressure drop on two sides of the wall; while the pressure profiles throughout the column are estimated using pressure drop correlations (more on this last point below).

Our model is based on Montz-Pak B1-350 packing because the parameters needed to properly model Montaz-Pak B1-350MN – as used in the design by Dejanović et al. (2011) – are not available in the literature. The expected HETP of Montz-Pak B1-350 is between 0.2 – 0.4 m (Olujić et al., 2003).

Mass transfer coefficients were estimated from a hybrid model composed of the Rocha et al. (1996) correlation for the gas phase mass transfer coefficient, the Song et al. (2014) correlations for the liquid phase mass transfer coefficient, and the Tsai et al. (2011) correlation for the effective area. Geometric parameters of Montz-Pak B1-350 structured packing (needed for these correlations) used in our simulations are as follows: specific surface area 346/m, void fraction 0.98, channel base 16.7 mm, crimp height 7.9 mm, channel side, 11.6 mm, and channel flow angle 45o. Both vapor and liquid phases were assumed to be in plug flow. The pressure drop for a corrugated sheet metal packing was estimated from the model proposed by Rocha et al. (1993). Other sources of pressure drop, e.g. liquid distributors and collectors, are ignored in this simulation.

We use the Peng-Robinson (PR) equation of state thermodynamic model as we did in the equilibrium-stage PCM (model parameters are available in Appendix C). For this particular set of simulations the following models were used for estimation of other physical properties:

Vapor density	Peng-Robinson EOS
Liquid density	COSTLD method
Vapor viscosity	Brokaw method
Liquid viscosity	Mass fraction average of log
Vapor pressure	Antoine
Vapor diffusivity	Fuller et al.

Liquid diffusivity (at infinite dilution)	Modified Wilke-Chang
Liquid diffusivity (at finite concentration)	Kooijman-Taylor + Vignes

3.3.2 Simulation Results

The rate-based PCM takes only 7 iterations to converge this case, compared to 6 iterations (0.7 seconds) for the corresponding equilibrium-stage simulation of the same case (see Chapter 2). With the liquid split ratio specified to be 40% / 60% at the top of the dividing wall, the vapor split ratio at the bottom of the dividing wall is estimated as 65.7% / 34.3% by balancing the pressures on two sides of the wall. This is very close to the ratio of 66% / 34% given by Dejanović (2017). Table 3.1 summarizes the pressure drop in each section, where the pressure drops in the pre-fractionator and main-fractionator are equal (17.04 mbar).

Other pressure drop correlations could be used in the simulations of this aromatic DWC. The vapor split ratios calculated from this type of model will vary slightly depending on the pressure drop model that has been selected. For this column the vapor split ratio is estimated to be 67.4% / 32.6% using the model of Stichlmair et al. (1989) ; 66.0% / 34.0% using the model of Billet and Schultes (1992); and 65.0% / 35.0% using the model of Bravo et al. (1992).

The fact that the simulations with different pressure drop models all converge easily suggests that the approximation of the dynamic part of pressure drop specifically for the purpose of calculating the derivative terms in the Jacobian matrix works well. (We have also simulated this column using packings other than Montz-Pak, and with pressure drop models other than those mentioned above, so far with complete success in the sense that all converged easily. We should add a caveat that operation under different flow regimes – e.g. above the loading point – might alter this conclusion, but we have not yet encountered such conditions.)

Table 3.1 Basic dimensions and estimated pressure drop in each packed bed section.

			Pre-fractionator		Main-fractionator		
Section	I	II	III	IV	V	VI	VII
First stage	2	15	28	37	50	62	72
Last stage	14	27	36	49	61	71	87
Section height, m	5.2	5.2	3.6	5.2	4.8	4.0	6.4
Diameter, m	1.7	1.7	1.2	1.43	1.2	0.92	1.7
ΔP, mbar	9.1	9.0	6.8	10.3	6.9	10.1	15.0

Figure 3.4 shows the temperature profiles for this column conducted with simulations with decreasing the integration height over the beds, which increases the number of stages used in the model. It illustrates that the temperature profiles appear to be converging towards the profiles that would result from an infinite number of stages. Table 3.2 shows the resulting product compositions for the key components and the error in the key components using the values in the last row of Table 3.2 as the basis. We see the mole fractions converging towards their infinite-stage value smoothly as the number of stages per unit height of packing increases. In this particular case a stage/integration height equivalent to HETP/3 provides a reasonable compromise between accuracy of prediction of the mole fractions of the impurities and major products in product streams. A more coarse-grained simulation using a stage height approximately equal to the expected HETP will still yield useful results if the composition of the minor components is not a consideration. Stage heights greater than the expected HETP are not recommended. (Not shown here is a similar table created using a well-mixed liquid flow model; the plug flow model in Table 3.2 converges significantly more rapidly than does the mixed flow model.)

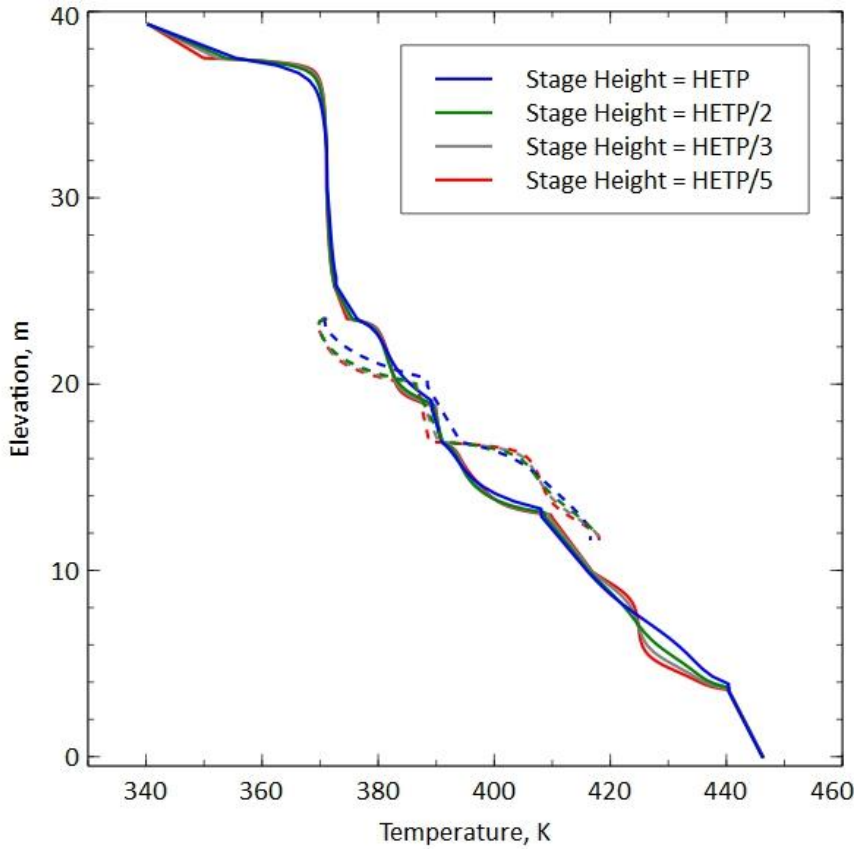

Figure 3.4 Temperature profiles of the aromatic DWC predicted from the rate-based PCM. The solid lines represent the temperature profiles in the main-fractionator, while the dashed lines are the profiles in the pre-fractionator.

Table 3.2 Selected product mole fractions as a function of stage height.

Stage height		x Top		x Heart cut			x Bottoms		Key comp's
Effective	m	2MP	B	2MP	B	3MH	3MH	T	error
1.5 HETP	0.6	0.2766	0.0347	0.0485	0.6757	0.1160	0.0062	0.4224	6.1%
HETP	0.4	0.2863	0.0247	0.0284	0.7103	0.1179	0.0056	0.4266	1.5%
HETP / 2	0.2	0.2962	0.0155	0.0075	0.7359	0.1163	0.0059	0.4280	2.2%
HETP / 3	0.13	0.2981	0.0132	0.0033	0.7408	0.1170	0.0057	0.4282	0.8%
HETP / 5	0.08	0.2989	0.0119	0.0015	0.7436	0.1174	0.0056	0.4282	-

2MP= 2-methylpentane, B= benzene, 3MH= 3-methylhexane, T= toluene
HETP reference value = 0.4 m

3.4 Remarks

In this chapter, we have described an equation-oriented non-equilibrium or rate-based Parallel Column Model (PCM) and used it for the simulation of dividing wall columns. The rate-based PCM described here is an extension of the earlier equation oriented equilibrium stage model (discussed in Chapter 2) and, therefore, inherits all of the advantages of the equilibrium-stage PCM, namely significantly reduced effort required to create a model of a DWC compared to the effort needed to set-up a multi-column model in a commercial simulator, and rapid and stable convergence from an automated initialization procedure, again when compared to the performance of multi-column models. Heat transfer across the dividing wall can be accounted for very easily in an equation-oriented PCM.

A significant aspect of DWC simulation that usually is ignored in multi-column models is the fact that in a real column the vapor flows to each side of the wall cannot be known a-priori because the actual vapor split depends on the pressure drop in the walled part of the column. To be precise: the flows to each side of the wall will self-adjust in an operating column to ensure that the pressure drops on each side of a wall are equal. This is impossible in a true equilibrium stage simulation because such a model has no connection to real process equipment. We have shown here how to include a pressure balance in an equation-oriented and rate-based model in a flexible way suitable for a range of internals types (and, hence, their underlying pressure drop models).

A case study involving an aromatics processing column demonstrates that it is also possible to simultaneously determine the vapor split ratio, and that such calculation can be done quite easily using different pressure drop models. In this case the estimated vapor splits were all close to the value provided in the original paper.

The proposed rate-based PCM can be used as a single, standard DWC unit model within commercial process simulation tools via the CAPE-OPEN mechanism. This aspect of the model is discussed in more detail in Section 2.5.

A factor apparently not previously considered by DWC researchers (i.e. not written about anyway) is that changes in the flow rate (made in order to equalize the pressure drops) necessarily changes the stripping factors on opposite sides of the walled section(s) of the column. This in turn, means the HETP will change and so the precise number of stages on opposite sides of the wall must change to accommodate this. The appropriate number of equilibrium stages should, therefore, be adjusted during a DWC simulation. This dynamic adjustment of the number of stages cannot be adequately anticipated using an equilibrium stage model. We conclude that a rate-based model such as that described in this paper is the proper way to simulate dividing wall columns.

Reference

Billet, R., and Schultes, M., 1992. Advantage in correlating packed column performance. In: *Inst. Chem. Eng. Symp. Ser.* Distillation and Absorption 1992. Hemsphere Publishing Corporation, p.B129.

Bravo, J.L., Rocha, J.A., and Fair, J.R., 1992. A comprehensive model for the performance of columns containing structured packings. In: *Inst. Chem. Eng. Symp. Ser.* Distillation and Absorption 1992. Hemisphere Publishing Corporation, pp.A439–A457.

Dejanović, I., 2017. Private communication to R. Taylor.

Dejanović, I., Matijašević, L., Jansen, H., and Olujić, Ž., 2011. Designing a packed dividing wall column for an aromatics processing plant. *Industrial & Engineering Chemistry Research*, 50(9), pp.5680–5692.

Kister, H.Z., Haas, J.R., Hart, D.R., and Gill, D.R., 1992. Distillation design. McGraw-Hill New York.

Lockett, M.J., 1986. Distillation tray fundamentals, Cambridge University Press.

Olujić, Ž., et al., 2003. Performance characteristics of a new high capacity structured packing. *Chemical Engineering and Processing: Process Intensification*, 42(1), pp.55–60.

Rocha, J.A., Bravo, J.L., and Fair, J.R., 1993. Distillation columns containing structured packings: a comprehensive model for their performance. 1. Hydraulic models. *Industrial & Engineering Chemistry Research*, 32(4), pp.641–651.

Rocha, J.A., Bravo, J.L., and Fair, J.R., 1996. Distillation columns containing structured packings: a comprehensive model for their performance. 2. mass-transfer model. *Industrial & Engineering Chemistry Research*, 35(5), pp.1660–1667.

Song, D., Seibert, A.F., and Rochelle, G.T., 2014. Effect of liquid viscosity on the liquid phase mass transfer coefficient of packing. *Energy Procedia*, 63, pp.1268–1286.

Stichlmair, J., Bravo, J.L., and Fair, J.R., 1989. General model for prediction of pressure drop and capacity of countercurrent gas/liquid packed columns. *Gas Separation & Purification*, 3(1), pp.19–28.

Taylor, R., and Kooijman, H.A., 1991. Composition derivatives of activity coefficient models (for the estimation of thermodynamic factors in diffusion). *Chemical Engineering Communications*, 102(1), pp.87–106.

Taylor, R., Kooijman, H.A., and Hung, J.-S., 1994. A second generation nonequilibrium model for computer simulation of multicomponent separation processes. *Computers & Chemical Engineering*, 18(3), pp.205–217.

Taylor, R., and Krishna, R., 1993. Multicomponent mass transfer. John Wiley & Sons.

Tsai, R.E., Seibert, A.F., Eldridge, R.B., and Rochelle, G.T., 2011. A dimensionless model for predicting the mass-transfer area of structured packing. *AIChE Journal*, 57(5), pp.1173–1184.

CHAPTER 4 Model Validation with Pilot Data

4.1 Validation with the Pilot Data from University of Texas at Austin

A comprehensive experimental study of DWCs has recently been documented in the dissertation of Roach (2017), (see, also, Roach and Eldridge, 2017; Roach et al., 2017). The pilot DWC at the University of Texas, Austin, is composed of six sections, with each section fabricated using 6 inch schedule 40 pipe. There is a welded wall, made of a 1/4 in. thick 304 stainless steel plate, that divides the cross sectional area more or less exactly in half. The DWC has an internal diameter of 6.63 in. (0.17 m), and has 2 in. (0.051 m) of insulation on the outside of the shell. Sulzer Mellapak 500Y (M500Y) corrugated sheet metal structured packing is used in the column. Mellapak 500Y has a single element bed height of 8.125 in. (0.21 m), an effective packing area of 507, m^2/m^3, and a void fraction of 0.975 (see, again, Roach, 2017, for details).

Liquid and vapor distributors are four chimney trays in the column, each of which has a number of points for liquid distribution and four chimney columns for vapor distribution. An exception is the chimney tray right above the dividing wall, which is a liquid trap tray and has no distribution points or weep holes. The liquid from the rectifying section is collected on this trap tray and fed to a tank; the liquid is then pumped to two control valves that control the liquid splits to the two sides of the wall. The vapor split in the DWC is not controlled during the experiments; it must, therefore, self-adjust in order to balance the pressure drop on both sides of the wall.

Roach (2017) studied two different mixtures in the pilot DWC: an alcohol system and a hydrocarbon system. The alcohol system consists of n-hexanol, n-octanol, and n-decanol, and was run under vacuum conditions, approximately 0.9 psia. In total 11 experiments with differing liquid split ratios and feed compositions are recorded in detail in Appendix F of the thesis of Roach (2017). The hydrocarbon system consists of n-pentane, cyclohexane, and n-heptane, and for these tests the column was operated at around 20

psia. There are 22 experiments for the hydrocarbon system reported in her thesis. Table 4.1 summarizes different pilot tests at different liquid splits. The experiments documented in the thesis were conducted from February 2015 to May 2016 during which time the outside temperatures vary quite widely. It might, therefore, be expected that the column performance would have been affected by different amounts of heat lost to the environment.

4.1.1 Simulation with the Equilibrium-Stage PCM

We have carried out simulations of all of the experiments described by Roach (2017) using the equilibrium-stage PCM described in Chapter 2.

Figure 4.1 shows a schematic diagram of the DWC with the stage numbers used. Our model of the Austin DWC has 38 stages in total, with condenser and reboiler included in that number (this is the same number of stages used by Roach in her own equilibrium stage simulations). The feed is to stage 14 and the side product is taken from stage 25. The right side of Figure 3 shows the specifications of the column interconnections. The upper one is for the liquid flow on stage 7, which splits into two streams going to stage 8 and stage 20 with the ratios 30% / 70%. Shown at the bottom are the vapor split ratio and the heat transfer coefficient (denoted by U) of the dividing wall. Note that the vapor split ratio is specified in the equilibrium-stage PCM to be 50% / 50%.

Table 4.1 Summary of pilot tests in the thesis of Roach (2017).

Alcohol system		Hydrocarbon system	
Test	Liquid split	Test	Liquid split
Total Reflux			
A1	50/50	H13	50/50
A2	30/70	H14	30/70
A3	70/30	H15	70/30
A4	25/75	H16	60/40
		H17	40/60
Equimolar Feed			
A10i	25/75	H1	30/70
A10ii	32/68	H2	30/70
A12	75/25	H8	25/75
A13	50/50	H9	25/75
		H10	25/75
		H11	25/75
		H3	25/75
		H7	25/75
		H12	50/50
		H6	50/50
10/80/10 Feed			
A7	50/50	P4	50/50
A8	44/56	P5	50/50
A9	25/75	P6	50/50
		P1	50/50
		P3	44/56
		P7	55/45
		P2	40/60

The column inner diameter is given by Roach to be 6.63 inches, and the dividing wall divides the cross sectional area in half, hence the equivalent diameter in the wall region is about 4.69 inches. This DWC has six packed beds (two of which are, of course, parallel to two others), each with a height of 4.74 feet (56.88 inches).

The NRTL activity coefficient model is used to model the phase equilibrium of both mixtures (we used the parameters provided in Appendix D of Roach's dissertation).

Simulations of all the experiments described by Roach are carried out using the equilibrium-stage PCM discussed in Chapter 2, and three cases are selected for further discussion here.

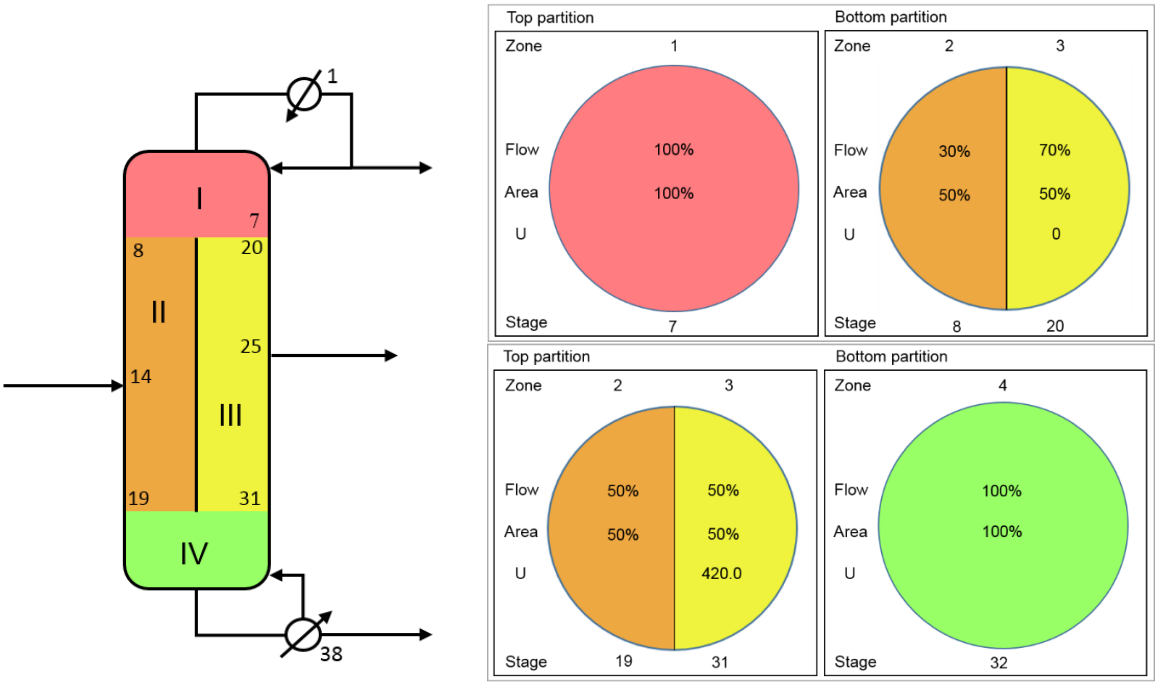

Figure 4.1 (left) Schematic diagram of the DWC with four packed beds (numbers indicate stages in model); (right) Initial liquid split at the top and vapor split at the bottom of the wall (specified by Roach, 2017).

4.1.1.1 Selected Case Studies

Three cases studied in this section are alcohol equimolar case A10ii, hydrocarbon equimolar case H1, and hydrocarbon equimolar case H12. Specifications for these cases are provided in Table 4.2. In these simulations, both heat transfer across the dividing wall and heat loss to the surroundings are considered. The heat transfer coefficients are denoted as Shell (for column shell) and Wall (for dividing wall), respectively.

In the equilibrium-stage PCM, pressures throughout the column are specified, according to the overall pressure drop and wall region pressure drop data provided by Roach. Vapor split ratios in the equilibrium-stage model are specified.

Table 4.2 Specifications for the selected DWC simulations (from Roach, 2017).

Case Number	A10ii	H1	H12
Feed flowrate (lb/h)	66.73	101.95	103.48
Feed temperature (^oF)	202.39	133.07	139.98
Feed pressure (psia)	1.00	25.00	25.00
Feed Composition (wt%)			
n-Hexanol	24.4		
n-Octanol	37.1		
n-Decanol	38.5		
n-Pentane		26.1	26.7
Cyclohexane		34.1	33.2
n-Heptane		39.7	40.1
Sidedraw rate (lb/h)	24.86	35.06	36.23
Bottom flowrate (lb/h)	25.66	40.45	39.75
Overhead reflux ratio	1.12	2.62	6.62
Flow split ratios (left % / right %)			
Vapor split	50/50	50/50	50/50
Liquid split	32/68	30/70	51/49
Pressure overhead (psia)	0.90	20.00	20.00
Overall pressure drop (in H_2O)	3.29	3.58	3.09
Wall region pressure drop (in H_2O)	1.52	2.11	1.79
Heat Transfer Coefficients			
Shell (W/m^2K)	14	85.4	85.4
Wall (W/m^2K)	400	420	850*
Surroundings temperature (^oF)	73.91	34	65

* Actual value in experiment of Roach (2017) was 1238.

4.1.1.2 Simulation Results

Case A10ii

In case A10ii, the pilot purity of the top, side, and bottom products are recorded to be 99.6 wt%, 99.8 wt%, and 99.8 wt%, respectively; while the purity from the simulation are 99.4 wt%, 99.2 wt%, and 99.6 wt%. Figure 4.2 shows the predicted temperature profiles and pilot data recorded from temperature sensors. Note that the elevations at the y-axis are estimated from the column detailed drawing in the thesis of Roach, where all the temperature sensors are shown.

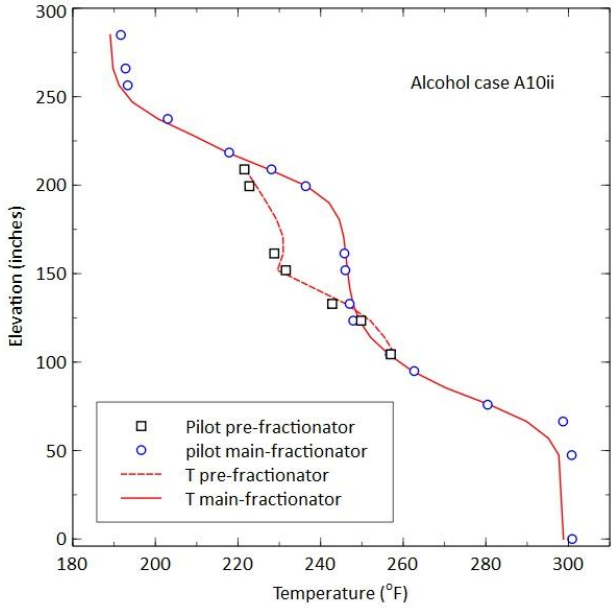

Figure 4.2 Temperature profiles of case A10ii (data from Roach, 2017).

Case H1

The product purity in the pilot column of case H1 is recorded as 100 wt% (top), 93.8 wt% (side), and 95.6 wt% (bottom), and the corresponding simulation results are 100 wt% (top), 92.6 wt% (side), and 94.0 wt% (bottom). The predicted purity in the side and bottom

products are slightly smaller than the experimental data. Figure 4.3 shows the predicted temperature profiles and the pilot data for case H1; good agreements are seen in the plot.

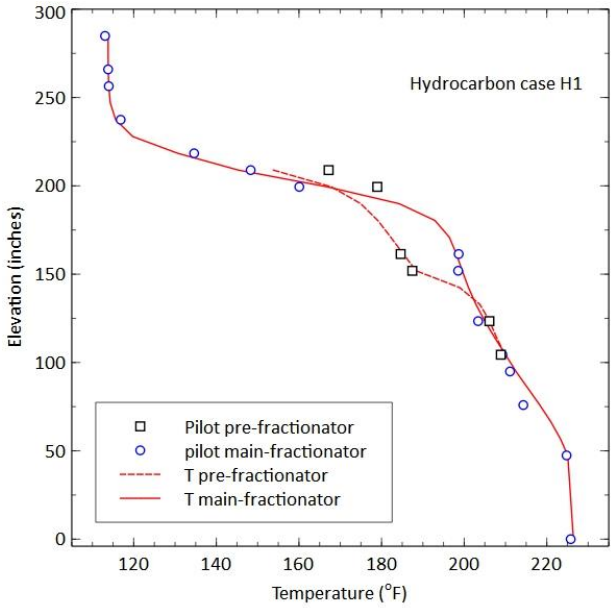

Figure 4.3 Temperature profiles of case H1 (data from Roach, 2017).

Case H12

Figure 4.4a shows the predicted temperature profiles and pilot data for case H12. Heat effects (this includes wall heat transfer and heat losses) are not considered in this simulation. However, the predicted temperature in the pre-fractionator show large deviations from the measured temperatures. Figure 4.4b shows the improved temperature profiles that result when we include the effects of heat transfer with the heat transfer coefficient for the shell, 85.4 W/m^2K, and the wall heat transfer coefficient, 850 W/m^2K, modified from the simulation of Roach (2017).

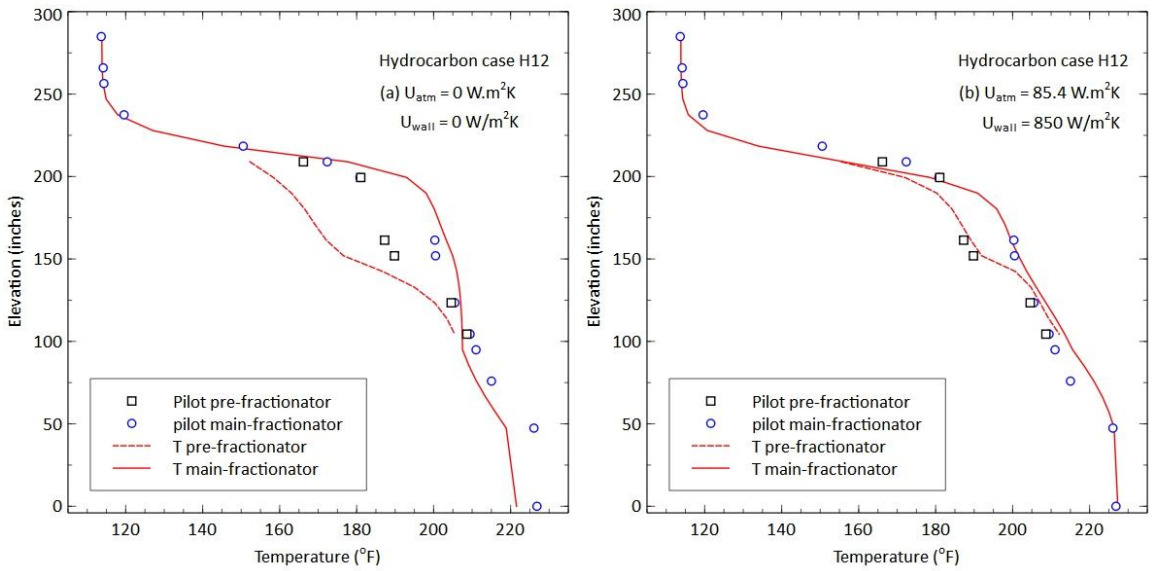

Figure 4.4 Predicted temperature profiles in case H12 using equilibrium-stage PCM with (a) no heat transfer, and (b) U_{atm} = 85.4 W/m^{2}K, U_{wall} = 850 W/m^{2}K. Data from Roach (2017).

The pilot product purity of case H12 are 100 wt% (top), 88.2 wt% (side), 97.1 wt% (bottom); the simulated purity with heat transfer effects (this includes heat transfer across the dividing wall and heat losses) included are 100 wt% (top), 87.35 wt% (side), 96.1 wt% (bottom). However, if heat effects are not included in the simulations, the purity of the side and bottom products would be significantly deteriorated (72.4 wt% in the side draw and 82.5 wt% in the bottom product). We infer that heat transfer effects are important in the model of this particular pilot scale DWC.

4.1.1.3 All Experimental Cases

All 22 experiments with the hydrocarbon system and all 11 cases involving alcohols (shown in Table 4.1) have been modeling using the equilibrium-stage PCM. Figure 4.5 shows a parity plot of column temperatures in all cases listed in the dissertation, in which green squares denote data for alcohol system, and red dots are hydrocarbon system data.

Points in dark colors (dark green and dark red) represents data points in the wall region, and the statistical data provided in this figure is only for the points in the wall region; the data in the top and bottom sections is not included in these numbers.

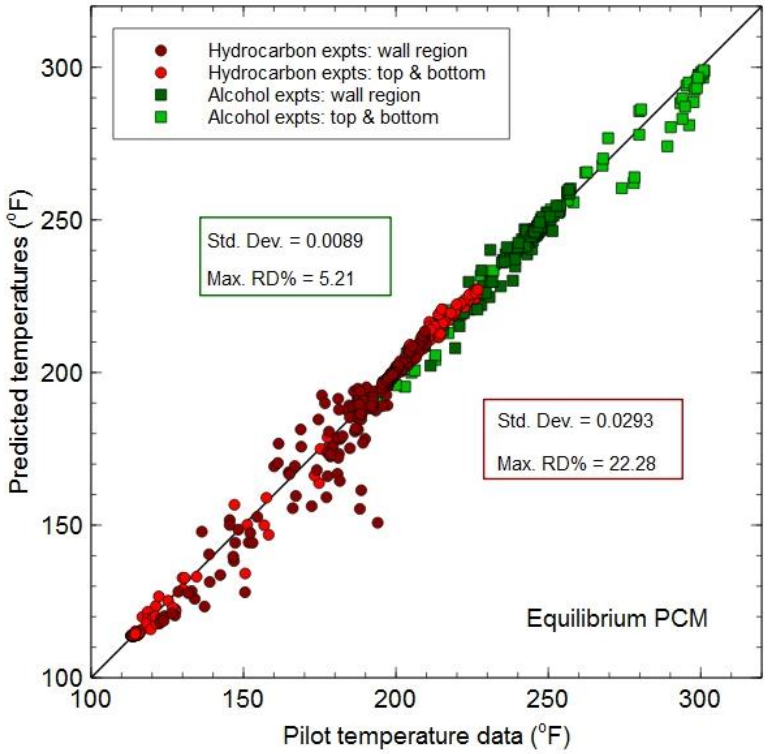

Figure 4.5 Parity plot of temperatures for all case studies in Roach (2017), predicted with the equilibrium-stage PCM.

We see from Figure 4.5 that the equilibrium-stage PCM gives good predictions to the temperatures in an extensive number of simulations. The predictions for the alcohol system are better than for the hydrocarbon system, as the green squares are collected more closely to the 45 degree line than the red points.

4.1.2 Simulation with the Rate-Based PCM

In the rate-based PCM, a same stage numbers as shown in Figure 4.1 is used for simulations. Note that the vapor split ratio is calculated in the rate-based PCM, in our case the ratio 50% / 50% shown in Figure 4.1b serves only as the initial estimate.

Mass transfer coefficients are estimated from a hybrid model composed of the Rocha et al. (1996) correlation for the gas phase mass transfer coefficient, the Song et al. (2014) correlation for the liquid phase mass transfer coefficient, and the Tsai et al. (2011) correlation for the effective area. The vapor is assumed to be in plug flow, while mixed flow model is used for the liquid phase. (The liquid flow model does not appear to have a significant impact on the results obtained in this study.) The pressure drop is estimated from the model proposed by Kooijman et al. (2002), with parameters listed in Table 4.3.

The vapor split ratios were specified to be 50% / 50% in the simulations of Roach (2017), here they are determined by equalizing the pressure drop on two sides of the wall with our rate-based PCM.

Table 4.3 Parameters used in Kooijman et al. (2002) pressure drop model for Sulzer M500Y packing.

Parameters	Description	Value
f_{pack}	Friction factor of the packing (the packed set of corrugations)	0.25
f_{vdir}	Friction factor for redirection	0.05
C_{load}	Onset of loading parameter	0.0047
C_p	Liquid loading pressure drop parameter	0.01
C_h	Liquid holdup parameter	3.5
C_{riv}	Rivulet formation parameter c, constant value of 0.3	0.3
σ_{crit}	Critical surface tension, below which full wetting occurs (N.m)	0.04
H_{el}	Height of an element (m)	0.206
w_w	Width of wall wipers (m)	0.005

4.1.3 Simulation Results

Three cases are selected for further discussion, specifications for which are provided in Table 4.4. Computed temperature profiles for hydrocarbon Case H1 and alcohol Case A10ii are shown in Figure 4.6, together with the corresponding measurements from Roach (2017). The red lines represent the liquid phase temperatures, and green lines show the vapor phase temperatures. The temperature profiles are plotted as a function of elevation, with single bed height given to be 4.74 feet; the height of the reboiler and condenser are estimated from the DWC drawing in the Appendix A of the thesis of Roach (2017). Both plots demonstrate good agreement between the predicted values and pilot plant data. The vapor split ratio estimated in Case H1 is 50% / 50%, and 46% / 54% in Case A10ii.

Figure 4.7 shows the predicted temperature profiles and pilot plant data for case H12. Figure 4.7a shows the profiles when heat effects (this includes wall heat transfer and heat losses to the environment) are not considered in this simulation. However, the predicted temperatures in the pre-fractionator show large deviations from the measured temperatures. Figure 4.7b shows the improved temperature profiles that result when we include the effects of heat transfer with the heat transfer coefficient for the shell, 85.4 W/m^2K, and the wall heat transfer coefficient, 1238 W/m^2K, values that are provided by Roach (2017). The vapor split ratios estimated by the model are included in Table 4.4. We infer that heat transfer effects (both heat transfer across the dividing wall and heat loss) are important in the model of this particular pilot scale dividing-wall column.

All 22 experiments with the hydrocarbon system and all 11 cases involving alcohols have also been modeled using our PCM. Figure 4.8 shows parity plots of column temperatures in all cases listed in the dissertation, obtained using the rate-based PCM. The statistical data provided in this figure is only for the points in the wall region; the data in the top and bottom sections are not included in these numbers (although points for the top and bottom sections are included in Figure 4.8). Compared to the parity plot obtained from

the equilibrium-stage PCM (Figure 4.5), we see that the rate-based PCM gives better predictions for the hydrocarbon cases than does the equilibrium-stage PCM, while both models give comparative predictions to the alcohol cases, with equilibrium-stage PCM performing slightly better.

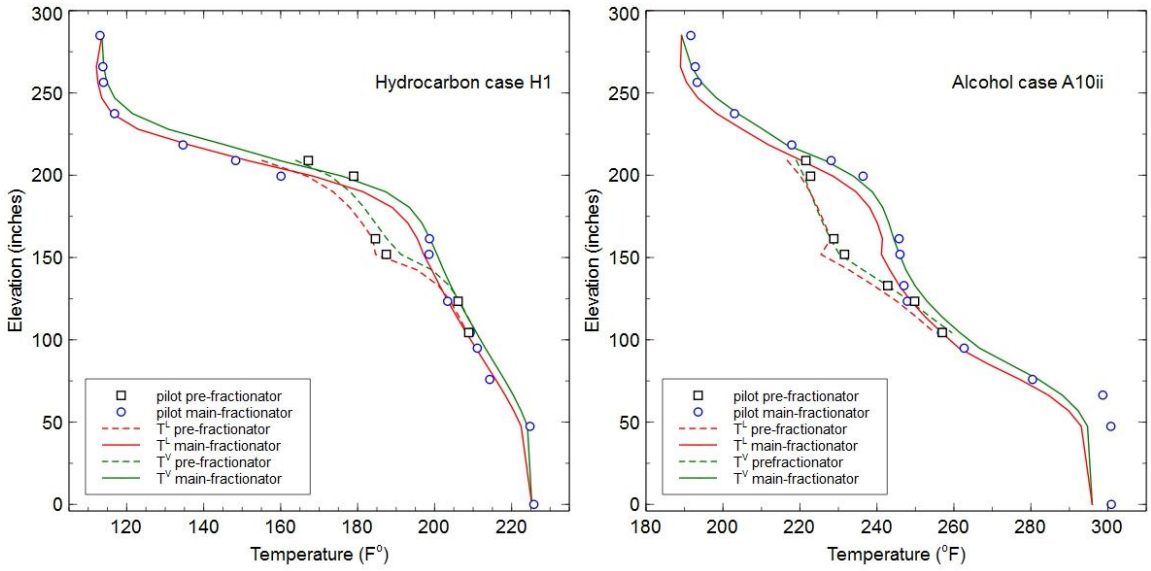

Figure 4.6 Temperature profiles in the DWC of two different systems described in Table 4.4. Data from Roach (2017).

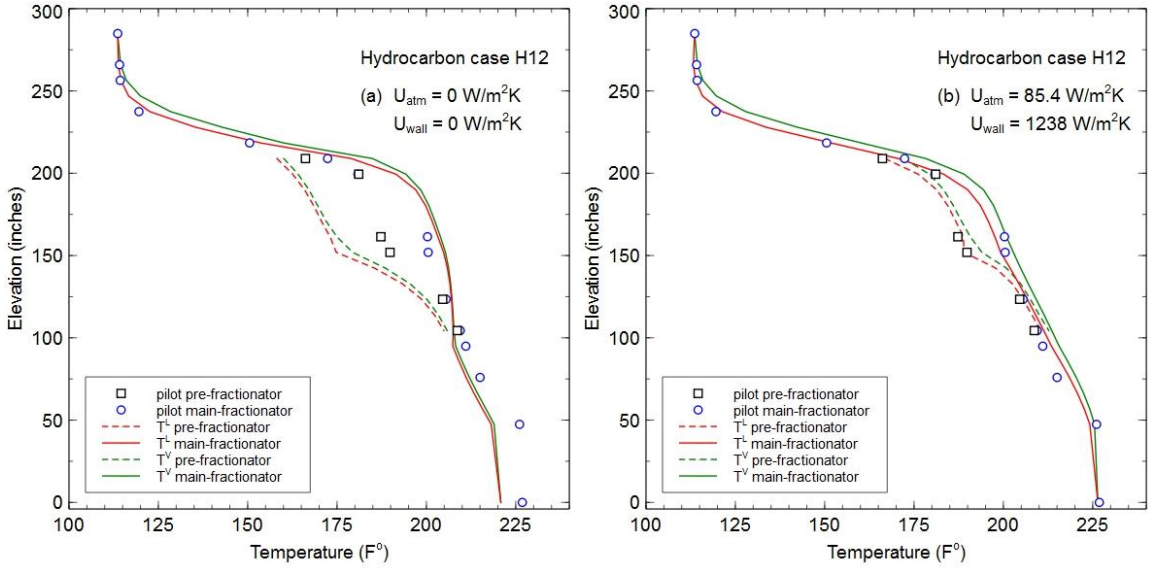

Figure 4.7 Predicted temperature profiles in hydrocarbon case H12 with (a) no heat transfer, and (b) U_{atm} = 85.4 W/m^{2}K, U_{wall} = 1238 W/m^{2}K. Data from Roach (2017).

Table 4.4 Specifications for selected dividing wall column simulations (from Roach, 2017).

Case Number	H1	H12	A10ii
Feed flowrate (lb/h)	101.95	103.48	66.73
Feed temperature (^oF)	133.07	139.98	202.39
Feed pressure (psia)	25.00	25.00	1.00
Feed Composition (wt%):			
n-Pentane	26.1	26.7	
Cyclohexane	34.1	33.2	
n-Heptane	39.7	40.1	
1-Hexanol			24.4
1-Octanol			37.1
1-Decanol			38.5
Pressure overhead (psia):	20.00	20.00	0.90
Overall pressure drop (in H_2O)	3.58	3.09	3.29
Wall region pressure drop (in H_2O)	2.11	1.79	1.52
Heat Transfer Coefficients:			
Shell (W/m^2K)	85.4	85.4	14
Wall (W/m^2K)	420	1238	400
Surroundings temperature (^oF)	34	65	73.91
Sidedraw rate (lb/h)	35.06	36.23	24.86
Bottoms flow rate (lb/h)	40.45	39.75	25.66
Overhead reflux ratio	2.62	6.62	1.12
Flow split ratios (left % / right %):			
Vapor split specified by Roach	50 / 50	50 / 50	50 / 50
Liquid split specified by Roach (and in this work)	30 / 70	51 / 49	32 / 68
Vapor split estimated in this work	50.1 / 49.9	47.7 / 52.3	46.1 / 53.9
Vapor split estimated when ignoring heat transfer		52.1 / 47.9	

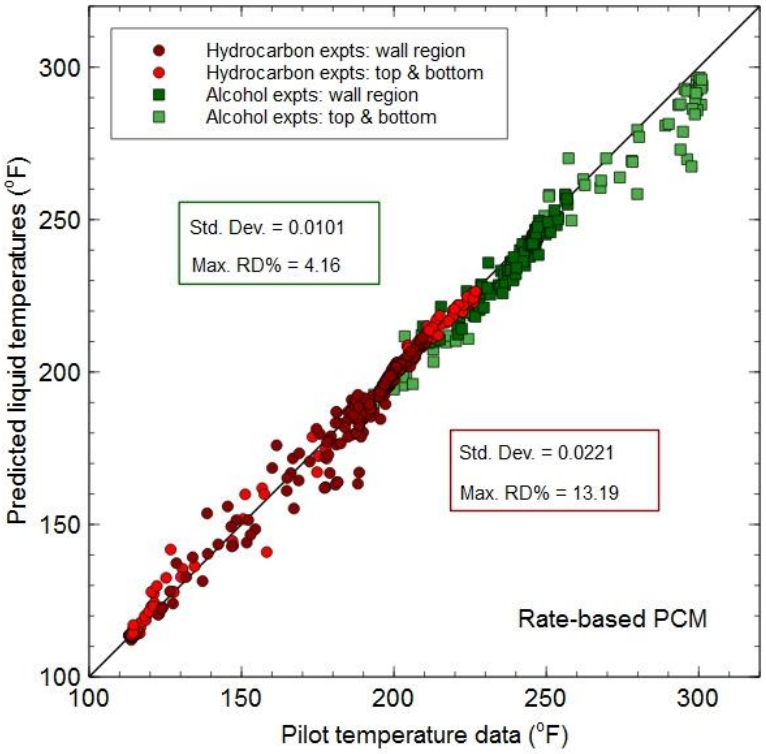

Figure 4.8 Parity plots of temperatures in dividing wall sections for all case studies in Roach (2017).

Simulation details (specifications and results) of all 22 experimental cases using both the equilibrium-stage PCM and the rate-based PCM are summarized in Appendix D.

4.2 Validation with the Mutalib Pilot Data

Figure 4.9 shows the PCM model established to simulate the pilot DWC in the work of Mutalib et al. (1998) where the dividing wall is off-centered to the left. Liquid and vapor split ratios are specified to be 17.24% / 82.76%, and 43.67% / 56.33%, respectively. The feed is an equimolar stream with flowrate 75 L/h, at temperature 78.5 °C. According to Mutalib et al. (1998), the volumetric feed flowrate is equivalent to 1.082 kmol/h molar flowrate. In the table that summarizes the results of steady state runs, information for conducting the simulations is not completely provided by them (this includes three

product flowrates). The following simulation is, instead, conducted based on the information of their base case simulation in Aspen Plus.

Based on the Figure 1 in Mutalib et al. (1998), the distillate from the column top is 15.14 L/h, and the reflux rate is 95.84 L/h. The volumetric reflux rate is equivalent to 2.174 kmol/h. Since the condenser is a total type, the density of the distillate equals to that of the reflux stream. Hence, the distillate in molar unit can be calculated as 0.3434 kmol/h. Similarly, the side draw flowrate in molar unit is calculated as 0.3549 kmol/h. Reboiler duty is given to be 23.981 kW.

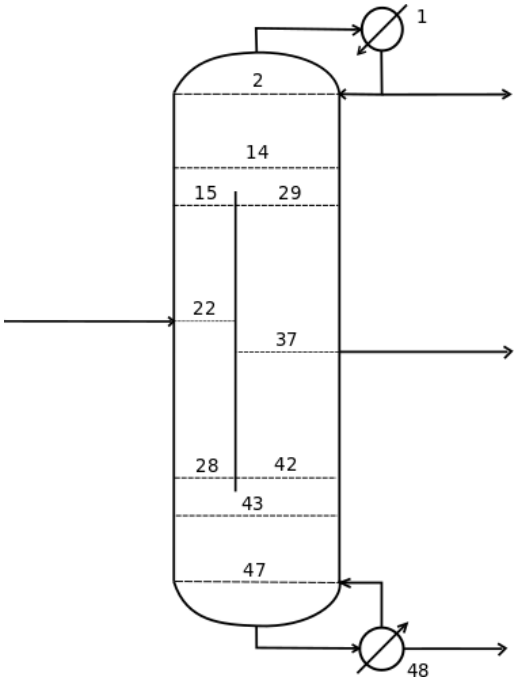

Figure 4.9 Schematic diagram of the pilot DWC in the work of Mutalib et al. (1998) (numbers indicate stages in the PCM).

The simulation results are compared with those given by Mutalib et al. (1998), and are shown in Table 4.5. The purity of the side draw and bottoms have relatively large differences. The explanations of the large deviations are possibly because, firstly, incomplete information is provided in the paper, and, secondly, the flowrates are given in volumetric unit, and there could be some inaccuracy converting the flowrate to molar unit. No further investigation is conducted with this case, due to the lack of information.

Table 4.5 Comparison of the simulated purity and those provided in the paper of Mutalib et al. (1998).

Mol frac, %	Top		Side		Bottom	
	Mutalib	PCM	Mutalib	PCM	Mutalib	PCM
Methanol	98.50	99.70	1.33	5.17	0	0
Isopropanol	1.50	0.30	98.50	94.78	1.50	6.03
1-Butanol	0	0	0.17	0.05	98.50	93.97

4.3 Remarks

In this chapter, both the equilibrium-stage PCM and the rate-based PCM are validated using an extensive set of experimental data from the thesis of Roach (2017), where two different chemical systems were investigated. One was a mixture of linear alcohols (n-C6, n-C8, and n-C10) and the other a mixture of n-pentane, cyclohexane, and n-heptane. Good agreement is observed between the model predictions and the pilot plant data.

A comparison of the parity plots from the equilibrium PCM and the rate-based PCM show that the rate-based PCM gives better predictions of the experiments with hydrocarbons than does the equilibrium PCM. The hydrocarbon case H12 highlights the importance of heat transfer effects in the simulations of such pilot scale DWC.

Although several papers have published pilot plant data for DWC operations, few of the papers provide complete information for one to reproduce the work.

Reference

Kooijman, H.A., Krishnamurthy, K.R., and Biddulph, M.W., 2002. A new pressure drop model for structured packing. In: IChemE Symp Ser. Distillation and Absorption. pp.A109–A123.

Mutalib, M.I.A., Zeglam, A.O., and Smith, R., 1998. Operation and control of dividing wall distillation columns: part 2: simulation and pilot plant studies using temperature control. *Chemical Engineering Research and Design*, 76(3), pp.319–334.

Roach, B.J., 2017. A design model for dividing wall distillation columns.

Roach, B.J., Barsotti, D., Eldridge, R.B., and Andrews, C., 2017. Novel optimization of a dividing wall distillation column. AIChE National Meeting. San Antonio, TX.

Roach, B.J., and Eldridge, R.B., 2017. Scaling up dividing wall distillation columns. AIChE National Meeting. Minneapolis, MN.

Rocha, J.A., Bravo, J.L., and Fair, J.R., 1996. Distillation columns containing structured packings: a comprehensive model for their performance. 2. mass-transfer model. *Industrial & Engineering Chemistry Research*, 35(5), pp.1660–1667.

Song, D., Seibert, A.F., and Rochelle, G.T., 2014. Effect of liquid viscosity on the liquid phase mass transfer coefficient of packing. *Energy Procedia*, 63, pp.1268–1286.

Tsai, R.E., Seibert, A.F., Eldridge, R.B., and Rochelle, G.T., 2011. A dimensionless model for predicting the mass-transfer area of structured packing. *AIChE Journal*, 57(5), pp.1173–1184.

CHAPTER 5 Multiple Steady-State Solutions in a Dividing Wall Column Simulation

5.1 Introduction

The existence of multiple steady states (MSS) in multicomponent distillation has been known for a long time. First reports were from analytical or simulation-based studies (see, e.g. Bekiaris et al. (1993); Güttinger & Morari (1996) for nearly complete historical surveys). To the best of our knowledge the earliest documented case of MSS in multicomponent distillation can be found in the Ph.D. thesis of C.F. Shewchuk (1974) who found two different solutions for ethanol dehydration using benzene (a system frequently used in later studies of MSS). A later paper by Magnussen et al. (1979) – which often is said by many others to be the first report of MSS in multicomponent distillation – found three steady-state solutions for the same system. It was, however, the Magnussen paper that led to increased interest in MSS with many subsequent publications reporting the occurrence of MSS in different systems, or with different specifications, proposing explanations of why MSS exist, and, relatively recently, experimental studies that confirm that MSS is not a phenomenon that arises solely from the nature of our mathematical models (see, e.g. Müller & Marquardt (1997); Güttinger et al. (1997)). One of the findings of some of the many studies on MSS is that interlinked column systems can exhibit multiplicity, an observation that may lie behind the results reported in this paper.

Wayburn, Seader, and coworkers (see Wayburn and Seader (1984), Chavez C et al. (1986), and Lin et al. (1987)) used a differential arc length homotopy continuation method and found MSS for the well-known Petlyuk column configuration. A simple DWC is structurally equivalent in some ways at least to a Petlyuk column. Thus, it could, perhaps, be anticipated that a DWC can exhibit multiple steady states. However, the MSS reported in the works of Wayburn, Seader and colleagues, who specified product purities, is what others refer to as input multiplicity, meaning that two or more independent sets of input variables result in the same output condition (see, e.g., Jacobsen and Skogestad (1991)).

It is, therefore, unlikely that a real DWC with a fixed wall could exhibit that type of multiplicity (a fixed wall implies that operating specifications should remain more or less the same for each steady state). Output multiplicity is when a single set of input specifications leads to multiple independent sets of outputs; it is an example of that type of multiplicity for a DWC that we report in this chapter.

5.2 Case Study

The simulation described here was carried out using an equation-oriented equilibrium-stage parallel column model (PCM) described in Chapter 2. In other words, the simulation code uses Newton's method to solve simultaneously all of the model equations. One of the advantages of an equation-based approach is that it becomes very easy to include in the model heat transfer across the wall. Accounting for heat transfer across the wall is not straightforward in the more widely used approach in which a DWC is modeled using a multi-column model in a sequential-modular simulator. Complete details of the parallel column model, the solution procedure, and the initialization (which is of some importance here) are given in Appendix B.

The example that exhibits multiple steady states is derived from a comprehensive experimental study conducted by Roach (2017) at the University of Texas at Austin.

The pilot DWC at the University of Texas, Austin, uses Sulzer Mellapak 500Y with an HETP of 9.5 inches/stage (as indicated by Sulzer). The welded dividing wall (1/4 inch 304 SS) divides the cross sectional area exactly in half.

The DWC is simulated with 38 equilibrium stages in total, with condenser and reboiler included in that number (this is the same number of stages used by Roach in her simulations). Figure 5.1b shows the diagram of the DWC with the stage numbers we use in our parallel column model. The feed enters on stage 14, and the liquid side product is taken from stage 25. Specifications for our simulation are provided in Table 1 (at the end

of the paper); the case study is adapted from experiment A9ii in the dissertation of Roach (2017). The important specification that differs from her experimental values is the reflux ratio, 12 here instead of 6.

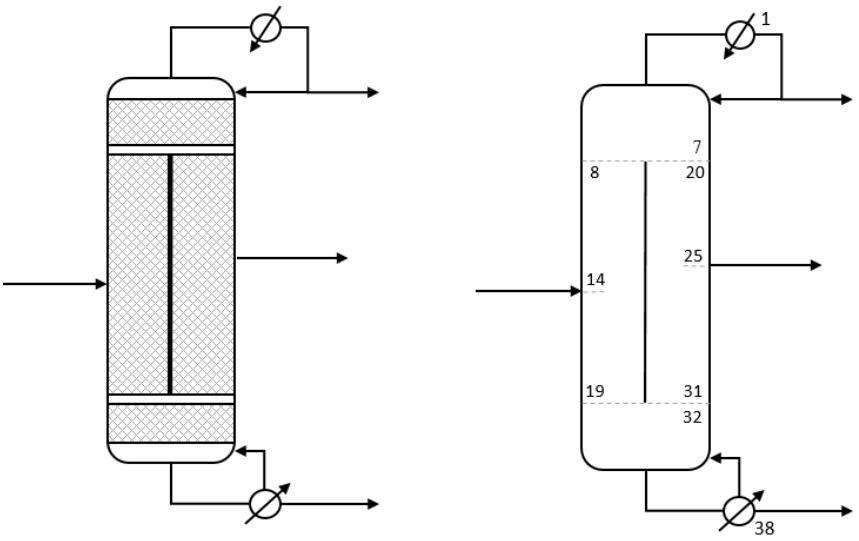

Figure 5.1 (a) Diagram of the packed DWC; (b) Diagram of the DWC with numbers indicating stages in model

Table 5.1 Specifications for dividing wall column simulation

Base Case Number in Roach (2017)	A9ii		
Feed flowrate (lb/h)	51.57	Shell heat transfer coefficient (W/m^{2}K)	14
Feed state	Saturated**	Wall heat transfer coefficient (W/m^{2}K)	1600***
Feed Composition (wt%)		Surroundings temperature (^{o}F)	75.75
1-Hexanol	7.6		
1-Octanol	74.6	Sidedraw rate (lb/h)	38.72
1-Decanol	17.8	Bottoms flow rate (lb/h)	8.99
Pressure overhead (psia)	0.90	Overhead reflux ratio	12*
Overall pressure drop (in H_2O)	2.41		
Wall region pressure drop (in H_2O)	1.09	Vapor split (left % / right %)	50 / 50
		Liquid split (left % / right %)	26 / 74

* Actual value in experiment of Roach (2017) was 6

** Actual feed in the experiment was not saturated

*** See discussion

The NRTL activity model is used to model vapor liquid equilibrium, with parameters obtained from Appendix D of Roach's dissertation. Vapor pressures are estimated from a correlation of experimental vapor pressure data.

Three steady state solutions to this simulation problem are summarized in Table 5.2 and in Figure 5.2 and Figure 5.3. Figure 5.2 shows temperature profiles of three steady state solutions to the simulation in Table 5.1; Figure 5.3 shows the flowrate and liquid mole fraction profiles for the three steady state solutions.

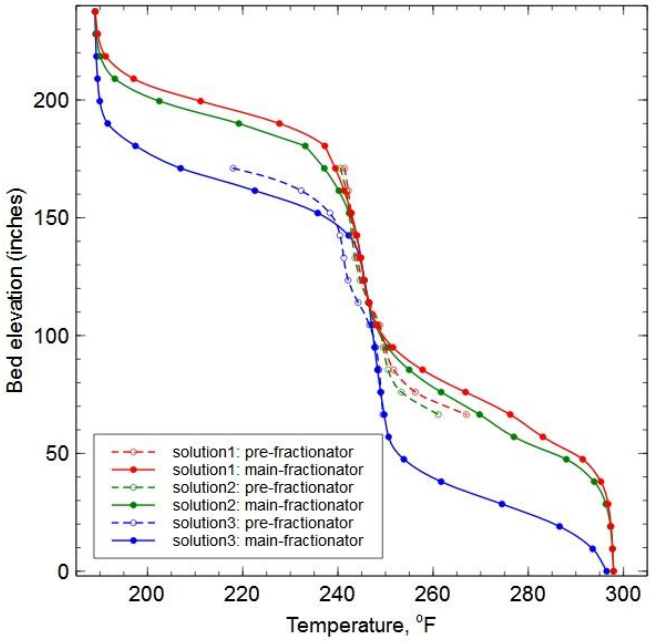

Figure 5.2 Temperature profiles of three steady-state solutions

Table 5.2 Summary of multiple steady state solutions

	Solution 1			Solution 2			Solution 3		
	Top	Side	Bottom	Top	Side	Bottom	Top	Side	Bottom
Recovery (%) *	98.1	99.7	97.9	98.3	99.9	97.9	98.5	99.7	96.7
Condenser duty (Btu/h)		-11589			-11583			-11586	
Reboiler duty (Btu/h)		24645			24478			23587	
Flowrates (lbmol/hr)									
from reboiler		0.906			0.900			0.861	
to condenser		0.490			0.491			0.491	

* 1-hexanol in top product, 1-octanol in side draw, 1-decanol in bottom product

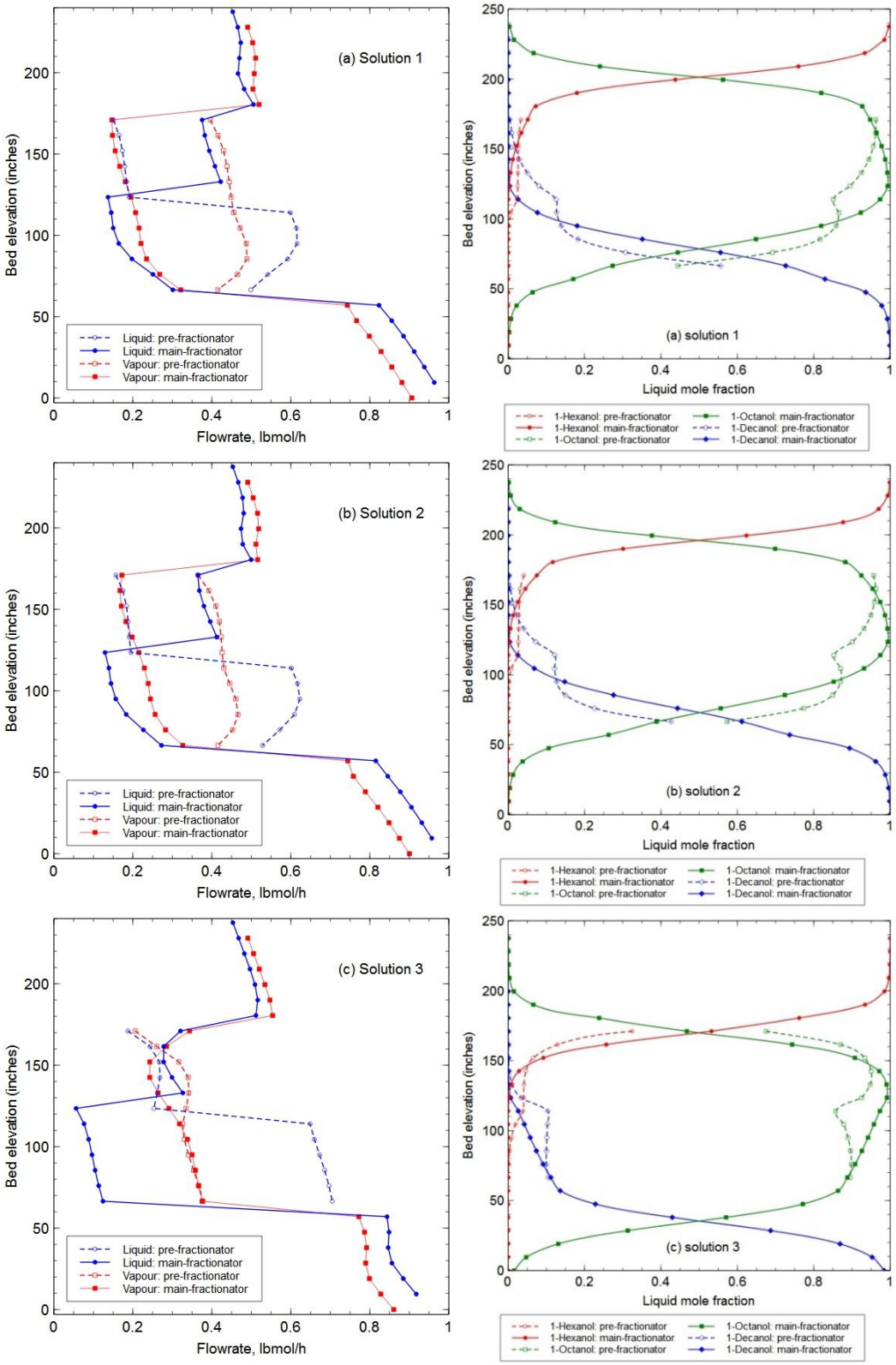

Figure 5.3 Flowrate and liquid phase mole fraction profiles for three steady-state solutions for the dividing wall column in Table 6.1

To gain further insight, we varied the side product mass flowrate from 38.68 lb/h to 38.75 lb/h, while retaining the bottom flowrate at 8.99 lb/h. The effect of varying the side product mass flowrate on the top and middle product purities is shown in Figure 5.4, with an s-shape curve (for the top product purity) and a bow-tie shape (for the middle product purity) shown in the plots. It is worth noting that the curves in Figure 4 should be continuous in the range of varying side product flowrate, although the curves are not closed at the connections of different solutions due to the extreme difficulty of obtaining convergence of the simulation in the close vicinity of the turning points. It can be concluded from the plots that three steady-state solutions exist if the side product flowrate is in the very narrow range of 38.702 lb/h to 38.724 lb/h. If the side product flowrate is less than 38.702 lb/h, only solution 1 exists; if the side product flowrate is greater than 38.724 lb/h, solution 3 is the only one.

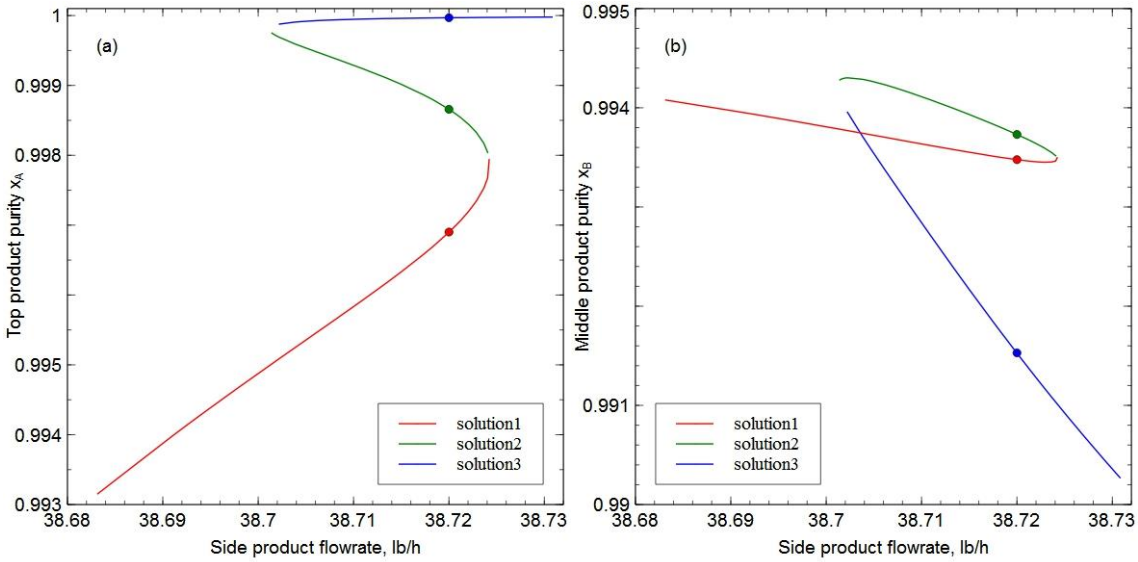

Figure 5.4 Product purity as a function of side product mass flowrates: (a) top product purity, and (b) middle product purity vs. side product mass flowrate. Points represent the solution in Figure 6.2 and 6.3

These MSS do not disappear when the vapor split below the wall is other than 50%/50% as, following the experimental work of Roach(Roach, 2017), specified in the simulations reported here.

Not shown are (because they are not sufficiently different) are similar plots that show the multiplicity as a function of the bottom and side flow rates expressed in molar units, rather than mass units. Thus, that the existence of multiple steady-state solutions is due to mass flow specifications when the model equations employ molar flows, advanced by Jacobsen and Skogestad (1991) as a potential explanation for MSS in some distillation systems, seems unlikely here.

Figure 5.5 shows the result of varying both side draw and bottoms rate at the same time. The side product flowrate is varied over the same range as before, and bottom product flowrate varied from 8.96 lb/h to 9.03 lb/h. At each combination of side draw rate and bottoms rate the simulation is run from 3 different starting points; the results used to create the surface plots in Figure 5.5. These figures show a three-dimensional s-shaped surface corresponding to the curve in Figure 5.4a and a bow-tie surface corresponding to the curve in Figure 5.4b.

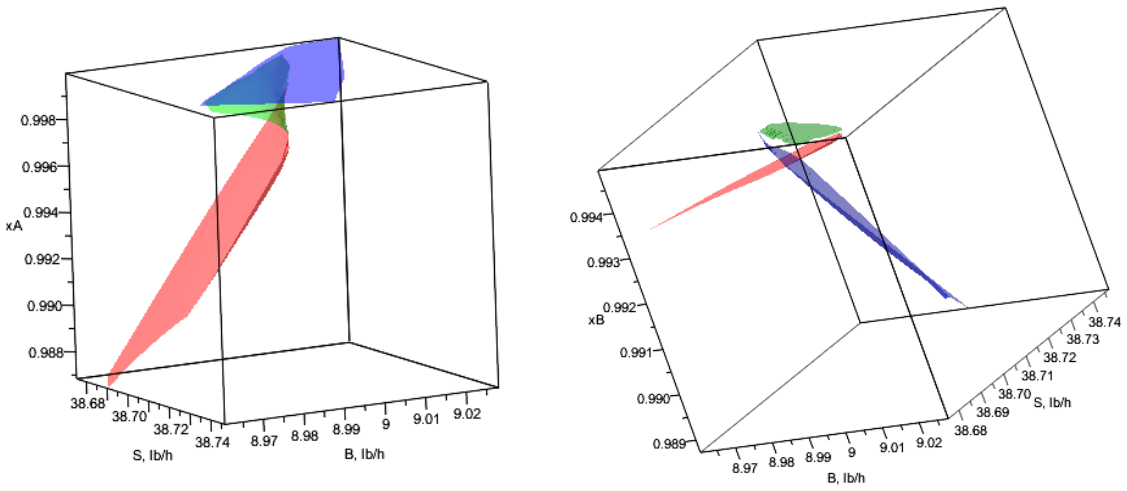

Figure 5.5 Multiple steady-state solutions obtained when varying side product and bottom product flowrates simultaneously: (a) Purity of main compound in the distillate (left), and (b) mole fraction of main product in the sidedraw. B = Bottom mass flow, S = Sidedraw rate (both in lb/h)

5.3 Discussion

Our discovery of multiple steady state solutions shown above came about entirely by accident. We were experimenting with different ways to initialize the flow rates, temperatures, and mole fractions in the parallel column model and obtained different solutions depending on what particular method was used for the initialization.

In the example shown here the window for MSS is quite narrow and is somewhat sensitive to the value of the wall heat transfer coefficient. For this simulation we used a value at the upper end of the range indicated by Roach (2017) (she quotes values of the wall heat transfer coefficient from 14 to more than 1800 W/m^2K, with one very high value for about 30,000 W/m^2K). We were not able to find MSS for this particular simulation when heat transfer across the wall was ignored. This might mean that these MSS are dependent on wall heat transfer; it may, instead, mean that the window for MSS has moved to a location we were not able to find.

Given the large number of more or less conventional distillation processes already demonstrated to show MSS, we speculate that it is likely that there are many other DWC operations that exhibit multiplicity. However, we have not yet been able routinely to find MSS in other DWC systems. It is possible that MSS in other cases will be hard for others to find because the vast majority of DWC simulations are carried out with multi-column models in commercial sequential modular simulation systems in which it is not straightforward to include heat transfer. (It is not, however, impossible to do so, as evidenced by the work of Roach). In addition, it is not easy to exercise any control over the computational process in a commercial simulation program. It is very easy to include heat transfer in the PCM that is described in the previous chapter. What may help here is to couple the PCM to an arc length continuation method that can assist with the automatic location of MSS in DWCs (see, for example, the works of Wayburn, Seader and coworkers cited in the introduction).

5.4 Conclusion

Multiple steady-state solutions are found in simulations of a DWC with two product flowrates specified in mass units. Variation of both specified mass flowrates result in a narrow region where three solutions exist. The reasons underlying multiplicity in the DWC model remain unclear. Possible factors that may cause multiple steady-state solutions include heat transfer across the dividing wall, heat loss to the surroundings, fixed vapor and liquid traffic on both sides of the dividing wall, and more. Further investigation is needed to gain deeper understanding of the multiplicity in modeling DWCs. Such investigation might be helped considerably by using differential arc-length continuation.

We will encounter another case involving multiple steady state solutions in the next chapter.

Given that multiplicity has been verified experimentally in simple distillation columns we suspect that it is only a matter of time before the experimental verification of MSS in a real DWC is confirmed.

Reference

Bekiaris, N., Meski, G.A., Radu, C.M., and Morari, M., 1993. Multiple steady states in homogeneous azeotropic distillation. *Industrial & Engineering Chemistry Research*, 32(9), pp.2023–2038.

Chavez C., R., Seader, J.D., and Wayburn, T.L., 1986. Multiple steady-state solutions for interlinked separation systems. *Industrial & Engineering Chemistry Fundamentals*, 25(4), pp.566–576.

Güttinger, T.E., Dorn, C., and Morari, M., 1997. Experimental study of multiple steady states in homogeneous azeotropic distillation. *Industrial & Engineering Chemistry Research*, 36(3), pp.794–802.

Güttinger, T.E., and Morari, M., 1996. Multiple steady states in homogeneous separation sequences. *Industrial & Engineering Chemistry Research*, 35(12), pp.4597–4611.

Jacobsen, E.W., and Skogestad, S., 1991. Multiple steady states in ideal two-product distillation. *AIChE Journal*, 37(4), pp.499–511.

Lin, W.-J., Seader, J.D., and Wayburn, T.L., 1987. Computing multiple solutions to systems of interlinked separation columns. *AIChE Journal*, 33(6), pp.886–897.

Magnussen, T., Michelsen, M.L., and Fredenslund, A., 1979. Azeotropic distillation using UNIFAC. In: Inst. Chem. Eng. Symp. Ser. pp.1–4.

Müller, D., and Marquardt, W., 1997. Experimental verification of multiple steady states in heterogeneous azeotropic distillation. *Industrial & Engineering Chemistry Research*, 36(12), pp.5410–5418.

Roach, B.J., 2017. A design model for dividing wall distillation columns.

Shewchuk, C.F., 1974. Computation of multiple distillation towers. University of Cambridge.

Wayburn, T.L., and Seader, J.D., 1984. Solution of systems of interlinked distillation columns by differential homotopy-continuation methods. In: Proceedings of the Second International Conference on Foundations of Computer-Aided Process Design. CACHE. Ann Arbor, pp.765–862.

CHAPTER 6 Process Plant Intensification with DWCs

6.1 LPG Recovery Plant

In a natural gas processing plant, the natural gas liquids (NGL), consisting of ethane (C_2), propane (C_3), butane (C_4), pentane (C_5), and heavies (C_{5+}), must be removed from natural gas streams to maintain methane (C_1) as dry gas, due to the fact that NGL may condense in methane pipe lines forming hydrates (ElBadawy et al., 2018). The separated NGL is then sent to an LPG (liquefied petroleum gas) recovery plant to separate LPG, which comprises propane (C_3), isobutane (i-C_4) and normal butane (n-C_4). Several patents and papers are available in the open literature, in which new processes of LPG recovery were proposed (e.g. Khan and Haliburton, 1990; Phu, 2018; Mostafa et al., 2019). However, the LGP recovery processes are considered highly energy intensive. It is desirable to reduce the energy consumption while still maintaining high LPG recovery rate, and the product purity.

Dividing wall columns are considered a promising candidate for this application, due to its potential capital and energy savings. Seihoub et al., (2017) proposed a shortcut method for DWC design, and applied it to a LPG process. It is said that the process with DWC implemented saved about 21% energy compared to the conventional direct sequence; in addition, significant capital cost savings can also be achieved. More recently, Mostafa et al. (2019) also employed a DWC to replace the two conventional columns in a LPG recovery process.

In this section, we simulate the process based on the work of Mostafa et al. (2019), in which they compared a process employing conventional columns with one using DWCs for a same separation task. Two approaches are compared from the perspective of economics, aiming at finding the most economic and optimum technology.

6.1.1 Process Description

According to Fig. 4 of Mostafa et al. (2019), the natural gas arriving from offshore is firstly sent to slug catchers to remove liquids; the resulting gas stream is then pressurized in the compression unit from 17 bar to 83 bar using two compressors. The high-pressure gas is processed in the temperature swing adsorption (TSA) section (in the dehydration unit). The LPG recovery section was added by Mostafa et al. (2019) after the dehydration unit; pentane (C_3), isobutene (i-C_4), normal butane (n-C_4), and natural gasoline (C_{5+}) are further separated for commercial use.

NGL Recovery

The stream coming out of the TSA section (in the dehydration unit) is the feed to the LPG recovery plant. The specification to this stream, adapted from the work of Mostafa et al. (2019), is shown in Table 6.1. The NGL recovery process shown in Fig. 5 of the paper of Mostafa et al. (2019) is created in COCO as shown in Figure 6.1. The Predictive Peng-Robinson equation of state (Jaubert and Mutelet, 2004) is chosen as the thermodynamic model in this simulation because the method provides excellent predictions of VLE for mixtures of alkanes, alkenes, aromatics, and light gases for which no experimental data exists (and, therefore, no binary interaction parameters have been published).

The feed stream exchanges heat with the sales gas out of the cold box, resulting in a temperature decrease (of the feed stream) from 30 ^{o}C to 10 ^{o}C. The cooled stream is sent through a pressure control valve (PCV-01), in which the pressure is reduced from 82.8 bar to 52.8 bar, and the temperature is reduced from 10 ^{o}C to -4.10 ^{o}C. The stream out from the control valve is then sent to the cold box to be cooled down to -60 ^{o}C, with a pressure drop of around 2 bar. The cold stream is then sent through a turboexpander (TE) section, which consists of a TE suction flash tank to remove the liquids, a TE to reduce the pressure from 50.8 bar to 35.8 bar, and a TE discharge vessel to separate the vapor and liquid phases. In order to save energy, the liquid flow from the TE suction flash tank and the vapor flow from the TE discharge vessel are both directed to the cold box to exchange

heat with the stream out of the control valve. The vapor flow of TE discharge vessel is heated from -77 ^{o}C to about -9.26 ^{o}C, and is directed to a heat exchanger to further exchange heat with the Feed Outlet TSA stream. The sales gas, containing mainly methane, is sent to a sales compressor for further processing and liquefaction.

Table 6.1 Natural gas feed (from Mostafa et al. 2019).

Property	Value
Mole flow, tonne/day	6868.99*
Pressure, bar	83
Temperature, ^{o}C	30
Mass fraction:	
N_2	0.0005
CO_2	0.0033
Methane	0.9461
Ethane	0.028
Propane	0.0098
i-Butane	0.0035
n-Butane	0.0028
i-Pentane	0.0016
n-Pentane	0.0011
n-Hexane	0.0016
Benzene	0.0001
Toluene	0.0001
n-Heptane	0.0011
n-Octane	0.0005

* The original value in Mostafa et al. (2019) is 350 MMsft^{3}d.

In the process shown in Figure 6.1, there are two streams containing NGL: one is the stream exiting the bottom of the TE suction flash tank, and the other is the bottom stream exiting the TE discharge vessel. Both streams are directed to the LPG recovery unit to produce LPG. More information of these two streams is shown in Table 6.2.

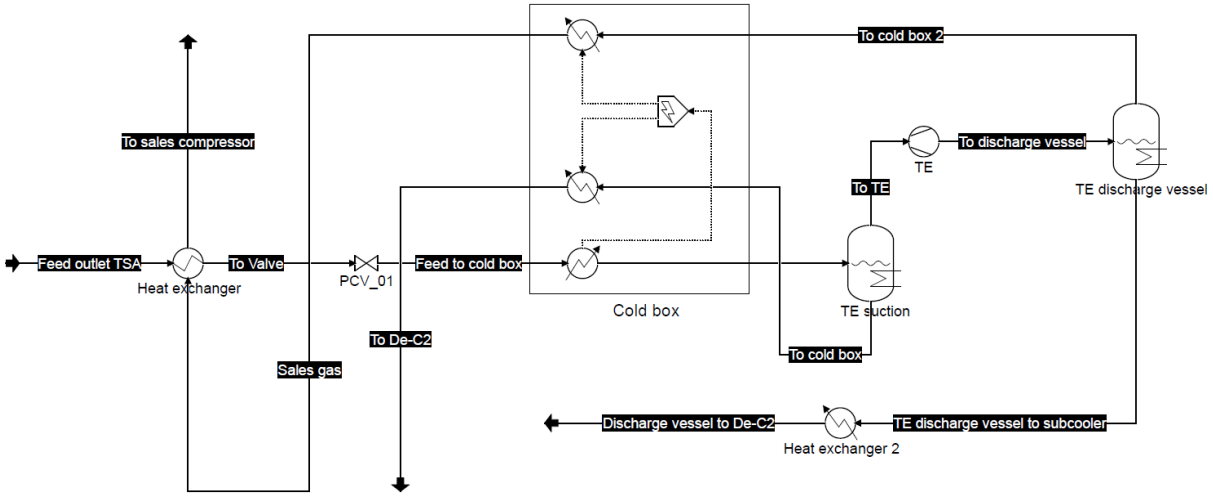

Figure 6.1 NGL recovery process simulated in COCO.

Table 6.2 Streams sent to the LPG recovery section (from Mostafa et al. 2019).

Streams	To DeC_2	Discharge vessel to De-C_2
Mole flow, tonne/day	618.49*	240.65**
Pressure, bar	50.2	35.4
Temperature, ^oC	-10.00	-21.39
Mole fractions:		
N_2	0.0000	0.0001
CO_2	0.0061	0.0078
Methane	0.6035	0.6997
Ethane	0.1003	0.1352
Propane	0.0902	0.0960
i-Butane	0.0471	0.0304
n-Butane	0.0417	0.0198
i-Pentane	0.0277	0.0061
n-Pentane	0.0191	0.003
n-Hexane	0.0298	0.0014
Benzene	0.0017	0.0001
Toluene	0.0010	0.0000
n-Heptane	0.0213	0.0003
n-Octane	0.0095	0.0000

* The original value is 17.74 $MMsft^3d$ in Mostafa et al. (2019)

** The original value is 9.151 $MMsft^3d$ in Mostafa et al. (2019)

LPG Recovery

Two streams in Table 6.2 are fed to the LPG recovery section as two feed streams. In the LPG recovery section, NGL is separated into three different fractions: sales gas containing mainly C_1 and C_2, LPG containing C_3 and C_4 (i-C_4 and n-C_4), and heavies (C_{5+}). Two different approaches are discussed by Mostafa et al. (2019), a conventional direct sequence, and a process that includes a dividing wall column. The details of the two simulations are discussed in the next section.

6.1.2 Simulation of the LPG Recovery

Conventional Method Simulation

The LPG recovery unit is first simulated using a conventional direct sequence. A short-cut calculation was conducted by Mostafa et al. (2019) in order to get initial estimates for this sequence. In the first column, a deethanizer, a mixture of methane and ethane is obtained in the distillate, thus the light key in the deethanizer is ethane (C_2), while the heavy key is propane (C_3). It is specified that the light key in the bottoms should be less than 0.005 mole fraction, and the heavy key in the distillate should be less than 0.005 mole fraction as well. In the second column, a debutanizer, LPG (C_3, i-C_4, n-C_4) is separated from the heavies (C_{5+}). The light key in this column is n-butane (n-C_4), and the heavy key is isopentane (i-C_5). It is specified that the light key in the bottoms is less than 0.0004 mole fraction, while the heavy key in the distillate is less than 0.021 mole fraction (see Mostafa et al. (2019) for more details). The results of the short-cut calculation and the results after optimization are tabulated in Table 3 and 4 in the article of Mostafa et al. (2019). The results obtained from the short-cut calculation indicate that the number of stages in the deethanizer is 22, while 36 are needed in the debutanizer (condenser and reboiler are counted as two equilibrium stages). The optimal feed stages for the two columns are 6 and 18, respectively. The condenser pressure in the deethanizer is 25.8 bar, and 26.2 bar

in the reboiler; the condenser pressure in the debutanizer is 10 bar, and 11 bar in the reboiler.

The flowsheet for LPG recovery using the conventional direct sequence is shown in Figure 6.2. Two feed streams enters the deethanizer from the same stage (stage 6). In the deethanizer, the reflux ratio is specified to be 0.25, and ethane recovery in the bottoms is specified to 0.01. The bottom product (C_{3+}) from the deethanizer is sent through a pressure control valve to decrease the pressure from 26.2 bar to 11 bar. In the debutanizer, the mole fraction of i-pentane (i-C_5) is specified to be 0.021, while the mole fraction of n-butane (n-C_4) in the bottoms is set to 0.0004; all these values are from Mostafa et al. (2019). The product purities from these two columns are shown in Table 6.3, with underlined values represent the design requirements.

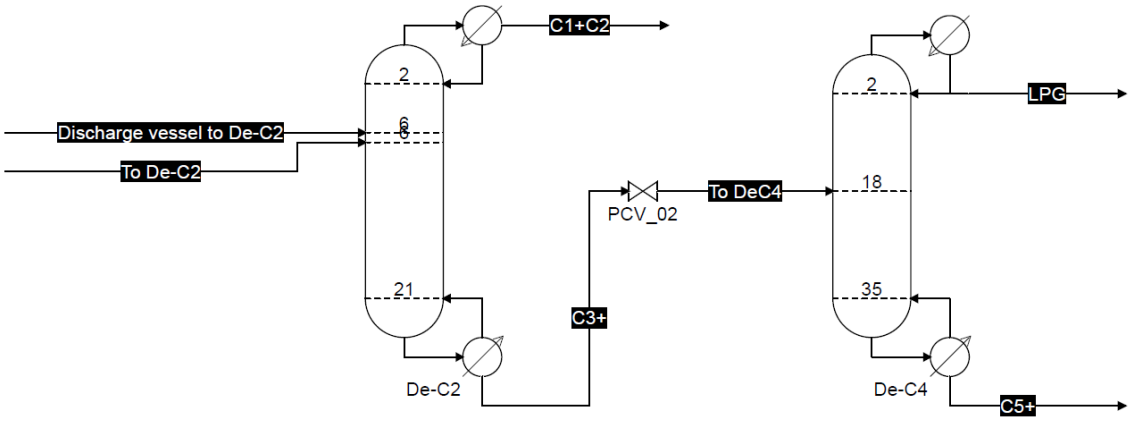

Figure 6.2 LPG recovery flowsheet of the conventional method simulated in COCO.

As is indicated from Table 6.3, the top product from the deethanizer is mostly methane and ethane; the mole fraction of propane in the top product is 0.0047, which is less than the design value (0.005). The mole fraction of ethane in the bottoms (stream C_{3+}) is 0.0045 which meets the design requirement of being less than 0.005. The LPG stream out of the debutanizer contains mainly C_3, i-C_4, and n-C_4, the mole fraction of i-C_5 in the distillate is 0.021, while the mole fraction of n-C_4 in the bottoms is 0.0004; both satisfy the design

requirements. The condenser and reboiler duties of the deethanizer column are -863 kW and 2503 kW, respectively; and are -2027 kW and 1587 kW for the debutanizer column.

Table 6.3 Product purities from the conventional column sequence simulation.

Streams	C_1+C_2	C_{3+}	LPG	C_{5+}
Pressure, bar	25.8	26.2	10	11
Temperature, ^oC	-57.8	118.0	43.8	157.0
Flowrate, tonne/day	406.23	452.91	258.6	194.31
Mole fraction:				
N_2	0.0001	0	0	0
CO_2	0.0079	0	0	0
Methane	0.8370	0	0	0
Ethane	0.1503	0.0045	0.0066	0
Propane	0.0047	0.3552	0.5147	0
i-Butane	0	0.1724	0.2497	0
n-Butane	0	0.1425	0.2064	0.0004
i-Pentane	0	0.0850	0.0210	0.2274
n-Pentane	0	0.0586	0.0016	0.1854
n-Hexane	0	0.0855	0	0.2761
Benzene	0	0.0053	0	0.0172
Toluene	0	0.0053	0	0.0173
n-Heptane	0	0.0588	0	0.1899
n-Octane	0	0.0267	0	0.0863

DWC Process Simulation

To model the DWC, Mostafa et al. (2019) used a short-cut calculation for the DWC based on a three-column model. The top product from the DWC was permitted to contain no more than 0.0001 mole fraction of propane (C_3); the side product is the LPG stream, containing no more than 0.08 mole fraction of ethane (C_2) and no more than 0.01 mole fraction of i-pentane (i-C_5); the bottom product from the DWC is the heavies (C_{5+}), which should contain no more than 0.01 mole fraction of n-butane (n-C_4).

According to Table 6 of Mostafa et al. (2019), the prefractionator has 28 stages, and the main column has 52 stages with condenser and reboiler included. The feed location for

the prefractionator is at stage 9 counting from top down; the liquid from the bottom of the prefractionator is sent to the main column on stage 32, while the vapor from the top of the prefractionator is directed to the main column on stage 5. The liquid and vapor recycles to the prefractionator are from stage 5 and 32 of the main column, respectively. The equivalent DWC configuration for the parallel column model (PCM) is shown in Figure 6.3.

At the column top the mole fraction of propane is set to 0.0001; the sidedraw mass flowrate is 260.76 tonne/day; the mole fraction of n-butane in the bottom product is 0.01. The condenser pressure is 9 bar, and the bottom pressure is 11 bar; constant pressure drop of 0.0148 bar/stage is assumed in the simulation.

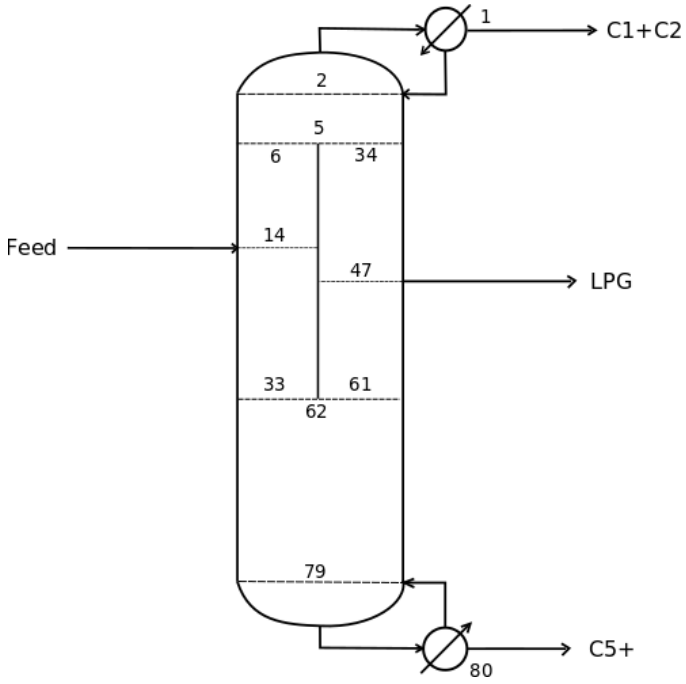

Figure 6.3 DWC model for LPG recovery column (numbers represent stages in the PCM).

The vapor and liquid split ratios are not provided in the article of Mostafa et al. (2019). In our simulation, a vapor split of 22% / 78% (meaning that 22% of vapor flows to the left side of the wall), and a liquid split of 76% / 24% (meaning that 76% of liquid flows to the left side of the wall) was used, as these ratios lead to the lowest energy demand. Figure

6.4 shows the flowsheet using the DWC. The resulting temperature profiles of the DWC are shown in Figure 6.5. The product purities are summarized in Table 6.4 (underlined values are the design requirements). All three products satisfy the design requirements.

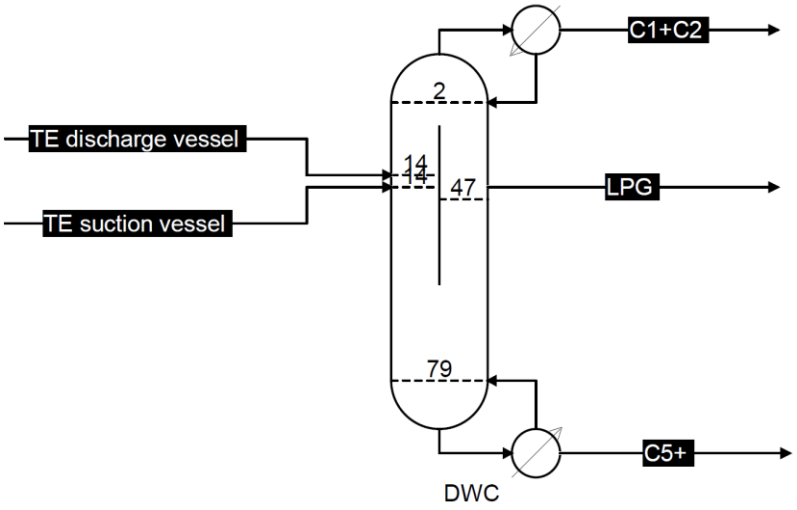

Figure 6.4 LPG recovery flowsheet of the DWC method simulated in COCO.

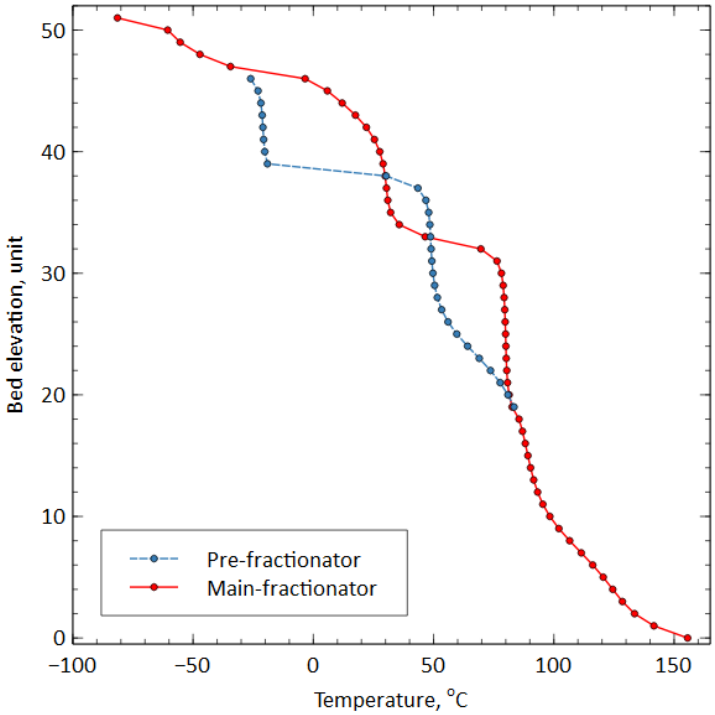

Figure 6.5 Temperature profiles of the DWC.

Table 6.4 Product purities from the DWC simulation.

Streams	C_1+C_2	LPG	C_{5+}
Pressure, bar	10	10.568	11
Temperature, ^oC	-81.43	46.55	155.59
Flowrate, tonne/day	402.28	260.76	219.92
Mole fraction:			
N_2	0	0	0
CO_2	0.0088	0	0
Methane	0.8449	0	0
Ethane	0.1462	0	0
Propane	0.0001	0.5289	0
i-Butane	0	0.2504	0.0003
n-Butane	0	0.2075	0.0100
i-Pentane	0	0.0100	0.2445
n-Pentane	0	0.0032	0.1728
n-Hexane	0	0	0.2709
Benzene	0	0	0.0155
Toluene	0	0	0.0090
n-Heptane	0	0	0.1918
n-Octane	0	0	0.0852

Table 6.5 summarizes the reboiler duties for both the conventional flowsheet and the DWC column simulations. We assume that the reboiler duty can be used to approximate the energy consumption in the distillation system. We see that the DWC column requires about 21% less energy than the conventional direct sequence.

Table 6.5 Comparison of the reboiler duty between direct sequence and DWC column.

	De-C2	De-C4	DWC
Reboiler duty, kW	2503	1587	3228
Sum, kW	4090		3228
Savings, %	-		21

6.1.3 Summary

In the first part of this chapter, we adopted a LPG recovery plant case and simulated the process using both the conventional direct sequence method and the DWC method. The DWC method simulation employs the parallel column model (discussed in Chapter 2) as a standard DWC module. The entire flowsheet, including the NGL recovery, created in COCO, is shown in Figure 6.6, where the DWC icon in COCO correctly shows the appearance of the column. A comparison between the conventional and the DWC configurations indicates that, with the given simulation information, the flowsheet with the DWC saves about 21% of the energy required by the direct sequence.

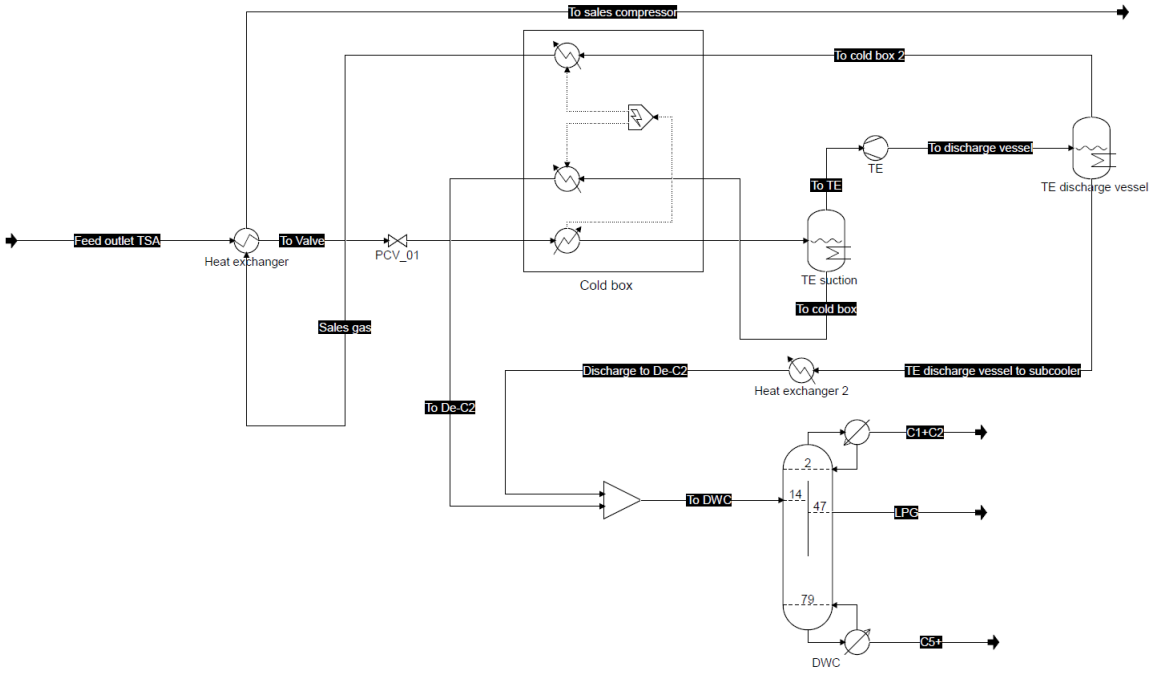

Figure 6.6 The entire flowsheet of the DWC method setup in COCO.

6.2 Shell Higher Olefin Process (SHOP)

Linear alpha olefins (LAOs), also known as normal alpha olefins (NAOs), with carbon numbers greater or equal to four are important chemical intermediates; they are the key building blocks for a wide variety of petrochemical products. The applications of LAOs vary with the carbon numbers, among which an important use of LAOs is to convert them into fatty alcohols that are mainly used for PVC plasticizers ($<C_{11}$) or detergent alcohols ($>C_{11}$) (Behr and Keim, 1985). The products that have the primary market are the $C_{12} – C_{18}$ fractions valuable for the detergent market, while the markets for light LAOs ($<C_{12}$) and heavy LAOs ($>C_{18}$) are relatively small (Keim, 2013).

Commercially, there are two processes for manufacturing LAOs: one is through the thermal cracking of waxes, and the other is based on the oligomerization of ethylene (Turner, 1983; Lappin, 1989). Prior to the 1970s, the main approach to manufacturing LAOs was through thermal cracking of high molecular weight n-paraffins. However, the products from thermal cracking strongly depend on the n-paraffin content and the conditions in the cracking furnace, the manufactured LAOs usually have low purity (less than 90 wt%); the products also contain some undesired byproducts, such as secondary olefins, dienes, and aromatics (Turner, 1983). On the other hand, the ethylene oligomerization processes produce higher purity LAOs with even-numbered chains (LAOs manufactured from thermal cracking have a mixture of both odd and even numbered chains). During the 1970s and 80s, companies that employed the ethylene oligomerization processes include Ethyl, Chevron, Shell, and Mitsubish with different catalytic systems used (Lappin, 1989; Al-Jarallah et al., 1992). Due to the fact that LAOs produced from ethylene oligomerization have higher purity and less costs, many thermal cracking plants eventually shut down in the 70s and 80s. As a result, ethylene oligomerization became the primary approach for manufacturing LAOs.

The Shell Higher Olefins Process (SHOP) from the Shell Oil Company is considered the most remarkable, as the products can be readily adjusted to meet various market

demands (Freitas and Gum, 1979). The SHOP comprises three steps: oligomerization, isomerization, and methathesis. In the ogilomerization step, ethylene reacts over a nickel complex catalyst to produce linear even-numbered α-olefins ranging from C_4 to C_{20+}, which follows a certain geometric distribution. By adjusting the reaction conditions, the distribution of the LAOs can be controlled in response to the market needs. The products are then separated using distillation technique into three fractions: $C_4 – C_8$, $C_{10} – C_{14}$, and C_{16+}. The middle cut LAOs ($C_{10} – C_{14}$) can be converted to $C_{11} – C_{15}$ alcohols through a hydroformylation reactor. The light and heavy LAOs can be converted to internal olefins in the isomerization step, in which the double bond is shifted from the primary position to a different position. Then the light ($C_4 – C_8$) and heavy (C_{16+}) internal olefins react over a heterogeneous catalyst to generate internal olefins in the detergent range ($C_{10} – C_{14}$) via the metathesis (or disproportionation) mechanism. An example is that one mole C_4 internal olefin and one mole C_{20} internal olefin react to produce two moles C_{12} internal olefin. Therefore, the relatively less valuable light and heavy LAOs can be upgraded to detergent range through the combination of isomerization and metathesis (Turner, 1983).

The main focus of this section is on the separation of the oligomers produced from the SHOP oligomerization reactor. As the LAOs products from the oligomerization range from C_4 to C_{20+}, the physical properties of each cut vary quite considerably; a separation train comprising of several distillation columns, operating at different conditions, is required. In this section, we first simulate the SHOP ethylene oligomerization process, and then we use a conventional direct sequence of distillation columns to separate the products. Three different configurations employing dividing wall column techniques are introduced to perform a same separation task, capital and energy costs are compared among different configurations. The simulations of the DWCs employ the parallel column model discussed in Chapter 2, and the entire flowsheet is built up in the COCO simulator.

6.2.1 Oligomerization Reaction

The SHOP oligomerization reaction produces α-olefins from the monomer ethylene using a nickel complex catalyst dissolved in an organic solvent, e.g. 1,4-butanediol (O'Donnell and Gum, 1981). The reaction is homogeneous, and occurs at relatively low temperature (80 – 120 ^{o}C) and high ethylene pressure (70 – 140 atm), which is essential to control the product linearity (Olah and Molnár, 2003). It should be noted that olefins made by ethylene oligomerization have a very broad chain length distribution ranging from $C_{4=}$ to $C_{40=}$, and only olefins with an even number of carbons exist.

The chain lengths of the α-olefins follow the Schulz-Flory type distribution (see Figure 6.7), and a molar growth factor, *K*, is often used to characterize the product compositions, which is defined as (Kister and Lutz, 1977; Freitas and Gum, 1979):

$$K = \frac{Moles\ of\ C_{n+2}\ olefin}{Moles\ of\ C_n\ olefin};\ n = 4, 6, 8 \ldots$$

The K-factor varies with catalyst composition and reaction conditions, e.g. reaction temperature and pressure. Typical values of K-factor in industries are usually set in the range of 0.6 to 0.8. It is reported by Lappin (1989) that K-factor varies from about 0.5 to 0.75 for Chevron, and from about 0.6 to 0.85 for Shell.

The product of the SHOP oligomerization process contains 96 – 97.5 wt% α-olefins; byproducts involve branched olefins (1.0 – 3.0 wt%), internal olefins (1.0 – 2.4 wt%), and paraffins (<0.1 wt%) (see Al-Jarallah et al., 1992). In this work, linear α-olefins with even carbon numbers from $C_{4=}$ to $C_{20=}$ are considered the major products, and 2-methyl-1-alkene type of branched α-olefins with even carbon numbers from $C_{6=}$ to $C_{20=}$ are considered the only byproducts in the system. We assume that the major α-olefins make up 97.5 wt%, 2-methyl-1-pentene (or b-$C_{6=}$) and b-$C_{8=}$ make up 1.0 wt%, and b-$C_{10=}$ to b-$C_{20=}$ make up 1.5 wt%. Together with the molecular weight of each component, mass compositions can be easily converted to molar compositions. Table 6.6 shows the product molar compositions at K-factors 0.6, 0.65, and 0.7.

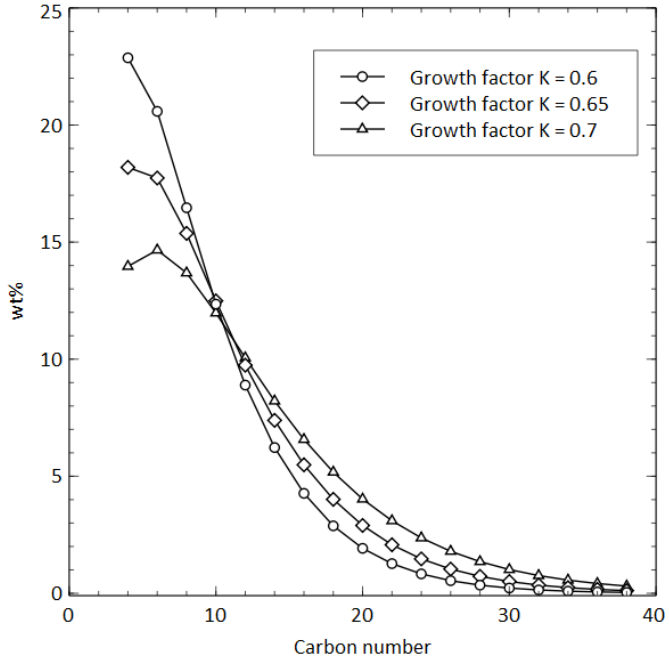

Figure 6.7 Schulz-Flory type distribution (plotted at K = 0.65).

For simplicity, we lump all of the possible reactions together into one long reaction, where ethylene is the only reactant. All the olefins with chain length from $C_{4=}$ to $C_{20=}$ are considered products from ethylene oligomerization; the stoichiometric parameters of this lumped reaction are determined from the molar compositions shown in Table 6.6 at different K-factors.

Although some researchers have studied the kinetics of ethylene oligomerization reaction with different types of catalyst (see, for example, Peuckert and Keim, 1983; Galtier et al., 1988; Al-Jarallah et al., 1992), our interest is not in modeling of such reactions; instead, we focus more on the separation train coming after the reaction. As a result, the oligomerization reaction is modeled using a simple conversion reactor in COCO, with K-factor and reaction conversion as the two parameters that determine the reactor output.

Table 6.6 Ethylene oligomerization product compositions at different K-factors.

Component name	Chain length	Growth factor K 0.6	0.65 (mole %)	0.7
α-olefins:				
1-Butene	$C_{4=}$	39.73	35.1	30.66
1-Hexene	$C_{6=}$	23.84	22.81	21.46
1-Octene	$C_{8=}$	14.3	14.83	15.02
1-Decene	$C_{10=}$	8.58	9.64	10.52
1-Dodecene	$C_{12=}$	5.15	6.27	7.36
1-Tetradecene	$C_{14=}$	3.09	4.07	5.15
1-Hexadecene	$C_{16=}$	1.85	2.65	3.61
1-Octadecene	$C_{18=}$	1.11	1.72	2.52
1-Eicosene	$C_{20=}$	0.67	1.12	1.77
Byproducts:				
2-Methyl-1-pentene	b-$C_{6=}$	0.49	0.53	0.57
2-Methyl-1-heptene	b-$C_{8=}$	0.49	0.53	0.57
2-Methyl-1-nonene	b-$C_{10=}$	0.11	0.12	0.13
2-Methyl-1-undecene	b-$C_{12=}$	0.11	0.12	0.13
2-Methyl-1-tridecene	b-$C_{14=}$	0.11	0.12	0.13
2-Methyl-1-pentadecene	b-$C_{16=}$	0.11	0.12	0.13
2-Methyl-1-heptadecene	b-$C_{18=}$	0.11	0.12	0.13
2-Methyl-1-nonadecene	b-$C_{20=}$	0.11	0.12	0.13

6.2.2 Process Simulation

6.2.2.1 Simulation of the Reaction System

The SHOP oligomerization process comprises of two parts, the reaction system and the separation train. This section mainly focuses on the description of the reaction system and the simulation of it in COCO. Figure 6.8 shows the reaction system setup in COCO. The flowsheet consists of the ethylene oligomerization reactor, which forms C_4 – C_{20+} linear olefin products, the separation and recycle of the unreacted ethylene, and the separation and recycle of the organic solvent as well as of the catalyst. In this simulation, the polar organic solvent used is 1,4-butanediol (BDO), which is substantially insoluble in the hydrocarbon product phase (Kister and Lutz, 1977).

The thermodynamic vapor-liquid equilibrium (VLE) model used for the reaction modeling is the Peng-Robinson equation of state with the Universal Mixing Rule (PR-UMR) (Voutsas et al., 2006), which uses the UNIFAC activity coefficient model in the mixing rules. The reason for the change (from PPR78) is because of the need to model strongly non-ideal systems with compounds that have a molecular structure that cannot be represented by the PPR78 model (BDO here).

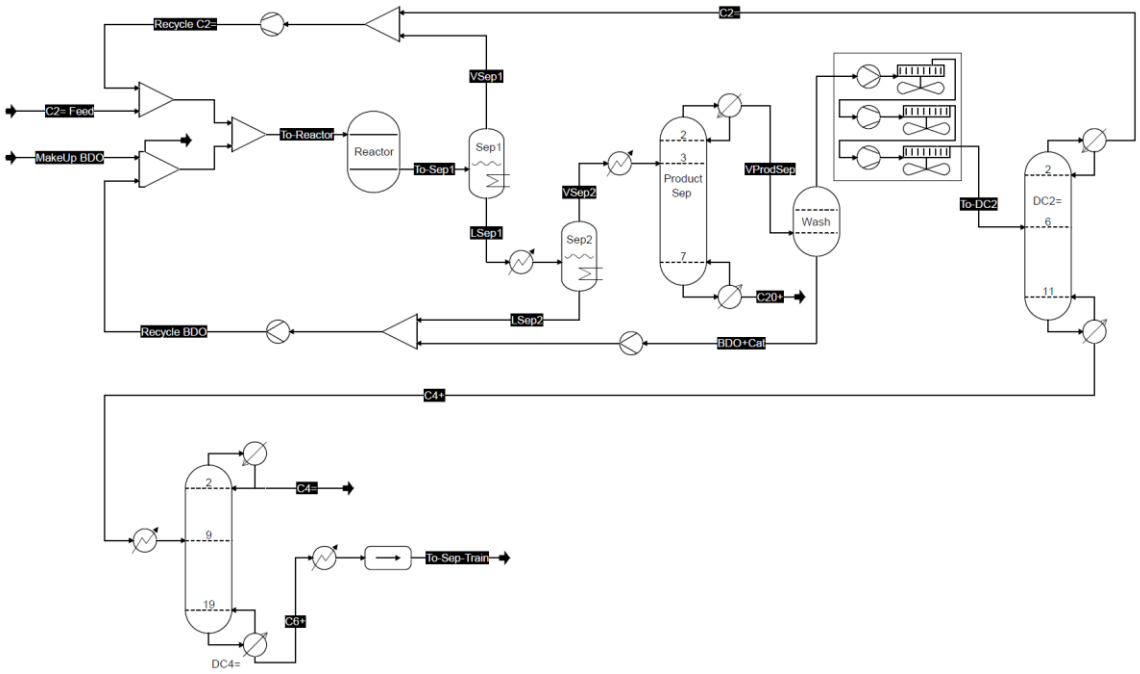

Figure 6.8 Simulation of the oligomerization reaction system in COCO.

A news report in early 2018 stated that Shell's alpha olefin project (also known as the Tiger AO4 Project) in Geismar, Louisiana, was to be commercially operated by the end of 2018 (Veazey, 2018). This project adds 425000 tons of capacity at Geismar, which makes "the site the largest alpha olefin producer in the world." To create a similarly sized process plant, the capacity of the plant in our simulation is set to be about 425000 tons per year, assuming an uptime of 8500 hours (96%/year). The feed flowrate of pure ethylene is therefore set to 50 tons per hour.

According to O'Donnell and Gum (1981), the solvent/oligomer weight ratio is about 10:1. Both the ethylene-rich stream and the BDO-rich stream are mixed together and fed to the reactor. The reaction temperature is preferably from about 70 to 100 ^{o}C (Kister and Lutz, 1977), and here we use 90 ^{o}C in this simulation; the pressure is chosen from the range 20 to 345 bar (300 to 5000 psig) (Kister and Lutz, 1977), and here we use 90 bar in this simulation. We take the growth factor K of the oligomerization reaction a value of 0.65, and assume the ethylene conversion is about 80%. The information of streams 'To-Reactor' and 'To-Sep1' are shown in Table 6.7.

Table 6.7 Simulation results for the oligomerization reactor inlet and outlet streams.

Streams	To-Reactor	To-Sep1
Pressure, bar	90	90
Temperature, ^{o}C	47.4	90
Flowrate, tonne/h	501.07	501.07
Vapor fraction	0.201	0.198
Mass compositions:		
$C_{2=}$	0.1247	0.0249
$C_{4=}$	0.0779	0.0969
$C_{6=}$ + b-$C_{6=}$	0.0299	0.0488
$C_{8=}$ + b-$C_{8=}$	0.0128	0.0293
$C_{10=}$ + b-$C_{10=}$	0.0054	0.0185
$C_{12=}$ + b-$C_{12=}$	0.0023	0.0127
$C_{14=}$ + b-$C_{14=}$	0.001	0.009
$C_{16=}$ + b-$C_{16=}$	0.0004	0.0064
$C_{18=}$ + b-$C_{18=}$	0.0002	0.0047
$C_{20=}$ + b-$C_{20=}$	0.0001	0.0034
BDO	0.7453	0.7453

An essential step is to remove the catalyst in the hydrocarbon phase as soon as possible; this is because polyethylene tends to form when ethylene and nickel complex catalyst exist in a hydrocarbon medium (Kister and Lutz, 1977). The polyethylene has little value, and would reduce the yield, and rapidly foul the downstream equipment.

The stream out of the reactor is a vapor-liquid-liquid three-phase mixture, containing a large amount of solvent (75 wt%). The organic solvent with catalyst in it is mostly

immiscible with the hydrocarbon liquid phase. Before conducting a liquid-liquid separation, removal of the gaseous ethylene using a flash tank (Sep1) is preferred (Kister and Lutz, 1977). The flash (Sep1) is operated at a reduced pressure, 20 bar, and 90 ^{o}C. The vapor cut from the flash, containing mainly ethylene ($C_{2=}$), 1-butene ($C_{4=}$), and 1-hexene ($C_{6=}$), is directed to the reactor as part of the ethylene recycle. The liquid cut from Sep1 is first cooled to 35 ^{o}C, and then directed to a liquid phase separator (Sep2). The liquid-liquid equilibrium (LLE) thermodynamic model in this separation is UNIFAC-LLE.

In the liquid-liquid separator (Sep2), the organic phase, containing BDO and catalyst, is separated at 20 bar and 35 ^{o}C from the hydrocarbon phase, the latter containing mainly the oligomerization reaction products and some dissolved ethylene, as well as a small amount of catalyst. The heavy BDO rich liquid from Sep2 is recycled back to the reactor. The light LAOs rich liquid is first cooled to 27 ^{o}C, and then directed to a vacuum column, which separates the heavies (C_{20+}) via the bottom. The normal boiling point of these heavies are greater than that of BDO (501.15 K). In order to separate the remainder of the BDO for recycle use, the heavies need to be removed first. The product separation column has 8 stages including a partial condenser and a partial reboiler, and the feed stage is stage 3. The column is operated at high vacuum (20 mbar). The reflux ratio is specified to be 0.4, and the fraction of combined feeds recovered at the bottom is very small (only 0.8% on molar base).

After removal of the heavies, a water wash removes all BDO and pumped back to the feed vessel, where recycled BDO is topped up with make-up BDO. Note that in our simulation, the homogeneous catalyst is not actually simulated.

Table 6.8 Inlet and outlet stream information of column DC2=.

Stream	To-DC2	C2=	C4+
Pressure, bar	33	30	30
Temperature, ^{o}C	8.0	54.8	187.4
Flowrate, tonne/h	49.72	0.87	48.85
Vapor fraction	0	1	0
Mass compositions:			
$C_{2=}$	0.0123	0.7032	0
$C_{4=}$	0.1964	0.2967	0.1946
$C_{6=}$ + b-$C_{6=}$	0.1907	0.0002	0.1941
$C_{8=}$ + b-$C_{8=}$	0.1673	0	0.1703
$C_{10=}$ + b-$C_{10=}$	0.1329	0	0.1353
$C_{12=}$ + b-$C_{12=}$	0.1044	0	0.1063
$C_{14=}$ + b-$C_{14=}$	0.0799	0	0.0813
$C_{16=}$ + b-$C_{16=}$	0.0604	0	0.0614
$C_{18=}$ + b-$C_{18=}$	0.0451	0	0.0459
$C_{20=}$ + b-$C_{20=}$	0.0106	0	0.0108
BDO	0	0	0

To separate the remaining ethylene from the olefin products, the stream from the top of the water wash column is pressured to 33 bar via a three-stage compressor. The resulting liquid stream at 88 ^{o}C is directed to a distillation column (DC2=) to remove ethylene. The DC2= has 12 stages (this includes the partial condenser and the reboiler), with the feed at stage 6. Column pressure is assumed constant at 30 bar. The reflux ratio is 0.2, and the mole fraction of ethylene in the bottoms is specified to be 10^{-5}. Table 6.8 shows the feed and products of the column DC2=. The overhead product (C2=) is recycled and mixed with the vapor cut from Sep1 and then pressurized through a compressor back to the feed pressure of 90 bar.

6.2.2.2 Products Separation Using a Direct Sequence

Stream 'C4+' contains olefins ranging from $C_{4=}$ to $C_{18=}$, with a trace amount of $C_{20=}$. The product mixture is first separated to different fractions using conventional direct sequence of distillation columns. Figure 6.9 shows the flowsheet of product separation using the conventional method simulated in COCO, where the feed (C4+) is separated to seven fractions (i.e. streams C4=, C6=, C8=, C10=, C12=, C14=, and C16=, C18=) using six conventional columns in a direct sequence.

The feed stream C4+ is cooled down to 100 ^{o}C before it enters column DC4=; the pressure drop of the cooler is 0.5 bar. Column DC4= has 20 stages with a total condenser and a reboiler counted as two equilibrium stages; the feed enters the column from stage 9. The condenser pressure is 7 bar, and the reboiler pressure is 7.6 bar. Since this column separates 1-butene ($C_{4=}$) from heavier alkenes, the heavy key component in this column is 1-hexene ($C_{6=}$). The mole fraction of $C_{6=}$ in the distillate is specified to 0.001, while the recovery of $C_{4=}$ in the bottoms is specified to 0.001. The purity of stream 'C4=' is shown in Table 6.9, where the mass fraction of $C_{4=}$ and b-$C_{4=}$ is 99.89 wt%.

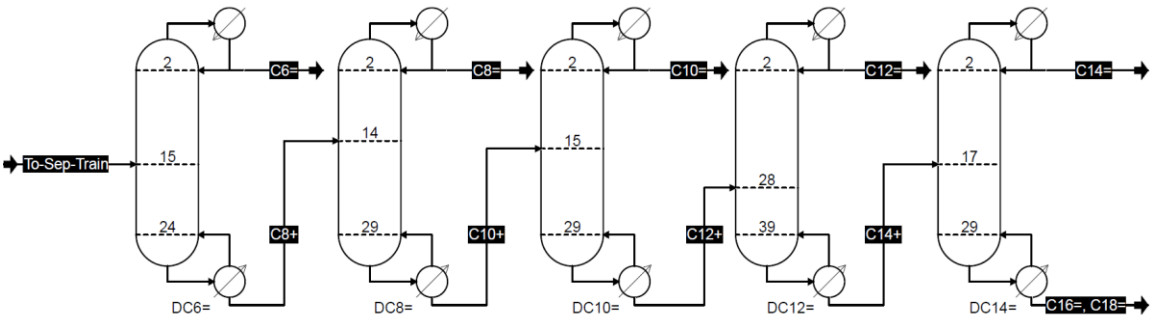

Figure 6.9 Flowsheet of α-olefin product separation using conventional direct sequence of columns.

The bottom stream (C_{6+}) from the column DC4= is cooled down from 197 ^{o}C to 80 ^{o}C before it enters column DC6=. After the DC4= column we switch thermodynamic models from PR-UMR to modified UNIFAC. The reason for using two different models is because the PR-UMR model is more suitable for modeling processes at high pressure operations –

this model is mainly used in the first part of the flowsheet – the columns after DC4= are operated at atmospheric or vacumm pressures, where the modified UNIFAC model (Weidlich and Gmehling, 1987; Lohmann et al., 2001) would be expected to be superior.

The column DC6= removes 1-hexene ($C_{6=}$) in the distillate. This column has 25 stages with a feed stream entering at stage 15. The condenser pressure is 1.1 bar with a pressure drop of 0.3 bar; the reboiler pressure is 1.8 bar. The reflux ratio of this column is 0.6, and the recovery of $C_{6=}$ at the bottom is specified to 0.001. The purity of stream C6= is shown in Table 6.9, where the sum of the fractions of $C_{6=}$ and b-$C_{6=}$ is 99.85 wt%.

Similar specifications are provided for the remaining four columns (DC8=, DC10=, DC12=, and DC14=). Details of the column setup in COCO are summarized in Table 6.10. The Fenske-Underwood-Gilliland (FUG) short-cut methods are employed to determine the minimum theoretical stages and minimum reflux ratio in each column. The actual reflux ratio is taken to be about 1.2 times the minimum value. A McCabe-Thiele diagram was used to optimize the feed stage in each column.

Table 6.9 Summary of the product streams simulated with the conventional method.

Stream	C6=	C8=	C10=	C12=	C14=	C16=, C18=
Pressure, bar	1.1	1.1	0.1	0.1	0.1	0.15
Temperature, °C	65.9	124.1	97.5	135.2	169.3	221.5
Flowrate, tonne/h	9.47	8.32	6.61	5.20	3.96	5.78
Mass compositions:						
$C_{2=}$	0	0	0	0	0	0
$C_{4=}$	0.0010	0	0	0	0	0
$C_{6=}$ + b-$C_{6=}$	0.9990	0.0011	0	0	0	0
$C_{8=}$ + b-$C_{8=}$	0	0.9985	0.0012	0	0	0
$C_{10=}$ + b-$C_{10=}$	0	0.0003	0.9986	0.0013	0	0
$C_{12=}$ + b-$C_{12=}$	0	0	0.0001	0.9987	0.0006	0
$C_{14=}$ + b-$C_{14=}$	0	0	0	0	0.9991	0.0020
$C_{16=}$ + b-$C_{16=}$	0	0	0	0	0.0003	0.5189
$C_{18=}$ + b-$C_{18=}$	0	0	0	0	0	0.3875
$C_{20=}$ + b-$C_{20=}$	0	0	0	0	0	0.0915

The sum of the mass fractions of α-olefin and the corresponding branched olefin are shown for each product stream in Table 6.10. The simulation results of condenser and reboiler temperatures and duties in each column are also summarized in Table 6.10. The sum of the reboiler duties in these columns is an estimation of the total energy requirement, which is 8.54 MW for the conventional separation method.

Table 6.10 Summary of column specifications and some simulation results.

Column Specification	DC6=	DC8=	DC10=	DC12=	DC14=
Number of stages	25	30	30	40	30
Feed stage	15	14	15	28	17
Pressures (bar):					
Condenser pressure	1.1	1.1	0.1	0.1	0.1
Condenser pressure drop	0.3	0.3	0.05	0.02	0.02
Reboiler pressure	1.8	1.8	0.25	0.25	0.15
Top Specs:					
Reflux ratio	0.6	1.2	2.0	2.3	1.7
Bottom Specs:					
Recovery of the light key*	0.001	0.001	0.001	5.00E-04	0.003
Simulation Results:					
Boilup ratio	1.4	1.3	0.6	2.0	1.8
Condenser temperature, ^{o}C	65.9	124.1	97.5	135.2	169.3
Reboiler temperature, ^{o}C	178.5	227.4	183.5	214.4	221.5
Condenser duty, MW	-1.47	-1.65	-1.84	-1.47	-0.87
Reboiler duty, MW	3.41	2.13	0.73	1.51	0.77
Sum of reboiler duties, MW			8.54		

* The light key components in each column are $C_{6=}$, $C_{8=}$, $C_{10=}$, $C_{12=}$, $C_{14=}$

6.2.2.3 Product Separation with DWCs

In this section we consider replacing the conventional columns in the product separation part, in Figure 6.9, with DWCs. Table 6.10 indicates that columns DC6= and DC8= have similar operating pressures, and columns DC10=, DC12=, and DC14= operate at more or less the same pressure. Therefore, columns DC6= and DC8= can be combined into a DWC operating at about 1.1 bar, and columns DC10=, DC12=, and DC14= can also be combined.

All the dividing wall columns modeled in this section employ the standard DWC module, discussed in Chapter 2. The use of the PCM considerably reduces the time and effort in setting up, and converging a DWC simulation, no matter the column configuration.

Combining DC6= and DC8=

Columns DC6= and DC8= are combined into a three-product DWC with the wall in the center of the column. The top product of the dividing wall column is 1-hexene ($C_{6=}$), the sidedraw product is 1-octene ($C_{8=}$), and the bottom stream is C10+.

For the design of this DWC, we first use a very large number of stages (300 in this case) to find out the minimum (or close to the minimum) reflux ratio necessary to attain particular product purities. When the purity requirements are satisfied, one then needs to vary the vapor and liquid split ratios to reduce the reflux and boilup ratios in order to lower the energy consumption. Then for the final design, we take about 1.2 times the minimum reflux ratio as the actual value, and gradually reduce the number of stages in each section to ensure that the column configuration can still reach the required purities.

The DWC was modeled initially with 300 stages in total, 75 stages in each section, assuming equal number of stages in each column section; the feed and sidedraw positions are in the middle of their respective section (c.f. Figure 2.1 in Chapter 2). The condenser pressure is 1.1 bar, with a pressure drop of 0.3 bar; all other stages (this includes the

reboiler) are assumed at constant pressure 1.4 bar. The liquid sidedraw flowrate is specified to be 8323 kg/h. The column design requires the sum of mass fractions of $C_{6=}$ and b-$C_{6=}$ reaches 99.90 wt% in the distillate, while the sum of the mass fractions of $C_{8=}$ and b-$C_{8=}$ reaches 99.85 wt% in the liquid sidedraw. Vapor and liquid split ratios are both initially 50% / 50%.

After running simulations at different vapor and liquid split ratios, we found that, with fixed product purities, changing the vapor and liquid split ratios in a simulation can result in different reflux ratio and boilup ratio. Therefore, the minimum reflux ratio can be found by varying the split ratios.

We varied the liquid split ratio from 0.10 (this means 10% liquid flows to the left side of the wall) to 0.50, and vapor split ratio from 0.45 (this means 45% vapor flows to the left side of the wall) to 0.75, the change of reflux ratio is plotted in Figure 6.10. It is obvious that, in this particular case, increasing the vapor split ratio, or decreasing the liquid split ratio, can decrease reflux ratio. The minimum (or close to minimum) reflux ratio is found to be 1.36 at a combination of vapor split ratio 0.74 and liquid split ratio 0.10. Hence, we take 1.6 as the actual reflux ratio for this DWC.

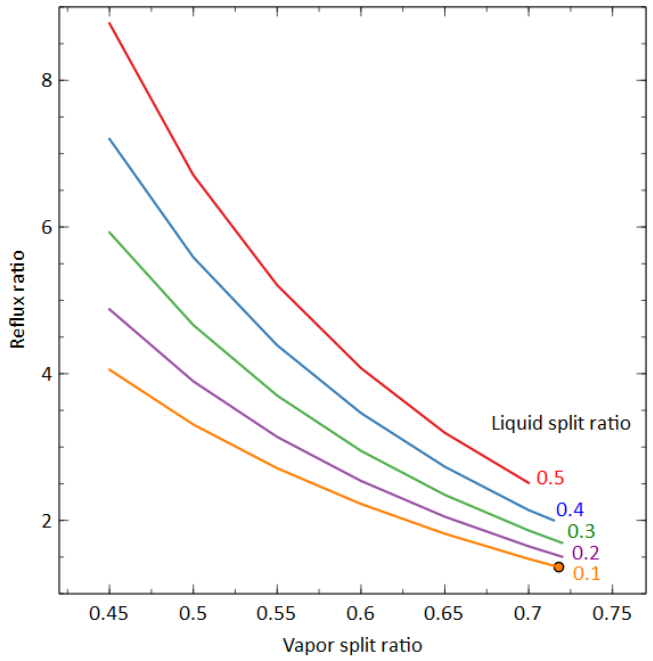

Figure 6.10 Reflux ratio as a function of vapor and liquid split ratios (point indicates the found minimum reflux ratio)

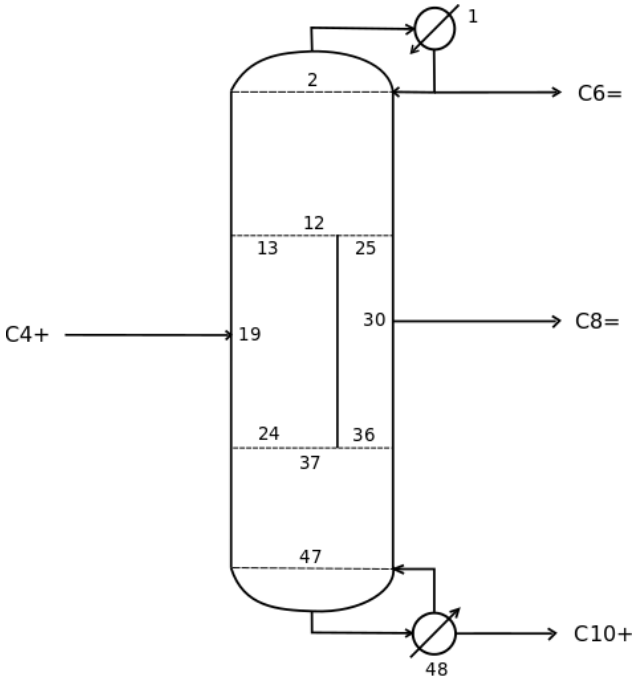

Figure 6.11 DWC configuration separating $C_{6=}$ and $C_{8=}$.

Then, we gradually decrease the number of stages in each section, while keeping the product purities in the top and middle products unchanged. A potential DWC configuration is shown in Figure 6.11 with 12 theoretical stages in each section. The reflux ratio that gives the required purities is 1.6; the vapor and liquid split ratios are 0.77 and 0.21, respectively. The dividing wall is off-centered to the right, as more vapor flows to the left side of the wall.

It is worth noting that when solving this DWC simulation, we found multiple solutions! Perhaps it is because product purities are specified in the simulation, and there is more than one way to reach that purity. The reflux ratio in the second solution is 1.92. Temperature profiles and flowrate profiles of two solutions for this DWC simulation are shown in Figure 6.12 and Figure 6.13 (we do not know how many solutions in total exist). It should be noted that the multiple solutions here belong to the category of "input multiple steady states" where the product purities are specified; they are not in the same category as the MSS reported in Chapter 5. In this case, we take Solution one with the reflux ratio of 1.6 in our simulation.

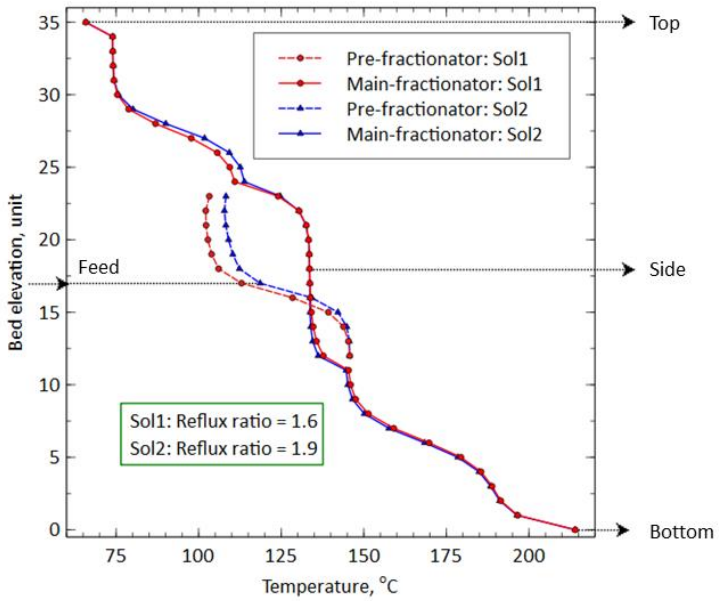

Figure 6.12 Two solutions of the temperature profiles of the DWC simulation.

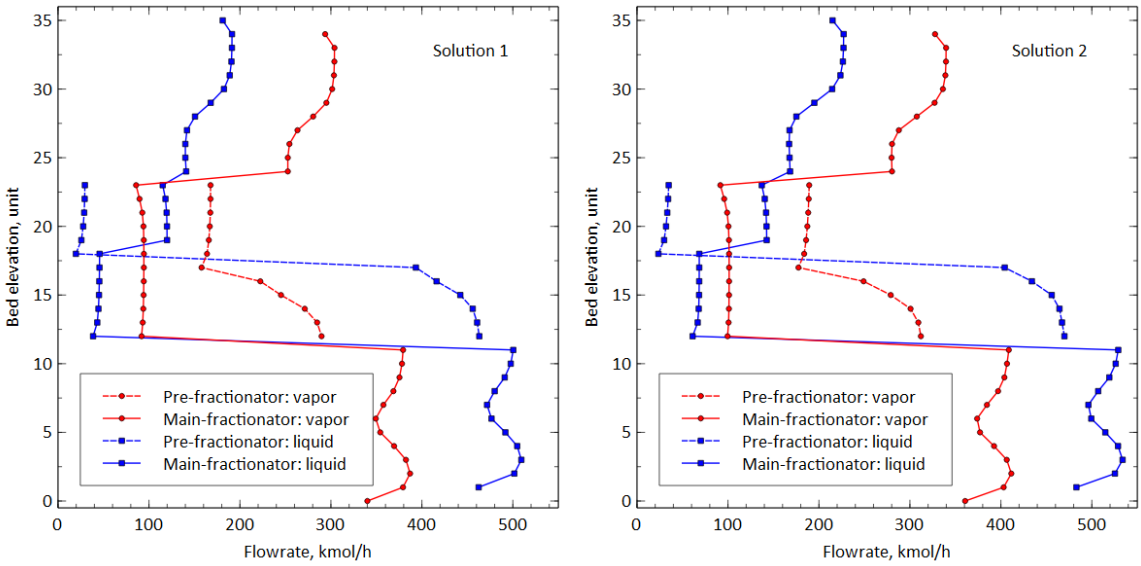

Figure 6.13 Two solutions of the flowrate profiles of the DWC simulation.

Combining DC10=, DC12=, and DC14=

There are more possible configurations. A more straightforward way is to use a four-product DWC; available options are, for example, the Kaibel column with one wall, the satellite column system with two walls (discussed in Section 2.2.2), and the fully extended Petlyuk column with three walls (see Dejanović et al., 2011). The Kaibel column is not a wise choice, since the required purity for each product cut is quite high (>99.85 wt%), and it may require a large number of stages between the two sidedraws to get two high-purity sidedraws. The fully extended Petlyuk column as yet has no industrial application, mainly because of its complexity in design and control. Therefore, for a four-product DWC, we choose the satellite configuration with two walls. In order to distinguish different configurations, we give names to them according to the number of product streams each column processes. For example, the configuration comprised of a three-product DWC (replacing columns DC6= and DC8=) and a four-product DWC (replacing columns DC10= to DC14=) is named configuration “3-4”.

Other options include combining two conventional columns into a three-product DWC, while leaving the other column a conventional two-product column. In the following discussion, columns DC10= and DC12= are combined into a three-product DWC. Based on where the heavies ($C_{16=}$, $C_{18=}$) will go, two different configurations, namely "3-3-2" and "3-2-3", are possible.

6.2.2.3.1 Configuration "3-3-2"

Figure 6.14 shows the flowsheet for configuration "3-3-2". The columns DC6= and DC8= in Figure 6.9 are replaced with the DWC1, and columns DC10= and DC12= are replaced with the DWC2. The number of columns reduces from five to three. Similar to the simulation setup for DWC1 (discussed above), the DWC2 has 72 stages in total, with each section containing 18 stages. Feed and sidedraw stages are 29 and 46, respectively (this follows the way of numbering stages in the PCM). The condenser pressure is at 0.1 bar, with a pressure drop of 0.04 bar; the pressures of all other stages are assumed constant at 0.14 bar. Liquid sidedraw mass flowrate is specified to 5195 kg/h. Product purities of $C_{10=}$ in the distillate and $C_{12=}$ in the sidedraw are specified to guarantee the mass fraction of both ($C_{10=}$ + b-$C_{10=}$) and ($C_{12=}$ + b-$C_{12=}$) reach 99.85 wt%. Vapor and liquid split ratios are adjusted to lower the boilup ratio, which is considered proportional to the energy consumption. It is essential to mention that when varying the vapor and liquid split ratios, multiple solutions similar to the one shown in Figure 6.12 and Figure 6.13 are found; it also poses some convergence problems as the simulation becomes extremely difficult to converge if the initial guess happens to be in the vicinity of two solutions that are "close" to each other. In this case, we found the vapor and liquid split ratios are 0.59 and 0.50, respectively.

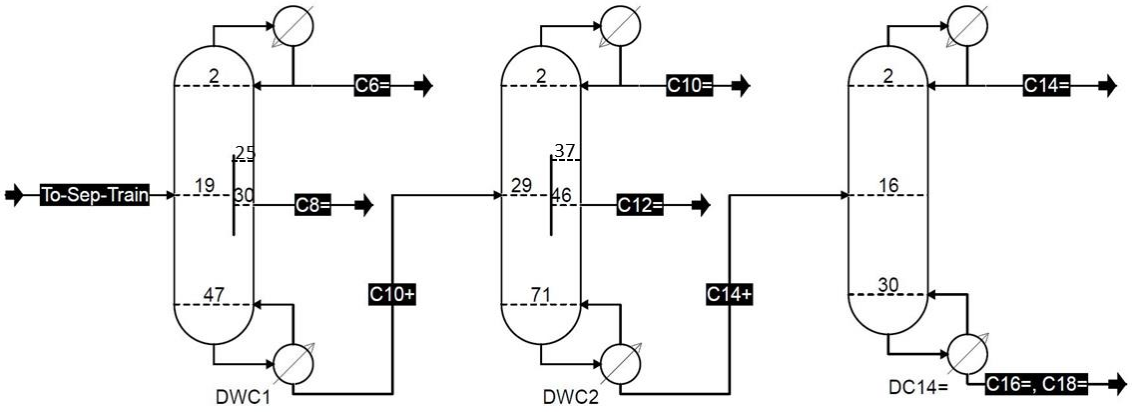

Figure 6.14 Flowsheet of the "3-3-2" configuration.

The last column (DC14=) is a conventional column similar to the last column in Figure 6.9. The column condenser operates at 0.1 bar, with a pressure drop of 0.02 bar; the reboiler pressure is 0.15 bar. The FUG short-cut method estimates that the number of stages is about 30, with feed from stage 16. We specify the distillate purity to ensure that ($C_{14=}$ + b-$C_{14=}$) is no less than 99.85 wt%; the smallest boilup ratio is found to be 2.3 by conducting a parametric study. A comparison of the required hardware between the conventional columns configuration and the "3-3-2" configuration is shown in Table 6.11. Both configurations have more or less the same total number of stages; the "3-3-2" configuration requires 4 fewer heat exchangers, and 2 fewer column shells. The simulation results are summarized in Table 6.12.

The condenser and reboiler temperatures and heat duties of each column are summarized in Table 6.11. A comparison in Table 6.11 indicates that the configuration "3-3-2" requires 24% less energy than the conventional direct sequence configuration.

Table 6.11 Comparison between the conventional and the "3-3-2" configurations.

	Conventional					"3-3-2"		
	DC6=	DC8=	DC10=	DC12=	DC14=	DWC1	DWC2	DC14=
Number of stages	25	30	30	40	30	48	72	30
Sum of stages			155				151	
Number of HE*			10				6	
Pressure, bar:								
Cond** pressure	1.1	1.1	0.1	0.1	0.1	1.1	0.1	0.1
Cond** pressure drop	0.3	0.3	0.05	0.02	0.02	0.3	0.03	0.02
Reb** pressure	1.8	1.8	0.25	0.25	0.15	1.4	0.14	0.15
Reflux ratio	0.6	1.2	2.0	2.3	1.7	1.6	2.1	1.7
Boilup ratio	1.4	1.3	0.6	2.0	1.8	2.8	1.2	2.2
Vapor split ratio	-	-	-	-	-	0.77	0.59	-
Liquid split ratio	-	-	-	-	-	0.21	0.50	-
Simulation results:								
Cond T, °C	65.9	124.1	97.5	135.2	169.3	65.8	97.5	169.2
Reb T, °C	178.5	227.4	183.5	214.4	221.5	214.0	195.1	221.7
Cond duty, MW	-1.47	-1.65	-1.84	-1.47	-0.87	-2.40	-1.89	-0.88
Reb duty, MW	3.41	2.13	0.73	1.51	0.77	4.66	0.92	0.92
Sum of Reb duties, MW			8.54				6.49	

* HE: heat exchangers

** Cond: condenser, Reb: reboiler

Table 6.12 Summary of the product streams simulated with the configuration "3-3-2".

Streams	C6=	C8=	C10=	C12=	C14=	C16=, C18=
Pressure, bar	1.1	1.4	0.1	0.14	0.1	0.15
Temperature, °C	65.8	133.6	97.5	144.6	169.2	221.5
Flowrate, tonne/h	9.47	8.32	6.60	5.19	3.97	5.78
Mass compositions:						
$C_{2=}$	0	0	0	0	0	0
$C_{4=}$	0.0010	0	0	0	0	0
$C_{6=}$ + b-$C_{6=}$	0.9990	0.0003	0	0	0	0
$C_{8=}$ + b-$C_{8=}$	0	0.9985	0.0015	0	0	0
$C_{10=}$ + b-$C_{10=}$	0	0.0013	0.9985	0.0007	0	0
$C_{12=}$ + b-$C_{12=}$	0	0	0	0.9987	0.0008	0
$C_{14=}$ + b-$C_{14=}$	0	0	0	0.0005	0.9991	0.0003
$C_{16=}$ + b-$C_{16=}$	0	0	0	0	0.0001	0.5199
$C_{18=}$ + b-$C_{18=}$	0	0	0	0	0	0.3882
$C_{20=}$ + b-$C_{20=}$	0	0	0	0	0	0.0917

6.2.2.3.2 Configuration "3-2-3"

Figure 6.15 shows the simulation of the "3-2-3" configuration in COCO. Five columns in Figure 6.9 reduce to only three columns with the addition of a pump. After the DWC1, the heavies ($C_{16=}$, $C_{18=}$) are separated first, then $C_{10=}$, $C_{12=}$, and $C_{14=}$ are separated in the DWC2. By removing the heavies first, the last DWC is a "clean" column that separates three almost pure components. In addition, $C_{10=}$ to $C_{14=}$ are important products in the detergent range, this configuration could be superior in terms of the product quality.

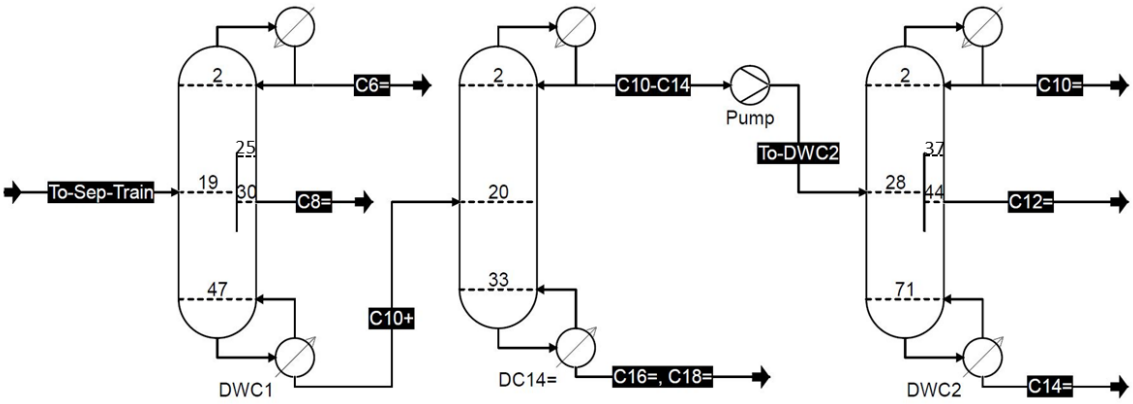

Figure 6.15 Flowsheet of the "3-2-3" configuration.

The bottom stream from the DWC1 (C10+) is directed to DC14= to separate $C_{14=}$ from $C_{16=}$. According to the FUG short-cut method, the number of stages in this column is about 34, with feed entering from stage 20. The condenser pressure is 0.1 bar, with a pressure drop of 0.02 bar; the reboiler pressure is 0.15 bar. The reflux ratio in this column is set to 0.33, and, at the bottom, $C_{14=}$ recovery is specified to be 0.002.

The top stream from the column DC14= contains mainly $C_{10=}$ to $C_{14=}$ olefins, which is directed to a pump to increase the pressure to 0.2 bar. The pressurized stream is then sent to the DWC2 for further separation.

DWC2 has 72 stages in total, with 18 stages in each section. Feed and sidedraw stages are 28 and 44, respectively (these numbers are the stage numbers in the PCM). The

condenser pressure is 0.1 bar, with a pressure drop of 0.04 bar; pressures of all other stages in this column are assumed constant at 0.14 bar. Column top and bottom product purities are specified to ensure that the mass fractions of ($C_{10=}$ + b-$C_{10=}$) and ($C_{14=}$ + b-$C_{14=}$) are both above 99.85 wt%. The liquid sidedraw flowrate is adjusted to control the purity of $C_{12=}$, which turns out to be 5199 kmol/h. Vapor and liquid split ratios of 0.78 and 0.30, respectively, result in a small boilup ratio, thus a low energy requirement.

Table 6.13 compares the hardware requirements between the conventional and the "3-2-3" configurations. Both configurations require more or less the same number of theoretical stages; the "3-2-3" configuration requires 4 less heat exchangers and 2 less columns shells, but one more pump, which will add considerably to the capital cost.

Table 6.14 summarizes the results of some streams in the configuration "3-2-3". All the product steams reach the required purity. A comparison in Table 6.13 shows that the configuration "3-2-3" saves 13% energy compared to the conventional separation train. It should not come with surprise that the configuration "3-3-2" saves much more energy than the configuration "3-2-3", since more energy is needed to vaporize the $C_{10=}$ to $C_{14=}$ contents in the "3-2-3" configuration.

Table 6.13 Comparison between the conventional and the "3-2-3" configurations.

	Conventional					"3-2-3"		
	DC6=	DC8=	DC10=	DC12=	DC14=	DWC1	DC14	DWC2
Number of stages	25	30	30	40	30	48	72	34
Sum of stages			155				154	
Number of HE*			10				6	
Pressures, bar								
Cond** pressure	1.1	1.1	0.1	0.1	0.1	1.1	0.1	0.1
Cond** pressure drop	0.3	0.3	0.05	0.02	0.02	0.3	0.02	0.04
Reb** pressure	1.8	1.8	0.25	0.25	0.15	1.4	0.15	0.14
Reflux ratio	0.6	1.2	2.0	2.3	1.7	1.6	0.3	1.4
Boilup ratio	1.4	1.3	0.6	2.0	1.8	2.8	2.5	5.6
Vapor split ratio	-	-	-	-	-	0.77	-	0.78
Liquid split ratio	-	-	-	-	-	0.21	-	0.30
Simulation results:								
Cond T, °C	65.9	124.1	97.5	135.2	169.3	65.8	112.9	97.5
Reb T, °C	178.5	227.4	183.5	214.4	221.5	214.0	221.6	179.1
Cond duty, MW	-1.47	-1.65	-1.84	-1.47	-0.87	-2.40	-2.18	-1.48
Reb duty, MW	3.41	2.13	0.73	1.51	0.77	4.66	1.04	1.71
Sum of Reb duties, MW			8.54				7.41	

* HE: heat exchangers

** Cond: condenser, Reb: reboiler

Table 6.14 Summary of streams information in the configuration “3-2-3”.

Streams	C6=	C8=	C10-C14	C16=, C18=	C10=	C12=	C14=
Pressure, bar	1.1	1.4	0.1	0.15	0.1	0.14	0.14
Temperature, °C	65.8	133.6	112.9	221.6	97.5	144.6	179.1
Flowrate, tonne/h	9.47	8.32	15.76	5.78	6.60	5.20	3.96
Mass compositions:							
$C_{2=}$	0	0	0	0	0	0	0
$C_{4=}$	0.0010	0	0	0	0	0	0
$C_{6=}$ + b-$C_{6=}$	0.9990	0.0003	0	0	0	0	0
$C_{8=}$ + b-$C_{8=}$	0	0.9985	0.0006	0	0.0013	0	0
$C_{10=}$ + b-$C_{10=}$	0	0.0012	0.4185	0	0.9987	0.0006	0
$C_{12=}$ + b-$C_{12=}$	0	0	0.3293	0	0	0.9985	0.0004
$C_{14=}$ + b-$C_{14=}$	0	0	0.2514	0.0013	0	0.0009	0.9992
$C_{16=}$ + b-$C_{16=}$	0	0	0.0001	0.5192	0	0	0.0004
$C_{18=}$ + b-$C_{18=}$	0	0	0	0.3878	0	0	0
$C_{20=}$ + b-$C_{20=}$	0	0	0	0.0916	0	0	0

6.2.2.3.3 Configuration “3-4”

The configuration “3-4” combines the columns DC10=, DC12=, and DC14= into one DWC with two walls. Figure 6.16 shows the flowsheet of the “3-4” configuration simulated in COCO; the total number of columns decreases from five, in Figure 6.9, to only two. The sum of the number of stages in columns DC10=, DC12=, and DC14= are 100; in order not to add too much capital cost, the four-product DWC (DWC2) has 110 stages. The DWC2 takes the column configuration of the satellite column system in Figure 2.8, discussed in Chapter 2. The feed enters the column from stage 55; two sidedraws are taken from stages 24 and 85, respectively (the numbers here are the stages numbered in the PCM). The condenser pressure is 0.1 bar, with a pressure drop of 0.05 bar; all the other stages (this includes the reboiler) are assumed at constant pressure 0.15 bar.

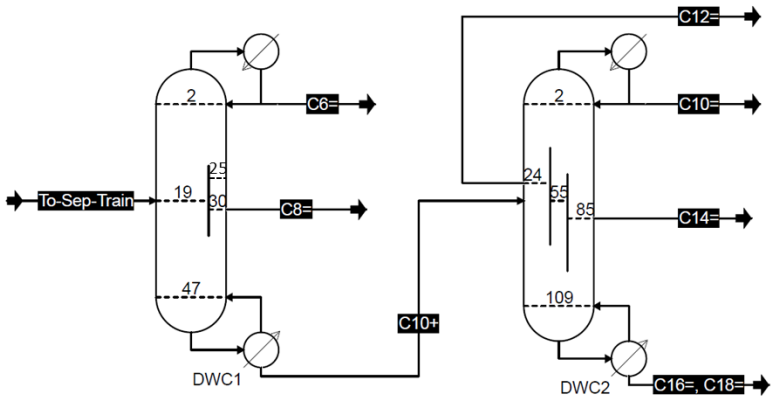

Figure 6.16 Flowsheet of the "3-4" configuration.

The liquid sidedraw from stage 24 has mass flowrate 5199 kg/h, and the other liquid sidedraw has a mass flowrate 3962 kg/h. The purities of $C_{10=}$ and $C_{14=}$ are, respectively, specified for the column top product and the sidedraw product from stage 85; by adjusting the specified values, we aim to reach 99.85 wt% for the sum of α-olefins and branched olefins in each product stream. When the purities are satisfied, varying the vapor and liquid split ratios can change the reflux ratio, as well as the boilup ratio, which relates to the energy consumption of this column system.

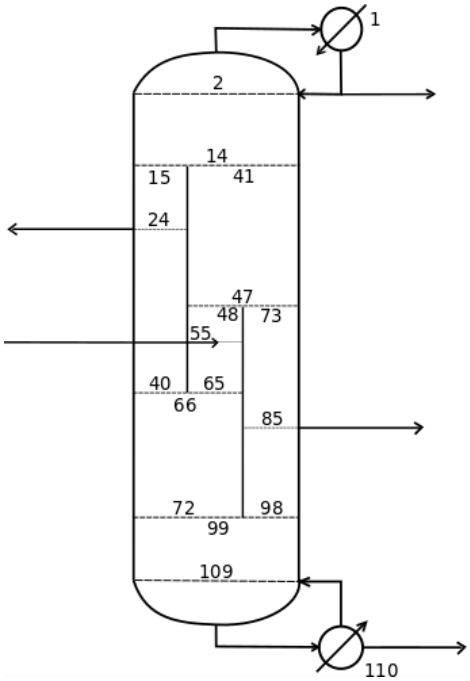

Figure 6.17 Diagram of the DWC2 in the "3-4" configuration (numbers indicate stage numbers in the PCM).

Figure 6.17 shows a close look of the DWC2 configurations. With extensive simulations, we found that when the liquid split ratio from stage 14 to stage 15 is 0.45, the liquid split ratio from stage 47 to stage 48 is 0.26, the vapor split ratio from stage 66 to stage 40 is 0.59, the vapor split ratio from stage 99 to stage 72 is 0.59, the boilup ratio is close to the minimum; therefore, at this combination of the split ratios, the energy consumption is low.

Table 6.15 compares the hardware requirements between the conventional and the “3-4” configurations. Both configurations require more or less the same number of theoretical stages, while the “3-4” configuration requires 6 less heat exchangers and 3 less column shells.

Product purities are summarized in Table 6.16, with all the products reach their purity requirements. A comparison with the reboiler heat duties in Table 6.15 indicates that the “3-4” configuration requires 17% less energy.

Table 6.15 Comparison between the conventional and the "3-4" configurations.

	Conventional					"3-4"	
	DC6=	DC8=	DC10=	DC12=	DC14=	DWC1	DWC2
Number of stages	25	30	30	40	30	48	110
Sum of stages			155			158	
Number of HE*			10			4	
Pressures, bar							
Cond** pressure	1.1	1.1	0.1	0.1	0.1	1.1	0.1
Cond** pressure drop	0.3	0.3	0.05	0.02	0.02	0.3	0.05
Reb** pressure	1.8	1.8	0.25	0.25	0.15	1.4	0.15
Reflux ratio	0.6	1.2	2.0	2.3	1.7	1.6	4.4
Boilup ratio	1.4	1.3	0.6	2.0	1.8	2.8	5.8
Vapor split ratio	-	-	-	-	-	0.77	(See text)
Liquid split ratio	-	-	-	-	-	0.21	(See text)
Simulation results:							
Cond T, °C	65.9	124.1	97.5	135.2	169.3	65.84	97.51
Reb T, °C	178.5	227.4	183.5	214.4	221.5	214.02	221.64
Cond duty, MW	-1.47	-1.65	-1.84	-1.47	-0.87	-2.40	-3.35
Reb duty, MW	3.41	2.13	0.73	1.51	0.77	4.66	2.45
Sum of Reb duties, MW			8.54			7.11	

* HE: heat exchangers

** Cond: condenser, Reb: reboiler

Table 6.16 Summary of the product stream information in the configuration "3-4".

Streams	C6=	C8=	C10=	C12=	C14=	C16=, C18=
Pressure, bar	1.1	1.4	0.1	0.14	0.1	0.15
Temperature, °C	65.9	133.6	97.5	144.6	169.2	221.5
Flowrate, tonne/h	9.48	8.32	5.60	5.20	3.96	5.78
Mass compositions:						
$C_{2=}$	0	0	0	0	0	0
$C_{4=}$	0.0010	0	0	0	0	0
$C_{6=}$ + b-$C_{6=}$	0.9990	0.0003	0	0	0	0
$C_{8=}$ + b-$C_{8=}$	0	0.9985	0.0013	0	0	0
$C_{10=}$ + b-$C_{10=}$	0	0.0012	0.9987	0.0000	0	0
$C_{12=}$ + b-$C_{12=}$	0	0	0	0.9986	0.0005	0
$C_{14=}$ + b-$C_{14=}$	0	0	0	0.0014	0.9991	0.0004
$C_{16=}$ + b-$C_{16=}$	0	0	0	0	0.0004	0.5197
$C_{18=}$ + b-$C_{18=}$	0	0	0	0	0	0.3882
$C_{20=}$ + b-$C_{20=}$	0	0	0	0	0	0.0917

6.2.3 Simulations at Different Growth Factors

The oligomerization reaction products follow the Schulz-Flory type distribution that is characterized by the growth factor, *K*; see Figure 6.7. The previous simulations described in the preceding section were conducted at *K* = 0.65, and in this section, we attempt to find one configuration that can obtain products at all three K-factors, 0.60, 0.65, and 0.70.

The specifications for columns in the separation trains remain unchanged, where the reflux ratio at the column top and component recovery at the bottom are specified. Four different configurations, namely the conventional direct sequence, the "3-3-2" configuration, the "3-2-3" configuration, and the "3-4" configuration, are investigated at K-factor equals 0.60, 0.65, and 0.70, and the separation at *K* = 0.65 has already been discussed.

At K-factor equals 0.60, with the same specifications as the K-factor equals 0.65, the product purities from the conventional direct sequence are only slightly affected; all the product purities are still above 99.85 wt%, and hence no change is required in this configuration. The product purities from the "3-3-2" configuration are significantly different when the K-factor is changed from 0.65 to 0.60, the purities of $C_{6=}$ and $C_{12=}$ have dropped to less than 99.85 wt%, although the others remain above the required purity. Similar behavior is observed in the "3-2-3" and "3-4" configurations. Simply adjusting the sidedraw flowrates and column reflux rates in the columns can bring all of the purities back to the required value.

At K-factor equals 0.70, with the same specifications as the K-factor equals 0.65, the $C_{8=}$ purity in the conventional direct sequence drops from 99.85 wt% to 99.19 wt%, while the other purities are still above the required value. Slightly increasing the reflux rate in the column DC8= can increase the purity to 99.85 wt%. In the other three configurations with DWCs, more than two products fail to meet the purity requirement. However, the product purities in DWC1 cannot meet the requirement (this applies to all three configurations with DWCs), although all other product purities can be increased by adjusting the

sidedraw flowrates and the reflux rates in the columns. The possible reasons for this could be either the DWC1 has too few stages to achieve the necessary separation, or the preceding column separating $C_{4=}$ is insufficiently complete that some $C_{4=}$ slips through to contaminate the top of the DWC1.

In the new flowsheet shown in Figure 6.8 we change the specification in the column DC4= by tightening the recovery specification in the bottoms from 0.001 to 0.0001, so the amount of $C_{4=}$ in the bottoms significantly decreases. Figure 6.18 shows the new flowsheet of the "3-3-2" configuration, where the first DWC has 72 stages in total, with each section containing 18 stages (these include the condenser and reboiler). Here we discuss the use of the "3-3-2" configuration to separate oligomerization reaction products to high purities at three different K-factors.

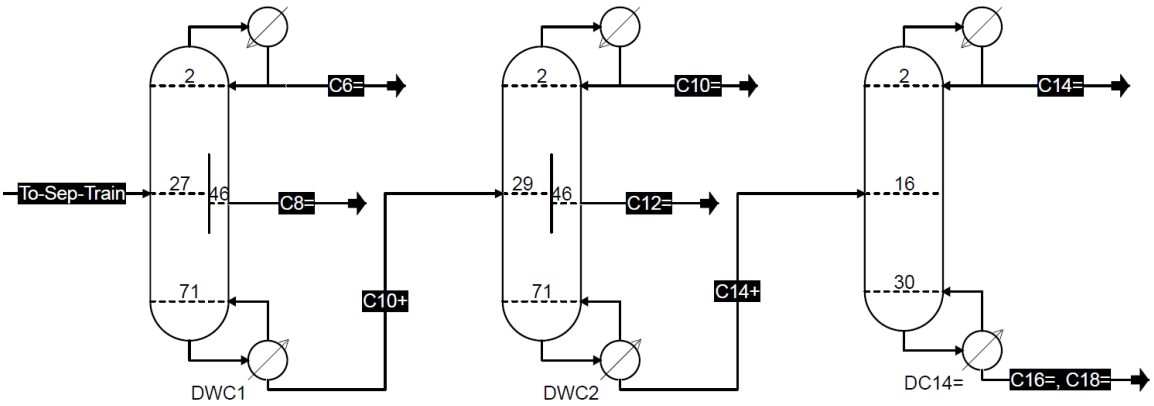

Figure 6.18 New flowsheet of the "3-3-2" configuration.

At K-factor equals 0.60, the purities obtained from the conventional direct sequence are 99.92 wt% for $C_{6=}$, 99.89 wt% for $C_{8=}$, 99.99 wt% for $C_{10=}$, 99.99 wt% for $C_{12=}$, and 99.98 wt% for $C_{14=}$. The same separation is obtained by using the "3-3-2" configuration, and Table 6.17 summarizes the simulation results in both configurations. The resulting energy saving of the "3-3-2" configuration is about 20%, compared to the corresponding conventional direct sequence at K-factor equals 0.60.

Table 6.17 Comparison between the conventional and the "3-3-2" configurations for separations at K-factor equals 0.60.

	Conventional					"3-3-2"		
	DC6=	DC8=	DC10=	DC12=	DC14=	DWC1	DWC2	DC14=
Number of stages	25	30	30	40	30	72	72	31
Sum of stages			155				175	
Number of HE*			10				6	
Pressures, bar								
Condenser pressure	1.1	1.1	0.1	0.1	0.1	1.1	0.1	0.1
Condenser pressure drop	0.3	0.3	0.05	0.02	0.02	0.3	0.03	0.02
Reboiler pressure	1.8	1.8	0.25	0.25	0.15	1.4	0.14	0.15
Reflux ratio	0.5	1.0	2.2	1.5	1.6	1.3	2.4	1.5
Boilup ratio	1.5	1.4	1.0	1.8	2.2	3.1	2.1	2.5
Vapor split ratio	-	-	-	-	-	0.78	0.65	-
Liquid split ratio	-	-	-	-	-	0.21	0.55	-
Simulation results:								
Condenser T, ^{o}C	66.2	124.3	97.7	135.2	169.3	66.2	97.7	169.3
Reboiler T, ^{o}C	174.0	222.0	180.8	211.8	218.8	210.3	192.6	218.6
Condenser duty, MW	-1.52	-1.53	-1.89	-0.97	-0.69	-2.38	-1.98	-0.66
Reboiler duty, MW	3.14	1.88	0.94	0.98	0.61	4.25	1.14	0.68
Sum of reboiler duties, MW			7.55				6.07	
Energy savings			-				20%	

* HE: heat exchanger

Table 6.18 and Table 6.19 show the results of separating the oligomerization products at K-factors of 0.65 and 0.70, respectively, using the conventional direct sequence and the “3-3-2” configurations. The DWC configuration can save about 22% energy at K-factor of 0.65, and 16% energy at a K-factor of 0.70.

Table 6.18 Comparison between the conventional and the "3-3-2" configurations for separations at K-factor equals 0.65.

	Conventional					"3-3-2"		
	DC6=	DC8=	DC10=	DC12=	DC14=	DWC1	DWC2	DC14=
Number of stages	25	30	30	40	30	48	72	31
Sum of stages			155				151	
Number of HE*			10				6	
Pressures, bar								
Condenser pressure	1.1	1.1	0.1	0.1	0.1	1.1	0.1	0.1
Condenser pressure drop	0.3	0.3	0.05	0.02	0.02	0.3	0.03	0.02
Reboiler pressure	1.8	1.8	0.25	0.25	0.15	1.4	0.14	0.15
Reflux ratio	0.7	1.2	2.2	1.9	1.7	1.4	2.6	1.8
Boilup ratio	1.4	1.3	0.7	1.8	1.8	2.7	1.6	2.3
Vapor split ratio	-	-	-	-	-	0.78	0.585	-
Liquid split ratio	-	-	-	-	-	0.2	0.495	-
Simulation results:								
Condenser T, ^{o}C	66.2	124.2	97.7	135.3	169.3	66.2	97.7	169.3
Reboiler T, ^{o}C	178.6	227.5	183.6	214.5	221.5	214.1	195.1	221.7
Condenser duty, MW	-1.52	-1.64	-1.97	-1.26	-0.87	-2.23	-2.19	-0.91
Reboiler duty, MW	3.47	2.13	0.86	1.31	0.77	4.49	1.21	0.95
Sum of reboiler duties, MW			8.53				6.66	
Energy savings			-				22%	

* HE: heat exchanger

Table 6.19 Comparison between the conventional and the "3-3-2" configurations for separations at K-factor equals 0.70.

	Conventional					"3-3-2"		
	DC6=	DC8=	DC10=	DC12=	DC14=	DWC1	DWC2	DC14=
Number of stages	25	30	30	40	30	48	72	31
Sum of stages			155				151	
Number of HE*			10				6	
Pressures, bar								
Condenser pressure	1.1	1.1	0.1	0.1	0.1	1.1	0.1	0.1
Condenser pressure drop	0.3	0.3	0.05	0.02	0.02	0.3	0.03	0.02
Reboiler pressure	1.8	1.8	0.25	0.25	0.15	1.4	0.14	0.15
Reflux ratio	0.5	1.2	2.5	1.8	2.2	1.6	3.4	1.9
Boilup ratio	1.3	1.1	0.6	1.5	1.8	2.4	1.7	2.0
Vapor split ratio	-	-	-	-	-	0.78	0.585	-
Liquid split ratio	-	-	-	-	-	0.19	0.495	-
Simulation results:								
Condenser T, ^{o}C	66.2	124.3	97.7	135.3	169.3	66.2	97.7	169.3
Reboiler T, ^{o}C	183.2	230.2	186.3	216.8	223.6	218.1	197.3	223.8
Condenser duty, MW	-1.21	-1.56	-2.17	-1.35	-1.20	-2.08	-2.76	-1.11
Reboiler duty, MW	3.47	2.10	0.89	1.43	1.08	4.74	1.66	1.17
Sum of reboiler duties, MW			8.97				7.57	
Energy savings			-				16%	

* HE: heat exchanger

6.2.4 Remarks

This work has described an industrial process for production of linear α-olefins. This process comprises two part: the reaction and the product separation. The reaction part takes ethylene as its feed and produces linear α-olefins with a wide range of carbon numbers. The oligomerization reaction process was modeled using a simple conversion reactor. In the product separation part, the conventional direct sequence of distillation columns were used to separate the reaction products into different fractions. Based on the conventional separation train, three different, more advanced, configurations

containing dividing wall columns were proposed, namely the “3-3-2”, “3-2-3”, and “3-4” DWC configurations.

We compared the sum of the reboiler duties in the three configurations; this is considered an approximation to the energy consumption of the column system. The results indicate that all three proposed DWC configurations can save at least 13% of the energy required by a conventional process, with the configuration “3-3-2” saving the most (24%) energy. In addition, all three configurations require fewer heat exchangers and fewer columns shells which can reduce the capital costs. The “3-4” configuration requires 17% less energy than the conventional direct sequence, and furthermore it employs only two DWCs (the second DWC contains two walls) to achieve the same separation task, which is considered to have the most capital savings among the three configurations.

A modified “3-3-2” configuration is proposed to separate the oligomerization reaction products at three different K-factors. We show that, by using the “3-3-2” configuration, one only needs to slightly change the reflux rates, product withdraw rates, or split ratios to maintain the high separation purities at different K-factors. The configuration with DWCs has similar flexibilities to handle different feed compositions as the conventional direct sequence, and, more attractively, the configuration with DWCs can save up to 22% energy compared to its corresponding conventional sequence. It is useful to note that the purity specifications on this process are somewhat higher than might be typical in actual practice (Turner, 1983). This was done in part to demonstrate that it is possible to obtain very high purities from a sequence of DWCs.

It should also be noted that multiple solutions were found in the DWC simulations. The existence of MSS could pose a challenges for DWC process design. The simulation can be extremely difficult to converge if the starting point is in the vicinity of two nearby solutions.

Reference

Al-Jarallah, A.M., et al., 1992. Ethylene dimerization and oligomerization to butene-1 and linear α-olefins: a review of catalytic systems and processes. *Catalysis Today*, 14(1), pp.1–121.

Behr, A., and Keim, W., 1985. The nickel-complex catalyzed synthesis of α-olefins. *Arabian journal for science and engineering*, 10(4), pp.377–390.

Dejanović, I., et al., 2011. Designing four-product dividing wall columns for separation of a multicomponent aromatics mixture. *Chemical Engineering Research and Design*, 89(8), pp.1155–1167.

ElBadawy, K.M., Teamah, M.A., Shehata, A.I., and A Hanfy, A., 2018. Simulation of liquefied petroleum gas (LPG) production from natural gas using fractionation towers. *International Journal of Advanced Scientific and Technical Research*, 6(7).

Freitas, E.R., and Gum, C.R., 1979. Shell's Higher Olefins Process. *Chemical engineering progress*. Jan.

Galtier, P.A., Forestière, A.A., Glaize, Y.H., and Wauquier, J.P., 1988. Mathematical modeling of ethylene oligomerization. In: J.R. Bourne, W. Regenass and W. Richarz, eds., *Tenth International Symposium on Chemical Reaction Engineering*. Pergamon, pp.1855–1860.

Jaubert, J.-N., and Mutelet, F., 2004. VLE predictions with the Peng–Robinson equation of state and temperature dependent kij calculated through a group contribution method. *Fluid Phase Equilibria*, 224(2), pp.285–304.

Keim, W., 2013. Oligomerization of ethylene to α-Olefins: discovery and development of the Shell Higher Olefin Process (SHOP). *Angewandte Chemie International Edition*, 52(48), pp.12492–12496.

Khan, S.A., and Haliburton, J., 1990. *Process for LPG recovery*. USRE33408E.

Kister, A.T., and Lutz, E.F., 1977. *Oligomerization reaction system*. US4020121A.

Lappin, G.R., 1989. *Alpha olefins applications handbook*. 1st ed. Bosa Roca, United States: Taylor & Francis Inc.

Lohmann, J., Joh, R., and Gmehling, J., 2001. From UNIFAC to Modified UNIFAC (Dortmund). *Industrial & Engineering Chemistry Research*, 40(3), pp.957–964.

Mostafa, M.M., EL-Emam, N.A., EL-Shafie, M.A., and Aboul-Fotouh, T.M., 2019. *Upgrade a gas plant to produce LPG by DWC and conventional methods—part 1*.

O'Donnell, A.E., and Gum, C., 1981. *Nickel complexes in diol solvents and their use as oligomerization catalyst precursors*. US4260844A.

Olah, G.A., and Molnár, Á., 2003. Oligomerization and polymerization. In: *Hydrocarbon Chemistry*. John Wiley & Sons, Ltd, pp.723–806.

Peuckert, M., and Keim, W., 1983. A new nickel complex for the oligomerization of ethylene. *Organometallics*, 2(5), pp.594–597.

Phu, N.P., 2018. *Process for LPG recovery*. US20180216011A1.

Seihoub, F.-Z., Benyounes, H., Shen, W., and Gerbaud, V., 2017. An improved shortcut design method of divided wall columns exemplified by a liquefied petroleum gas process. *Industrial & Engineering Chemistry Research*, 56(34), pp.9710–9720.

Turner, A.H., 1983. Purity aspects of higher alpha olefins. *Journal of the American Oil Chemists' Society*, 60(3), pp.623–627.

Veazey, M.V., 2018. *Shell pouncing on AO top spot with Louisiana 'Tiger' project*.

Voutsas, E., et al., 2006. Thermodynamic property calculations with the universal mixing rule for EoS/GE models: Results with the Peng–Robinson EoS and a UNIFAC model. *Fluid Phase Equilibria*, 241(1), pp.216–228.

Weidlich, U., and Gmehling, J., 1987. A modified UNIFAC model. 1. Prediction of VLE, hE, and .gamma..infin. *Industrial & Engineering Chemistry Research*, 26(7), pp.1372–1381.

CHAPTER 7 Conclusions and Future Work

7.1 Conclusions

This thesis includes proposals for two equation-oriented models for simulating dividing wall columns: the equilibrium-stage PCM (parallel column model), and the rate-based PCM. Several case studies with different DWC configurations (these include DWCs with multiple walls, and multiple condensers) are modeled with the equilibrium-stage PCM, elaborating that the equilibrium PCM is capable of simulating DWCs of arbitrary configuration. The simulations from the equilibrium-stage PCM were verified by comparison with those from other flowsheet simulation software packages (VMGSim, UniSim® Design, and COCO) that use multi-column models. The comparisons between the proposed PCM and the multi-column models show that, while leading to more or less equivalent results, the proposed PCM takes considerably less effort to setup a DWC flowsheet, and converges more rapidly from the automatically generated initial guess (the multi-column model requires engineers to provide good initial guesses to initiate the simulation) for most cases. Heat transfer across the wall can be modeled in the PCM in a quite straightforward way, due to the equation-oriented nature of the model.

The equilibrium-stage PCM was extended to a rate-based PCM, where model equations for vapor and liquid phases are considered separately. The rate-based PCM has all the above-mentioned advantages for the equilibrium-stage PCM; furthermore, it considers the column geometry and column internals in a more detailed way compared to the equilibrium-stage PCM. A significant aspect of DWC simulations is that the vapor split ratio is, in fact, a consequence of pressure balancing on two sides of the wall. The rate-based PCM is capable of predicting the self-regulating vapor split ratio by equalizing the pressures on two sides of the wall. Various pressure drop models for conventional columns can also be applied to DWCs, as long as the geometry used in the model is correct. For heat transfer across the wall in the rate-based PCM, it is considered adequate to only account for heat transfer between two liquid phases. A case study on the impact

of stage height shows that, when decreasing the stage height while keeping the product of stage height and number of stages the same, the rate-based PCM converges to a fixed point (this should always be true for rate-based models, although some other rate-based models fail to converge).

Both the equilibrium-stage PCM and the rate-based PCM are validated using an extensive set of experimental data from the University of Texas at Austin, where two different chemical systems were investigated. One is a mixture of linear alcohols with n-hexanol, n-octanol, and n-decanol; the other is a mixture of n-pentane, cyclohexane and n-heptane. Both models give good predictions to the temperature profiles in the column. The results from the rate-based PCM are statistically superior to those from the equilibrium-stage PCM.

The two proposed PCMs can, via the CAPE-OPEN mechanism, be used as a standard DWC module in any major commercial flowsheeting systems. Two industrial case studies, LPG recovery process and the Shell Higher Olefins Process (SHOP), are used to demonstrate the application of the PCM in flowsheet intensification. Three different process configurations were discussed in modeling the SHOP process, with hardware requirement and energy requirement in each configuration shown, based on which engineers can select the “best” configuration.

In addition, multiple steady-state solutions are found in DWC simulations by solving the model equations from different starting points. The existence of multiplicity poses some challenges to DWC design, as it is sometimes difficult for engineers to tell which solution is the practically feasible one if no experimental work is done a priori. Further investigations are needed to either find the physical explanations for such multiplicity, or find a criteria to distinguish a feasible solution from the others.

7.2 Future Work

With the results shown in this research, here are some promising avenues for future DWC studies:

- Material leakage around the wall

Since more and more DWCs use stacked wall elements as an alternative to welded walls, leakage of liquid and vapor is unavoidable. The parallel column model can easily include the flow around the wall by adding terms to the mass balance equations. A knowledge of how mass leakage would affect the separation, and how engineers should react in order to diminish its negative effects might be interesting.

- Dynamics and control

Dynamic models can provide information on how columns respond to some unwanted disturbances. Dynamic simulation allows engineers to gain further insights into the flexibility, operability, and safety of a process. Effective control schemes of a unit can be proposed according to its dynamic behavior. Current studies of DWC dynamics and control mainly use multi-column models. The proposed equation-oriented models in this thesis can significantly ease the dynamic simulations of DWCs. Different control schemes can also be studied for various DWC operations.

- Multiple steady-state solutions

The reasons for the multiplicity reported in Chapter 5 are still unknown. Finding multiple solutions by just randomly varying the initial guess is extremely difficult. One possible way of automatically locating all solutions is to couple the PCM to an arc length continuation method. On the other hand, experimental work may be required to tell which solution is practically feasible; criteria may be set up to screen the practical solutions if experiments are not available.

- Flowsheet intensification with rate-based PCM

All the flowsheets simulated in Chapter 6 use the equilibrium-stage PCM with the vapor split ratios specified by engineers. It would be interesting to employ the rate-based PCM for DWC modeling with vapor split ratios estimated from pressure equalizing. Pumparound (or bypass) may be used to change the internal liquid flows, and pressure drop in different sections, and hence indirectly regulate the vapor split ratios to find the optimum operation.

- CAPEX and OPEX estimations of the SHOP process

The SHOP work discussed in Chapter 6 compared the energy consumption and the hardware requirements between the conventional direct sequence and the configurations with DWCs. A more rigorous model is required to predict the capital expenditure (CAPEX) and the operational expenditure (OPEX), and hence to predict the total annualized cost (TAC). Additional savings are possible because the cost of stages in the center section of a DWC can be less than the cost of additional stages in the top or bottom sections or of those in a conventional column.

- Automated hardware design with the account for maldistribution

The parallel column model in this thesis can be used to model maldistribution in packed columns. It would be interesting if practical procedures can be proposed to design packed columns with maldistribution automatically taken into consideration.

Appendix A: Counting Stages – Additional Discussion

In the main body of the paper we outlined a scheme for enumerating the different sections of a DWC. While we prefer a scheme that requires the fewest non-adjacent stage connections, the method we actually employ in our software, while straightforward, does not guarantee that we end up with the fewest connections.

The table below identifies the number of different ways to order varying numbers of column sections.

Number of Sections	Number of Possible Section Orders
4	24
5	120
6	720
7	5040
8	40320
9	362880
10	3628800

Consider the 3-wall, 4-product DWC in Fig. A1. By drawing horizontal lines across the column at the top and bottom of each wall (but only between the nearest vertical lines to the left and right) we will find that there are ten sections in this column.

From the table above we see that there are more than three million ways in which to order the ten sections of this column. Three possible sequences are shown in Fig. A2. The configuration to the left follows the guidelines for assigning section identities outlined in the main body of the paper. The configuration in the center follows a scheme in which we start at the top of the column and assign section identities as we move down the column while staying to the left of all walls encountered as we do so. We stop this sequence when we reach the bottommost section which is assigned the identity for the total number of column sections (J for the tenth section in this case). Then we move up the right hand side of the column reducing the section identity, from section J, by one every time we

encounter the start or end of a wall while staying to the right of each wall. The last two sections are numbered by moving up from Section D or down from Section G (both approaches yield the same result). The configuration on the right hand side follows the column from top to bottom while staying to the left of walls until we reach the bottom section which will, as before, be assigned a section identity equal to the total number of sections. Then from Section D we ascend the column staying to the left of any walls encountered to the right (note that for Section F that is the column shell itself). When we encounter a section above that already is numbered (Section B here) we move right again (if required) and continue numbering sections while moving down. In all of these schemes the top section is A and the bottom section has an identity equal to the total number of sections.

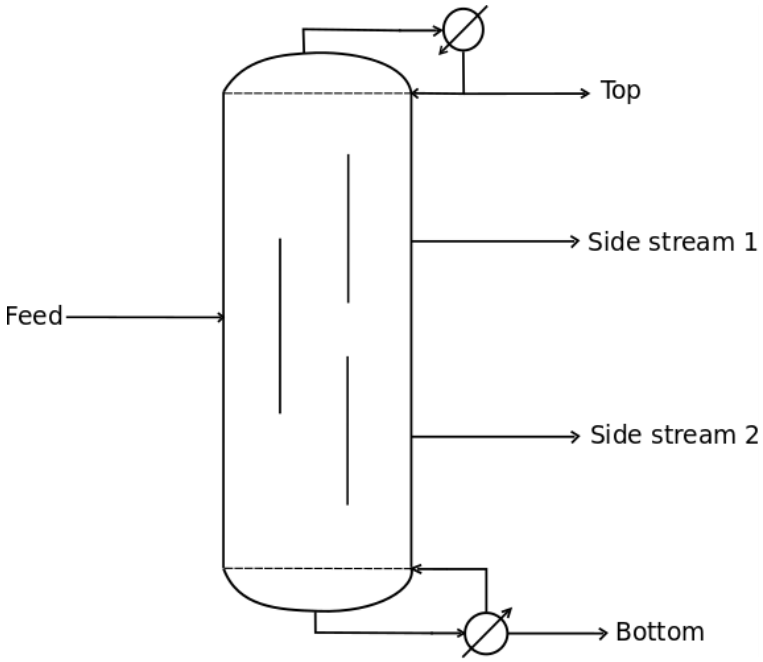

Fig. A1 3-Wall, 4-product Dividing Wall Column.

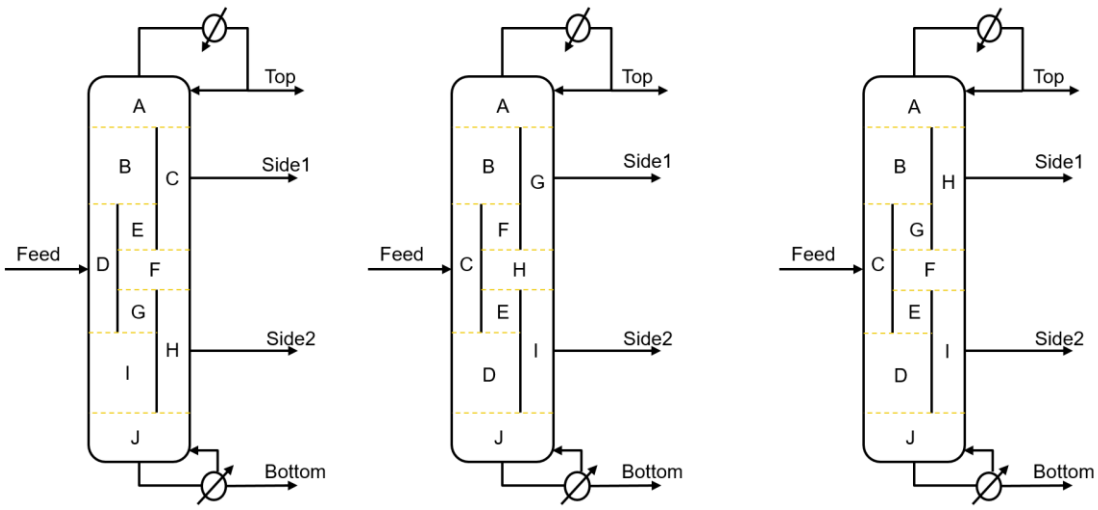

Fig. A2 Three possible sequences of column sections for 3-wall, 4-product Dividing Wall Column.

The numbers of non-consecutively numbered stage connecting streams (NCCs) in these three variants are 8, 6, and 8 respectively. (Liquid NCCs occur when the split leaving the bottom stage of Section S, say, goes to a stage in any section not next in the sequence A-Z, or when a vapor split leaving the top of a stage in Section S goes to any stage in a section not next in the sequence Z-A.) Our simulation program defaults to the first scheme in Fig. A2.

Figure A3 shows three different section sequences for a 3-wall 5-product DWC devised by Halvorsen et al. (2011) the column also has 3 walls and 10 sections.

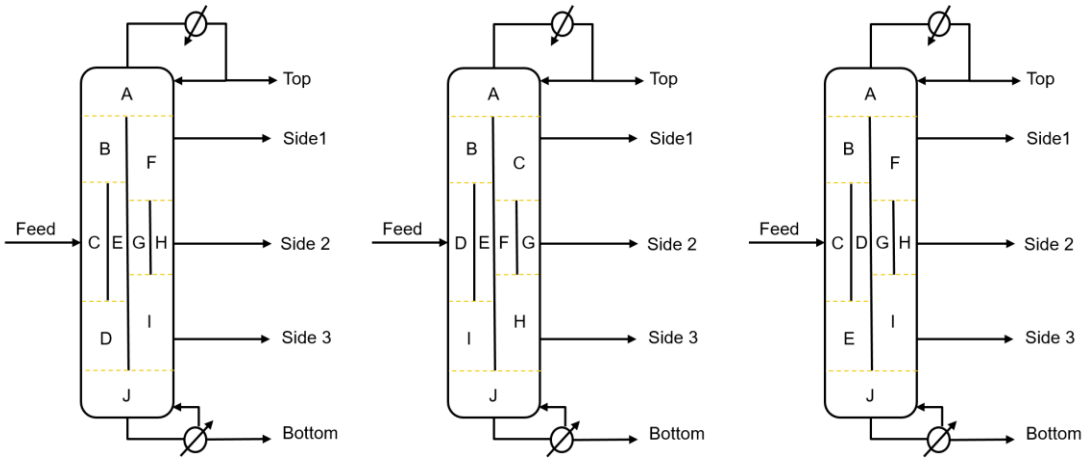

Fig. A3 Three possible sequences of column sections for 3-wall, 5-product Dividing Wall Column. After Halvorsen et al. (2011).

Scheme (i) in Figure A3 has 10 NCCs; Scheme (ii) has 10 and Scheme (iii) also has 6 NCCs. Our software will normally prefer Scheme (ii) (although the calculation module can handle any of these or any other scheme).

Reference

Halvorsen, I.J., et al., 2011. Multi-product dividing wall columns: a simple and effective assessment and conceptual design procedure, *Chemical Engineering Transactions*. 25, pp.611-616.

Appendix B: PCM Initialization

In this work, the bubble point (BP) method, proposed by Wang and Henke (1966), is used to provide initial estimates for the PCM. The algorithm for the BP method, adapted from Seader and Henley (2011), is shown in Fig. B1.

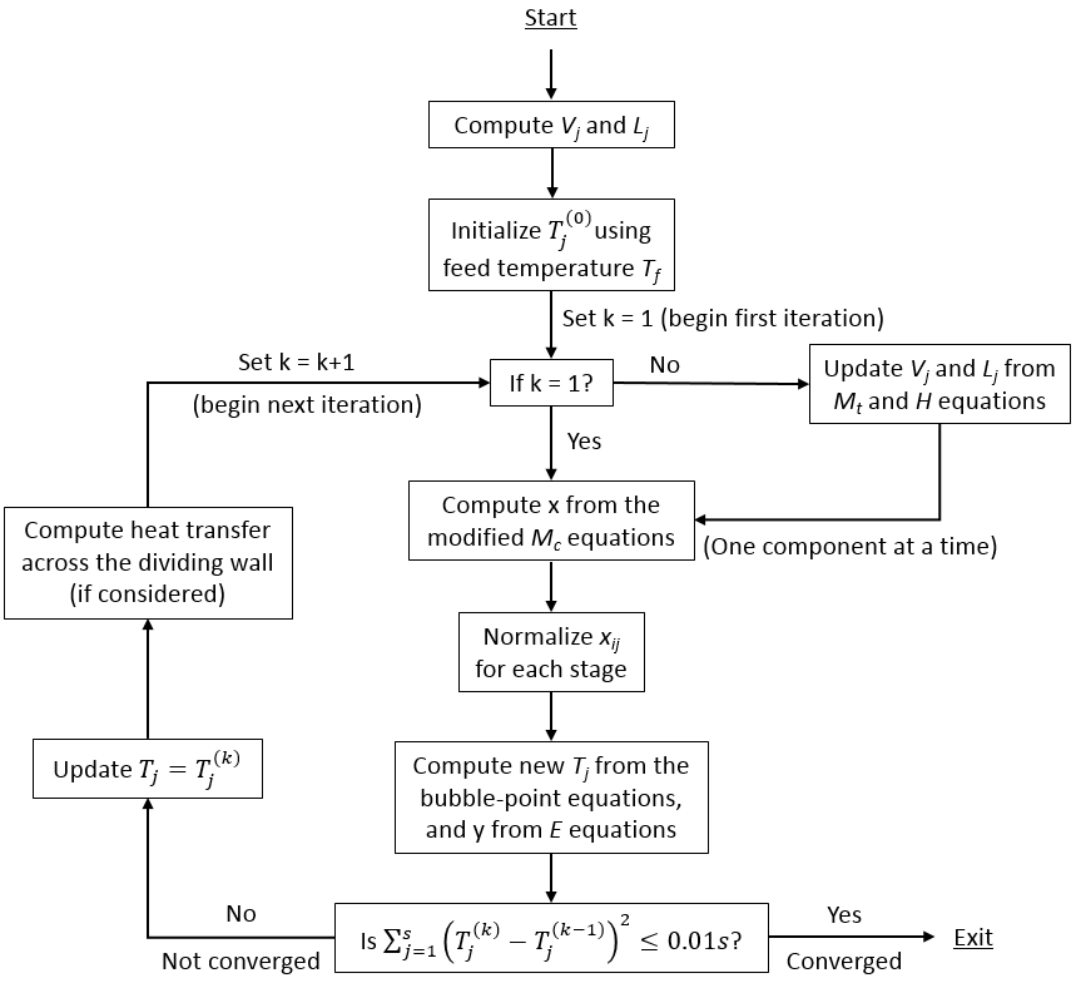

Fig. B1 Flowchart for the PCM initialization.

To initiate the calculation, vapor and liquid molar flowrates are first estimated. Due to the lack of temperature information, enthalpies cannot be calculated at this moment, and, thus, energy balance equations cannot be used. To deal with this, constant molar overflow is assumed.

The total material balance equation on stage *j* in Eq. (2.2) is re-arranged to Eq. (B.1), and can be extended to *s* equations, with one for each stage.

$$M_{tj} \equiv V_j - \delta^V_{j,j+1} \cdot V_{j+1} - \delta^L_{j,j-1} \cdot L_{j-1} + L_j - \sum_{m=1}^{s} \left(G^V_{jm} + G^L_{jm}\right) = F_j - S^L_j - S^V_j \tag{B.1}$$

This form of the balance equations is a system of linear equations with variables the vapor and liquid flowrates $(V_1, V_2, \dots, V_s, L_1, L_2, \dots, L_s)^T$. To solve for these $2s$ variables, another s equations are required. These additional equations come from the energy balances using the constant molar overflow assumption, as well as the specification equations for condensers and reboilers if they exist. The constant molar overflow assumption for liquid phase is written in a general form as in Eq. (B.2).

$$L_j - \delta^L_{j,j-1} \cdot L_{j-1} + \sum_{m=1}^{s} G^L_{jm} = F^L_j - S^L_j \tag{B.2}$$

Equation (B.2) can be extended to $(s-2)$ equations with *j* from 2 to $(s-1)$. The last two equations depend on the column configuration as discussed below.

1) Columns with one condenser and one reboiler

   For this type, the specifications (or estimates) of the reflux ratio and boilup ratio (or top or bottom product flowrate, etc.) constitute the last two equations.

2) Columns with one condenser and no reboiler

   The condenser specification is written as one equation; since there is no reboiler, a vapor feed should enter the column from the last stage, thus the last equation is:

$$V_s = F^V_s \tag{B.3}$$

3) Columns with no condenser and one reboiler

   Similar to type 2), the reboiler specification is written as one equation, while the other equation comes from the liquid feed to the first stage, that is:

$$L_1 = F_1^L \tag{B.4}$$

4) Columns with no condenser and no reboiler

For this type of columns, one liquid and one vapor feed should enter the column from the first and last stage, respectively. Therefore, Eqs. (B.3) and (B.4) should hold at the same time.

5) Columns with multiple condensers and/or reboilers

To illustrate this more complicated type, take a column with two condensers and no reboiler as an example. Assume that the first condenser is stage 1 (it should be if one follows the stage numbering rule in Section 2.1.1), and the second condenser is stage 11. The first equation is the specification of the condenser with stage number 1, while the second equation is Eq. (B.3) for the bottom of the column. Note that stage 11 is presumed to be a general stage while the equation for stage 11 is written as in Eq. (B.5) assuming no liquid interlinked stream to stage 11, and $\delta_{11,10}^L$ is one.

$$L_{11} - L_{10} = F_{11}^L - S_{11}^L \tag{B.5}$$

However, stage 11 is, in fact, a condenser, and Eq. (B.5) does not apply. Therefore, Eq. (B.5) is replaced with the specification of this extra condenser. Similar procedures apply to cases with multiple reboilers.

The $2s$ linearized equations can be solved by Gaussian elimination for the initial vapor and liquid flowrates. The temperature on each stage is initialized as equal to the feed temperature, T_f.

The component mass balance equations in Eq. (2.1) and the equilibrium equations in Eq. (2.3) are combined to give

$$\begin{aligned}\left[\left(L_j + S_j^L\right) + \left(V_j + S_j^V\right)K_{ij}\right]x_{ij} - \delta_{j,j-1}^L \cdot L_{j-1}x_{i,j-1} - \delta_{j,j+1}^V \\ \cdot V_{j+1}K_{i,j+1}x_{i,j+1} - \sum_{m=1}^{s}\left(G_{jm}^V y_{im} + G_{jm}^L x_{im}\right) = -F_j z_{ij}\end{aligned} \tag{B.6}$$

The last term on the left-hand side of the Eq. (B.6) accounts for the interlinked streams, containing vapor and/or liquid flows from stages other than stage *j-1* and *j+1*. For conventional columns, which have no interlinked streams, this summation term is zero. The combined Eq. (B.6) can be extended to *s* equations, with one for each stage. This system of equations can be considered as linearized equations for component *i*, with variables $x_{i,1}, x_{i,2}, \dots, x_{i,s}$, and can be written in a matrix-vector multiplication form as $Ax = b$. If no interlinked stream exists, as for conventional columns, the matrix *A* has a tridiagonal structure, which can be solved with the Thomas algorithm. If the interlinked term is nonzero, the structure of the matrix *A* is a large sparse matrix with most nonzero elements in the tridiagonal positions, thus a general sparse Gaussian elimination algorithm can be used to solve the equations.

The computed set of x_{ij} values in each iteration do not necessarily satisfy the summation equation that the component mole fractions on each stage should sum up to one; therefore, it is advisable to normalize the computed x_{ij} values.

With normalized liquid mole fractions computed, new temperature on each stage can be obtained by bubble-point calculations from Eq. (B.7).

$$\sum_{i=1}^{c} K_{ij}\, x_{ij} - 1.0 = 0 \tag{B.7}$$

As the temperature on each stage is determined, the K-value is then computed, thus the vapor mole fractions, y_{ij}, can be obtained easily.

The solution is converged if the criterion below is satisfied. This convergence criterion is proposed by Wang and Henke (1966), and is considered adequate (Seader and Henley, 2011).

$$\tau = \sum_{j=1}^{s} \left(T_j^{(k)} - T_j^{(k-1)} \right)^2 \leq 0.01s \tag{B.8}$$

If the criterion is not satisfied, another iteration is needed. In the next iterations, temperatures are updated to the newly computed bubble-point temperatures, and, if heat transfer across the dividing wall is considered, the amount of heat transfer on each stage alongside the dividing wall is computed using Eq. (2.6) in Section 2.1.3 . As the temperature on each stage is estimated, enthalpies are able to be computed, thus the energy balance equations can be used to update the vapor and liquid flowrates.

The total material balance equations in Eq. (2.2) and the energy balance equations in Eq. (2.7) can be re-arranged in terms of the vapor and liquid flowrates to Eqs. (B.1) and (B.9), respectively. Equation (B.1) is extended to *s* equations, one for each stage, and Eq. (B.9) is extended to $(s-2)$ equations with *j* from 2 to $(s-1)$. The rest two equations are determined using similar procedures as the estimation of the vapor and liquid flowrates with constant molar overflow assumed.

$$\begin{aligned} H_j \equiv\ & H_j^V \cdot V_j - \delta_{j,j+1}^V \cdot H_{j+1}^V \cdot V_{j+1} + H_j^L \cdot L_j - \delta_{j,j-1}^L \cdot H_{j-1}^L \cdot L_{j-1} \\ & - \sum_{m=1}^{s} \left(G_{jm}^V H_m^V + G_{jm}^L H_m^L \right) \\ & = -S_j^L H_j^L - S_j^V H_j^V - Q_j^S - \sum_{m=1}^{s} Q_{mj}^W \end{aligned} \tag{B.9}$$

The total $2s$ equations can be written in a linearized matrix form $Ax = b$, where x is a column vector containing vapor and liquid flowrates $(V_1, V_2, \dots, V_s, L_1, L_2, \dots, L_s)^T$, and can be obtained by solving this matrix equation with the Gaussian elimination algorithm.

With the updated vapor and liquid flowrates, the algorithm is continued for a few (4 or 5) iterations (but not usually until convergence is reached).

Reference

Seader, J.D., and Henley, E.J., 2011. Separation process principles. Hoboken, NJ : Wiley.

Wang, J.C., 1966. Tridiagonal Matrix for Distillation. *Hydroc. Process.*, 45, pp.155–163.

Appendix C: Additional Case Studies and Supplementary Material to Chapter 2

1. BTX Separation

Figure C1 shows a dividing wall column flowsheet for separating benzene, toluene, and o-xylene, adapted from Ling and Luyben (2009). The column has 9 stages in the top section (the total condenser is counted as one stage), 24 stages in each section along the dividing wall, and 12 stages in the bottom section (the partial reboiler is counted as one equilibrium stage). Other necessary information for modeling this column is also shown in Figure C1.

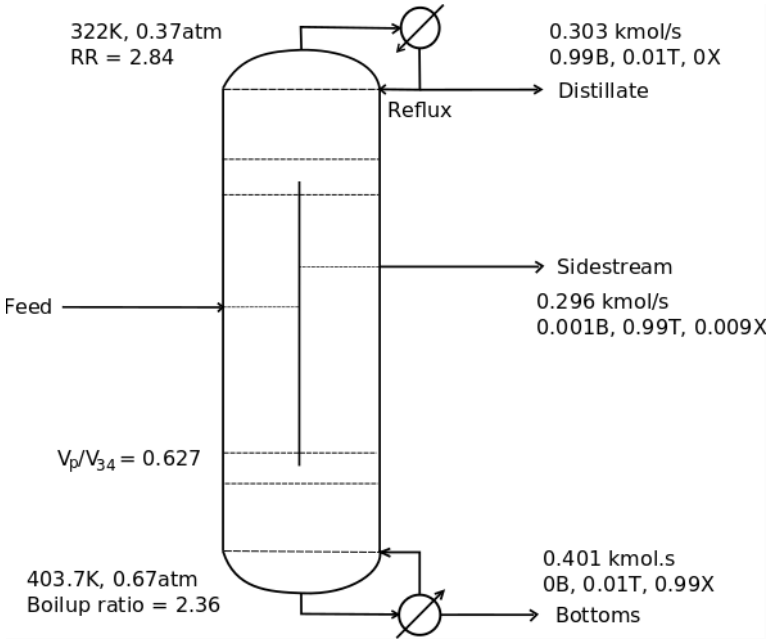

Figure C1 Dividing wall column flowsheet adapted from Ling and Luyben (2009).

1.1 Simulation with Multi-Column Model

This column is first modeled in UniSim® Design using a four-column model (see Figure C2). The NRTL thermodynamic model is used for the liquid phase, and vapor phase is assumed ideal. The pressure in the condenser is 0.37 atm, and the pressure drop is 0.0068 atm.

The pressure profiles in the column can be easily worked out, noting that, at the top and bottom of the dividing wall, the pressures on two sides of the wall should be equal. Vapor and liquid split ratios are given by Ling and Luyben (2009) as 62.7% / 37.3% and 35.3% / 64.7%, respectively. Condenser reflux ratio and bottom product flowrate are specified as indicated in Figure C1.

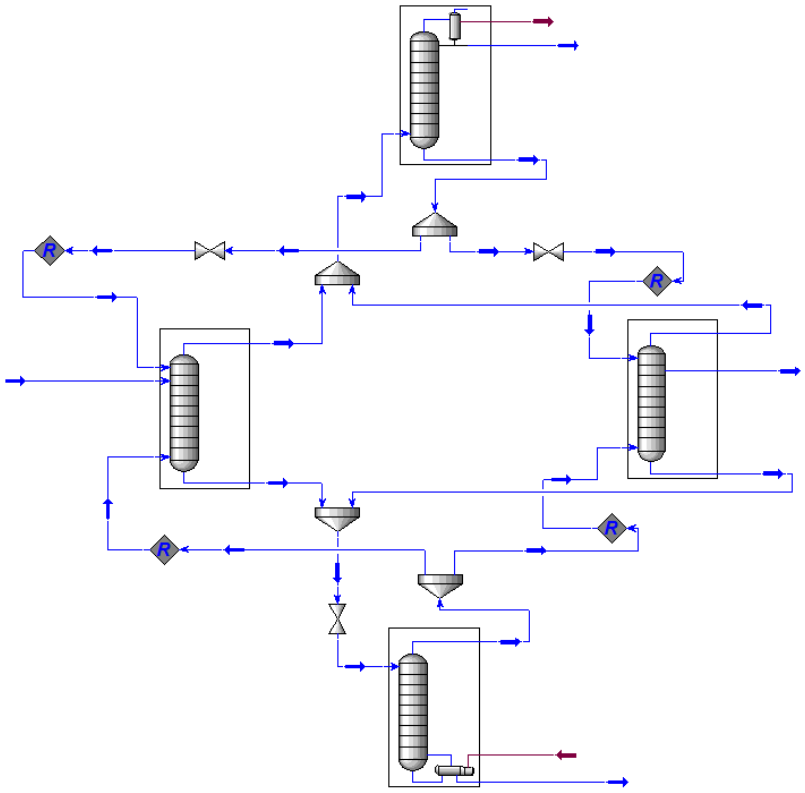

Figure C2 Four-column model built in UniSim® Design for modeling the DWC.

1.2 Simulation with the PCM

Figure C3 represents the dividing wall column established in the PCM. NRTL thermodynamic model is used, with interaction parameters obtained from UniSim® Design. Other specifications are the same as described in Figure C1 and the above section.

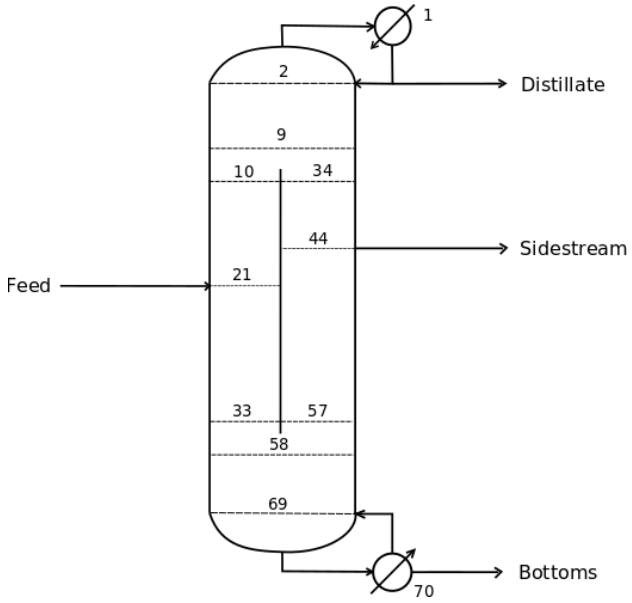

Figure C3 Schematic diagram of the DWC built in the PCM.

1.3 Simulation Results

The simulation results from the multi-column model and the PCM are compared. Figure C4 shows the temperature profiles predicted from two models. The two models give almost identical predictions throughout the column.

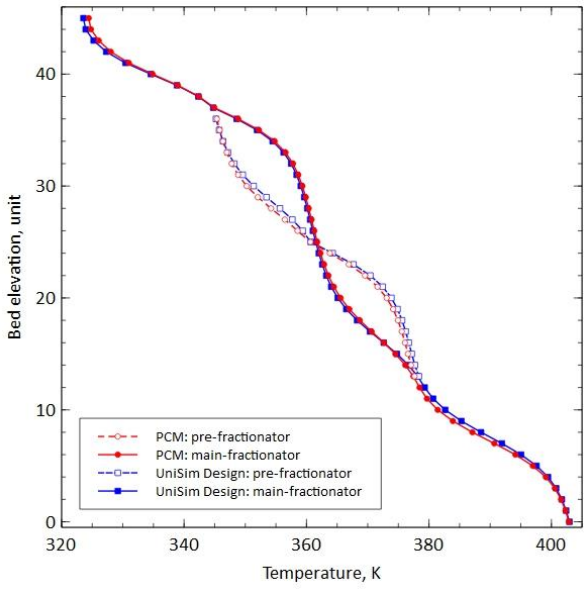

Figure C4 Comparisons of temperature profiles, assuming equal HETP.

Product purities are compared in Table C1, where two models results in very close agreement. Three products from the DWC all have high purity (around 99%). The liquid composition profiles throughout the column, predicted from the PCM, are shown in Figure C5.

Table C1 Comparisons of product purities.

	Top		Middle		Bottom	
	PCM	[a]UD	PCM	UD	PCM	UD
Temperature, K	324.44	323.57	361.27	361.04	402.85	402.95
Flowrate, kmol/s	0.303	0.303	0.296	0.296	0.401	0.401
Benzene, mol %	0.9897	0.9897	0.0005	0.0004	0	0
Toluene, mol %	0.0103	0.0103	0.9978	0.9978	0.0038	0.0038
o-Xylene, mol %	0	0	0.0018	0.0018	0.9962	0.9962

[a]UD represents UniSim® Design

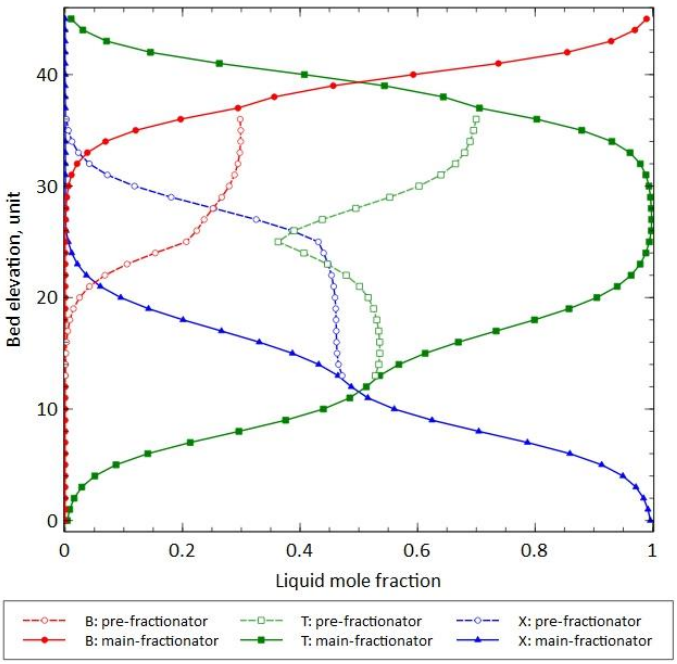

Figure C5 Liquid composition profiles predicted from the PCM, assuming equal HETP.

2. Aromatics Separation

The aromatics separating DWC discussed in Chapter 2 is also simulated in other simulation software, using multi-column models. Figure C6 shows two flowsheets established in COCO and UniSim® Design for modeling the DWC. The BIP information from UniSim® Design is shown in Table C2.

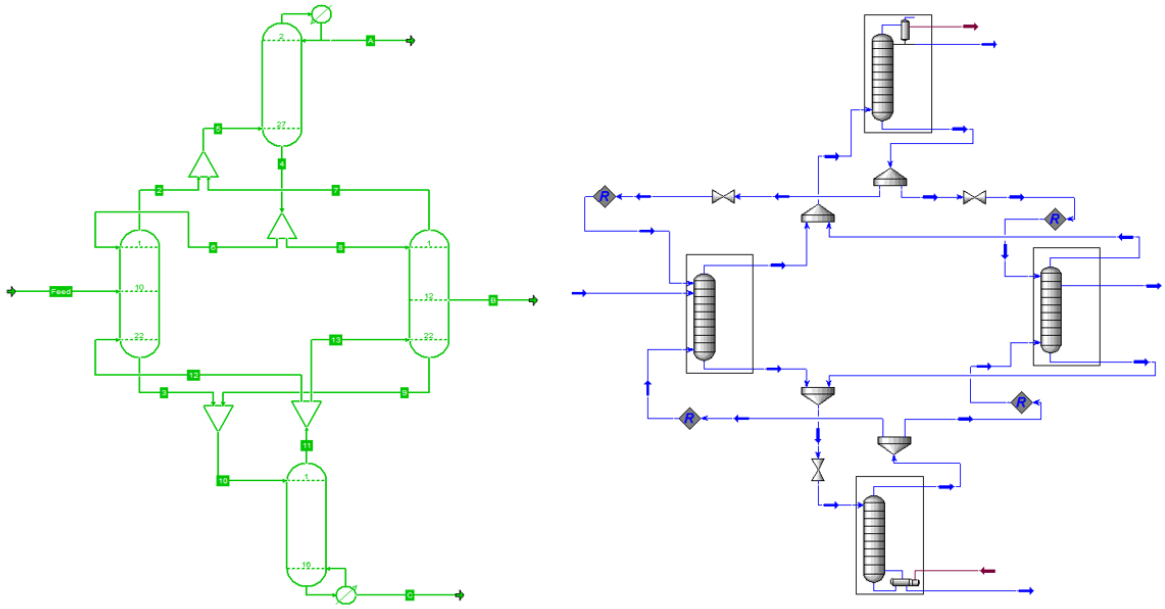

(a) (b)

Figure C6 Aromatics separating DWC flowsheets established in (a) COCO and (b) UniSim® Design.

Table C2. BIPs of the PR model from UniSim® Design.

	n-Butane	i-Pentane	n-Pentane	2-Mpentane	n-Hexane	Benzene	3-Mhexane	Toluene	E-Benzene	p-Xylene	m-Xylene	o-Xylene	1M3-Ebenzene	135-Mbenzene	14-Ebenzene
n-Butane	...	0.00050	0.00055	0.00182	0.00187	0.00001	0.00293	0.00064	0.00203	0.00218	0.00208	0.00190	0.00581	0.00388	0.00553
i-Pentane	0.00050	...	0.00000	0.00042	0.00044	0.00040	0.00102	0.00001	0.00052	0.00060	0.00055	0.00046	0.00293	0.00161	0.00273
n-Pentane	0.00055	0.00000	...	0.00037	0.00039	0.01600	0.00095	0.00000	0.00047	0.00054	0.00050	0.00041	0.00280	0.00152	0.00261
2-Mpentane	0.00182	0.00042	0.00037	...	0.00000	0.00163	0.00013	0.00030	0.00001	0.00002	0.00001	0.00000	0.00113	0.00039	0.00101
n-Hexane	0.00187	0.00044	0.00039	0.00000	...	0.00700	0.00012	0.00032	0.00000	0.00001	0.00001	0.00000	0.00110	0.00037	0.00098
Benzene	0.00001	0.00040	0.01600	0.00163	0.00700	...	0.00269	0.00053	0.00183	0.00197	0.00188	0.00170	0.00547	0.00360	0.00520
3-Mhexane	0.00293	0.00102	0.00095	0.00013	0.00012	0.00269	...	0.00084	0.00008	0.00006	0.00007	0.00011	0.00049	0.00007	0.00041
Toluene	0.00064	0.00001	0.00000	0.00030	0.00032	0.00053	0.00084	...	0.00039	0.00046	0.00042	0.00034	0.00261	0.00137	0.00242
E-Benzene	0.00203	0.00052	0.00047	0.00001	0.00000	0.00183	0.00008	0.00039	...	0.00000	0.00000	0.00000	0.00098	0.00030	0.00086
p-Xylene	0.00218	0.00060	0.00054	0.00002	0.00001	0.00197	0.00006	0.00046	0.00000	...	0.00000	0.00001	0.00088	0.00024	0.00077
m-Xylene	0.00208	0.00055	0.00050	0.00001	0.00001	0.00188	0.00007	0.00042	0.00000	0.00000	...	0.00000	0.00094	0.00028	0.00083
o-Xylene	0.00190	0.00046	0.00041	0.00000	0.00000	0.00170	0.00011	0.00034	0.00000	0.00001	0.00000	...	0.00108	0.00035	0.00096
1M3-Ebenzene	0.00581	0.00293	0.00280	0.00113	0.00110	0.00547	0.00049	0.00261	0.00098	0.00088	0.00094	0.00108	...	0.00020	0.00000
135-Mbenzene	0.00388	0.00161	0.00152	0.00039	0.00037	0.00360	0.00007	0.00137	0.00030	0.00024	0.00028	0.00035	0.00020	...	0.00015
14-Ebenzene	0.00553	0.00273	0.00261	0.00101	0.00098	0.00520	0.00041	0.00242	0.00086	0.00077	0.00083	0.00096	0.00000	0.00015	...

Flow rate profiles and temperature profiles estimated from COCO, ChemSep PCM, and UniSim® Design are compared with the ones simulated in ChemCAD by Dejanović (2017), see Figure C7 and C8. The differences between Figure C7a and other profiles are the vapor flowrates on stage 28 and stage 50 of the main-fractionator (red solid line). The reason for these differences is because of the way that the stream flowrates are reported by Dejanović (2017). Apart from this, the results are almost identical with each other.

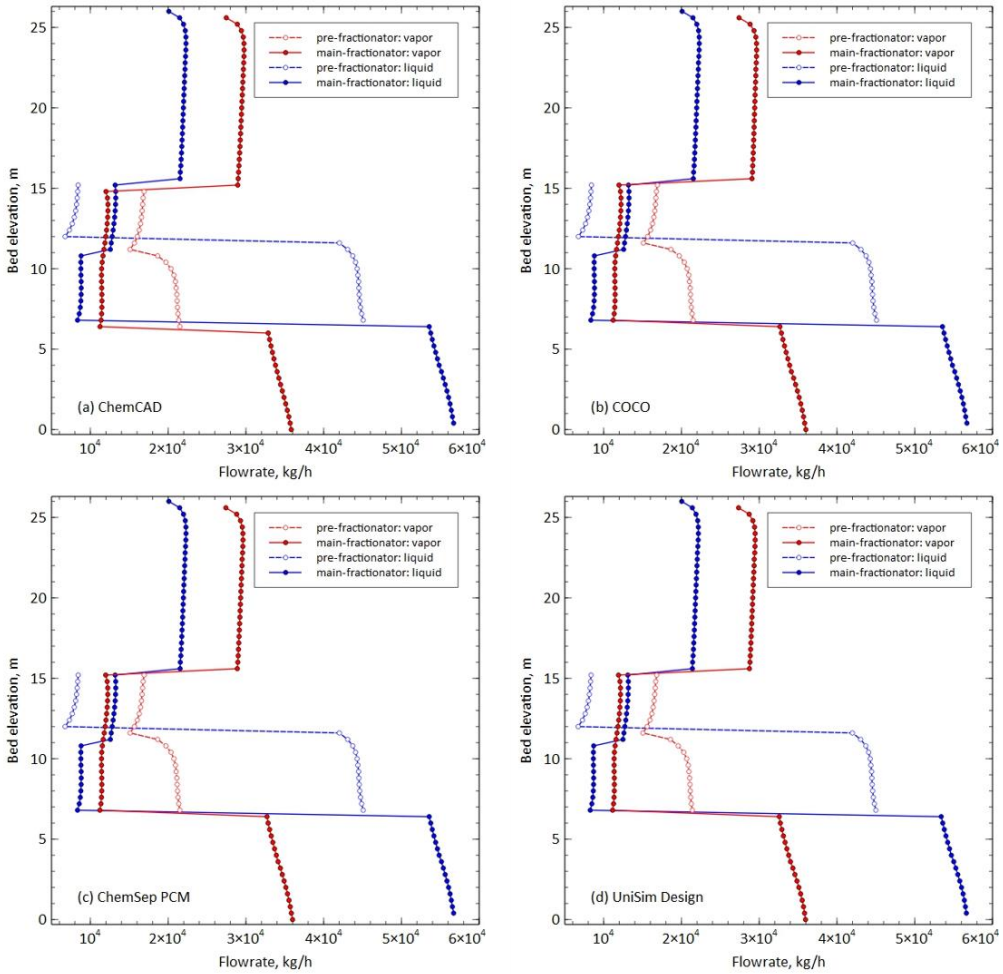

Figure C7 Flow rate profiles from (a) ChemCAD, (b) COCO, (c) ChemSep PCM, and (d) UniSim® Design.

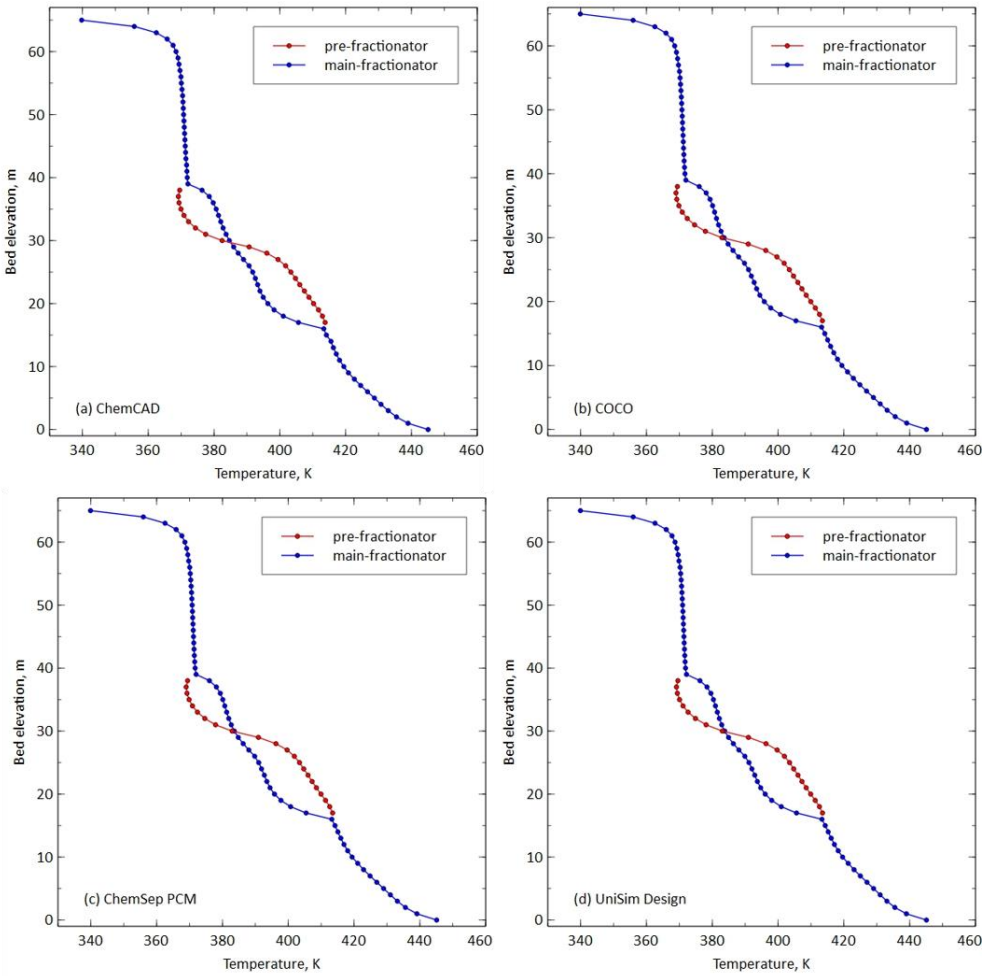

Figure C8 Temperature profiles from (a) ChemCAD, (b) COCO, (c) ChemSep PCM, and (d) UniSim® Design.

3. Satellite Column Simulation

The satellite column system is also simulated in COCO and UniSim® Design. Figure C9 shows the flowsheets established in COCO and UniSim® Design using two different multi-column models.

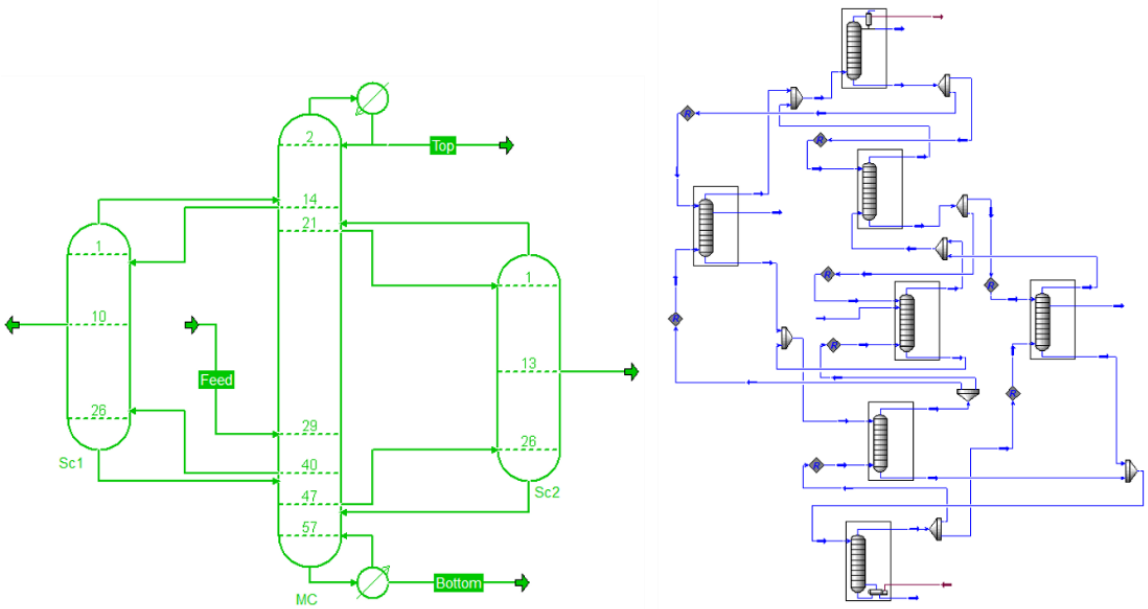

Figure C9 Flowsheets for modeling the satellite column in (a) COCO and (b) UniSim® Design.

Flow rate profiles and temperature profiles simulated in UniSim® Design are compared with the ones from ChemSep PCM, shown in Figure C10 and C11. The results are almost identical with each other.

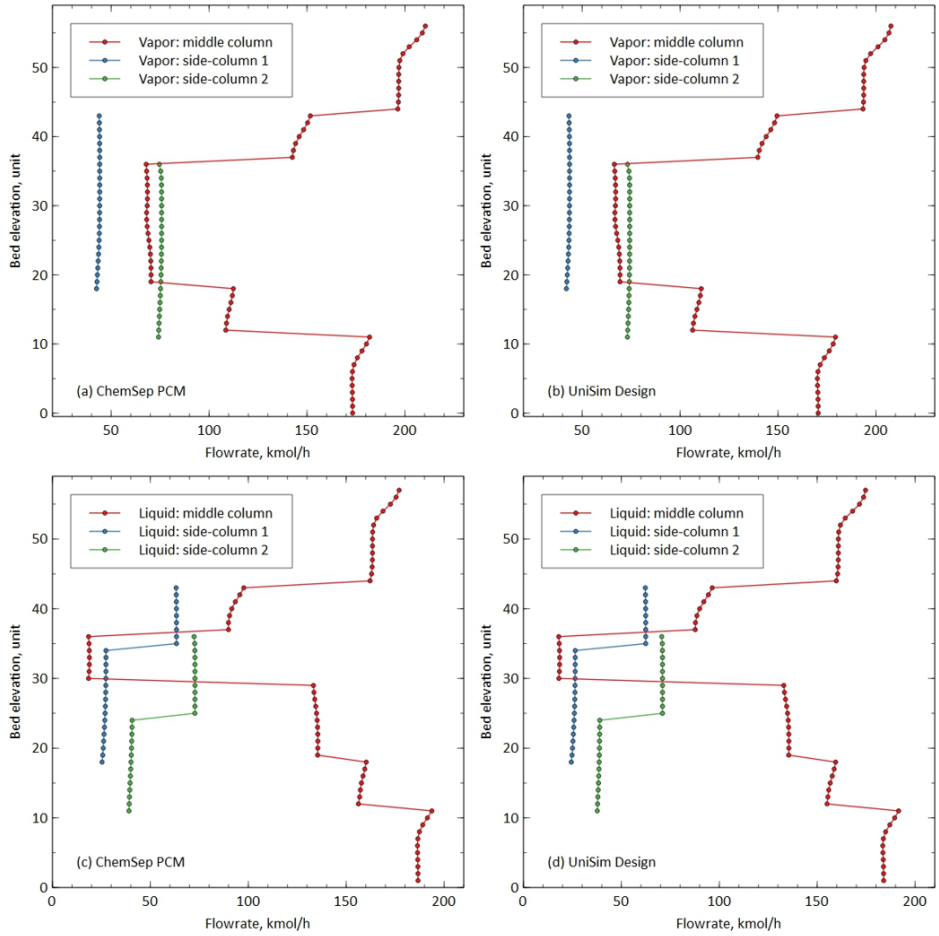

Figure C10 Flowrate profiles simulated from ChemSep PCM and UniSim® Design.

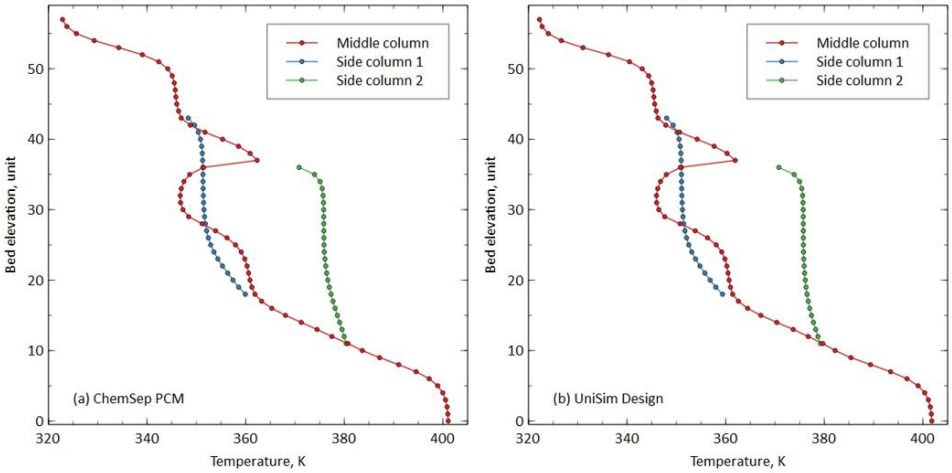

Figure C11 Temperature profiles simulated from (a) ChemSep PCM and (b) UniSim® Design.

4. LNG Simulation

This example is described in detail by Ashrafian (2014). Figure C12 shows a schematic diagram of the multi-partitioned DWC in the LNG production.

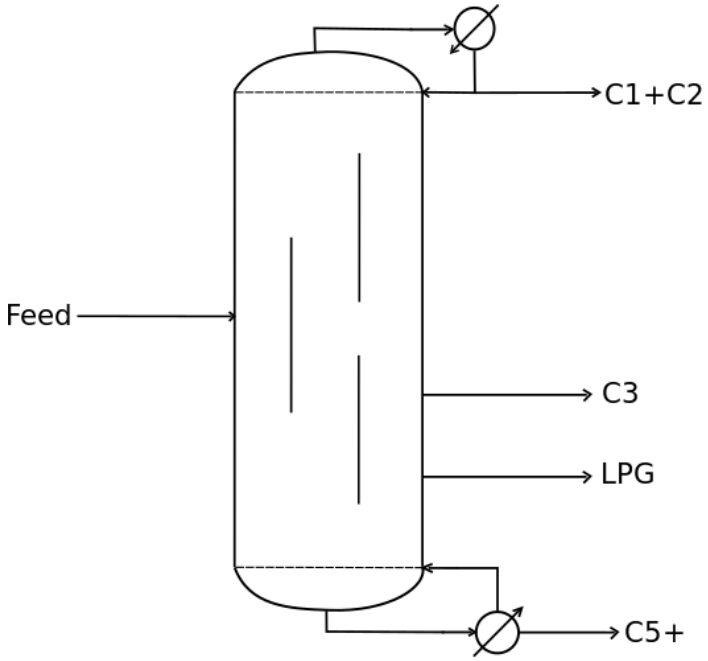

Figure C12 Configuration of a multi-partitioned DWC.

4.1 Simulation with multi-column models

The DWC is simulated by Ashrafian in Aspen Hysys® using a nine-column model to separate ten components (C1 to C8) into four fractions, with all stream information reported in the thesis of Ashrafian (2014). The same multi-column model is built in UniSim® Design to reproduce the work (see Figure C13), with initial guesses obtained from the converged PCM results. The Peng-Robinson equation of state thermodynamic model is used for the simulation.

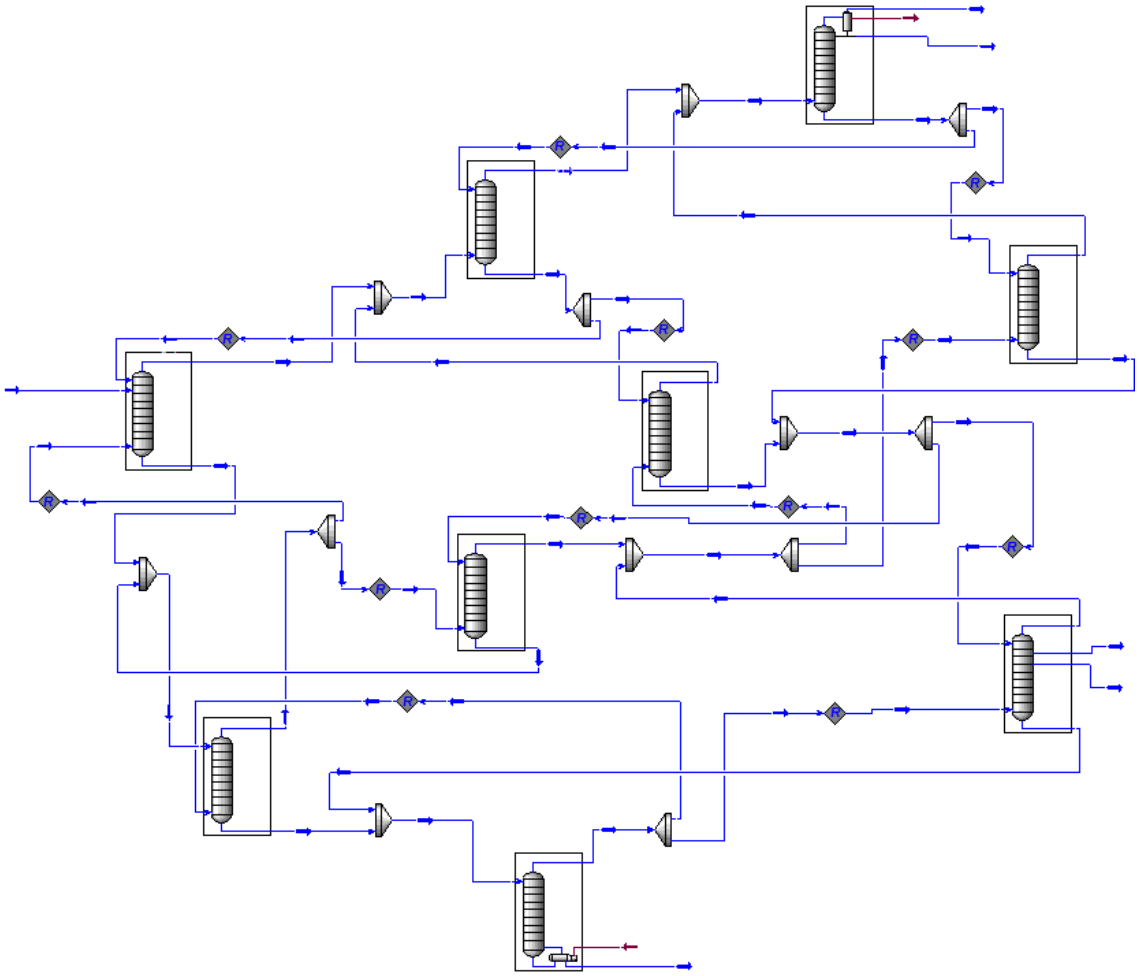

Figure C13 Flowsheet built in UniSim® Design to simulate DWC with three dividing walls.

4.2 Simulation with the PCM

According to the information provided by Ashrafian (2014), the following column structure is built in the PCM (Figure C14), with stages numbered following the rule in Chapter 2.

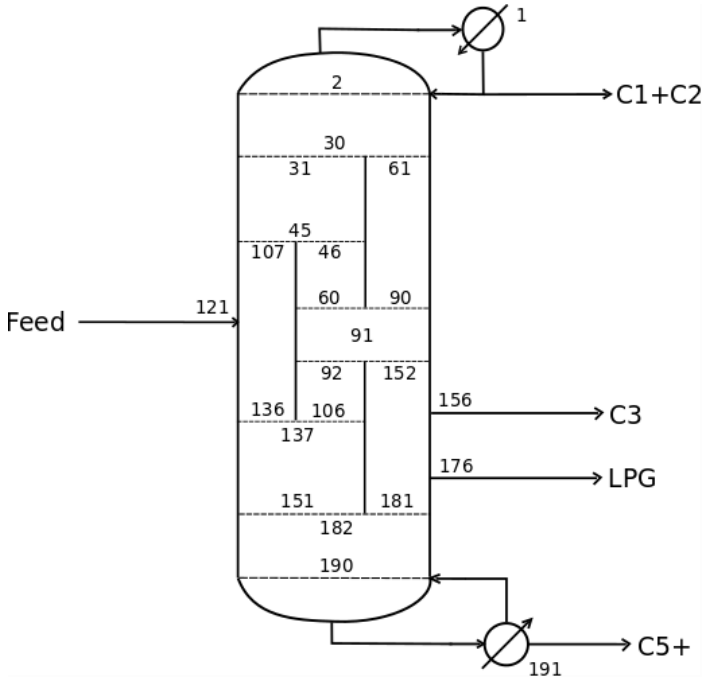

Figure C14 Schematic diagram of the multi-partitioned DWC built in the PCM.

Note that one stage (stage 91 in Figure C14) is added to the PCM, which plays a role as both collector and splitter, thus the mass transfer effeciency for stage 91 is set to a tiny number (e.g. 10^{-15}) in the PCM. The Peng-Robinson equation of state, with binary interaction parameters obtaied from UniSim® Design, is used in the simulation. Vapor and liquid split ratios are summarized in Table C3.

Table C3 Summary of vapor and liquid split ratios in the multi-partitioned DWC.

Phase	From Stage	To Stage	Split Ratio
Liquid	30	31	0.3
		61	0.7
	45	107	0.25
		46	0.75
	60	61	0
		91	1.0
	91	92	0.2
		152	0.8
	106	107	0
		137	1.0
	151	152	0
		182	1.0
Vapor	182	151	0.55
		181	0.45
	152	151	0
		91	1.0
	137	136	0.05
		106	0.95
	107	106	0
		45	1.0
	91	60	0.8
		90	0.2
	61	60	0
		30	1.0

Due to the complexity of this multi-partitioned DWC, temperature or composition profiles are not shown, and only product purities are compared among three simulations (Aspen Hysys, UniSim® Design, and ChemSep PCM), and summarized in Table C4. The three different simulation software predict similar results for the four product streams.

As the two side products are withdrawn from the same column section, we suspect that the upper dividing wall has little function in separating the products. Figure C15 shows the DWC structure with the upper dividing wall omitted from Figure C9. This column is modeled with the PCM, and we compare the product purities with those obtained from Figure C14, see Table C5.

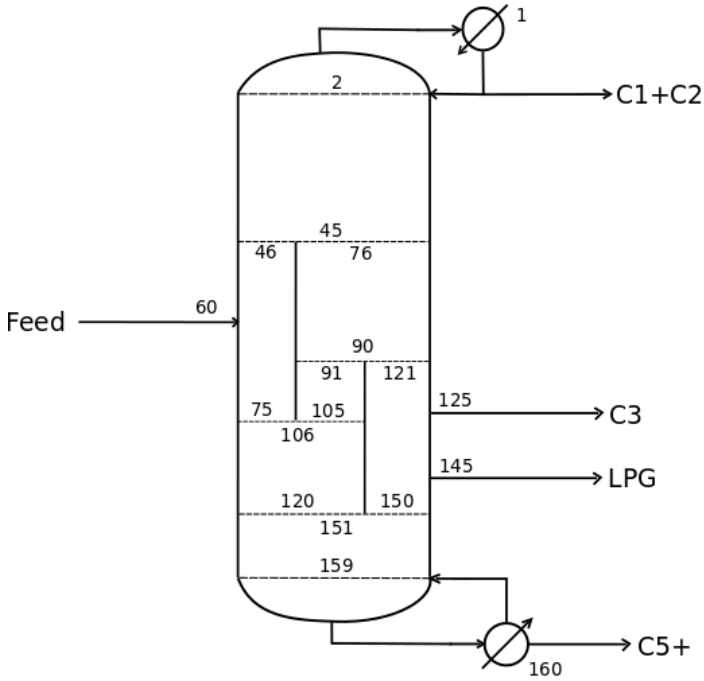

Figure C15 DWC structure with the upper dividing wall omitted from Figure C14.

As is indicated from Table C5, the two-wall DWC and the three-wall DWC tend to give almost identical purities. Therefore, the upper dividing wall does not seem to be necessary in this DWC.

Table C4 Comparisons of product purities from three simulation software.

	C1+C2			C3		
	Hysys	[a]UD	PCM	Hysys	UD	PCM
Temperature, K	238.41	238.44	238.41	337.58	337.59	337.61
Pressure, kPa	2535	2535	2535	2604	2604	2604
Molar flowrate, kmol/h	305.3	305.2	305.3	150	149.9	150
Compositions:						
Methane	0.5939	0.5935	0.5939	0	0	0
Ethane	0.4061	0.4065	0.4061	0.0783	0.0783	0.0786
Propane	0	0	0	0.8899	0.8897	0.8889
i-Butane	0	0	0	0.0159	0.0161	0.0162
n-Butane	0	0	0	0.0159	0.0159	0.0163
i-Pentane	0	0	0	0	0	0
n-Pentane	0	0	0	0	0	0
n-Hexane	0	0	0	0	0	0
n- Heptane	0	0	0	0	0	0
n-Octane	0	0	0	0	0	0
	LPG			C5+		
	Hysys	UD	PCM	Hysys	UD	PCM
Temperature, K	380.45	380.35	380.43	502.75	502.95	502.01
Pressure, kPa	2626	2625	2626	2640	2640	2640
Molar flowrate, kmol/h	315.7	315.8	315.7	75	74.99	75
Compositions:						
Methane	0	0	0	0	0	0
Ethane	0.0008	0.0008	0.0009	0	0	0
Propane	0.2950	0.2952	0.2953	0.0010	0.0010	0.0016
i-Butane	0.2189	0.2192	0.2181	0.0139	0.0138	0.0162
n-Butane	0.4591	0.4597	0.4575	0.0913	0.0902	0.0972
i-Pentane	0.0139	0.0136	0.0152	0.0747	0.0744	0.0689
n-Pentane	0.0101	0.0097	0.0110	0.1030	0.1028	0.0992
n-Hexane	0.0021	0.0017	0.0019	0.2452	0.2464	0.2459
n- Heptane	0.0002	0.0001	0.0001	0.1810	0.1814	0.1811
n-Octane	0	0	0	0.2900	0.2901	0.2898

[a]UD represents UniSim® Design

Table C5 Comparisons of product purities from a two-wall DWC and a three-wall DWC.

	C1+C2		C3		LPG		C5+	
	3-wall	2-wall	3-wall	2-wall	3-wall	2-wall	3-wall	2-wall
Temperature, K	238.41	238.41	337.61	337.54	380.43	380.49	502.01	501.96
Flowrate, kmol/h	305.3	305.3	150	150	315.7	315.7	75	75
Compositions:								
Methane	0.5939	0.5939	0	0	0	0	0	0
Ethane	0.4061	0.4061	0.0786	0.0785	0.0009	0.0009	0	0
Propane	0	0	0.8889	0.8908	0.2953	0.2943	0.0016	0.0016
i-Butane	0	0	0.0162	0.0156	0.2181	0.2184	0.0162	0.0163
n-Butane	0	0	0.0163	0.0151	0.4575	0.4580	0.0972	0.0976
i-Pentane	0	0	0	0	0.0152	0.0153	0.0689	0.0688
n-Pentane	0	0	0	0	0.0110	0.0111	0.0992	0.0990
n-Hexane	0	0	0	0	0.0019	0.0019	0.2459	0.2458
n- Heptane	0	0	0	0	0.0001	0.0001	0.1811	0.1811
n-Octane	0	0	0	0	0	0	0.2898	0.2898

5. Dividing Wall Column Simulation with the ChemSep PCM in UniSim® Design

In this section we demonstrate the simulation of a dividing wall column (DWC) with the Parallel Column Model (PCM) in UniSim® Design. The example used for demonstration is from Ling and Luyben (2009), also discussed in Section 1 of this Appendix.

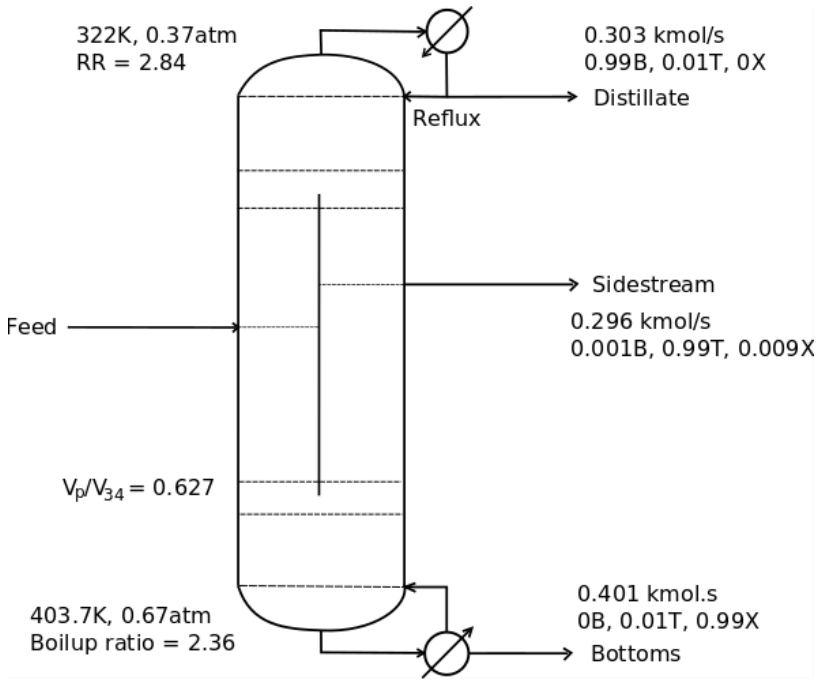

Figure C1 Dividing wall column flowsheet adapted from Ling and Luyben (2009).

A schematic diagram of the column was given above, Figure C1. It is repeated here for convenience of this part of the presentation.

From the diagram, there are 9 stages (including a condenser) in the section above the dividing wall, 24 stages on each side of the wall, and 13 stages (including a reboiler) at the bottom section below the wall. Liquid split ratio is given by Ling and Luyben (2009) as 0.353. Pressure drop is considered in the simulation of Ling and Luyben (2009); for simplicity, we assume constant pressure throughout the whole DWC. The procedures of setting up the ChemSep PCM, via the CAPE-OPEN mechanism, in UniSim® Design are discussed as follows.

1. Open UniSim® Design, then add benzene, toluene, and o-xylene to the simulation.

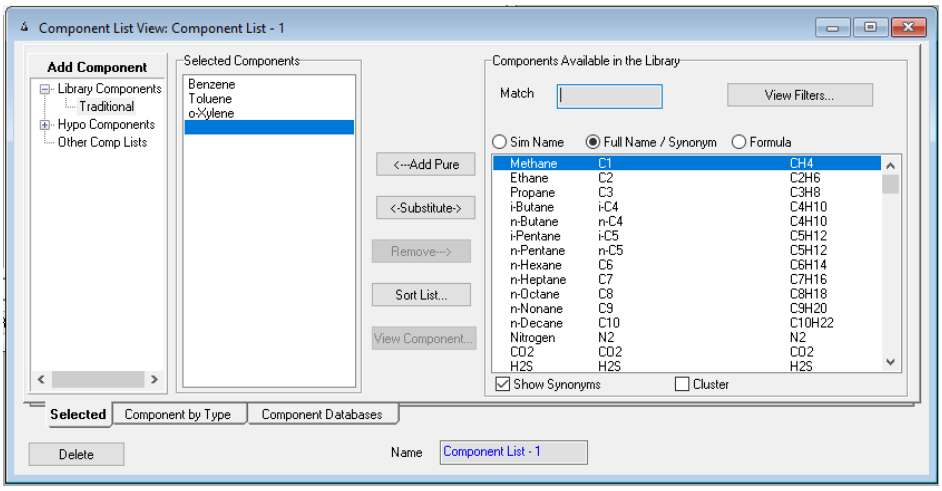

2. Select a fluid package (thermodynamic model) for the simulation. In this case, we use General NRTL model with default parameters from UniSim® Design.

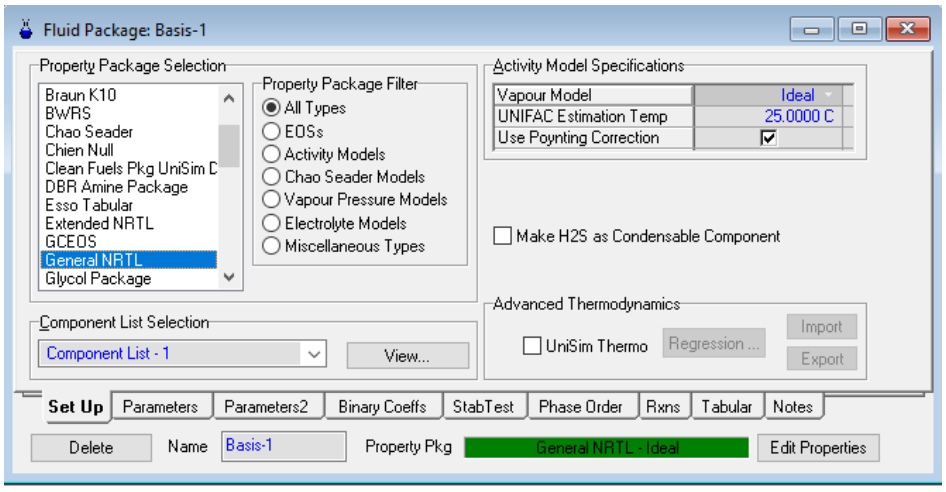

3. Enter the simulation environment, and then insert a material stream (Feed) as the feed to the column.

4. Specify the feed stream temperature, pressure, molar flowrate, and compositions as shown below.

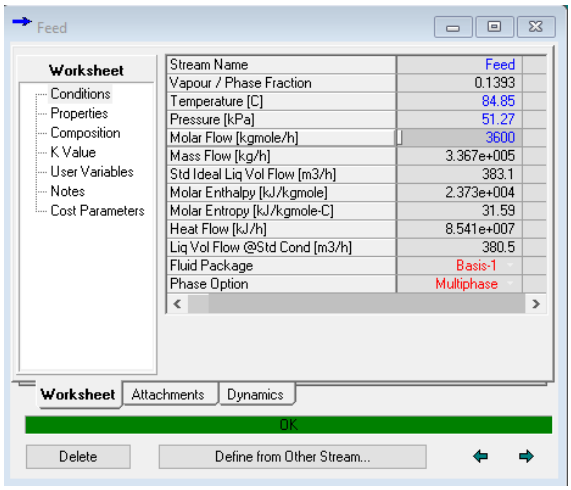

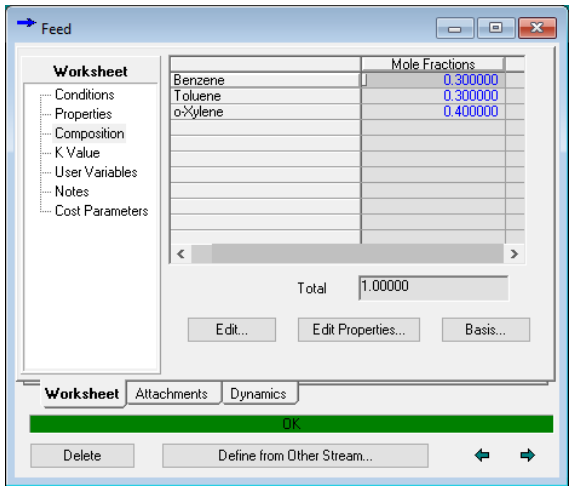

5. Go to Flowsheet -> Add Operation

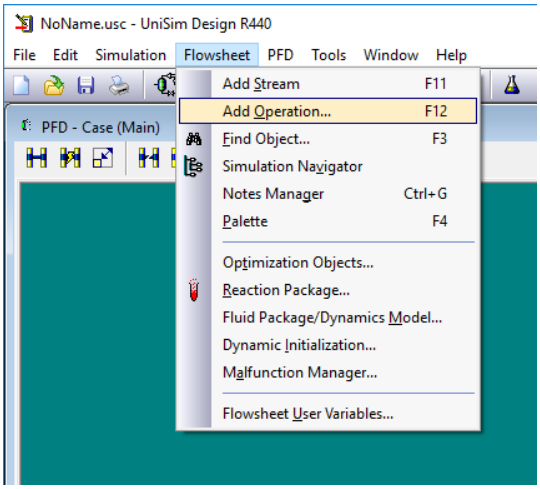

6. In the pop up window, select CAPE-OPEN Unit Operation, and click on the “Add” button.

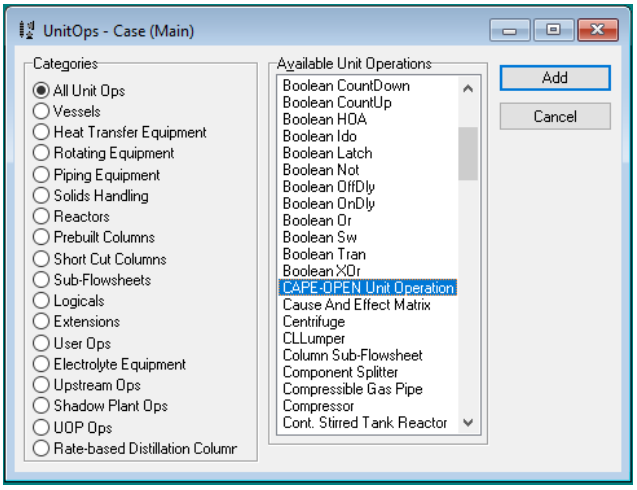

7. Select ChemSep and click on “OK”.

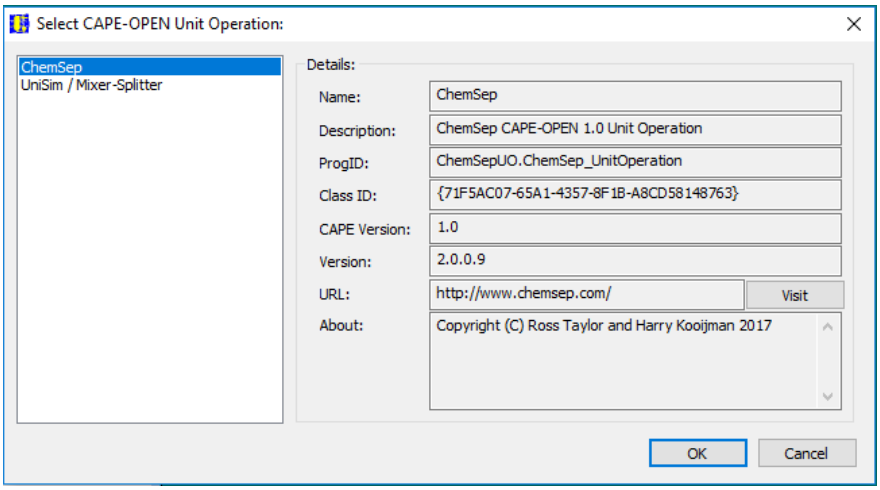

8. In the new pop up window (shown below), clicking on the “Show Unit GUI” button would open the CAPE-OPEN window of ChemSep.

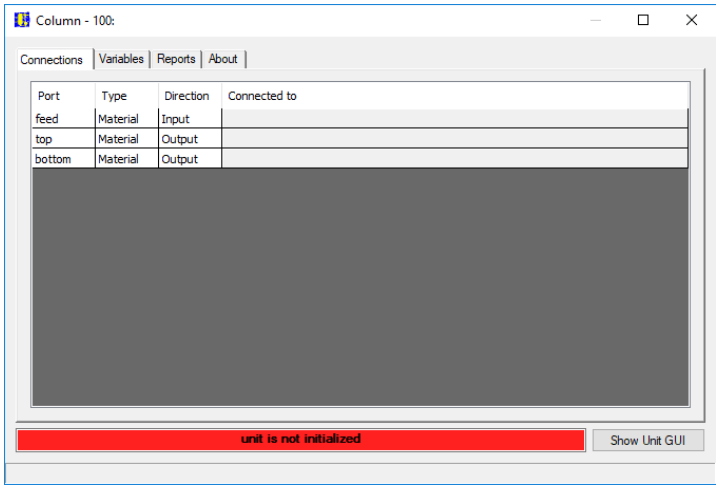

9. In the ChemSep CAPE-OPEN window, do some basic specifications to the column as follows. Users can use Cape-Open thermodynamic model (UniSim® Design in this case), or the thermodynamic model from ChemSep. Clicking on the “OK” button would enter the ChemSep interface.

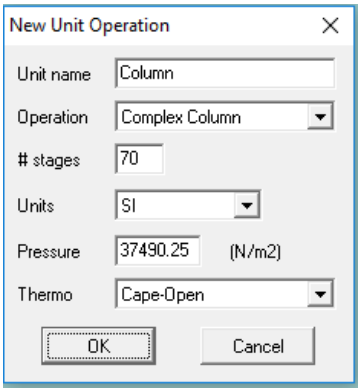

10. In the ChemSep Operation panel, specify the column interconnections for DWC.

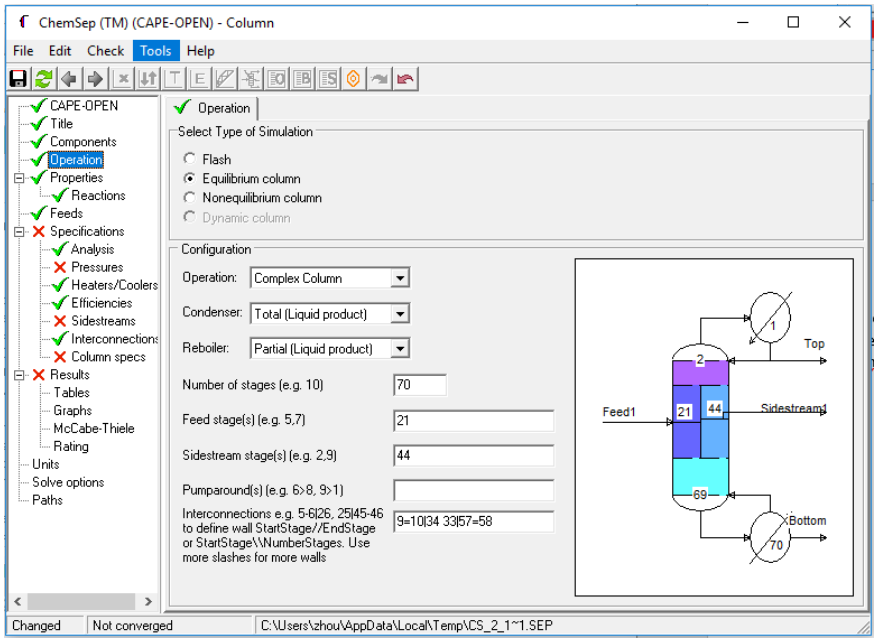

11. Assume the column pressure is constant at 0.37 atm; specify the liquid sidestream molar flowrate to be 0.296 kmol/s.

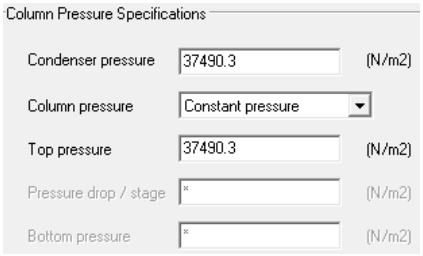

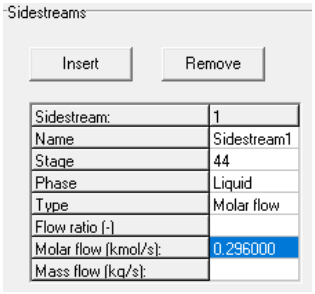

12. In the Interconnections panel, specify the liquid split ratio to be 0.353 / 0.647, while the vapor split ratio to be 0.627 / 0.373:

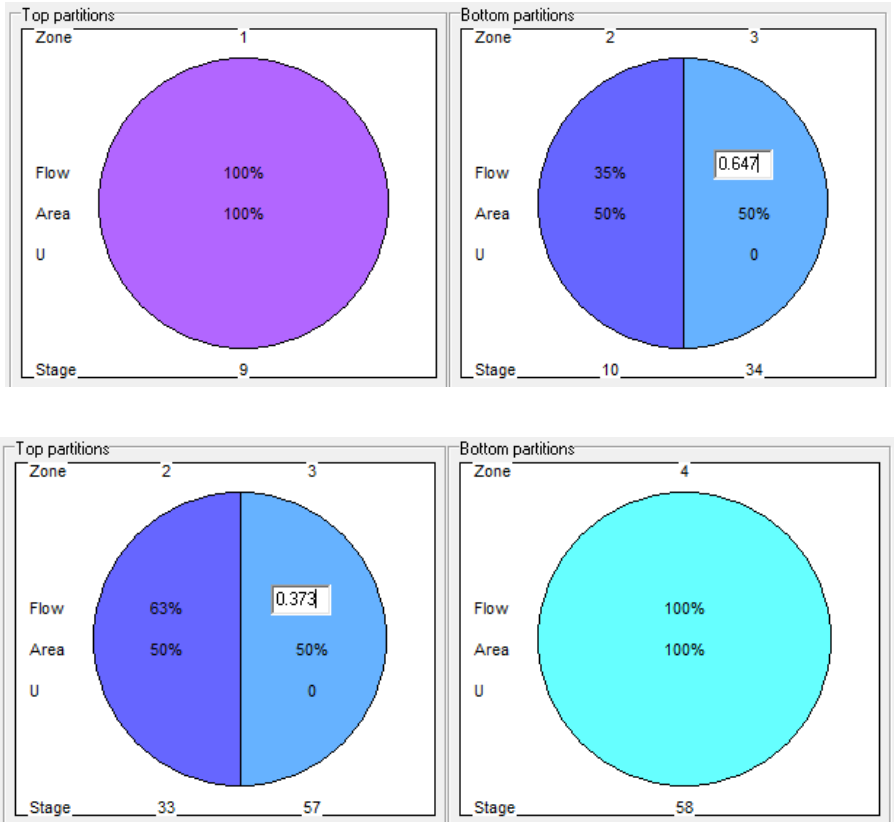

13. Specify the reflux ratio at the top to be 2.83, and the bottom product flow rate to be 0.401 kmol/s.

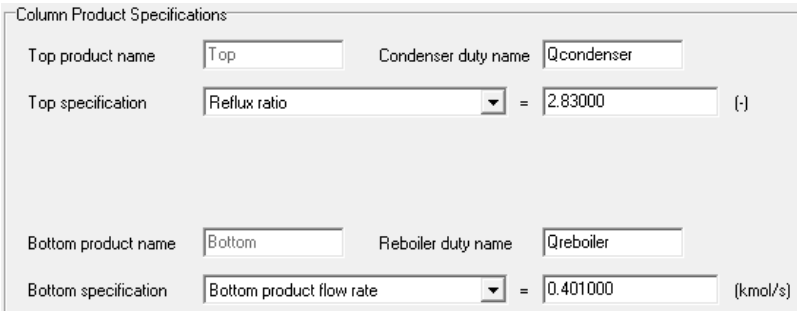

14. Save the ChemSep file, and close the ChemSep interface. A CAPE-OPEN column icon appears now on the flowsheet. Then add three streams, denoted as Top, Side, and Bottom.

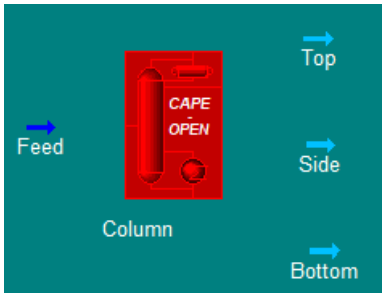

15. Double click on the column icon, and connect the streams to the right ports.

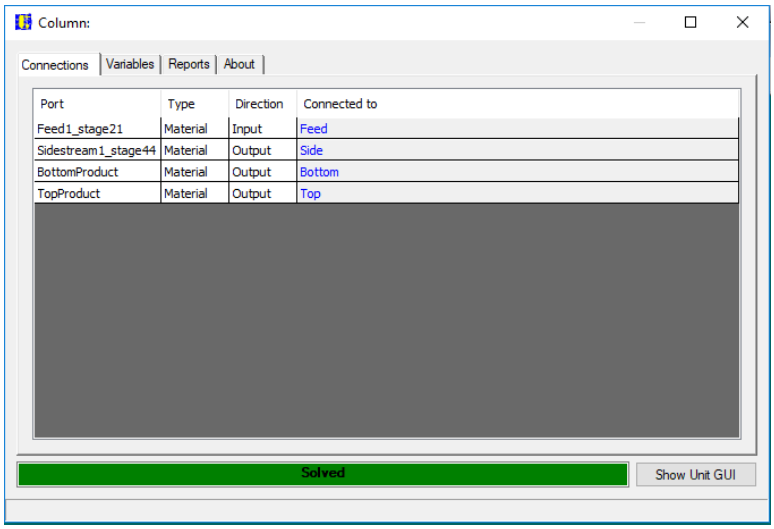

16. Close the Column window, and in the flowsheet the column is now solved.

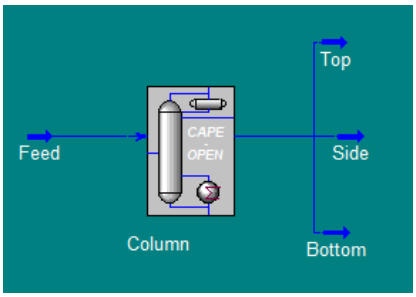

17. Users can then check the results from either UniSim® Design or ChemSep interface. The three product compositions from UniSim® Design are shown below; the simulation results from the ChemSep GUI are also shown below.

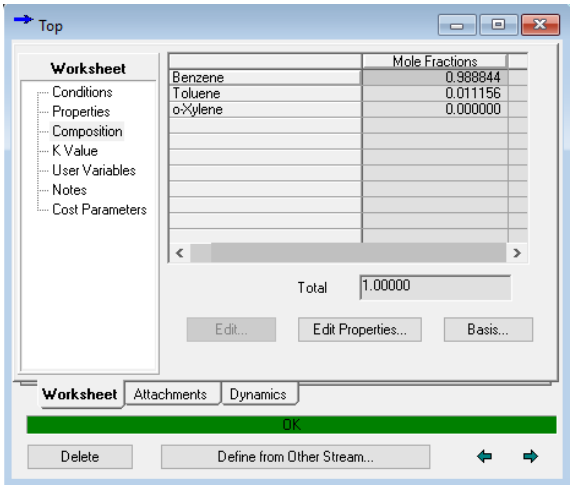

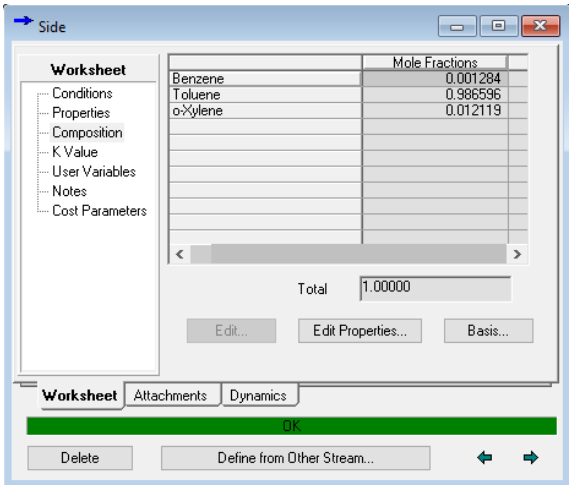

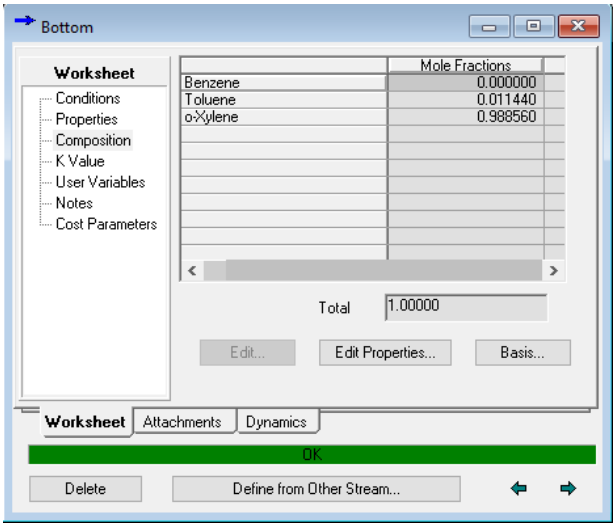

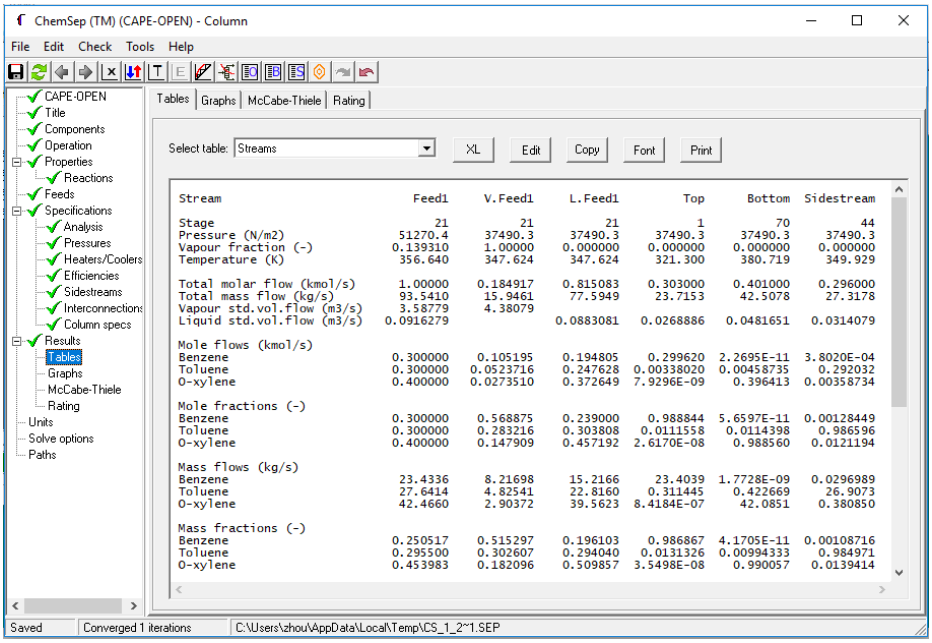

The figure below shows the composition profiles from the ChemSep interface.

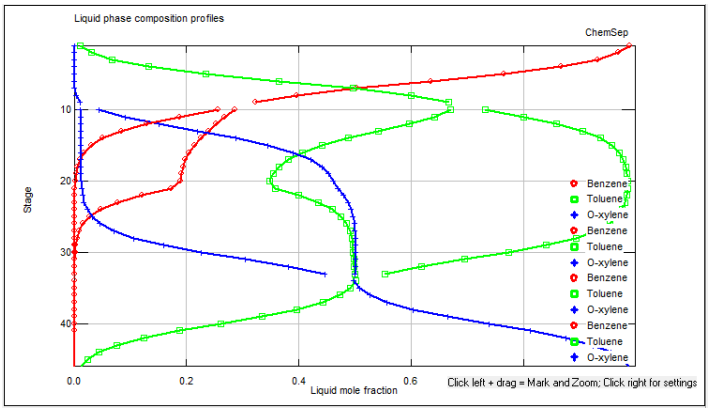

Software Used in This Work

COCO (v3.3) – a modular chemical process simulator available free from www.cocosimulator.org. The column model used in the COCO simulations is a standard ChemSep column model, not the PCM.

UniSim® Design (v6.61.0.0) – a modular process simulator available from Honeywell Inc.

ChemSep™ (v8.0) – A CAPE-OPEN compliant column simulation program. A version of ChemSep including some DWC capability is available free from www.chemsep.org.

Reference

Ashrafian, R., 2014. Using dividing wall columns (DWC) in LNG production: dividing wall column, double dividing wall column, prefractionator arrangement, Petlyuk column, NGL recovery, distillation (Thesis).

Dejanović, I., 2017. Private communication to R. Taylor.

Ling, H., and Luyben, W.L., 2009. New Control Structure for Divided-Wall Columns. *Industrial & Engineering Chemistry Research*, 48(13), pp.6034–6049.

Appendix D: Simulation Results of Cases from Roach (2017)

Alcohol – Total Reflux Case A1

Specifications:

Case Number	A1 (eqm)	A1 (neq)
Feed flowrate (lb/h)	0.99	0.99
Feed temperature (^oF)	99.74	99.74
Feed pressure (psia)	1.0	1.0
Feed Composition (wt%)		
n-Hexanol	33.0	33.0
n-Octanol	33.4	33.4
n-Decanol	32.6	32.6
Sidedraw rate (lb/h)	0.33	0.33
Bottom flowrate (lb/h)	0.33	0.33
Overhead reflux ratio	98.03	98.03
Flow split ratios (left % / right %)		
Vapor split *	50/50	-
Liquid split	50/50	50/50
Pressure overhead (psia)	0.9	0.9
Overall pressure drop (in H_2O)	2.93	-
Wall region pressure drop (in H_2O)	2.3	-
Heat Transfer Coefficients		
Shell (W/m^2K)	0	0
Wall (W/m^2K)	14	14
Surroundings temperature (^oF)	71.00	71.00
* Vapor split ratio is estimated in the rate-based PCM		

eqm: equilibrium-stage PCM, neq: rate-based (or nonequilibrium-stage) PCM

Results:

Product Purity (equilibrium-stage PCM):

	Unit	Pilot	Sim
ovhd_LK	mass frac	0.998	1.000
sidedraw_MK		0.997	1.000
bot_HK		0.986	0.988

Product Purity (rate-based PCM):

	Unit	Pilot	Sim
ovhd_LK	mass frac	0.998	0.998
sidedraw_MK		0.997	0.998
bot_HK		0.986	0.988

Temperature profiles:

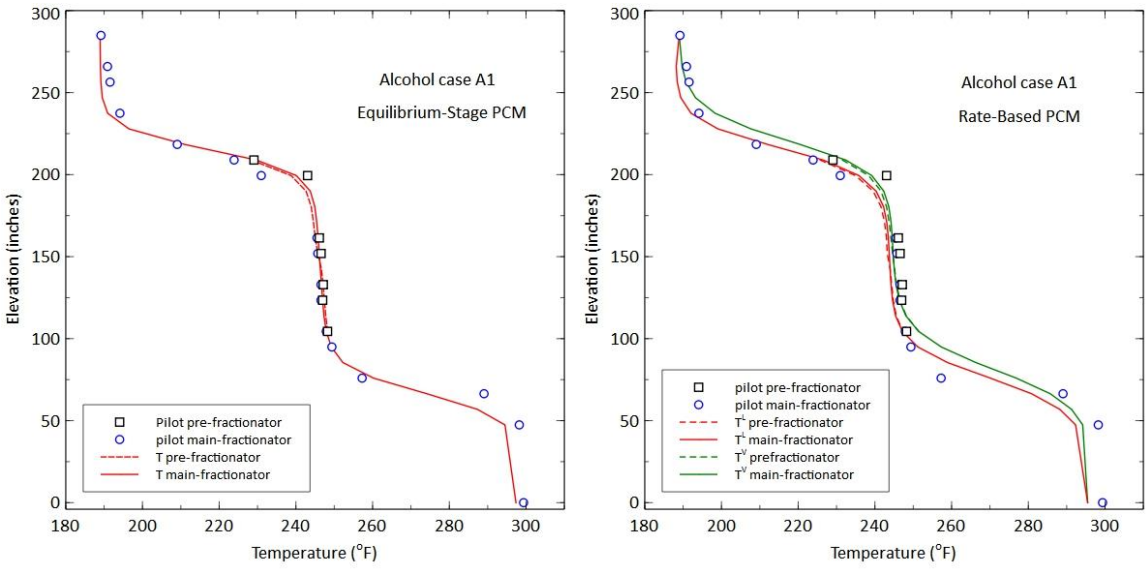

Pressure drop:

	Unit	Pilot	Sim
Overall dp	psia	0.1057	0.0606
Wall region dp		0.0830	0.0318

Estimated vapor split ratio: 50.17% / 49.83%

Alcohol – Total Reflux Case A2

Specifications:

Case Number	A2 (eqm)	A2 (neq)
Feed flowrate (lb/h)	0.99	0.99
Feed temperature (^oF)	118.76	118.76
Feed pressure (psia)	1.0	1.0
Feed Composition (wt%)		
n-Hexanol	33.5	33.5
n-Octanol	33.4	33.4
n-Decanol	32.1	32.1
Sidedraw rate (lb/h)	0.33	0.33
Bottom flowrate (lb/h)	0.33	0.33
Overhead reflux ratio	69.76	69.76
Flow split ratios (left % / right %)		
Vapor split *	50/50	-
Liquid split	30/70	30/70
Pressure overhead (psia)	0.9	0.9
Overall pressure drop (in H_2O)	1.80	-
Wall region pressure drop (in H_2O)	0.93	-
Heat Transfer Coefficients		
Shell (W/m^2K)	0	0
Wall (W/m^2K)	14	14
Surroundings temperature (^oF)	84.00	84.00
* Vapor split ratio is estimated in the rate-based PCM		

Results:

Product Purity (equilibrium-stage PCM):

	Unit	Pilot	Sim
ovhd_LK	mass frac	1.000	0.998
sidedraw_MK		0.982	0.998
bot_HK		0.971	0.988

Product Purity (rate-based PCM):

	Unit	Pilot	Sim
ovhd_LK	mass frac	1.000	0.999
sidedraw_MK		0.982	0.984
bot_HK		0.971	0.973

Temperature profiles:

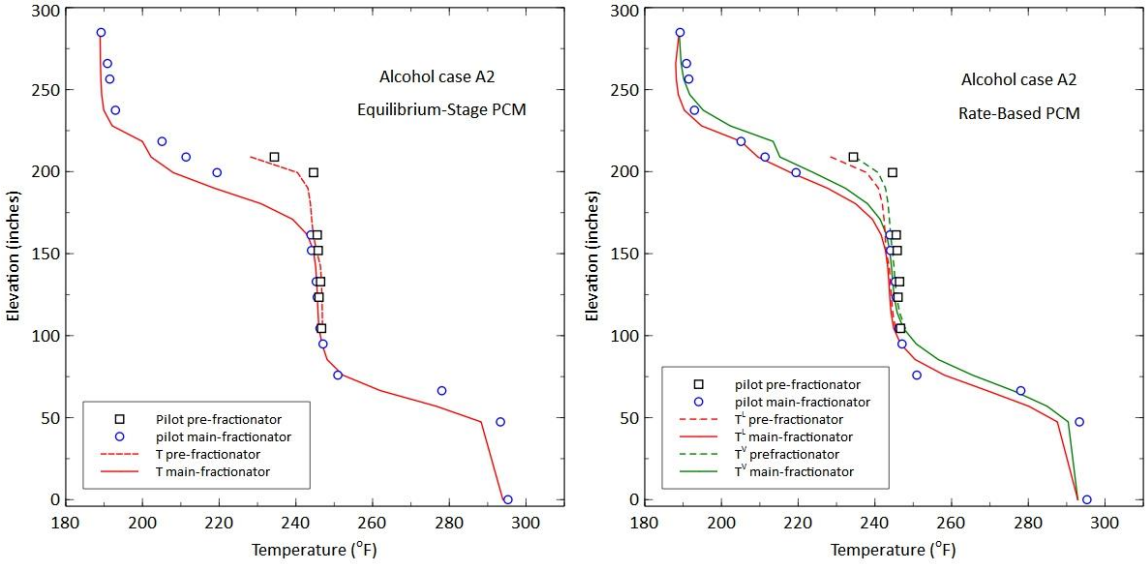

Pressure drop:

	Unit	Pilot	Sim
Overall dp	psia	0.0650	0.0401
Wall region dp		0.0336	0.0199

Estimated vapor split ratio: 50.03% / 49.97%

Alcohol – Total Reflux Case A3

Specifications:

Case Number	A3 (eqm)	A3 (neq)
Feed flowrate (lb/h)	0.99	0.99
Feed temperature (^oF)	95.01	95.01
Feed pressure (psia)	1.0	1.0
Feed Composition (wt%)		
n-Hexanol	33.1	33.1
n-Octanol	33.9	33.9
n-Decanol	32.0	32.0
Sidedraw rate (lb/h)	0.33	0.33
Bottom flowrate (lb/h)	0.33	0.33
Overhead reflux ratio	86.58	86.58
Flow split ratios (left % / right %)		
Vapor split *	50/50	-
Liquid split	70/30	70/30
Pressure overhead (psia)	0.9	0.9
Overall pressure drop (in H_2O)	2.51	-
Wall region pressure drop (in H_2O)	1.36	-
Heat Transfer Coefficients		
Shell (W/m^2K)	0	0
Wall (W/m^2K)	14	14
Surroundings temperature (^oF)	75.00	75.00
* Vapor split ratio is estimated in the rate-based PCM		

Results:

Product Purity (equilibrium-stage PCM):

	Unit	Pilot	Sim
ovhd_LK	mass frac	1.000	1.000
sidedraw_MK		1.000	0.997
bot_HK		0.973	0.970

Product Purity (rate-based PCM):

	Unit	Pilot	Sim
ovhd_LK	mass frac	1.000	1.000
sidedraw_MK		1.000	0.996
bot_HK		0.973	0.969

Temperature profiles:

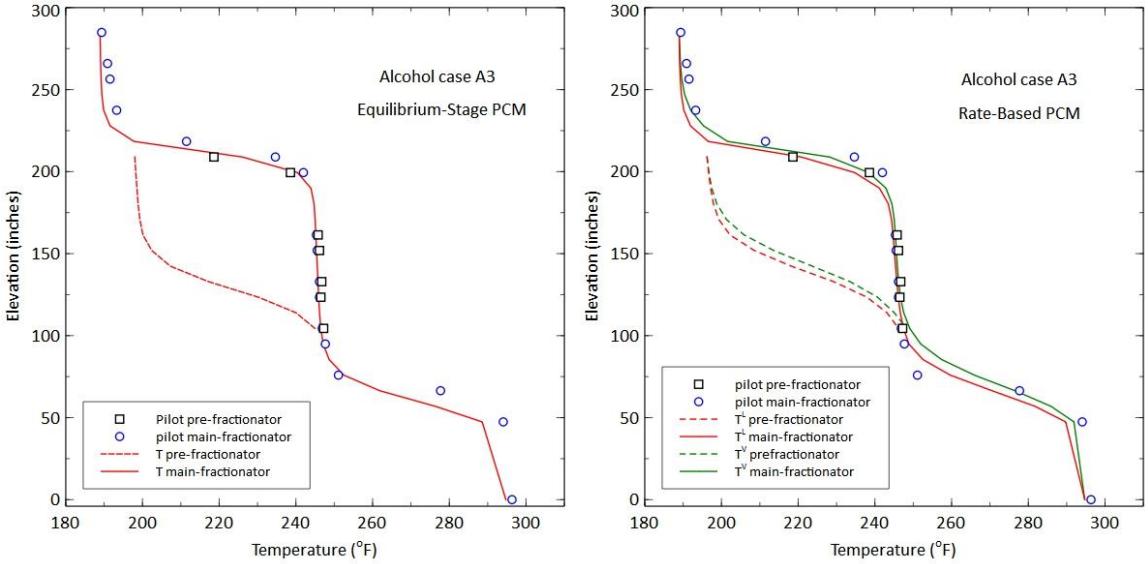

Pressure drop:

	Unit	Pilot	Sim
Overall dp	psia	0.0906	0.0906
Wall region dp		0.0491	0.0491

Estimated vapor split ratio: 50.00% / 50.00%

The predicted temperatures in the pre-fractionator have large deviations to the pilot data, and this case is considered an outlier when making the parity plot.

Alcohol – Total Reflux Case A4

Specifications:

Case Number	A4 (eqm)	A4 (neq)
Feed flowrate (lb/h)	0.99	0.99
Feed temperature (^oF)	92.11	92.11
Feed pressure (psia)	1.0	1.0
Feed Composition (wt%)		
n-Hexanol	33.7	33.7
n-Octanol	33.1	33.1
n-Decanol	32.2	32.2
Sidedraw rate (lb/h)	0.33	0.33
Bottom flowrate (lb/h)	0.33	0.33
Overhead reflux ratio	85.09	85.09
Flow split ratios (left % / right %)		
Vapor split *	50/50	-
Liquid split	20/80	20/80
Pressure overhead (psia)	0.9	0.9
Overall pressure drop (in H_2O)	2.27	-
Wall region pressure drop (in H_2O)	1.21	-
Heat Transfer Coefficients		
Shell (W/m^2K)	0	0
Wall (W/m^2K)	14	14
Surroundings temperature (^oF)	77.00	77.00
* Vapor split ratio is estimated in the rate-based PCM		

Results:

Product Purity (equilibrium-stage PCM):

	Unit	Pilot	Sim
ovhd_LK	mass frac	1.000	1.000
sidedraw_MK		0.975	0.978
bot_HK		0.972	0.975

Product Purity (rate-based PCM):

	Unit	Pilot	Sim
ovhd_LK	mass frac	1.000	0.999
sidedraw_MK		0.975	0.977
bot_HK		0.972	0.975

Temperature profiles:

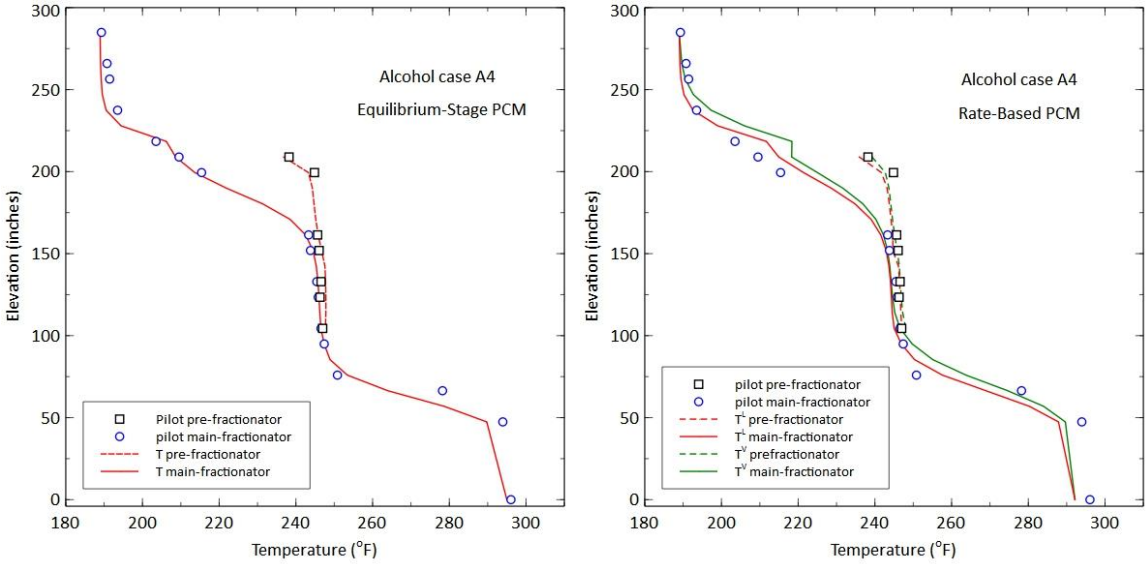

Pressure drop:

	Unit	Pilot	Sim
Overall dp	psia	0.0819	0.0187
Wall region dp		0.0437	0.0091

Estimated vapor split ratio: 50.41% / 49.59%

Alcohol – 10/80/10 Case A7

Specifications:

Case Number	A7 (eqm)	A7 (neq)
Feed flowrate (lb/h)	42.76	42.76
Feed temperature (^oF)	198.11	198.11
Feed pressure (psia)	1.0	1.0
Feed Composition (wt%)		
n-Hexanol	4.9	4.9
n-Octanol	71.6	71.6
n-Decanol	23.5	23.5
Sidedraw rate (lb/h)	30.68	30.74
Bottom flowrate (lb/h)	9.99	9.99
Overhead reflux ratio	19.54	19.54
Flow split ratios (left % / right %)		
Vapor split *	50/50	-
Liquid split	50/50	50/50
Pressure overhead (psia)	0.9	0.9
Overall pressure drop (in H_2O)	3.62	-
Wall region pressure drop (in H_2O)	1.78	-
Heat Transfer Coefficients		
Shell (W/m^2K)	14	14
Wall (W/m^2K)	1500	660
Surroundings temperature (^oF)	71.81	71.81

* Vapor split ratio is estimated in the rate-based PCM.

Results:

Product Purity (equilibrium-stage PCM):

	Unit	Pilot	Sim
ovhd_LK	mass frac	0.998	1.000
sidedraw_MK		0.994	0.995
bot_HK		0.997	0.991

Product Purity (rate-based PCM):

	Unit	Pilot	Sim
ovhd_LK	mass frac	0.998	0.999
sidedraw_MK		0.994	0.984
bot_HK		0.997	0.962

Temperature profiles:

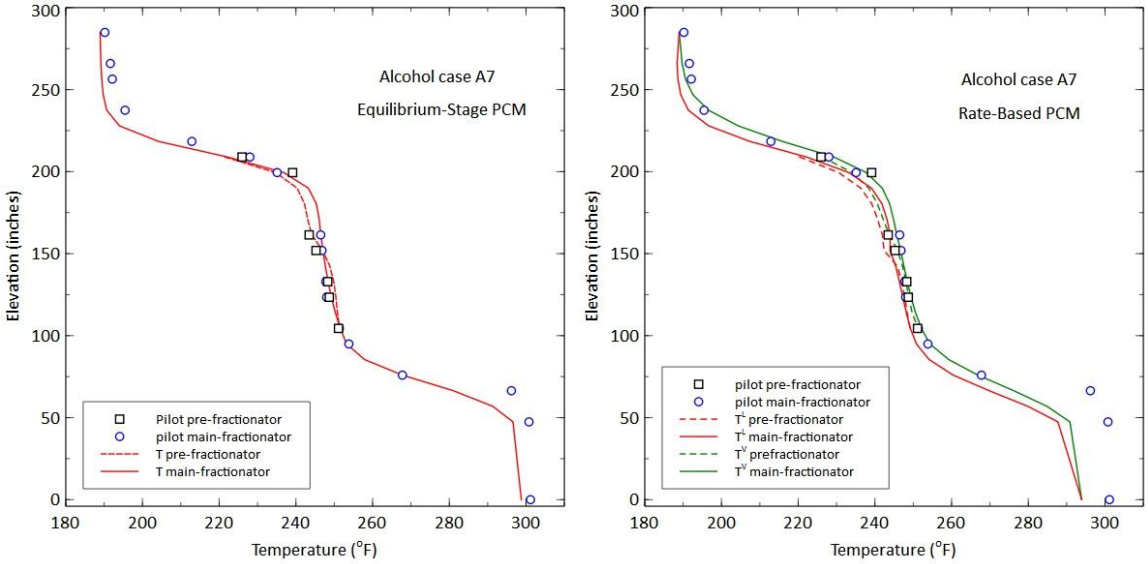

Pressure drop:

	Unit	Pilot	Sim
Overall dp	psia	0.1306	0.0878
Wall region dp		0.0642	0.0450

Estimated vapor split ratio: 51.12% / 48.82%

Alcohol – 10/80/10 Case A9i

Specifications:

Case Number	A9i (eqm)	A9i (neq)
Feed flowrate (lb/h)	41.47	41.47
Feed temperature (^oF)	198.00	198.00
Feed pressure (psia)	1.0	1.0
Feed Composition (wt%)		
n-Hexanol	7.9	7.9
n-Octanol	72.7	72.7
n-Decanol	19.4	19.4
Sidedraw rate (lb/h)	30.16	30.16
Bottom flowrate (lb/h)	8.08	8.08
Overhead reflux ratio	8.55	8.55
Flow split ratios (left % / right %)		
Vapor split *	50/50	-
Liquid split	44/56	44/56
Pressure overhead (psia)	0.9	0.9
Overall pressure drop (in H_2O)	2.57	-
Wall region pressure drop (in H_2O)	1.19	-
Heat Transfer Coefficients		
Shell (W/m^2K)	14	14
Wall (W/m^2K)	31317.3	31317.3
Surroundings temperature (^oF)	73.68	73.68

* Vapor split ratio is estimated in the rate-based PCM.

Results:

Product Purity (equilibrium-stage PCM):

	Unit	Pilot	Sim
ovhd_LK	mass frac	0.997	0.998
sidedraw_MK		0.997	0.998
bot_HK		0.990	0.994

Product Purity (rate-based PCM):

	Unit	Pilot	Sim
ovhd_LK	mass frac	0.997	0.994
sidedraw_MK		0.997	0.992
bot_HK		0.990	0.973

Temperature profiles:

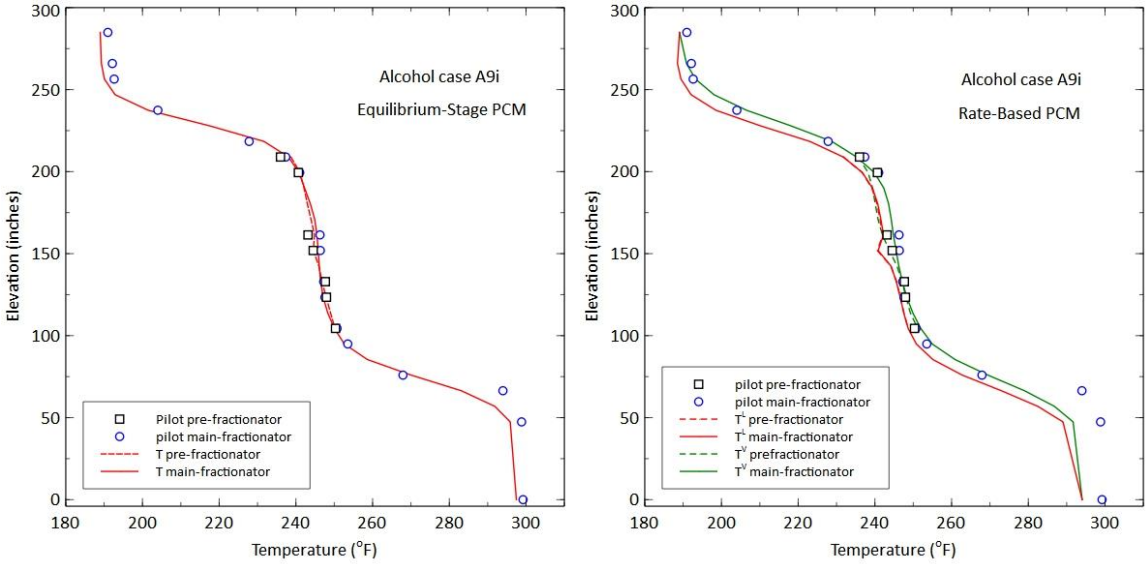

Pressure drop:

	Unit	Pilot	Sim
Overall dp	psia	0.0928	0.0648
Wall region dp		0.0429	0.0327

Estimated vapor split ratio: 48.45% / 51.55%

Alcohol – 10/80/10 Case A9ii

Specifications:

Case Number	A9ii (eqm)	A9ii (neq)
Feed flowrate (lb/h)	51.57	51.57
Feed temperature (^oF)	199.50	199.50
Feed pressure (psia)	1.0	1.0
Feed Composition (wt%)		
n-Hexanol	7.6	7.6
n-Octanol	74.6	74.6
n-Decanol	17.8	17.8
Sidedraw rate (lb/h)	38.72	38.72
Bottom flowrate (lb/h)	8.99	8.99
Overhead reflux ratio	6.45	6.45
Flow split ratios (left % / right %)		
Vapor split *	50/50	-
Liquid split	26/74	26/74
Pressure overhead (psia)	0.9	0.9
Overall pressure drop (in H_2O)	2.41	-
Wall region pressure drop (in H_2O)	1.09	-
Heat Transfer Coefficients		
Shell (W/m^2K)	14	14
Wall (W/m^2K)	1000	1000
Surroundings temperature (^oF)	75.75	75.75

* Vapor split ratio is estimated in the rate-based PCM.

Results:

Product Purity (equilibrium-stage PCM):

	Unit	Pilot	Sim
ovhd_LK	mass frac	0.995	0.682
sidedraw_MK		0.993	0.973
bot_HK		0.997	0.914

Product Purity (rate-based PCM):

	Unit	Pilot	Sim
ovhd_LK	mass frac	0.995	0.990
sidedraw_MK		0.993	0.983
bot_HK		0.997	0.959

Temperature profiles:

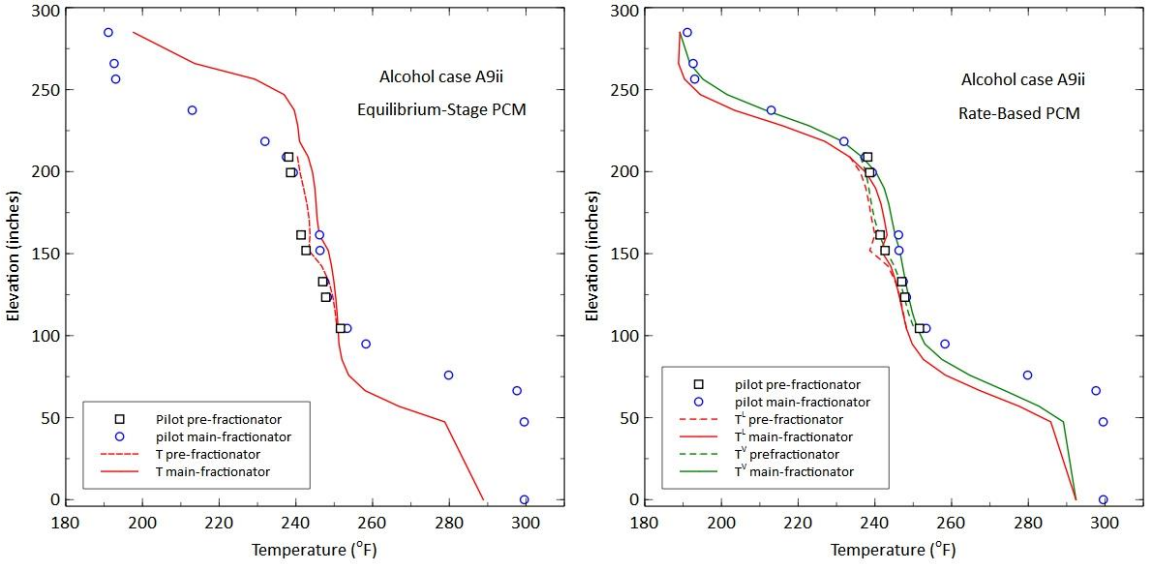

Pressure drop:

	Unit	Pilot	Sim
Overall dp	psia	0.0870	0.0612
Wall region dp		0.0393	0.0306

Estimated vapor split ratio: 49.87% / 50.13%

Alcohol – Equimolar Case A10i

Specifications:

Case Number	A10i (eqm)	A10i (neq)
Feed flowrate (lb/h)	67.15	67.15
Feed temperature (^oF)	203.55	203.55
Feed pressure (psia)	1.0	1.0
Feed Composition (wt%)		
n-Hexanol	24.5	24.5
n-Octanol	36.8	36.8
n-Decanol	38.7	38.7
Sidedraw rate (lb/h)	24.75	24.86
Bottom flowrate (lb/h)	25.96	25.96
Overhead reflux ratio	1.42	1.42
Flow split ratios (left % / right %)		
Vapor split *	50/50	-
Liquid split	26/74	26/74
Pressure overhead (psia)	0.9	0.9
Overall pressure drop (in H_2O)	2.97	-
Wall region pressure drop (in H_2O)	1.34	-
Heat Transfer Coefficients		
Shell (W/m^2K)	14	14
Wall (W/m^2K)	250	350
Surroundings temperature (^oF)	74.61	74.61

* Vapor split ratio is estimated in the rate-based PCM.

Results:

Product Purity (equilibrium-stage PCM):

	Unit	Pilot	Sim
ovhd_LK	mass frac	0.994	0.998
sidedraw_MK		0.989	0.994
bot_HK		0.998	0.997

Product Purity (rate-based PCM):

	Unit	Pilot	Sim
ovhd_LK	mass frac	0.994	0.992
sidedraw_MK		0.989	0.977
bot_HK		0.998	0.989

Temperature profiles:

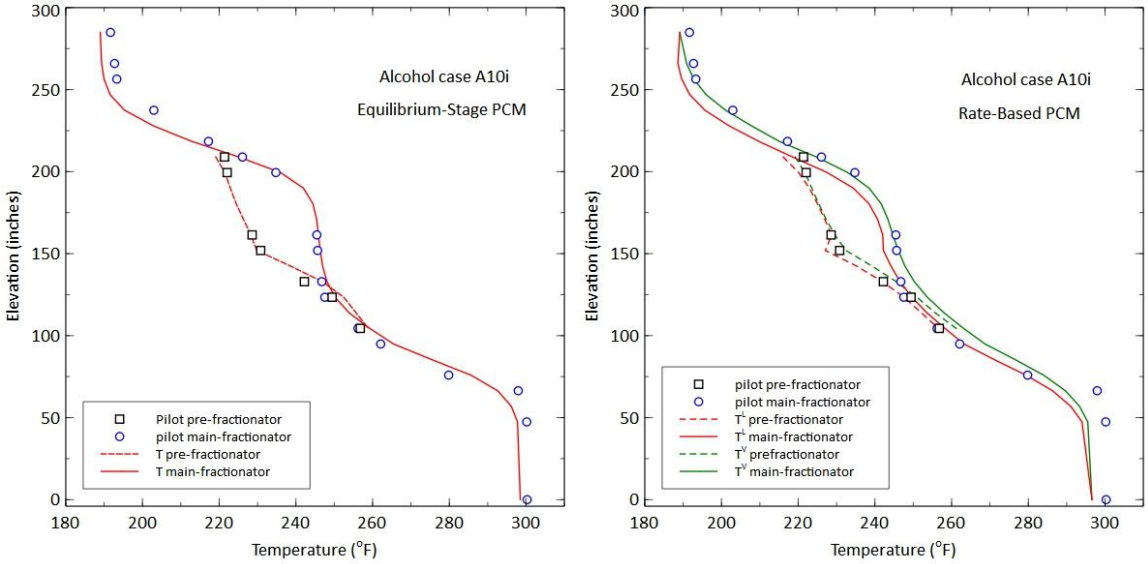

Pressure drop:

	Unit	Pilot	Sim
Overall dp	psia	0.1072	0.0822
Wall region dp		0.0484	0.0398

Estimated vapor split ratio: 47.93% / 52.07%

Alcohol – Equimolar Case A10ii

Specifications:

Case Number	A10ii (eqm)	A10ii (neq)
Feed flowrate (lb/h)	66.73	66.73
Feed temperature (°F)	202.39	202.39
Feed pressure (psia)	1.00	1.00
Feed Composition (wt%)		
n-Hexanol	24.4	24.4
n-Octanol	37.1	37.1
n-Decanol	38.5	38.5
Sidedraw rate (lb/h)	24.75	24.86
Bottom flowrate (lb/h)	25.66	25.66
Overhead reflux ratio	1.12	1.12
Flow split ratios (left % / right %)		
Vapor split *	50/50	-
Liquid split	32/68	32/68
Pressure overhead (psia)	0.9	0.9
Overall pressure drop (in H_2O)	3.29	-
Wall region pressure drop (in H_2O)	1.52	-
Heat Transfer Coefficients		
Shell (W/m^2K)	14	14
Wall (W/m^2K)	400	400
Surroundings temperature (°F)	73.91	73.91

* Vapor split ratio is estimated in the rate-based PCM.

Results:

Product Purity (equilibrium-stage PCM):

	Unit	Pilot	Sim
ovhd_LK	mass frac	0.994	0.994
sidedraw_MK		0.989	0.992
bot_HK		0.997	0.996

Product Purity (rate-based PCM):

	Unit	Pilot	Sim
ovhd_LK	mass frac	0.994	0.987
sidedraw_MK		0.989	0.974
bot_HK		0.997	0.987

Temperature profiles:

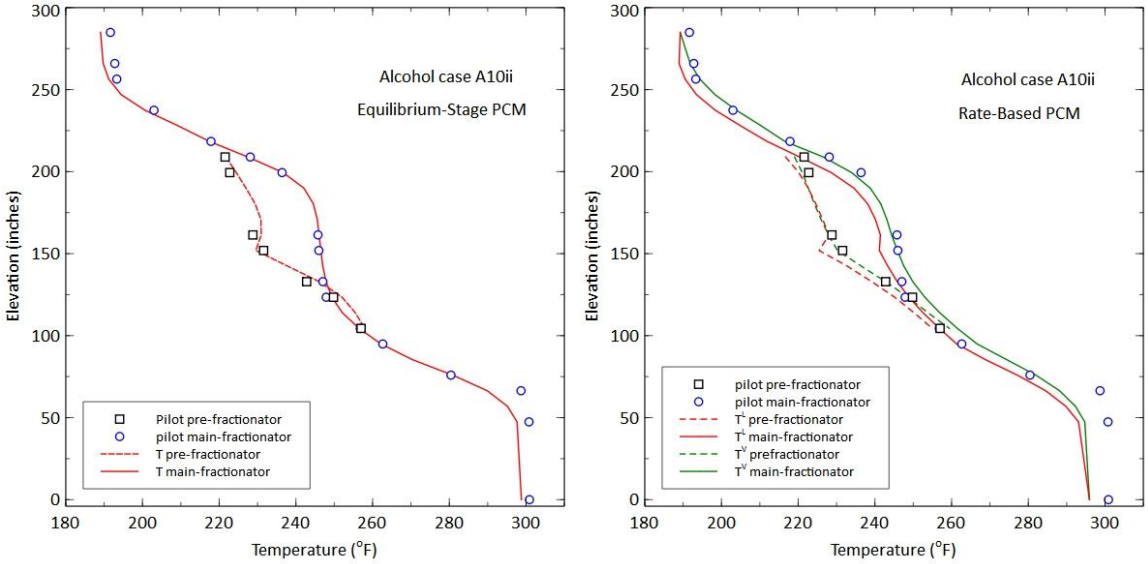

Pressure drop:

	Unit	Pilot	Sim
Overall dp	psia	0.1187	0.0723
Wall region dp		0.0548	0.0342

Estimated vapor split ratio: 46.15% / 53.85%

Alcohol – Equimolar Case A12

Specifications:

Case Number	A12 (eqm)	A12 (neq)
Feed flowrate (lb/h)	66.92	66.92
Feed temperature (^oF)	203.38	203.38
Feed pressure (psia)	1.00	1.00
Feed Composition (wt%)		
n-Hexanol	24.1	24.1
n-Octanol	36.2	36.2
n-Decanol	39.7	39.7
Sidedraw rate (lb/h)	23.24	23.24
Bottom flowrate (lb/h)	27.98	27.98
Overhead reflux ratio	2.17	2.17
Flow split ratios (left % / right %)		
Vapor split *	50/50	-
Liquid split	75/25	75/25
Pressure overhead (psia)	0.9	0.9
Overall pressure drop (in H_2O)	3.44	-
Wall region pressure drop (in H_2O)	1.61	-
Heat Transfer Coefficients		
Shell (W/m^2K)	14	14
Wall (W/m^2K)	90	120
Surroundings temperature (^oF)	67.42	67.42

* Vapor split ratio is estimated in the rate-based PCM.

Results:

Product Purity (equilibrium-stage PCM):

	Unit	Pilot	Sim
ovhd_LK	mass frac	0.995	0.999
sidedraw_MK		0.963	0.939
bot_HK		0.936	0.915

Product Purity (rate-based PCM):

	Unit	Pilot	Sim
ovhd_LK	mass frac	0.995	0.996
sidedraw_MK		0.963	0.937
bot_HK		0.936	0.915

Temperature profiles:

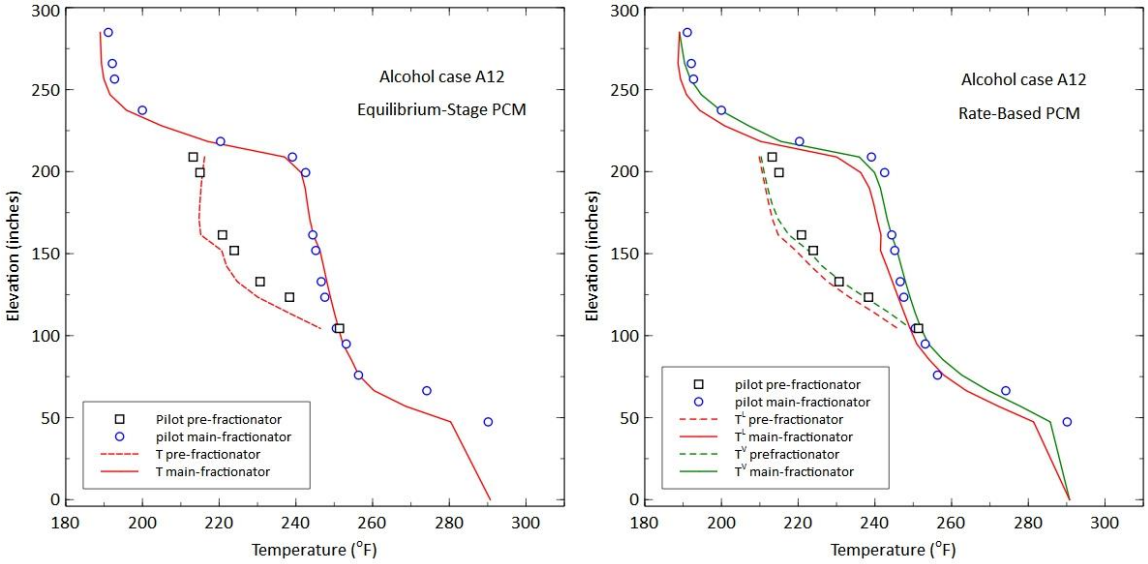

Pressure drop:

	Unit	Pilot	Sim
Overall dp	psia	0.1241	0.1221
Wall region dp		0.0581	0.0625

Estimated vapor split ratio: 49.10% / 50.90%

Alcohol – Equimolar Case A13

Specifications:

Case Number	A13 (eqm)	A13 (neq)
Feed flowrate (lb/h)	54.98	54.98
Feed temperature (^oF)	199.4	199.4
Feed pressure (psia)	1.00	1.00
Feed Composition (wt%)		
n-Hexanol	24.8	24.8
n-Octanol	37.0	37.0
n-Decanol	38.2	38.2
Sidedraw rate (lb/h)	20.87	20.87
Bottom flowrate (lb/h)	21.59	21.59
Overhead reflux ratio	1.63	1.63
Flow split ratios (left % / right %)		
Vapor split *	50/50	-
Liquid split	50/50	50/50
Pressure overhead (psia)	0.9	0.9
Overall pressure drop (in H_2O)	3.44	-
Wall region pressure drop (in H_2O)	1.61	-
Heat Transfer Coefficients		
Shell (W/m^2K)	14	14
Wall (W/m^2K)	150	300
Surroundings temperature (^oF)	74.40	74.40

* Vapor split ratio is estimated in the rate-based PCM.

Results:

Product Purity (equilibrium-stage PCM):

	Unit	Pilot	Sim
ovhd_LK	mass frac	0.994	0.996
sidedraw_MK		0.985	0.993
bot_HK		0.993	0.995

Product Purity (rate-based PCM):

	Unit	Pilot	Sim
ovhd_LK	mass frac	0.994	0.989
sidedraw_MK		0.985	0.981
bot_HK		0.993	0.987

Temperature profiles:

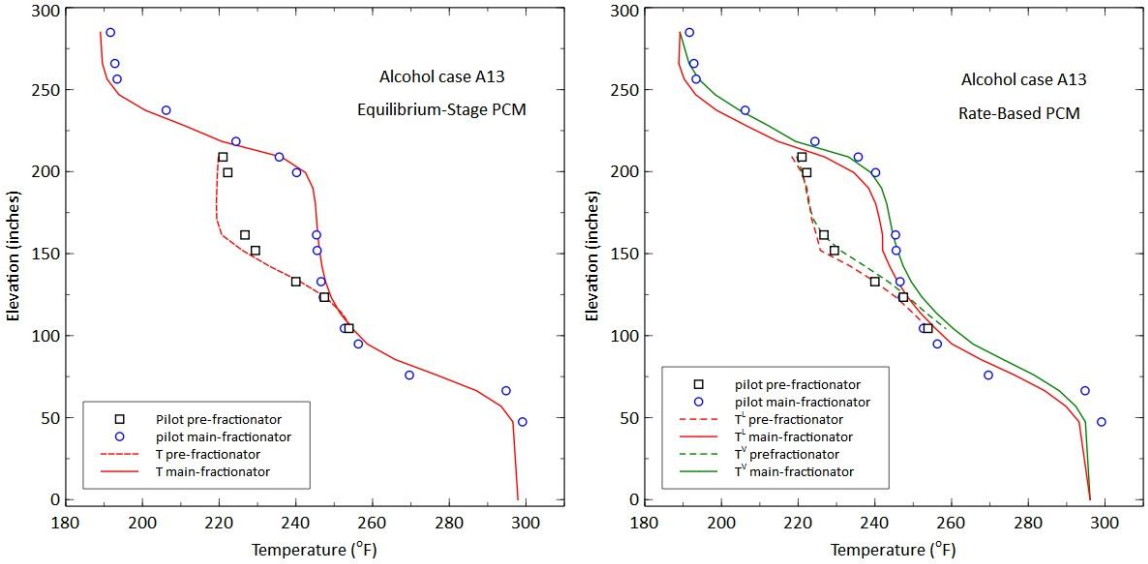

Pressure drop:

	Unit	Pilot	Sim
Overall dp	psia	0.1003	0.0761
Wall region dp		0.0451	0.0371

Estimated vapor split ratio: 47.15% / 52.85%

Hydrocarbon – Equimolar Case H1

Specifications:

Case Number	H1 (eqm)	H1 (neq)
Feed flowrate (lb/h)	101.95	101.95
Feed temperature (°F)	133.07	133.07
Feed pressure (psia)	25.00	25.00
Feed Composition (wt%)		
n-Pentane	26.1	26.1
Cyclohexane	34.1	34.1
n-Heptane	39.7	39.7
Sidedraw rate (lb/h)	34.92	35.06
Bottom flowrate (lb/h)	40.46	40.45
Overhead reflux ratio	4.22	2.62
Flow split ratios (left % / right %)		
Vapor split *	50/50	-
Liquid split	30/70	30/70
Pressure overhead (psia)	20.00	20.00
Overall pressure drop (in H_2O)	3.58	-
Wall region pressure drop (in H_2O)	2.11	-
Heat Transfer Coefficients		
Shell (W/m^2K)	85.4	85.4
Wall (W/m^2K)	1000	420
Surroundings temperature (°F)	34.00	34.00

* Vapor split ratio is estimated in the rate-based PCM.

Results:

Product Purity (equilibrium-stage PCM):

	Unit	Pilot	Sim
ovhd_LK	mass frac	0.999	1.000
sidedraw_MK		0.900	0.935
bot_HK		0.920	0.947

Product Purity (rate-based PCM):

	Unit	Pilot	Sim
ovhd_LK	mass frac	0.999	0.999
sidedraw_MK		0.900	0.895
bot_HK		0.920	0.916

Temperature profiles:

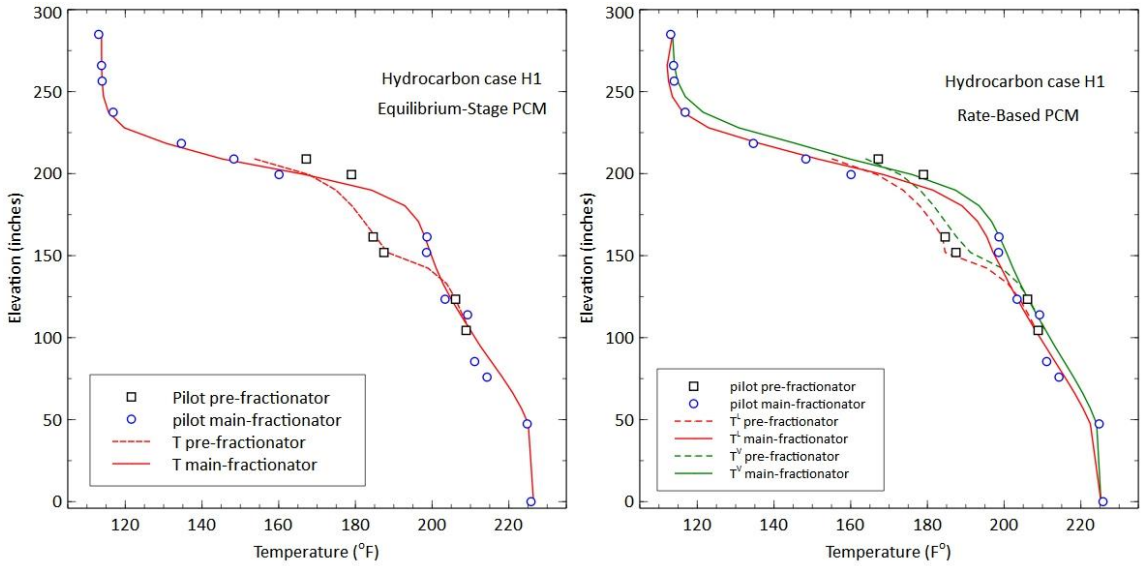

Pressure drop:

	Unit	Pilot	Sim
Overall dp	psia	0.1292	0.1355
Wall region dp		0.0762	0.0601

Estimated vapor split ratio: 50.06% / 49.94%

Hydrocarbon – Equimolar Case H2

Specifications:

Case Number	H2 (eqm)	H2 (neq)
Feed flowrate (lb/h)	103.56	103.56
Feed temperature (^oF)	133.07	133.07
Feed pressure (psia)	25.00	25.00
Feed Composition (wt%)		
n-Pentane	28.2	28.2
Cyclohexane	26.4	26.4
n-Heptane	45.5	45.5
Sidedraw rate (lb/h)	15.00	15.00
Bottom flowrate (lb/h)	59.04	59.04
Overhead reflux ratio	2.23	3.91
Flow split ratios (left % / right %)		
Vapor split *	50/50	-
Liquid split	30/70	30/70
Pressure overhead (psia)	20.00	20.00
Overall pressure drop (in H_2O)	3.58	-
Wall region pressure drop (in H_2O)	2.11	-
Heat Transfer Coefficients		
Shell (W/m^2K)	85.4	85.4
Wall (W/m^2K)	500	1000
Surroundings temperature (^oF)	34.00	34.00

* Vapor split ratio is estimated in the rate-based PCM.

Results:

Product Purity (equilibrium-stage PCM):

	Unit	Pilot	Sim
ovhd_LK	mass frac	0.987	0.988
sidedraw_MK		0.905	0.966
bot_HK		0.774	0.789

Product Purity (rate-based PCM):

	Unit	Pilot	Sim
ovhd_LK	mass frac	0.987	0.987
sidedraw_MK		0.905	0.936
bot_HK		0.774	0.781

Temperature profiles:

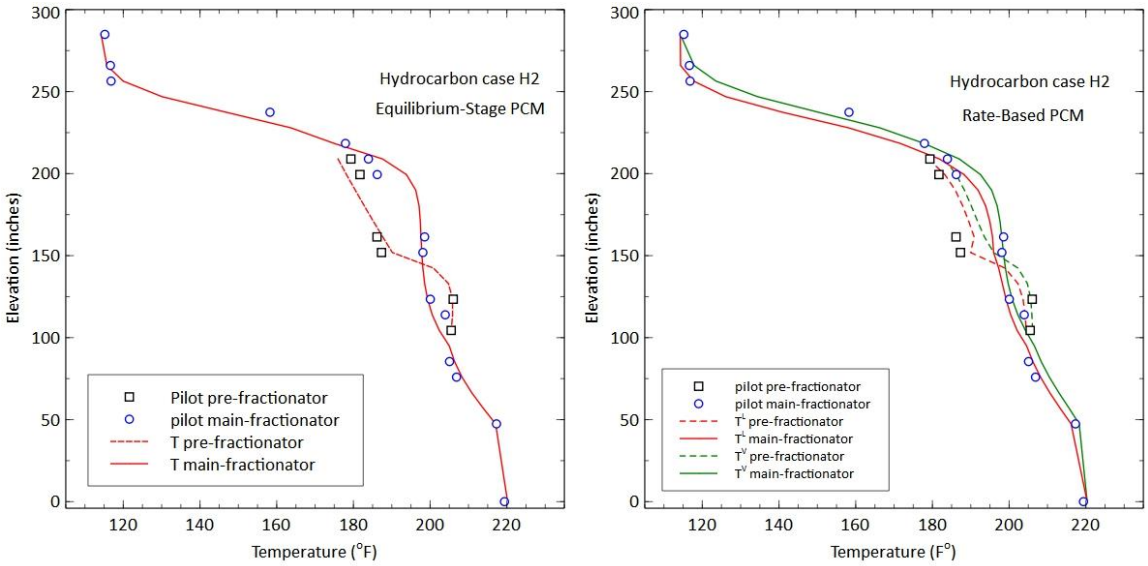

Pressure drop:

	Unit	Pilot	Sim
Overall dp	psia	0.1292	0.2628
Wall region dp		0.0762	0.0892

Estimated vapor split ratio: 51.61% / 48.39%

Hydrocarbon – Equimolar Case H3

Specifications:

Case Number	H3 (eqm)	H3 (neq)
Feed flowrate (lb/h)	103.96	103.96
Feed temperature (°F)	132.90	132.90
Feed pressure (psia)	25.00	25.00
Feed Composition (wt%)		
n-Pentane	31.7	31.7
Cyclohexane	32.2	32.2
n-Heptane	36.1	36.1
Sidedraw rate (lb/h)	34.74	34.97
Bottom flowrate (lb/h)	37.93	37.86
Overhead reflux ratio	7.8	4.99
Flow split ratios (left % / right %)		
Vapor split *	50/50	-
Liquid split	30/70	30/70
Pressure overhead (psia)	20.00	20.00
Overall pressure drop (in H_2O)	3.16	-
Wall region pressure drop (in H_2O)	2.08	-
Heat Transfer Coefficients		
Shell (W/m^2K)	85.4	85.4
Wall (W/m^2K)	0	280
Surroundings temperature (°F)	56.00	56.00

* Vapor split ratio is estimated in the rate-based PCM.

Results:

Product Purity (equilibrium-stage PCM):

	Unit	Pilot	Sim
ovhd_LK	mass frac	0.987	1.000
sidedraw_MK		0.905	0.936
bot_HK		0.774	0.959

Product Purity (rate-based PCM):

	Unit	Pilot	Sim
ovhd_LK	mass frac	0.987	0.999
sidedraw_MK		0.905	0.894
bot_HK		0.774	0.925

Temperature profiles:

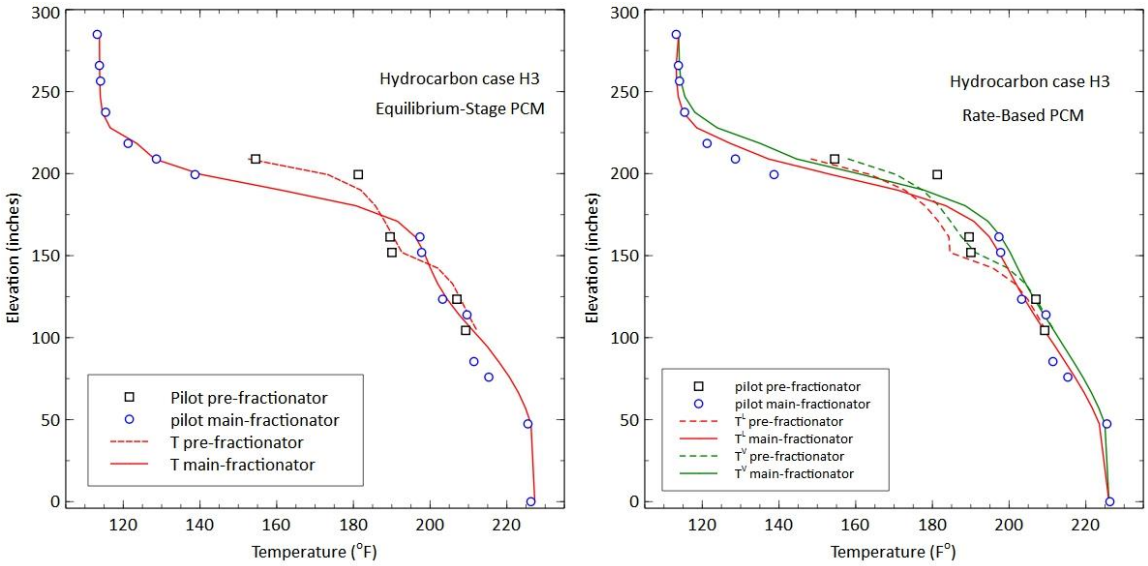

Pressure drop:

	Unit	Pilot	Sim
Overall dp	psia	0.1140	0.1977
Wall region dp		0.0751	0.0814

Estimated vapor split ratio: 50.60% / 49.40%

Hydrocarbon – Equimolar Case H6

Specifications:

Case Number	H6 (eqm)	H6 (neq)
Feed flowrate (lb/h)	96.89	96.89
Feed temperature (^oF)	130.75	130.75
Feed pressure (psia)	25.00	25.00
Feed Composition (wt%)		
n-Pentane	23.9	23.9
Cyclohexane	35.4	35.4
n-Heptane	40.7	40.7
Sidedraw rate (lb/h)	35.95	36.00
Bottom flowrate (lb/h)	37.77	37.80
Overhead reflux ratio	5.38	5.38
Flow split ratios (left % / right %)		
Vapor split *	50/50	-
Liquid split	50/50	50/50
Pressure overhead (psia)	20.00	20.00
Overall pressure drop (in H_2O)	3.77	-
Wall region pressure drop (in H_2O)	2.16	-
Heat Transfer Coefficients		
Shell (W/m^2K)	85.4	85.4
Wall (W/m^2K)	200	900
Surroundings temperature (^oF)	67.00	67.00

* Vapor split ratio is estimated in the rate-based PCM.

Results:

Product Purity (equilibrium-stage PCM):

	Unit	Pilot	Sim
ovhd_LK	mass frac	0.998	0.999
sidedraw_MK		0.891	0.876
bot_HK		0.942	0.927

Product Purity (rate-based PCM):

	Unit	Pilot	Sim
ovhd_LK	mass frac	0.998	0.999
sidedraw_MK		0.891	0.867
bot_HK		0.942	0.919

Temperature profiles:

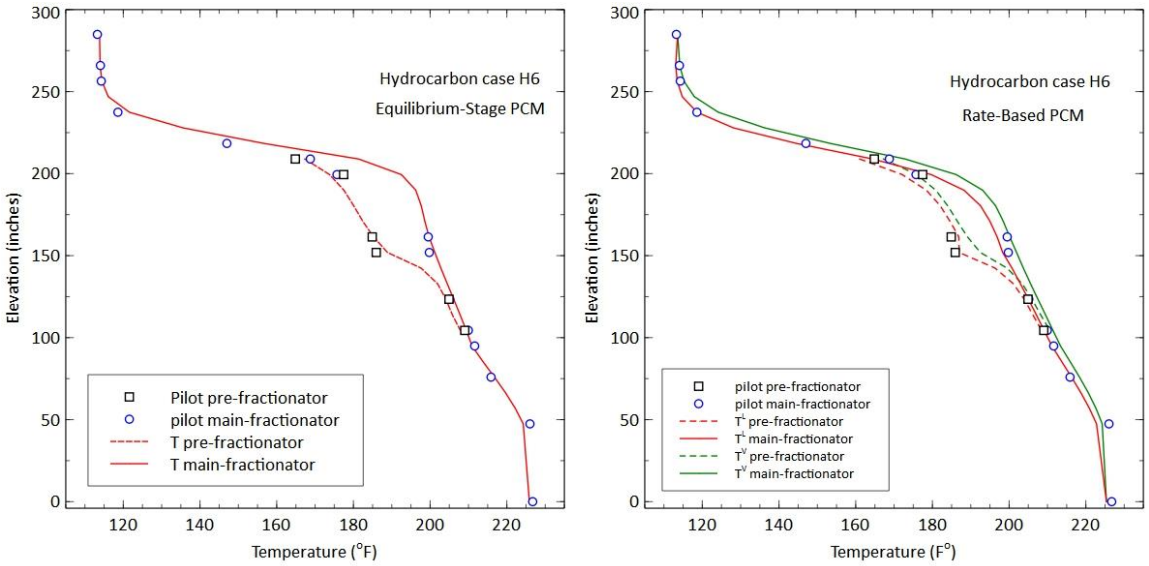

Pressure drop:

	Unit	Pilot	Sim
Overall dp	psia	0.1361	0.1351
Wall region dp		0.0780	0.0629

Estimated vapor split ratio: 48.27% / 51.73%

Hydrocarbon – Equimolar Case H7

Specifications:

Case Number	H7 (eqm)	H7 (neq)
Feed flowrate (lb/h)	108.49	108.49
Feed temperature (°F)	131.43	131.43
Feed pressure (psia)	25.00	25.00
Feed Composition (wt%)		
n-Pentane	32.2	32.2
Cyclohexane	30.8	30.8
n-Heptane	37.1	37.1
Sidedraw rate (lb/h)	14.99	14.90
Bottom flowrate (lb/h)	58.68	58.60
Overhead reflux ratio	6.5	3.6
Flow split ratios (left % / right %)		
Vapor split *	50/50	-
Liquid split	27/73	27/73
Pressure overhead (psia)	20.00	20.00
Overall pressure drop (in H_2O)	3.77	-
Wall region pressure drop (in H_2O)	2.16	-
Heat Transfer Coefficients		
Shell (W/m^2K)	85.4	85.4
Wall (W/m^2K)	320	2000
Surroundings temperature (°F)	67.00	67.00

* Vapor split ratio is estimated in the rate-based PCM.

Results:

Product Purity (equilibrium-stage PCM):

	Unit	Pilot	Sim
ovhd_LK	mass frac	1.000	0.999
sidedraw_MK		0.910	0.973
bot_HK		0.663	0.680

Product Purity (rate-based PCM):

	Unit	Pilot	Sim
ovhd_LK	mass frac	1.000	0.995
sidedraw_MK		0.910	0.928
bot_HK		0.663	0.669

Temperature profiles:

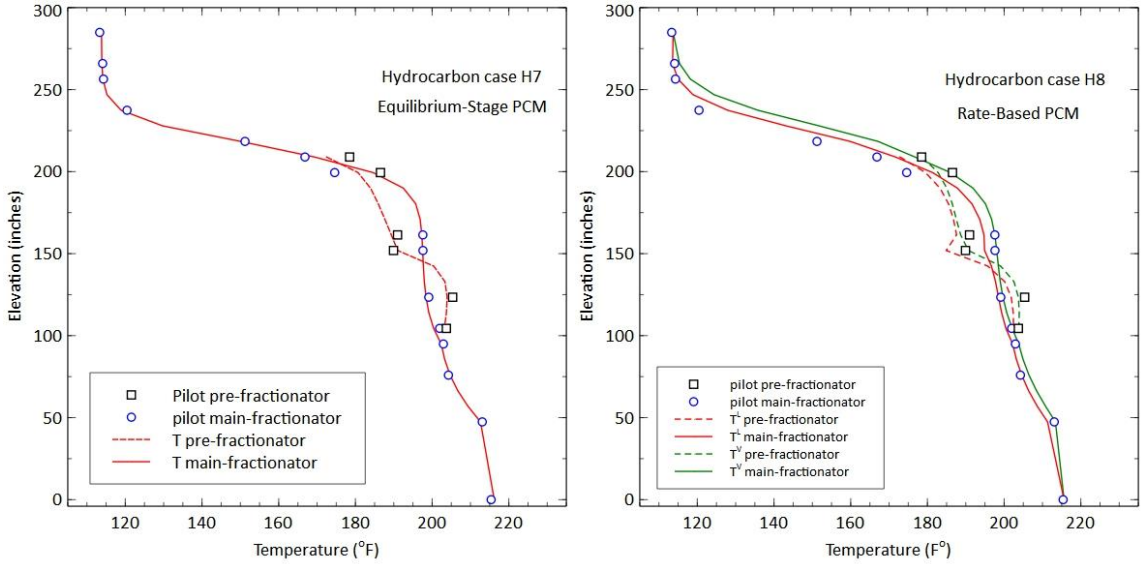

Pressure drop:

	Unit	Pilot	Sim
Overall dp	psia	0.1361	0.1424
Wall region dp		0.0780	0.0692

Estimated vapor split ratio: 50.52% / 49.48%

Hydrocarbon – Equimolar Case H8

Specifications:

Case Number	H8 (eqm)	H8 (neq)
Feed flowrate (lb/h)	106.17	106.17
Feed temperature (°F)	134.3	134.3
Feed pressure (psia)	25.00	25.00
Feed Composition (wt%)		
n-Pentane	27.8	27.8
Cyclohexane	31.2	31.2
n-Heptane	41.0	41.0
Sidedraw rate (lb/h)	36.96	36.94
Bottom flowrate (lb/h)	44.03	43.86
Overhead reflux ratio	8.00	7.00
Flow split ratios (left % / right %)		
Vapor split *	50/50	-
Liquid split	27/73	27/73
Pressure overhead (psia)	20.00	20.00
Overall pressure drop (in H_2O)	3.8	-
Wall region pressure drop (in H_2O)	2.18	-
Heat Transfer Coefficients		
Shell (W/m^2K)	85.4	85.4
Wall (W/m^2K)	0	0
Surroundings temperature (°F)	70.00	70.00

* Vapor split ratio is estimated in the rate-based PCM.

Results:

Product Purity (equilibrium-stage PCM):

	Unit	Pilot	Sim
ovhd_LK	mass frac	1.000	1.000
sidedraw_MK		0.803	0.830
bot_HK		0.923	0.944

Product Purity (rate-based PCM):

	Unit	Pilot	Sim
ovhd_LK	mass frac	1.000	1.000
sidedraw_MK		0.803	0.804
bot_HK		0.923	0.922

Temperature profiles:

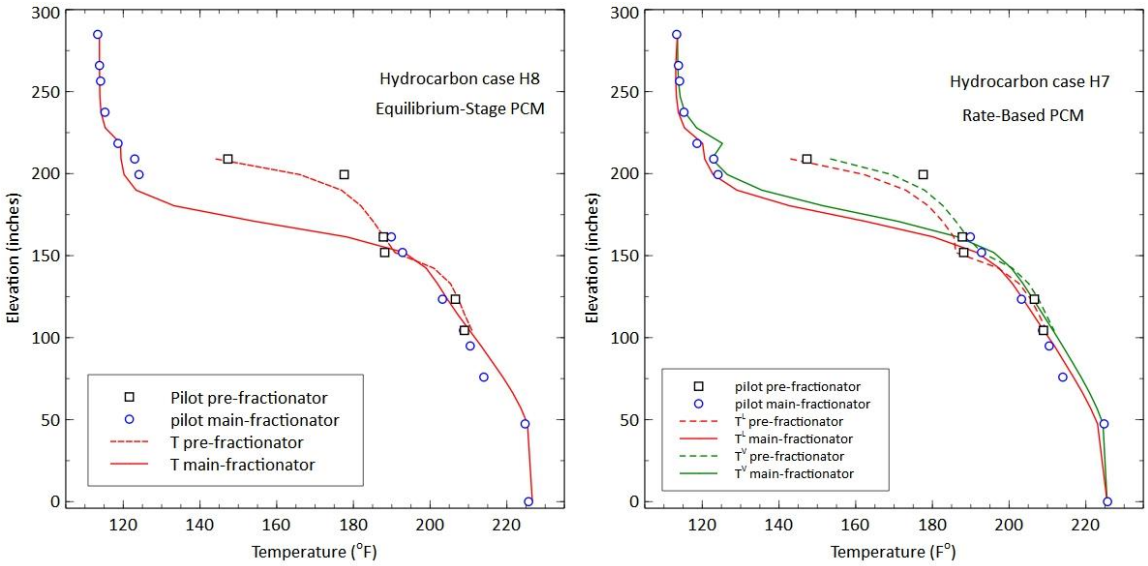

Pressure drop:

	Unit	Pilot	Sim
Overall dp	psia	0.1371	0.1540
Wall region dp		0.0787	0.0719

Estimated vapor split ratio: 51.41% / 48.59%

Hydrocarbon – Equimolar Case H9

Specifications:

Case Number	H9 (eqm)	H9 (neq)
Feed flowrate (lb/h)	106.42	106.42
Feed temperature (°F)	134.47	134.47
Feed pressure (psia)	25.00	25.00
Feed Composition (wt%)		
n-Pentane	28.4	28.4
Cyclohexane	29.8	29.8
n-Heptane	41.7	41.7
Sidedraw rate (lb/h)	36.11	36.11
Bottom flowrate (lb/h)	44.64	44.69
Overhead reflux ratio	6.8	7.0
Flow split ratios (left % / right %)		
Vapor split *	50/50	-
Liquid split	27/73	27/73
Pressure overhead (psia)	20.00	20.00
Overall pressure drop (in H_2O)	3.50	-
Wall region pressure drop (in H_2O)	2.15	-
Heat Transfer Coefficients		
Shell (W/m^2K)	85.4	85.4
Wall (W/m^2K)	0	0
Surroundings temperature (°F)	70.00	70.00

* Vapor split ratio is estimated in the rate-based PCM.

Results:

Product Purity (equilibrium-stage PCM):

	Unit	Pilot	Sim
ovhd_LK	mass frac	1.000	1.000
sidedraw_MK		0.792	0.810
bot_HK		0.930	0.944

Product Purity (rate-based PCM):

	Unit	Pilot	Sim
ovhd_LK	mass frac	1.000	1.000
sidedraw_MK		0.792	0.791
bot_HK		0.930	0.927

Temperature profiles:

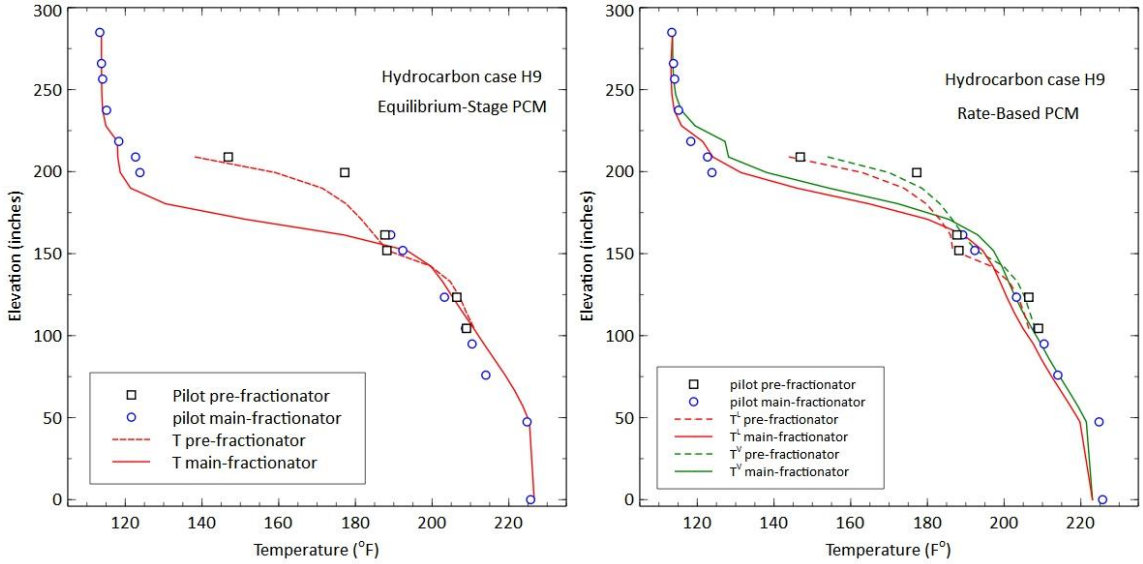

Pressure drop:

	Unit	Pilot	Sim
Overall dp	psia	0.1263	0.1555
Wall region dp		0.0776	0.0731

Estimated vapor split ratio: 51.44% / 48.56%

Hydrocarbon – Equimolar Case H10

Specifications:

Case Number	H10 (eqm)	H10 (neq)
Feed flowrate (lb/h)	106.42	106.42
Feed temperature (°F)	134.30	134.30
Feed pressure (psia)	25.00	25.00
Feed Composition (wt%)		
n-Pentane	26.9	26.9
Cyclohexane	33.3	33.3
n-Heptane	39.7	39.7
Sidedraw rate (lb/h)	32.18	32.26
Bottom flowrate (lb/h)	47.02	46.98
Overhead reflux ratio	8.0	7.0
Flow split ratios (left % / right %)		
Vapor split *	50/50	-
Liquid split	30/70	30/70
Pressure overhead (psia)	20.00	20.00
Overall pressure drop (in H_2O)	2.27	-
Wall region pressure drop (in H_2O)	2.00	-
Heat Transfer Coefficients		
Shell (W/m^2K)	85.4	85.4
Wall (W/m^2K)	0	0
Surroundings temperature (°F)	74.00	74.00

* Vapor split ratio is estimated in the rate-based PCM.

Results:

Product Purity (equilibrium-stage PCM):

	Unit	Pilot	Sim
ovhd_LK	mass frac	1.000	1.000
sidedraw_MK		0.903	0.928
bot_HK		0.883	0.880

Product Purity (rate-based PCM):

	Unit	Pilot	Sim
ovhd_LK	mass frac	1.000	1.000
sidedraw_MK		0.903	0.899
bot_HK		0.883	0.862

Temperature profiles:

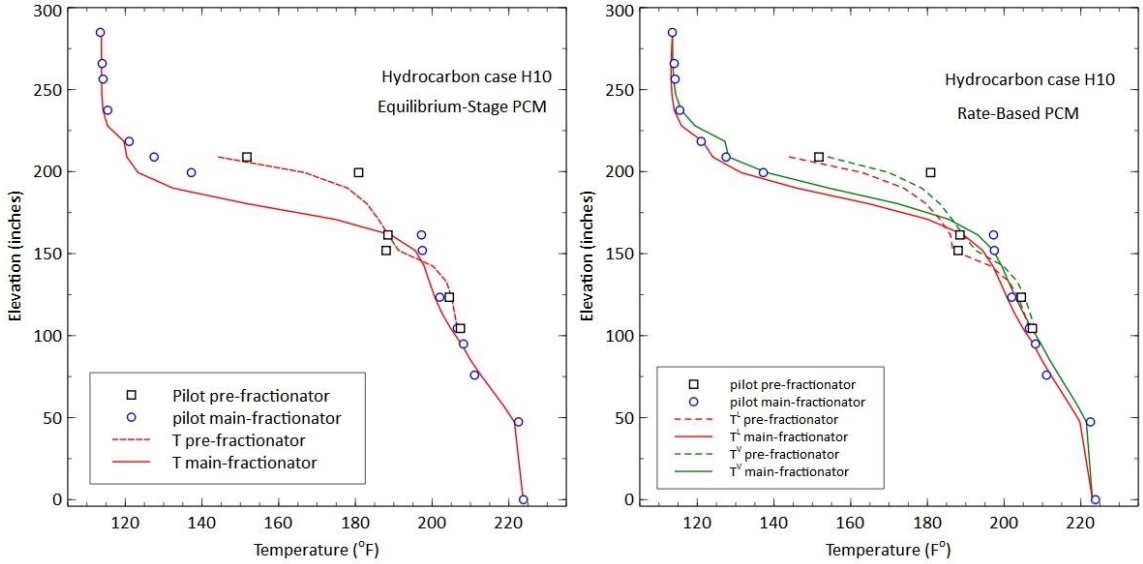

Pressure drop:

	Unit	Pilot	Sim
Overall dp	psia	0.0819	0.1529
Wall region dp		0.0722	0.0747

Estimated vapor split ratio: 51.13% / 48.87%

Hydrocarbon – Equimolar Case H11

Specifications:

Case Number	H11 (eqm)	H11 (neq)
Feed flowrate (lb/h)	102.43	102.43
Feed temperature (°F)	134.30	134.30
Feed pressure (psia)	25.00	25.00
Feed Composition (wt%)		
n-Pentane	27.3	27.3
Cyclohexane	31.0	31.0
n-Heptane	41.7	41.7
Sidedraw rate (lb/h)	30.69	30.69
Bottom flowrate (lb/h)	44.63	44.63
Overhead reflux ratio	5.58	5.56
Flow split ratios (left % / right %)		
Vapor split *	50/50	-
Liquid split	27/73	27/73
Pressure overhead (psia)	20.00	20.00
Overall pressure drop (in H_2O)	2.27	-
Wall region pressure drop (in H_2O)	2.00	-
Heat Transfer Coefficients		
Shell (W/m^2K)	85.4	85.4
Wall (W/m^2K)	0	84
Surroundings temperature (°F)	68.00	68.00

* Vapor split ratio is estimated in the rate-based PCM.

Results:

Product Purity (equilibrium-stage PCM):

	Unit	Pilot	Sim
ovhd_LK	mass frac	1.000	1.000
sidedraw_MK		0.890	0.923
bot_HK		0.902	0.923

Product Purity (rate-based PCM):

	Unit	Pilot	Sim
ovhd_LK	mass frac	1.000	1.000
sidedraw_MK		0.890	0.894
bot_HK		0.902	0.904

Temperature profiles:

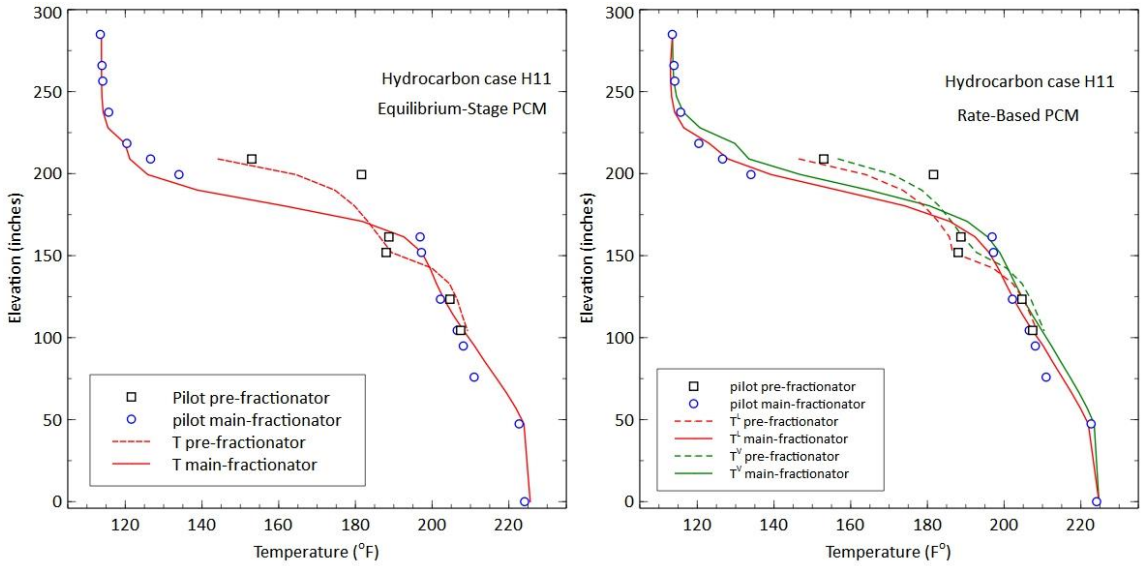

Pressure drop:

	Unit	Pilot	Sim
Overall dp	psia	0.0819	0.1389
Wall region dp		0.0722	0.0665

Estimated vapor split ratio: 51.11% / 48.89%

Hydrocarbon – Equimolar Case H12

Specifications:

Case Number	H12 (eqm)	H12 (neq)
Feed flowrate (lb/h)	103.48	103.48
Feed temperature (°F)	134.30	134.30
Feed pressure (psia)	25.00	25.00
Feed Composition (wt%)		
n-Pentane	26.6	26.6
Cyclohexane	32.1	32.1
n-Heptane	41.3	41.3
Sidedraw rate (lb/h)	36.23	36.23
Bottom flowrate (lb/h)	39.75	39.75
Overhead reflux ratio	6.62	6.62
Flow split ratios (left % / right %)		
Vapor split *	50/50	-
Liquid split	51/49	51/49
Pressure overhead (psia)	20.00	20.00
Overall pressure drop (in H_2O)	3.09	-
Wall region pressure drop (in H_2O)	1.79	-
Heat Transfer Coefficients		
Shell (W/m^2K)	85.4	85.4
Wall (W/m^2K)	850	1238
Surroundings temperature (°F)	65.00	65.00

* Vapor split ratio is estimated in the rate-based PCM.

Results:

Product Purity (equilibrium-stage PCM):

	Unit	Pilot	Sim
ovhd_LK	mass frac	1.000	1.000
sidedraw_MK		0.858	0.873
bot_HK		0.948	0.961

Product Purity (rate-based PCM):

	Unit	Pilot	Sim
ovhd_LK	mass frac	1.000	0.998
sidedraw_MK		0.858	0.848
bot_HK		0.948	0.938

Temperature profiles:

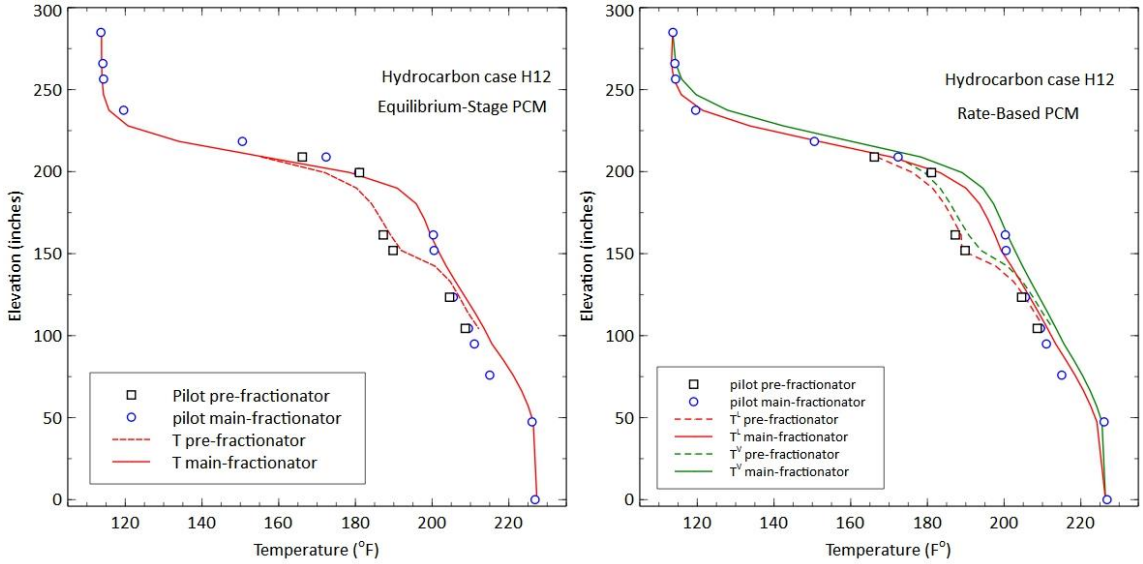

Pressure drop:

	Unit	Pilot	Sim
Overall dp	psia	0.1115	0.2001
Wall region dp		0.0646	0.0876

Estimated vapor split ratio: 47.74% / 52.26%

Hydrocarbon – Total Reflux Case H13

Specifications:

Case Number	H13 (eqm)	H13 (neq)
Feed flowrate (lb/h)	0.99	0.99
Feed temperature (^oF)	113.13	113.13
Feed pressure (psia)	25.00	25.00
Feed Composition (wt%)		
n-Pentane	33.1	33.1
Cyclohexane	38.1	38.1
n-Heptane	27.8	27.8
Sidedraw rate (lb/h)	0.33	0.33
Bottom flowrate (lb/h)	0.33	0.33
Overhead reflux ratio	533.09	533.09
Flow split ratios (left % / right %)		
Vapor split *	50/50	-
Liquid split	50/50	50/50
Pressure overhead (psia)	20.00	20.00
Overall pressure drop (in H_2O)	3.30	-
Wall region pressure drop (in H_2O)	2.83	-
Heat Transfer Coefficients		
Shell (W/m^2K)	0	0
Wall (W/m^2K)	85.4	85.4
Surroundings temperature (^oF)	78.00	78.00
* Vapor split ratio is estimated in the rate-based PCM.		

Results:

Product Purity (equilibrium-stage PCM):

	Unit	Pilot	Sim
ovhd_LK	mass frac	1.000	1.000
sidedraw_MK		0.980	0.989
bot_HK		0.827	0.835

Product Purity (rate-based PCM):

	Unit	Pilot	Sim
ovhd_LK	mass frac	1.000	1.000
sidedraw_MK		0.980	0.976
bot_HK		0.827	0.822

Temperature profiles:

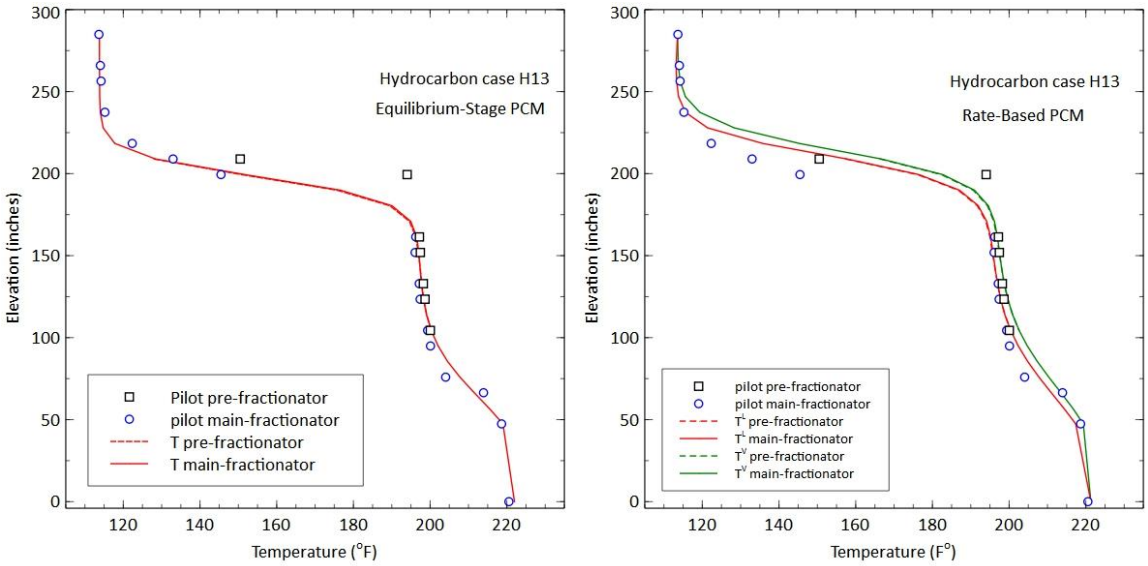

Pressure drop:

	Unit	Pilot	Sim
Overall dp	psia	0.1191	0.1292
Wall region dp		0.1021	0.0624

Estimated vapor split ratio: 50.01% / 49.99%

Hydrocarbon – Total Reflux Case H14

Specifications:

Case Number	H14 (eqm)	H14 (neq)
Feed flowrate (lb/h)	0.99	0.99
Feed temperature (^oF)	109.36	109.36
Feed pressure (psia)	25.00	25.00
Feed Composition (wt%)		
n-Pentane	34.6	34.6
Cyclohexane	36.4	36.4
n-Heptane	28.0	28.0
Sidedraw rate (lb/h)	0.33	0.33
Bottom flowrate (lb/h)	0.33	0.33
Overhead reflux ratio	579.3	579.3
Flow split ratios (left % / right %)		
Vapor split *	50/50	-
Liquid split	32/68	32/68
Pressure overhead (psia)	20.00	20.00
Overall pressure drop (in H_2O)	3.06	-
Wall region pressure drop (in H_2O)	3.02	-
Heat Transfer Coefficients		
Shell (W/m^2K)	0	0
Wall (W/m^2K)	85.4	85.4
Surroundings temperature (^oF)	78.00	78.00

* Vapor split ratio is estimated in the rate-based PCM.

Results:

Product Purity (equilibrium-stage PCM):

	Unit	Pilot	Sim
ovhd_LK	mass frac	1.000	1.000
sidedraw_MK		0.940	0.948
bot_HK		0.838	0.845

Product Purity (rate-based PCM):

	Unit	Pilot	Sim
ovhd_LK	mass frac	1.000	1.000
sidedraw_MK		0.940	0.939
bot_HK		0.838	0.837

Temperature profiles:

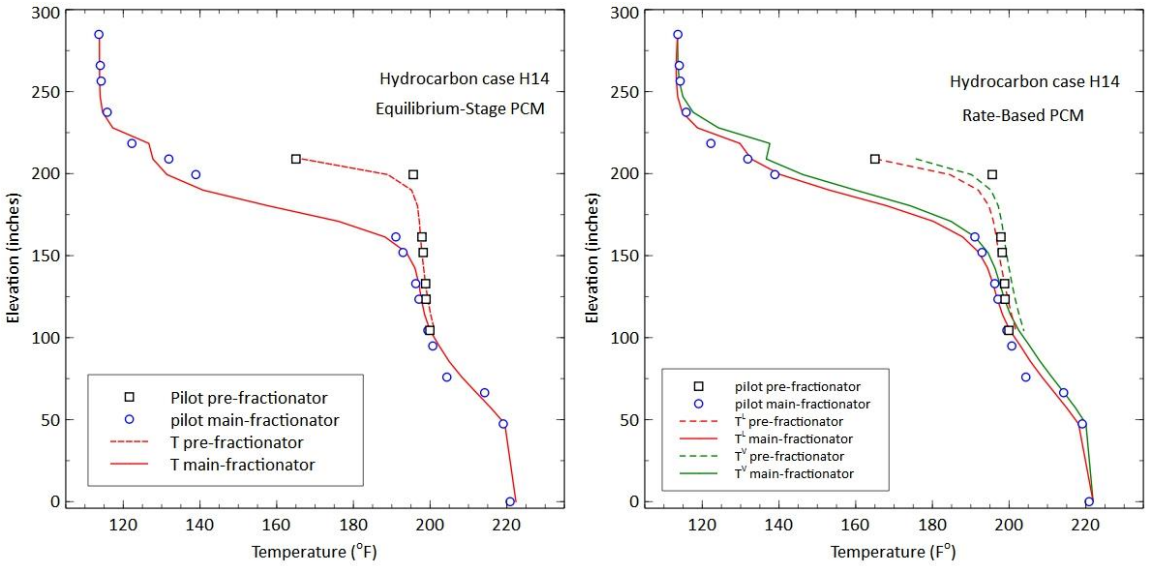

Pressure drop:

	Unit	Pilot	Sim
Overall dp	psia	0.1104	0.1310
Wall region dp		0.1090	0.0646

Estimated vapor split ratio: 50.50% / 49.50%

Hydrocarbon – Total Reflux Case H15

Specifications:

Case Number	H15 (eqm)	H15 (neq)
Feed flowrate (lb/h)	0.99	0.99
Feed temperature (^oF)	115.24	115.24
Feed pressure (psia)	25.00	25.00
Feed Composition (wt%)		
n-Pentane	33.0	33.0
Cyclohexane	36.9	36.9
n-Heptane	29.1	29.1
Sidedraw rate (lb/h)	0.33	0.33
Bottom flowrate (lb/h)	0.33	0.33
Overhead reflux ratio	636.39	636.39
Flow split ratios (left % / right %)		
Vapor split *	50/50	-
Liquid split	70/30	70/30
Pressure overhead (psia)	20.00	20.00
Overall pressure drop (in H_2O)	3.06	-
Wall region pressure drop (in H_2O)	2.09	-
Heat Transfer Coefficients		
Shell (W/m^2K)	0	0
Wall (W/m^2K)	85.4	85.4
Surroundings temperature (^oF)	85.00	85.00

* Vapor split ratio is estimated in the rate-based PCM.

Results:

Product Purity (equilibrium-stage PCM):

	Unit	Pilot	Sim
ovhd_LK	mass frac	1.000	1.000
sidedraw_MK		0.963	0.934
bot_HK		0.846	0.815

Product Purity (rate-based PCM):

	Unit	Pilot	Sim
ovhd_LK	mass frac	1.000	1.000
sidedraw_MK		0.963	0.884
bot_HK		0.846	0.766

Temperature profiles:

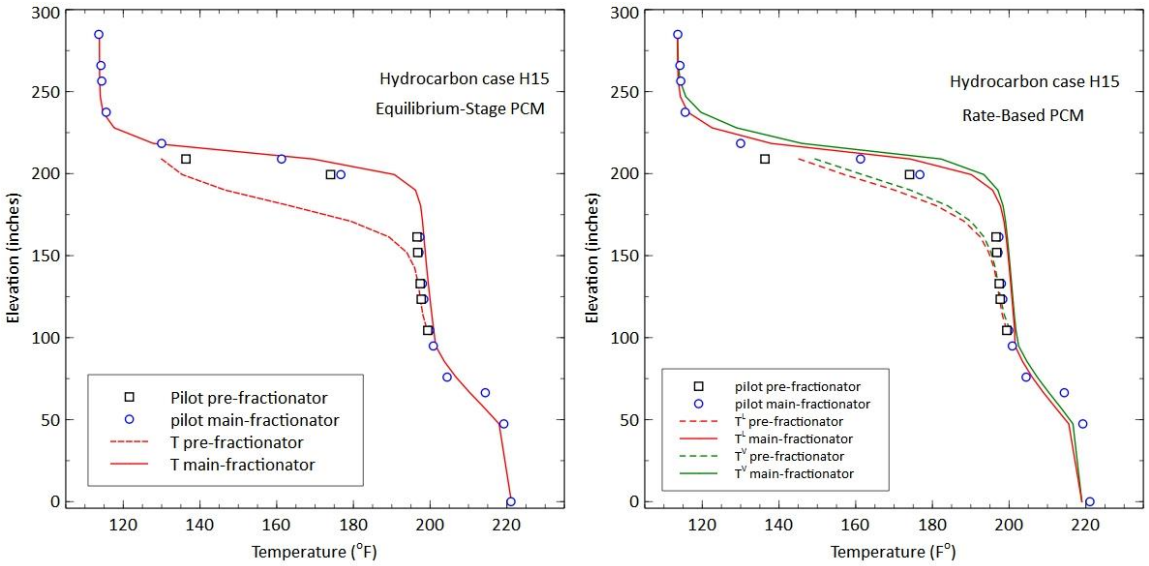

Pressure drop:

	Unit	Pilot	Sim
Overall dp	psia	0.1104	0.0786
Wall region dp		0.0754	0.0413

Estimated vapor split ratio: 48.65% / 51.35%

Hydrocarbon – Total Reflux Case H16

Specifications:

Case Number	H16 (eqm)	H16 (neq)
Feed flowrate (lb/h)	0.99	0.99
Feed temperature (°F)	122.62	122.62
Feed pressure (psia)	25.00	25.00
Feed Composition (wt%)		
n-Pentane	33.1	33.1
Cyclohexane	37.2	37.2
n-Heptane	28.7	28.7
Sidedraw rate (lb/h)	0.33	0.33
Bottom flowrate (lb/h)	0.33	0.33
Overhead reflux ratio	627.45	627.45
Flow split ratios (left % / right %)		
Vapor split *	50/50	-
Liquid split	60/40	60/40
Pressure overhead (psia)	20.00	20.00
Overall pressure drop (in H_2O)	2.97	-
Wall region pressure drop (in H_2O)	1.57	-
Heat Transfer Coefficients		
Shell (W/m^2K)	0	0
Wall (W/m^2K)	85.4	85.4
Surroundings temperature (°F)	85.00	85.00

* Vapor split ratio is estimated in the rate-based PCM.

Results:

Product Purity (equilibrium-stage PCM):

	Unit	Pilot	Sim
ovhd_LK	mass frac	1.000	1.000
sidedraw_MK		0.975	0.985
bot_HK		0.847	0.858

Product Purity (rate-based PCM):

	Unit	Pilot	Sim
ovhd_LK	mass frac	1.000	1.000
sidedraw_MK		0.975	0.953
bot_HK		0.847	0.826

Temperature profiles:

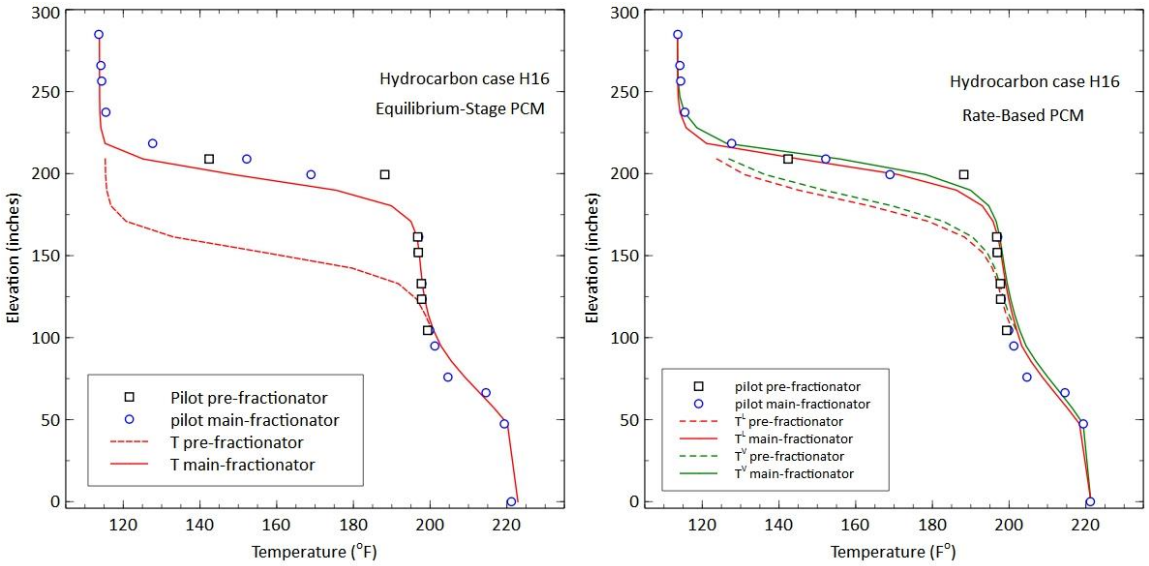

Pressure drop:

	Unit	Pilot	Sim
Overall dp	psia	0.1072	0.0803
Wall region dp		0.0567	0.0405

Estimated vapor split ratio: 48.95% / 51.05%

Hydrocarbon – Total Reflux Case H17

Specifications:

Case Number	H17 (eqm)	H17 (neq)
Feed flowrate (lb/h)	0.99	0.99
Feed temperature (^oF)	110.57	110.57
Feed pressure (psia)	25.00	25.00
Feed Composition (wt%)		
n-Pentane	33.6	33.6
Cyclohexane	36.3	36.3
n-Heptane	29.1	29.1
Sidedraw rate (lb/h)	0.33	0.33
Bottom flowrate (lb/h)	0.33	0.33
Overhead reflux ratio	622.30	622.30
Flow split ratios (left % / right %)		
Vapor split *	50/50	-
Liquid split	40/60	40/60
Pressure overhead (psia)	20.00	20.00
Overall pressure drop (in H_2O)	3.86	-
Wall region pressure drop (in H_2O)	2.27	-
Heat Transfer Coefficients		
Shell (W/m^2K)	0	0
Wall (W/m^2K)	85.4	85.4
Surroundings temperature (^oF)	85.00	85.00

* Vapor split ratio is estimated in the rate-based PCM.

Results:

Product Purity (equilibrium-stage PCM):

	Unit	Pilot	Sim
ovhd_LK	mass frac	1.000	1.000
sidedraw_MK		0.967	0.977
bot_HK		0.867	0.877

Product Purity (rate-based PCM):

	Unit	Pilot	Sim
ovhd_LK	mass frac	1.000	1.000
sidedraw_MK		0.967	0.969
bot_HK		0.867	0.869

Temperature profiles:

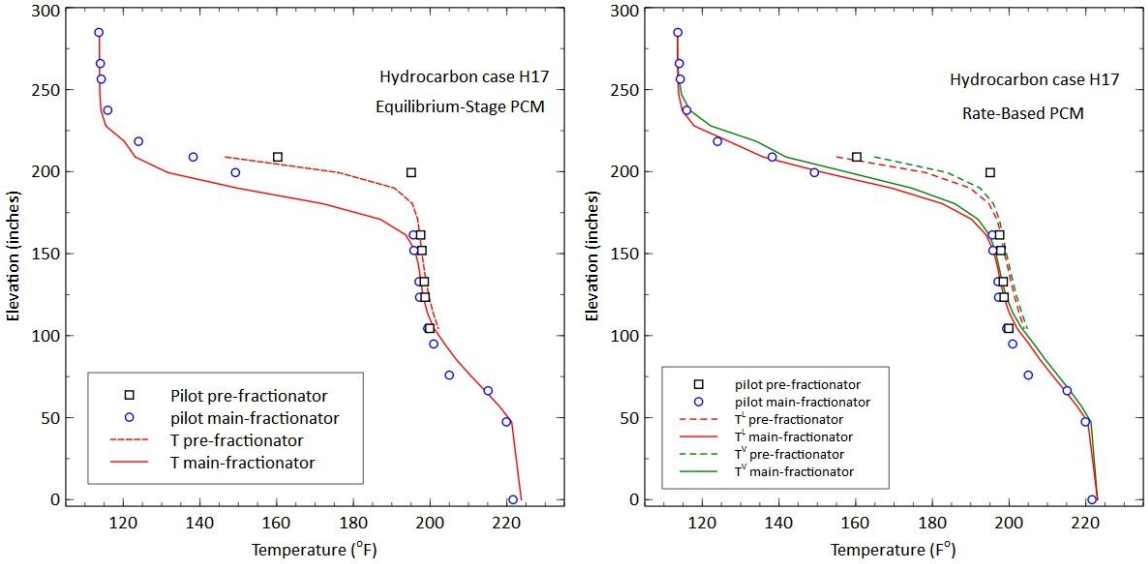

Pressure drop:

	Unit	Pilot	Sim
Overall dp	psia	0.1393	0.0759
Wall region dp		0.0819	0.0403

Estimated vapor split ratio: 50.81% / 49.19%

Hydrocarbon – 10/80/10 Case P1

Specifications:

Case Number	P1 (eqm)	P1 (neq)
Feed flowrate (lb/h)	52.02	52.02
Feed temperature (^oF)	121.63	121.63
Feed pressure (psia)	25.00	25.00
Feed Composition (wt%)		
n-Pentane	12.7	12.7
Cyclohexane	63.5	63.5
n-Heptane	23.8	23.8
Sidedraw rate (lb/h)	24.94	25.00
Bottom flowrate (lb/h)	20.49	20.49
Overhead reflux ratio	28.85	28.85
Flow split ratios (left % / right %)		
Vapor split *	50/50	-
Liquid split	50/50	50/50
Pressure overhead (psia)	20.00	20.00
Overall pressure drop (in H_2O)	2.98	-
Wall region pressure drop (in H_2O)	1.49	-
Heat Transfer Coefficients		
Shell (W/m^2K)	85.4	85.4
Wall (W/m^2K)	70	70
Surroundings temperature (^oF)	88.00	88.00

* Vapor split ratio is estimated in the rate-based PCM.

Results:

Product Purity (equilibrium-stage PCM):

	Unit	Pilot	Sim
ovhd_LK	mass frac	1.000	1.000
sidedraw_MK		0.976	0.989
bot_HK		0.579	0.592

Product Purity (rate-based PCM):

	Unit	Pilot	Sim
ovhd_LK	mass frac	1.000	1.000
sidedraw_MK		0.976	0.977
bot_HK		0.579	0.580

Temperature profiles:

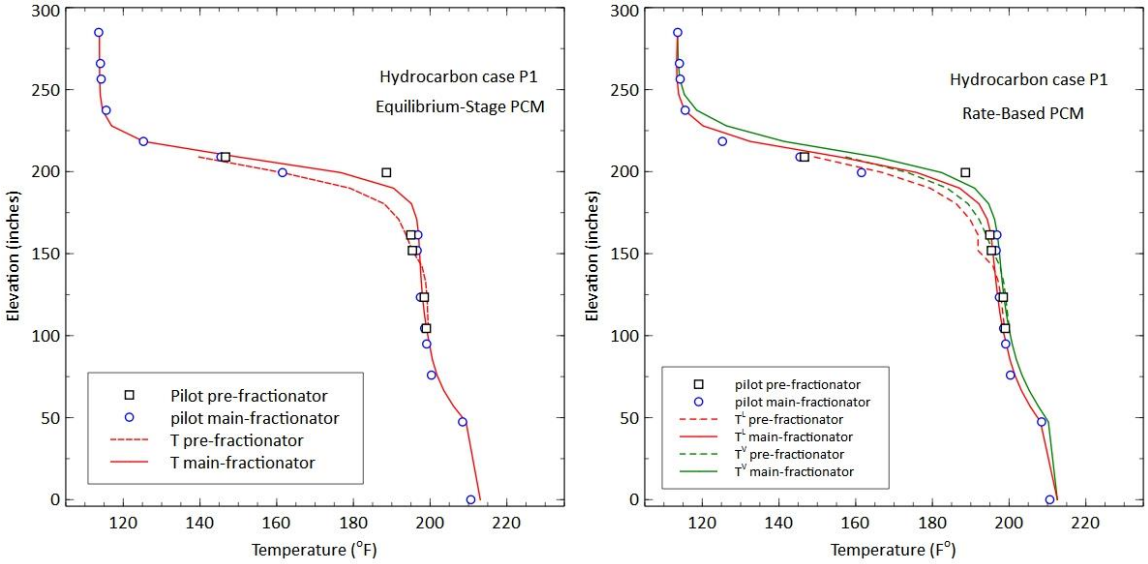

Pressure drop:

	Unit	Pilot	Sim
Overall dp	psia	0.1076	0.1314
Wall region dp		0.0538	0.0646

Estimated vapor split ratio: 50.45% / 49.55%

Hydrocarbon – 10/80/10 Case P2

Specifications:

Case Number	P2 (eqm)	P2 (neq)
Feed flowrate (lb/h)	51.99	51.99
Feed temperature (^oF)	123.21	123.21
Feed pressure (psia)	25.00	25.00
Feed Composition (wt%)		
n-Pentane	11.2	11.2
Cyclohexane	60.8	60.8
n-Heptane	28.0	28.0
Sidedraw rate (lb/h)	23.49	23.51
Bottom flowrate (lb/h)	22.68	22.70
Overhead reflux ratio	31.3	31.3
Flow split ratios (left % / right %)		
Vapor split *	50/50	-
Liquid split	40/60	40/60
Pressure overhead (psia)	20.00	20.00
Overall pressure drop (in H_2O)	3.09	-
Wall region pressure drop (in H_2O)	1.51	-
Heat Transfer Coefficients		
Shell (W/m^2K)	85.4	85.4
Wall (W/m^2K)	1000	1000
Surroundings temperature (^oF)	89.00	89.00

* Vapor split ratio is estimated in the rate-based PCM.

Results:

Product Purity (equilibrium-stage PCM):

	Unit	Pilot	Sim
ovhd_LK	mass frac	1.000	1.000
sidedraw_MK		0.976	0.992
bot_HK		0.618	0.634

Product Purity (rate-based PCM):

	Unit	Pilot	Sim
ovhd_LK	mass frac	1.000	0.998
sidedraw_MK		0.976	0.983
bot_HK		0.618	0.625

Temperature profiles:

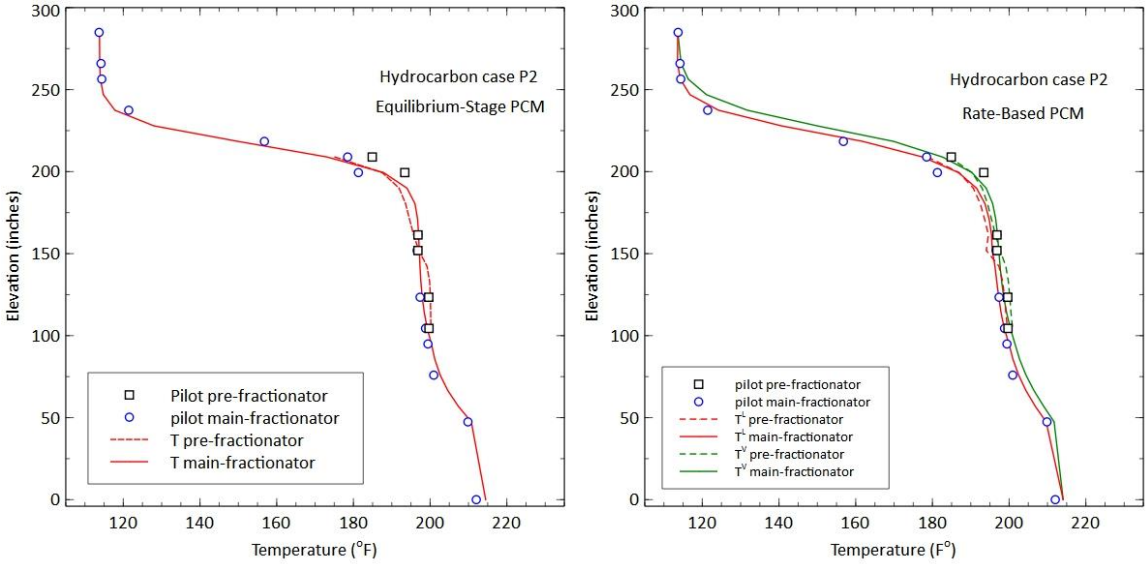

Pressure drop:

	Unit	Pilot	Sim
Overall dp	psia	0.1115	0.1339
Wall region dp		0.0545	0.0667

Estimated vapor split ratio: 51.44% / 48.56%

Hydrocarbon – 10/80/10 Case P3

Specifications:

Case Number	P3 (eqm)	P3 (neq)
Feed flowrate (lb/h)	52.70	52.70
Feed temperature (^oF)	122.57	122.57
Feed pressure (psia)	25.00	25.00
Feed Composition (wt%)		
n-Pentane	10.8	10.8
Cyclohexane	62.0	62.0
n-Heptane	27.2	27.2
Sidedraw rate (lb/h)	21.00	21.00
Bottom flowrate (lb/h)	26.01	26.04
Overhead reflux ratio	31.3	31.3
Flow split ratios (left % / right %)		
Vapor split *	50/50	-
Liquid split	45/55	45/55
Pressure overhead (psia)	20.00	20.00
Overall pressure drop (in H_2O)	2.79	-
Wall region pressure drop (in H_2O)	1.38	-
Heat Transfer Coefficients		
Shell (W/m^2K)	85.4	85.4
Wall (W/m^2K)	1000	1000
Surroundings temperature (^oF)	89.00	89.00

* Vapor split ratio is estimated in the rate-based PCM.

Results:

Product Purity (equilibrium-stage PCM):

	Unit	Pilot	Sim
ovhd_LK	mass frac	1.000	1.000
sidedraw_MK		0.979	0.993
bot_HK		0.535	0.545

Product Purity (rate-based PCM):

	Unit	Pilot	Sim
ovhd_LK	mass frac	1.000	0.998
sidedraw_MK		0.979	0.985
bot_HK		0.535	0.539

Temperature profiles:

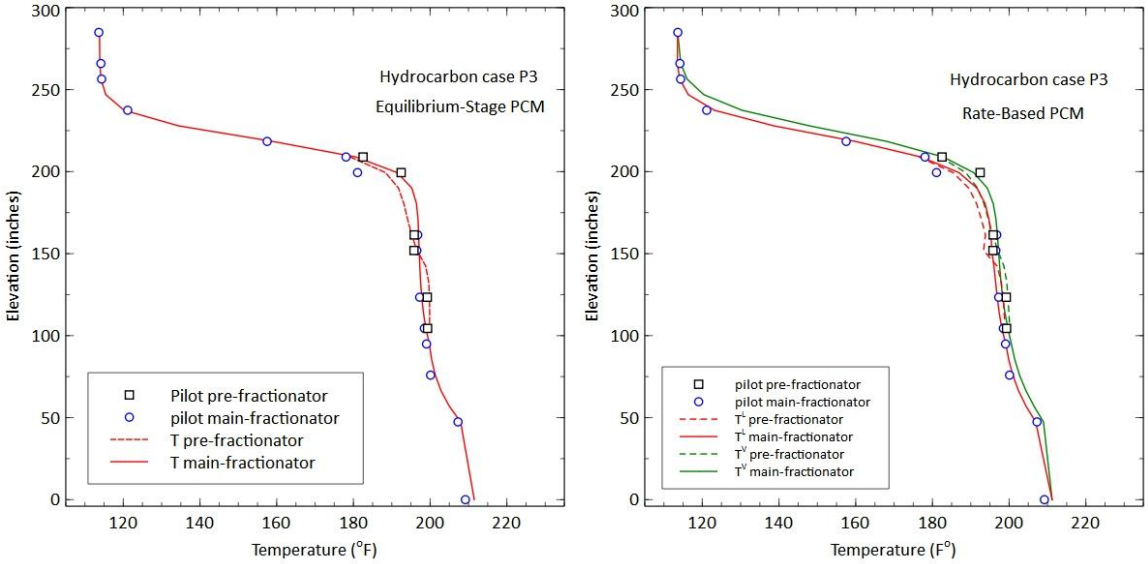

Pressure drop:

	Unit	Pilot	Sim
Overall dp	psia	0.1007	0.1187
Wall region dp		0.0498	0.0586

Estimated vapor split ratio: 50.93% / 49.07%

Hydrocarbon – 10/80/10 Case P4

Specifications:

Case Number	P4 (eqm)	P4 (neq)
Feed flowrate (lb/h)	52.71	52.71
Feed temperature (°F)	122.25	122.25
Feed pressure (psia)	25.00	25.00
Feed Composition (wt%)		
n-Pentane	9.9	9.9
Cyclohexane	61.1	61.1
n-Heptane	29.0	29.0
Sidedraw rate (lb/h)	15.00	15.00
Bottom flowrate (lb/h)	32.49	32.49
Overhead reflux ratio	39.87	30.66
Flow split ratios (left % / right %)		
Vapor split *	50/50	-
Liquid split	50/50	50/50
Pressure overhead (psia)	20.00	20.00
Overall pressure drop (in H_2O)	2.72	-
Wall region pressure drop (in H_2O)	1.45	-
Heat Transfer Coefficients		
Shell (W/m^2K)	85.4	85.4
Wall (W/m^2K)	1000	1000
Surroundings temperature (°F)	89.00	89.00

* Vapor split ratio is estimated in the rate-based PCM.

Results:

Product Purity (equilibrium-stage PCM):

	Unit	Pilot	Sim
ovhd_LK	mass frac	1.000	0.999
sidedraw_MK		0.982	0.994
bot_HK		0.463	0.468

Product Purity (rate-based PCM):

	Unit	Pilot	Sim
ovhd_LK	mass frac	1.000	0.997
sidedraw_MK		0.982	0.986
bot_HK		0.463	0.464

Temperature profiles:

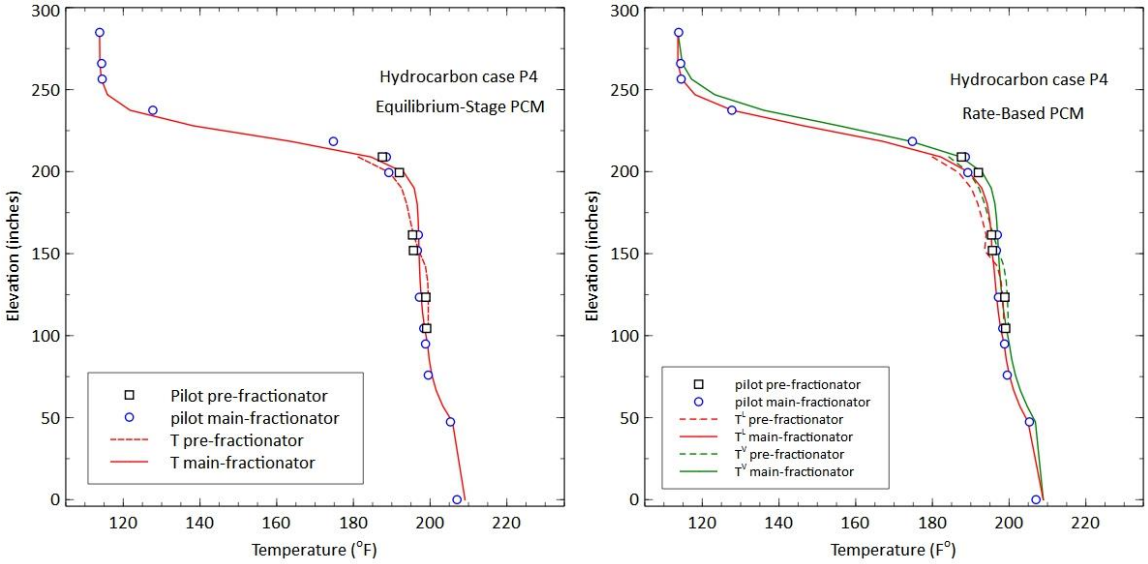

Pressure drop:

	Unit	Pilot	Sim
Overall dp	psia	0.0982	0.1219
Wall region dp		0.0523	0.0609

Estimated vapor split ratio: 50.84% / 49.16%

Hydrocarbon – 10/80/10 Case P5

Specifications:

Case Number	P5 (eqm)	P5 (neq)
Feed flowrate (lb/h)	51.68	51.68
Feed temperature (°F)	125.53	125.53
Feed pressure (psia)	25.00	25.00
Feed Composition (wt%)		
n-Pentane	10.2	10.2
Cyclohexane	63.0	63.0
n-Heptane	26.8	26.8
Sidedraw rate (lb/h)	31.00	31.00
Bottom flowrate (lb/h)	15.40	15.40
Overhead reflux ratio	32.16	32.16
Flow split ratios (left % / right %)		
Vapor split *	50/50	-
Liquid split	50/50	50/50
Pressure overhead (psia)	20.00	20.00
Overall pressure drop (in H_2O)	2.70	-
Wall region pressure drop (in H_2O)	1.28	-
Heat Transfer Coefficients		
Shell (W/m^2K)	85.4	85.4
Wall (W/m^2K)	1000	1000
Surroundings temperature (°F)	89.00	89.00

* Vapor split ratio is estimated in the rate-based PCM.

Results:

Product Purity (equilibrium-stage PCM):

	Unit	Pilot	Sim
ovhd_LK	mass frac	0.998	0.998
sidedraw_MK		0.962	0.973
bot_HK		0.824	0.844

Product Purity (rate-based PCM):

	Unit	Pilot	Sim
ovhd_LK	mass frac	0.998	0.995
sidedraw_MK		0.962	0.953
bot_HK		0.824	0.805

Temperature profiles:

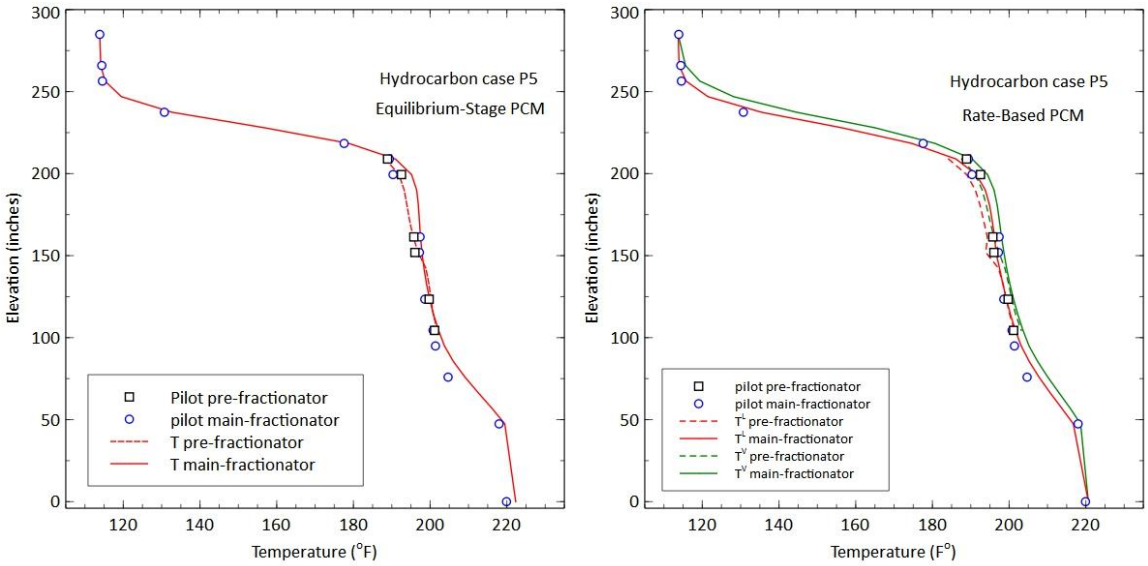

Pressure drop:

	Unit	Pilot	Sim
Overall dp	psia	0.0974	0.1322
Wall region dp		0.0462	0.0657

Estimated vapor split ratio: 49.87% / 50.13%

Hydrocarbon – 10/80/10 Case P6

Specifications:

Case Number	P6 (eqm)	P6 (neq)
Feed flowrate (lb/h)	51.17	51.17
Feed temperature (°F)	120.31	120.31
Feed pressure (psia)	25.00	25.00
Feed Composition (wt%)		
n-Pentane	10.1	10.1
Cyclohexane	62.4	62.4
n-Heptane	27.6	27.6
Sidedraw rate (lb/h)	24.98	24.98
Bottom flowrate (lb/h)	21.02	21.02
Overhead reflux ratio	26.05	26.05
Flow split ratios (left % / right %)		
Vapor split *	50/50	-
Liquid split	50/50	50/50
Pressure overhead (psia)	20.00	20.00
Overall pressure drop (in H_2O)	2.41	-
Wall region pressure drop (in H_2O)	1.17	-
Heat Transfer Coefficients		
Shell (W/m^2K)	85.4	85.4
Wall (W/m^2K)	1000	1000
Surroundings temperature (°F)	89.00	89.00

* Vapor split ratio is estimated in the rate-based PCM.

Results:

Product Purity (equilibrium-stage PCM):

	Unit	Pilot	Sim
ovhd_LK	mass frac	0.998	0.998
sidedraw_MK		0.976	0.987
bot_HK		0.643	0.656

Product Purity (rate-based PCM):

	Unit	Pilot	Sim
ovhd_LK	mass frac	0.998	0.996
sidedraw_MK		0.976	0.976
bot_HK		0.643	0.643

Temperature profiles:

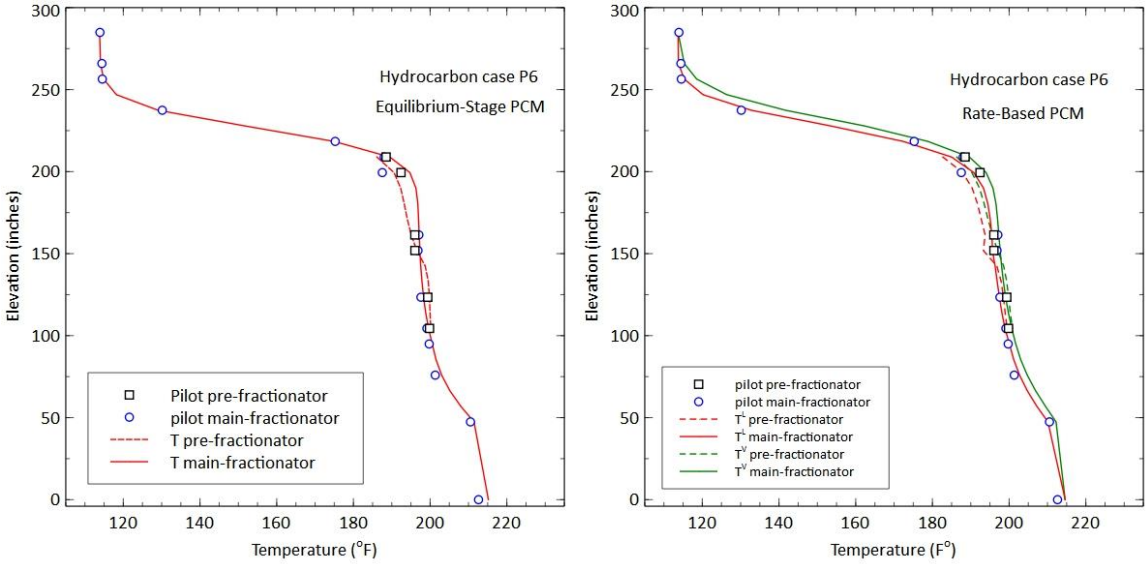

Pressure drop:

	Unit	Pilot	Sim
Overall dp	psia	0.0870	0.1099
Wall region dp		0.0422	0.0541

Estimated vapor split ratio: 50.47% / 49.53%

Hydrocarbon – 10/80/10 Case P7

Specifications:

Case Number	P7 (eqm)	P7 (neq)
Feed flowrate (lb/h)	51.05	51.05
Feed temperature (°F)	124.33	124.33
Feed pressure (psia)	25.00	25.00
Feed Composition (wt%)		
n-Pentane	10.6	10.6
Cyclohexane	63.7	63.7
n-Heptane	25.7	25.7
Sidedraw rate (lb/h)	25.08	25.05
Bottom flowrate (lb/h)	20.56	20.56
Overhead reflux ratio	32.67	35.27
Flow split ratios (left % / right %)		
Vapor split *	50/50	-
Liquid split	55/45	55/45
Pressure overhead (psia)	20.00	20.00
Overall pressure drop (in H_2O)	2.67	-
Wall region pressure drop (in H_2O)	1.27	-
Heat Transfer Coefficients		
Shell (W/m^2K)	85.4	85.4
Wall (W/m^2K)	1000	1000
Surroundings temperature (°F)	89.00	89.00

* Vapor split ratio is estimated in the rate-based PCM.

Results:

Product Purity (equilibrium-stage PCM):

	Unit	Pilot	Sim
ovhd_LK	mass frac	0.998	0.999
sidedraw_MK		0.969	0.987
bot_HK		0.603	0.623

Product Purity (rate-based PCM):

	Unit	Pilot	Sim
ovhd_LK	mass frac	0.998	0.992
sidedraw_MK		0.969	0.974
bot_HK		0.603	0.607

Temperature profiles:

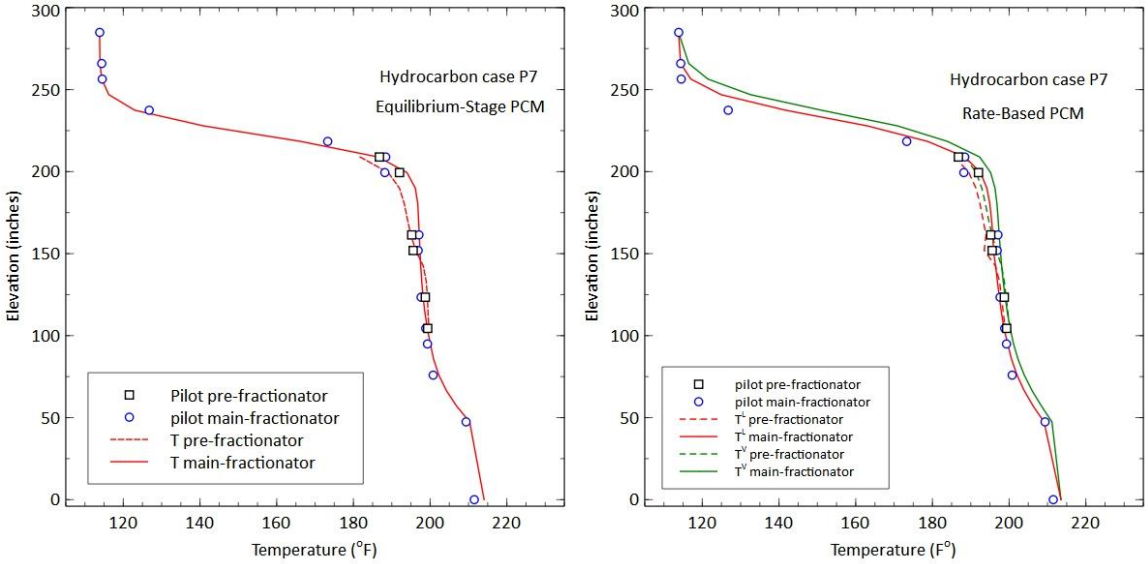

Pressure drop:

	Unit	Pilot	Sim
Overall dp	psia	0.0964	0.1462
Wall region dp		0.0458	0.0745

Estimated vapor split ratio: 50.01% / 49.99%